

Functional Nanostructures from well- defined Block Copolymers:

Stimuli-responsive Membranes, Multicompartment
Micelles, and Interpolyelectrolyte Complexes

DISSERTATION

zur Erlangung des akademisches Grades eines Doktors der
Naturwissenschaften (Dr. rer. Nat.) im Fach Chemie der Fakultät für
Biologie, Chemie und Geowissenschaften der Universität Bayreuth

vorgelegt von

Felix Schacher

Geboren in Lichtenfels / Deutschland

Bayreuth, 2009

Die vorliegende Arbeit wurde in der Zeit von Juli 2006 bis Februar 2009 am Lehrstuhl Makromolekulare Chemie II unter der Betreuung von Prof. Dr. Axel H. E. Müller angefertigt.

Vollständiger Abdruck der von der Fakultät für Biologie, Chemie und Geowissenschaften der Universität Bayreuth zur Erlangung des akademischen Grades eines Doktors der Naturwissenschaften genehmigten Dissertation.

Dissertation eingereicht am: 04.02.2009

Zulassung durch die Prüfungskommission: 17.02.2009

Wissenschaftliches Kolloquium: 15.05.2009

Amtierender Dekan: Prof. Dr. Axel H. E. Müller

Prüfungsausschuss:

Prof. Dr. Axel H. E. Müller (Erstgutachter)

Prof. Dr. Thomas Hellweg (Zweitgutachter)

Prof. Dr. Mukundan Thelakkat (Vorsitz)

Prof. Dr. Josef Breu

Erfahrung ist fast immer eine Parodie auf die Idee

(Johann Wolfgang v. Goethe)

Katharina

Margit

Moritz

Helmut

TABLE OF CONTENTS

	Summary / Zusammenfassung	
1.	Introduction	
1.1.	Functional Materials via Self-assembly	I-01
1.2.	Anionic Polymerization as a versatile Tool for Block Copolymer Synthesis	I-03
1.3.	Block Copolymer Membranes	I-06
1.3.1.	Membranes via Phase Inversion Processes	I-07
1.3.2.	Composite Membranes	I-09
1.4.	Block Copolymer Self-assembly in Solution	I-10
1.4.1.	Compartmentalized Polymeric Micelles	I-12
1.4.2.	Interpolyelectrolyte Complexes	I-15
1.4.3.	Hybrid Materials	I-17
1.5.	Objective of this Thesis	I-22
2.	Thesis Overview	II-01
	<i>Individual Contributions to Joint Publications</i>	II-23
3.	Synthesis, Characterization, and Bulk Crosslinking of Polybutadiene- <i>block</i> -poly(2-vinylpyridine)- <i>block</i> -poly(<i>tert</i> -butyl methacrylate) Block Terpolymers	III-01
4.	Towards Nanoporous Membranes based on ABC Triblock Terpolymers	IV-01
5.	New Block Copolymers with Poly(N,N-dimethylaminoethyl methacrylate) as Double Stimuli-responsive Block	V-01
6.	Self-supporting, Double Stimuli-responsive Porous Membranes from Polystyrene- <i>block</i> -poly(N,N-dimethylaminoethyl methacrylate) Diblock Copolymers	VI-01
7.	Double Stimuli-Responsive Ultrafiltration Membranes from Polystyrene- <i>block</i> -poly(N,N-dimethylaminoethyl methacrylate) Diblock Copolymers	VII-01

8.	Multicompartment-Core Micelles of ABC Triblock Terpolymers in Organic Media	VIII-01
9.	Dynamic Multicompartment-Core Micelles in Aqueous Media	IX-01
10.	Interpolyelectrolyte Complexes of Dynamic Multicompartment Micelles	X-01
11.	List of Publications	XI-01
12.	Conference Presentations	XII-01
13.	Abbreviations	XIII-01
14.	Danksagung	

Summary

This work describes the synthesis of different stimuli-responsive block co- and terpolymers of the AB- and ABC-type, their characterization, and their self-assembly in the bulk and in solution. Sequential anionic polymerization was used to obtain well-defined polymeric materials, which were utilized for the generation of functional nanostructures, e.g. for membrane applications.

In a first approach, five series of polybutadiene-*block*-poly(2-vinylpyridine)-*block*-poly(*tert*-butyl methacrylate) (BVT) block terpolymers were synthesized and their behavior in thin-films on substrates with different wettabilities was investigated. The aim was to generate microphase-separated structures which could serve as precursors for the fabrication of stimuli-responsive composite membranes. Thin films were prepared via spin-casting and the self-assembly processes were facilitated through subsequent solvent annealing. Although no smart membrane could be prepared and tested, model systems were intensively studied and in-depth knowledge could be gained concerning the morphological behavior of BVT terpolymers under such conditions. The thin film structures were always compared with the bulk ones.

Using a different strategy, smart ultrafiltration membranes could be fabricated via non-solvent induced phase separation (NIPS) processes. Amphiphilic polystyrene-*block*-poly(N,N-dimethylaminoethyl methacrylate) (PS-*b*-PDMAEMA) diblock copolymers were synthesized and cast onto planar glass substrates with a doctor blade. After final film formation in the coagulation bath, asymmetric membranes with tunable water flux and pore sizes were obtained. PS forms the matrix of these materials, while PDMAEMA covers the pore walls. The pH- and temperature-responsive properties of those systems were attributed to the hydrophilic PDMAEMA segments. The influence of several important parameters during the casting process onto the membrane morphology and permeability was thoroughly investigated: solvent composition, the cast film height, the "open-time", and the PDMAEMA content of the block copolymers.

Besides PS-*b*-PDMAEMA, several diblock copolymers with PDMAEMA as second block were also synthesized: PB-*b*-PDMAEMA, poly(*tert*-butoxystyrene)-*block*-PDMAEMA, and poly(ethylene oxide)-*block*-PDMAEMA. For the latter, a novel one-pot strategy

could be successfully employed, providing a facile changeover from an oxyanion to a carbanion. The kinetics of the DMAEMA polymerizations show that the reactions proceed considerably slower in presence of the *t*BuP₄-phosphazene base compared to polymerizations performed with an excess of alkoxides.

In a third approach, the self-assembly of BVT block terpolymers in solution was explored. Narrowly dispersed micelles with a patchy core were formed in acetone, a selective solvent for polybutadiene. The micelles exhibited a PB core, a non-continuous P2VP shell, and a P*t*BMA corona. The micellar core was then crosslinked via different methods, enabling the transfer of such polymeric colloids into non-selective solvents, like dioxane, while still preserving their structure and shape.

Finally, polymer analogous reactions were performed with the BVT terpolymers. After hydrolysis of the P*t*BMA block to PMAA and, eventually, quaternization of the middle block, P2VP, amphiphilic block terpolymers with either one or two pH-responsive segments were obtained. Their aggregation behavior in aqueous systems, depending on salinity and pH, was studied. Micelles with a soft PB core, a P2VP shell and a PMAA corona were formed. Under certain conditions intra-micellar interpolyelectrolyte complexes (IPECs) formed, generating multicompartement micelles with a patchy shell. Furthermore, the IPEC formation of those systems with oppositely charged double hydrophilic poly(*N*-methyl-2-vinylpyridinium)-*block*-poly(ethylene oxide) (P2VP_q-*b*-PEO) diblock copolymers was investigated. In that way, a second IPEC shell was formed by electrostatically driven co-assembly of PMAA and P2VP_q. PEO serves as the new corona of the resulting colloidal structures. The time-dependent evolution of such systems was studied and intermediate star-like structures were identified. Furthermore, the selective incorporation of in-situ generated gold nanoparticles inside the IPECs was demonstrated.

Zusammenfassung

In dieser Arbeit werden die Synthese, die Charakterisierung und die Selbstaggregation von Block Co- und Terpolymeren sowohl des AB- als auch des ABC-Typs beschrieben. Lebende anionische Polymerisation wurde herangezogen, um wohldefinierte Materialien zu erhalten. Diese wurden anschließend verwendet um Nanostrukturen mit definierten Funktionalitäten herzustellen, beispielsweise für die Anwendung als Membranen.

In einem ersten Ansatz wurden fünf Serien von Polybutadien-*block*-poly(2-vinylpyridin)-*block*-poly(*tert*-butylmethacrylat) (BVT) Blockterpolymeren synthetisiert. Daraufhin wurden deren Eigenschaften in Dünnschichten auf Oberflächen mit unterschiedlicher Benetzbarkeit untersucht. Die Zielsetzung bestand darin, mikrophasenseparierte Strukturen herzustellen und diese als mögliche Vorstufen zur Herstellung schaltbarer Komposit-Membranen zu verwenden. Dazu wurden Dünnschichten (Dicke unter 100 nm) durch Aufschleudern auf eine Oberfläche (z.B. Silizium) aufgebracht und der Prozess der Selbstanordnung durch nachfolgendes Quellen und Tempern im kontrollierten Lösungsmitteldampf beschleunigt. Obwohl auf diese Weise keine endgültigen Membranstrukturen erhalten und getestet werden konnten, gelangen intensive Untersuchungen an Modellsystemen. Außerdem wurde das morphologische Verhalten derartiger BVT-Terpolymere sorgfältig analysiert. Weiterhin wurden alle Dünnschicht-Strukturen stets mit den jeweiligen Volumenstrukturen verglichen.

Mittels einer anderen Strategie, nämlich über den Nichtlösungsmittel induzierten Phasenseparationsprozess (NIPS), konnten intelligente Ultrafiltrationsmembranen hergestellt werden. Dazu wurden amphiphile Polystyrol-*block*-poly(N,N-dimethylaminoethylmethacrylat) (PS-*b*-PDMAEMA) Diblockcopolymeren synthetisiert. Konzentrierte Lösungen dieser Materialien wurden mittels einer Rakel in definierten Schichtdicken auf Glasplatten aufgetragen. Nach dem endgültigen Ausfällen der Polymerfilme in einem Wasserbad wurden asymmetrische Membranen erhalten, deren Durchlässigkeit und Porengröße durch äußere Einflüsse regulierbar sind. PS bildet die Matrix während PDMAEMA hauptsächlich die Porenwände bedeckt. Das Ansprechen dieser Systeme auf Änderungen des pH-Wertes oder der Umgebungstemperatur wurde auf die Eigenschaften des hydrophilen PDMAEMA

Blocks zurückgeführt. Nach ersten Ergebnissen hinsichtlich der Poren dieser Membranen und ihrer Verwendung zur selektiven Filtration von Nanopartikeln unterschiedlicher Größe wurde der Einfluss verschiedener Parameter während der Filmherstellung auf Morphologie und Durchlässigkeit der Membranen untersucht. Dazu zählten die Zusammensetzung des Lösungsmittelgemisches, die Höhe des aufgetragenen Films, die Offenzeit vor dem Eintauchen in das Fällbad und der Anteil an PDMAEMA, bezogen auf den Volumenbruch im verwendeten Blockcopolymer.

Neben PS-*b*-PDMAEMA wurden verschiedene andere Blockcopolymerer mit PDMAEMA als zweitem Block hergestellt: PB-*b*-PDMAEMA, Poly(*tert*-Butoxystyrol)-*block*-PDMAEMA sowie Polyethylenoxid-*block*-PDMAEMA. Im letztgenannten Fall wurde eine neuartige Ein-Topf-Strategie angewandt. Dadurch wurde während der Reaktion direkt von einem Oxoanion-Kettenende auf ein Carbanion-Kettenende gewechselt. Die Kinetik aller DMAEMA-Polymerisationen zeigt, dass der Zusatz von Phosphazenen-Base im Falle der Polymerisation von PEO-*b*-PDMAEMA zu einer deutlich langsameren Reaktionsgeschwindigkeit verglichen mit Polymerisationen in Gegenwart von Alkoxiden führt.

Ein dritter Teil dieser Doktorarbeit befasste sich mit der Selbstanordnung von BVT Blockterpolymeren in Lösung. In Aceton, einem selektiven Lösungsmittel für PB, wurden sehr eng verteilte Mizellen mit einem uneinheitlichen Kern gebildet. Sie besaßen einen PB-Kern, eine uneinheitliche Schale aus P2VP sowie eine P*t*BMA-Corona. Der Mizellkern wurde mit verschiedenen Methoden vernetzt wodurch die Aggregate ohne Strukturveränderung in nicht-selektive Lösungsmittel wie z.B. Dioxan überführt werden konnten.

Schließlich wurden an den zuvor gebildeten und charakterisierten Mizellen polymeranaloge Modifikationen durchgeführt. Der P*t*BMA-Block wurde zu Polymethacrylsäure (MAA) hydrolysiert. Gegebenenfalls wurde zuvor der P2VP-Block durch Quaternisierung mit Methyljodid in einen starken Polyelektrolyten verwandelt. Auf diese Weise wurden amphiphile Blockterpolymere mit entweder einem oder zwei pH-sensitiven Blöcken erhalten. Das Aggregationsverhalten dieser Systeme in Abhängigkeit von pH-Wert und Salzgehalt wurde anschließend untersucht. Mizellen mit einem weichen PB-Kern, einer P2VP-Schale und einer MAA-Corona wurden gebildet. Unter bestimmten Voraussetzungen werden intermizellare

Interpolyelektrolytkomplexe (IPECs) gebildet. Daraus resultieren Multikompartiment-Mizellen mit einer uneinheitlichen Schale. Außerdem wurde die IPEC-Bildung dieser Systeme mit entgegengesetzt geladenen Poly(*N*-methyl-2-vinylpyridinium)-*block*-polyethylenoxid Diblockcopolymeren untersucht. Es konnte eine weitere Schale durch die elektrostatisch induzierte IPEC-Bildung zwischen PMAA und P2VPq geformt werden. PEO diente als stabilisierende Corona der neu gebildeten Strukturen. Die zeitliche Entwicklung solcher Aggregate wurde weiter untersucht und sternförmige Zwischenzustände konnten identifiziert werden. Abschließend wurde die Bildung von Gold-Nanopartikeln selektiv innerhalb der IPEC-Schale dieser Mizellen demonstriert.

1. Introduction

The development of block copolymers and, along with that, the concept of entropically and enthalpically driven phase separation^[1] had a great impact on a variety of different research areas.^[2, 3] Within this introduction, a brief overview will be given for several topics related to the concept of block copolymers with relevance concerning the content of this thesis.

1.1. Functional Materials via Self-assembly

Increasing complexity in nowadays problems is always accompanied with more demanding requirements on materials. Often, more and also different functional groups are desired in close proximity and on smaller length scales. Therefore, block copolymers with their ability to self-assemble into a large diversity of morphologies are promising starting materials for the fabrication of tomorrow's nanostructured materials.^[4] Moreover, depending on the block copolymer architecture, the composition, and on the environment or substrates employed these processes can be even further manipulated.^[5, 6] The blending of different block copolymers has also been shown to generate well-defined structural patterns.^[7, 8] Microphase-separated domains in such block copolymer patterns then are in the range of 10-100 nm. A short abstract of possible morphologies for a linear ternary system, polystyrene-*block*-polybutadiene-*block*-poly(methyl methacrylate) (SBM) as investigated by Stadler et. al., is displayed in Figure 1-1.

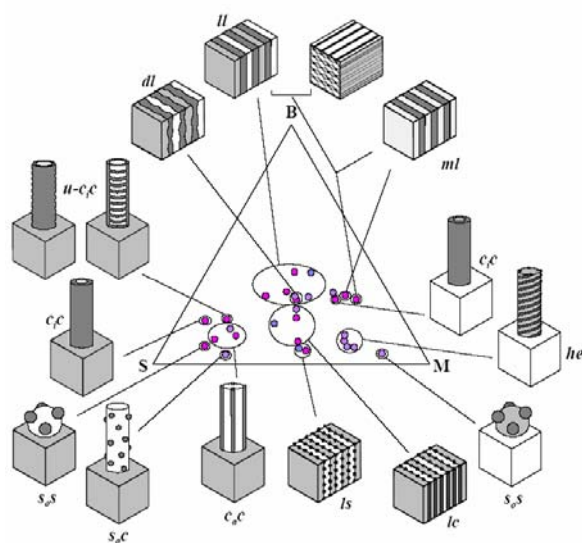


Figure 1-1: Ternary phase diagram obtained for different SBM block terpolymers.

Besides polymer architecture and sequence, the introduction of “smart” polymeric building blocks leads to novel, unexpected properties and broadened the scope of possible applications.^[9-11] “Smart”, or intelligent, polymers are able to change their properties or conformation in response to an external stimulus like pH,^[12] temperature,^[13] or light.^[14] Such materials could be used for, e.g., responsive membranes^[15] or bioreactors.^[16] Furthermore, block copolymer systems with photoaddressable segments are very interesting for lithography purposes^[17, 18] or for the preparation of scaffolds with pores in the nanometer size.^[19, 20]

Another possibility for the introduction of new functionalities into polymers is the generation of hybrid materials, e.g. polymers where inorganic compounds, like transition metal atoms, are either covalently bond or coordinated to the chains. This has been a drastically emerging field within the last decade.^[21] Metal-containing polymers, or metallopolymers, have caused a rapidly expanding interest due to the combination between the processability of polymers and the advanced functionality provided by metal centers. Alongside with that are superior chemical and electronic properties, rendering these materials suitable for applications in the fields of conducting polymers,^[22] colloidal crystals,^[23] thin-films (Figure 1-2),^[24] and displays.^[25]

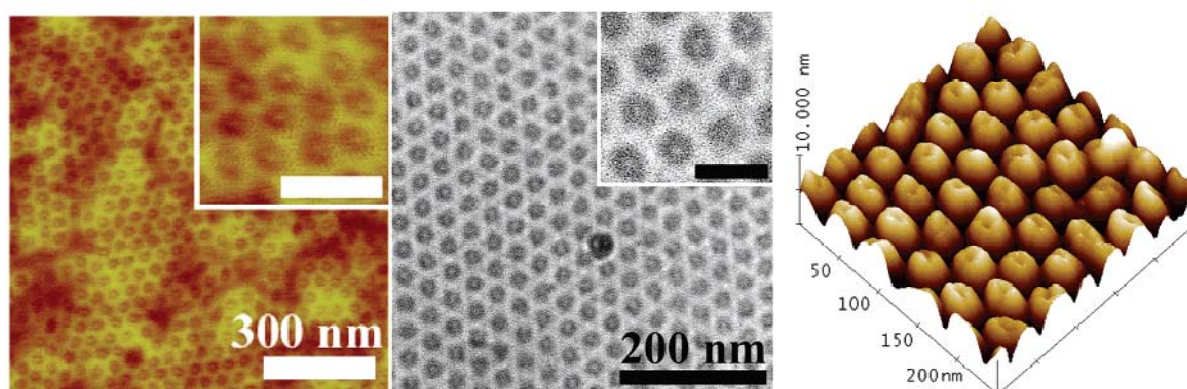


Figure 1-2: SFM height image (left), high-resolution TEM image (middle), and high-resolution SFM image (right) of a polystyrene-*block*-poly(ferrocenylethylmethylsilane) PS-*b*-PFEMS block copolymer thin film annealed via toluene evaporation exhibiting a cylindrical morphology.^[24]

1.2. Anionic Polymerization as a versatile tool for Block Copolymer Synthesis

Living anionic polymerization is a demanding but nevertheless versatile tool for the preparation of well-defined polymers. Since Szwarc's pioneering work in 1956^[26] the number of polymers and block copolymers prepared via this technique is huge. Among recently reported examples are linear block copolymers of the ABC^[27, 28] and the ABCD type,^[29] amphiphilic^[30] and / or double hydrophilic systems,^[31] and gradient block copolymers.^[32] The scope of accessible monomers also broadened, either through the use of additives^[33] or via a previously protected monomer to avoid side reactions during the polymerization step (Figure 1-3).^[34]

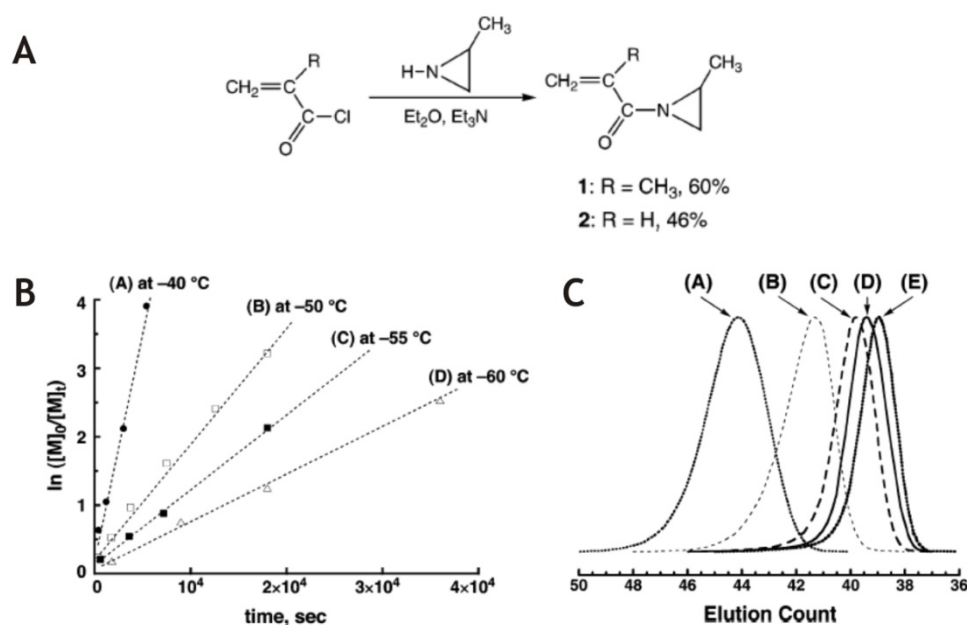


Figure 1-3: Living anionic polymerization of *N*-methacryloyl-2-methylaziridine; (A) monomer synthesis; (B) kinetic plots at different polymerization temperatures; (C) SEC traces of the polymers corresponding to the kinetic plots.^[34]

Increasing attention is drawn nowadays towards the controlled synthesis of block copolymers containing metallopolymer segments. Exemplarily, the synthesis of poly(ferrocenyldimethylsilane)-*block*-poly(2-vinylpyridine) (PFS-*b*-P2VP) via 1,1-dimethylsilacyclobutane (DMSB) mediated sequential anionic polymerization is shown in Figure 1-4.^[35]

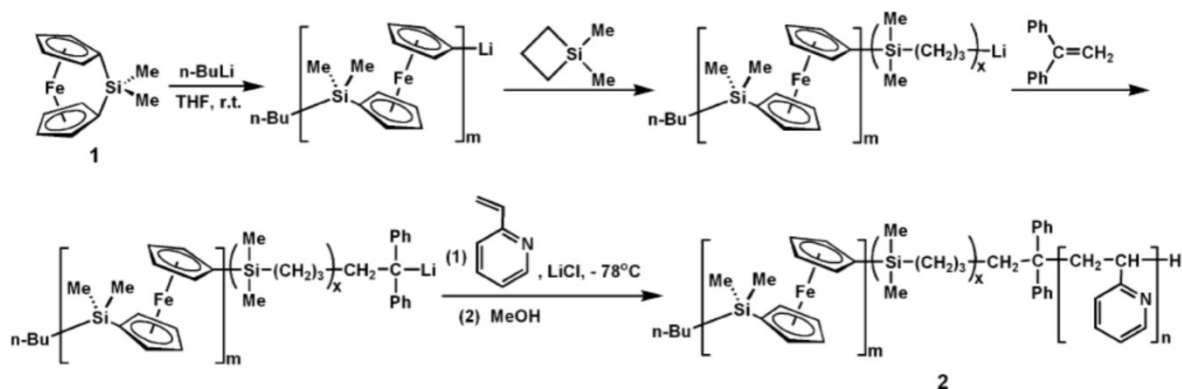


Figure 1-4: Synthesis of PFS-*b*-P2VP block copolymers via anionic polymerization.^[35]

Instead of using sophisticated monomers, changes in the resulting block copolymer architecture can also lead to complicated synthetic procedures and, hence, complex structural patterns in the bulk. This has been demonstrated for polystyrene-*block*-polybutadiene-*block*-poly(2-vinylpyridine)^[36] (SBV, Figure 1-5) and μ -poly(ethylene)-*block*-poly(ethylene oxide)-*block*-poly(perfluoropropylene oxide) [μ -(PEE)(PEO)(PFPO)] miktoarm terpolymers.^[37]

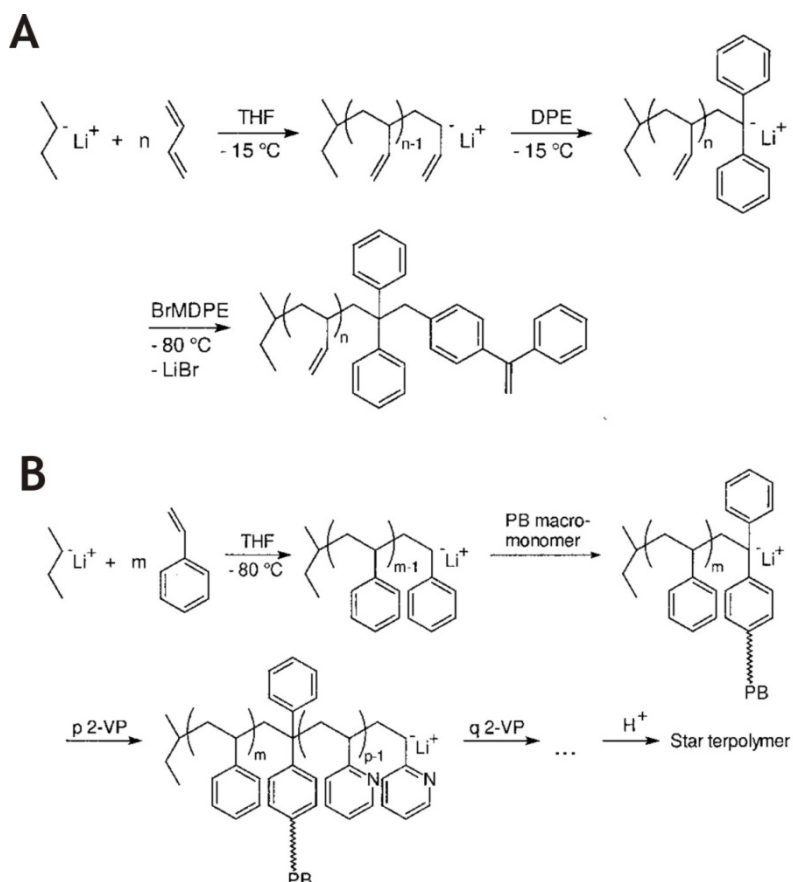


Figure 1-5: Synthesis of the PB macromonomer (A); synthetic procedure for SBV miktoarm terpolymers (B).^[36]

One peculiar advantage of anionic polymerization is that the chain-end functionality can be controlled with appropriate endcapping agents, like in the case of amino-endfunctionalized polybutadienes.^[38]

From the kinetic point of view, the monitoring of such polymerization reactions with in-situ NIR spectroscopy has become an approved and versatile method and has been applied to both known^[39] and novel systems.^[40]

1.3. Block Copolymer Membranes

Increasing complexity in modern separation processes is accompanied by demanding and further specialized requirements for a suitable membrane. Many state-of-the-art membranes are facing their limitations, especially when it comes to new technically challenging or commercially attractive separation problems. Polymers are by far the most important membrane materials, especially because of the relative ease and flexibility to manufacture a large diversity of effective barrier structures for different membrane processes. Possible pathways towards the design of novel membranes are the modification of already established membrane structures, an alteration of the preparation techniques, or the use of new building blocks with improved functionalities.^[41] The concept of block copolymers and, hence, self-assembly provides access to a large variety of functional groups. Moreover, the junction between two segments is covalent and therefore thermodynamically, chemically, and mechanically stable. Recently, well-defined asymmetric membranes from PS-*b*-P4VP diblock copolymers with a hexagonally arranged pattern typical for block copolymer morphologies in the top layer have been reported (Figure 1-6).^[42]

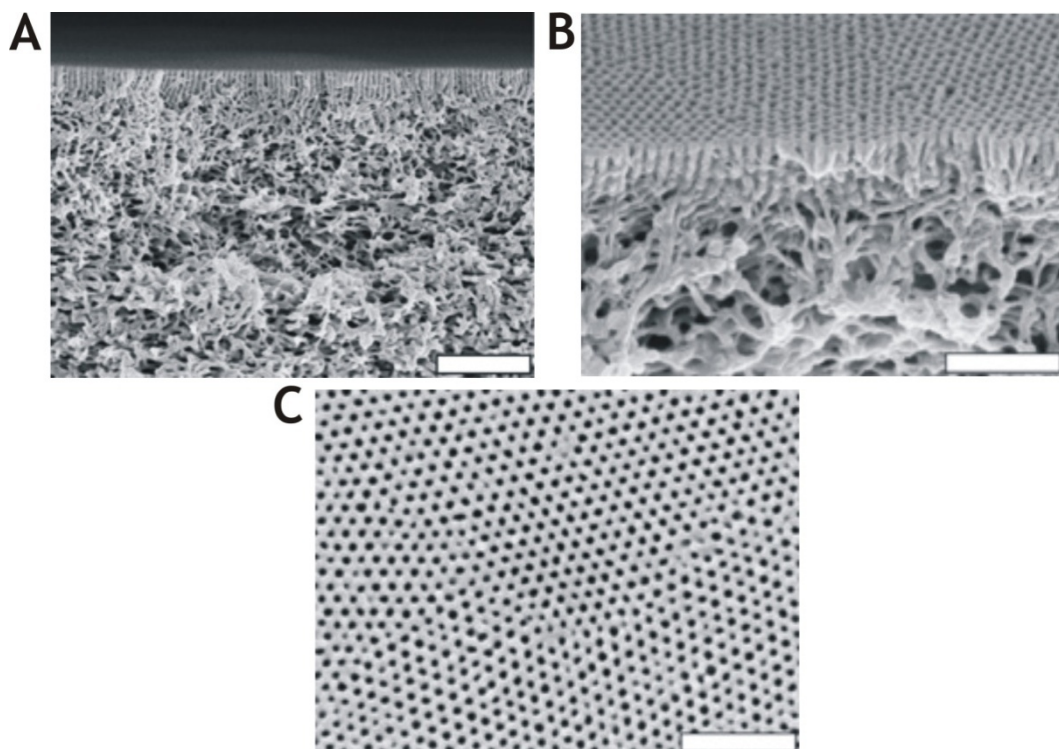


Figure 1-6: SEM micrographs of asymmetric membranes prepared from PS-*b*-P4VP diblock copolymers; cross-section (A), separation layer (B), and an on-top view (C); the scalebar corresponds to 1 μm (A) and 500 nm (B, C).^[42]

1.3.1. Membranes via Phase Inversion Processes

One of the most important industrial processes for the fabrication of integrally anisotropic (“asymmetric”) polymer membranes is non-solvent-induced phase separation (NIPS). Here, a previously casted film of a concentrated polymer solution is immersed in a precipitation bath. This is a straightforward and fast one-step procedure where both membrane morphology and barrier structure can be controlled by a wide range of parameters.^[43, 44] Membranes prepared via this technique usually exhibit an anisotropic cross section with a thin separation layer supported from underneath by a macroporous support. Such asymmetric structures find their applications in pressure-driven processes like ultrafiltration, nanofiltration, or reverse osmosis. To incorporate functional or stimuli-responsive groups into already existing materials often grafting-to processes are used prior to membrane formation via the NIPS technique.^[45, 46] As shown by Neoh and coworkers, poly(vinylidene fluoride)-*graft*-poly(N,N-dimethylaminoethyl methacrylate) (PVDF-*g*-PDMAEMA) membranes prepared via phase inversion were both pH- and temperature-responsive in terms of water flux.^[47] The proposed membrane formation mechanism is displayed in Figure 1-7.

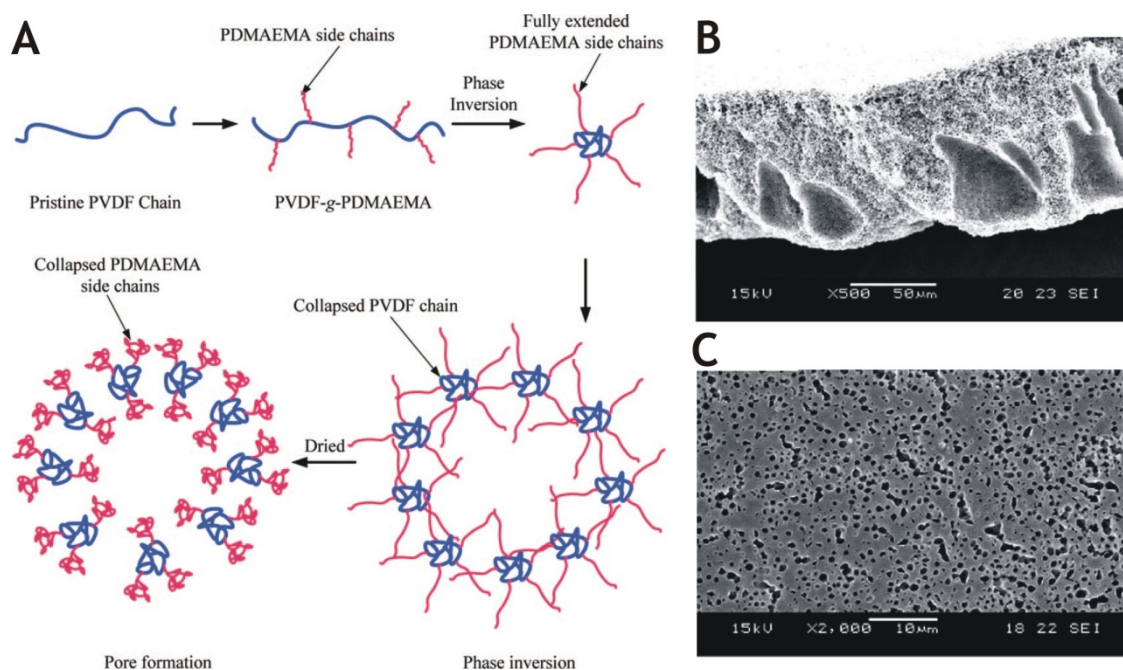


Figure 1-7: Proposed pore formation mechanism during the phase inversion for PVDF-*g*-PDMAEMA membranes (A); SEM cross-sectional view (B) and an on-top view (C).^[47]

If described for a linear block copolymer like PS-*b*-P4VP, the process is slightly more complex.^[42] Directly after the film casting, solvent evaporates and the polymer enriches at the air interface. At a certain concentration, the block copolymer self-assembles and, under the appropriate conditions, porous morphologies with a long range order are formed. This is schematically depicted in Figure 1-8.

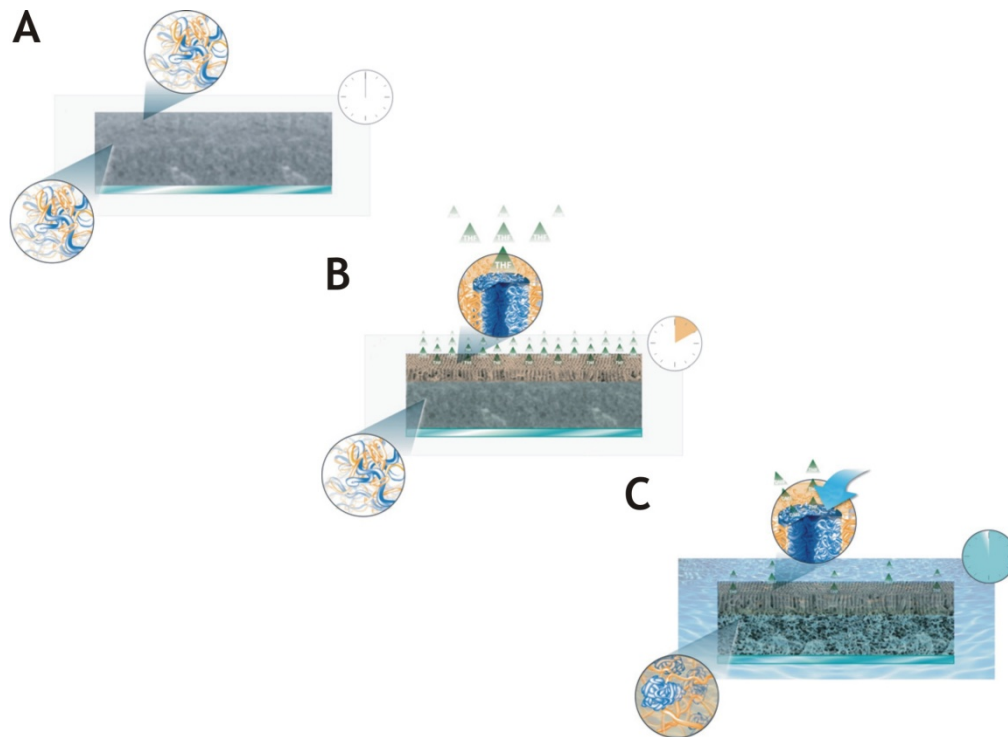


Figure 1-8: Membrane formation process during the phase inversion of PS-*b*-P4VP diblock copolymers; directly casted film (A), after 10 seconds (B), and after immersion into the coagulation bath (C).^[42]

1.3.2. Composite Membranes

Three types of composite membranes are commonly known: thin-film (TFC), pore-filling, and pore-surface-functionalized composite membranes.^[41] From those, thin-film composite structures are the only type related to the content of this thesis. TFC membranes can be further subdivided into porous and non-porous materials. Non-porous examples were often prepared via Langmuir-Blodgett (LB) techniques^[49] or layer-by-layer assemblies.^[50]

Several approaches for the block copolymer based fabrication of porous barriers as components of TFC membranes have been reported so far. Typically, materials containing at least one block which can be removed after final structure formation in thin-films are used. In that way, pores are introduced. Examples are the NaOH-assisted dissolution of the polylactide compartment in thin-films of poly(3-alkylthiophene)-*block*-polylactide,^[51] the UV-etching of PMMA in thin-films of PEO-*b*-PMMA-*b*-PS block terpolymers,^[52] or the ozonolysis of a polydiene block like polyisoprene from thin films of suitable block copolymers.^[53] The resulting porous polymeric thin-films should be transferred onto supporting membrane structures afterwards. First attempts towards nanoporous TFC membranes and their application for the filtration of viruses have been made for thin-films of PS-*b*-PMMA diblock copolymers. Those membranes then exhibited excellent solvent resistance and an improved pressure stability.^[54] The preparation scheme and SEM micrographs are shown in **Figure 1-9**. Another pathway for pore formation is to introduce additional PMMA homopolymer during the spin-casting of PS-*b*-PMMA diblock copolymer thin-films. Subsequent solvent-annealing, film transfer onto a porous substrate, and rinsing with acetic acid generated nanoporous composite membranes (Figure 1-9).^[55]

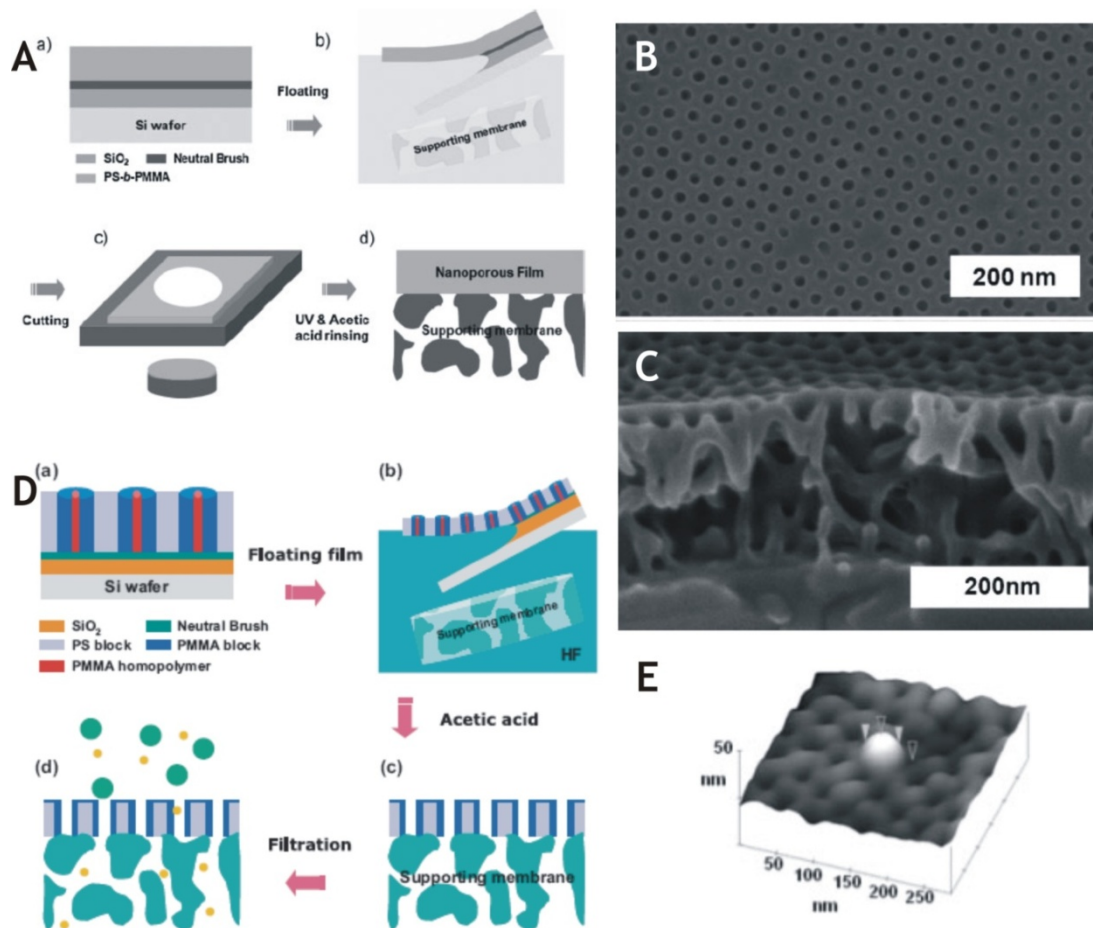


Figure 1-9: Thin-film composite membrane fabrication using PS-*b*-PMMA diblock copolymers transferred onto a porous substrate and UV-etched for pore formation (A); SEM on-top view onto the nanoporous membrane (B); cross-sectional view (C);^[54] TFC membrane preparation using additional PMMA homopolymer mixed with PS-*b*-PMMA diblock copolymer (D); SFM image revealing a blocked virus particle on top of such a TFC membrane structure (E).^[55]

One profound drawback of all mentioned systems is the brittleness of the matrix block, polystyrene. Sperschneider et al. reported on thin-films from polybutadiene-*block*-poly(2-vinylpyridine)-*block*-poly(*tert*-butyl methacrylate) (BVT) block terpolymers. Here, the first block could be crosslinked via an UV-photoinitiator while *Pt*BMA was etched via UV irradiation.^[56] The crosslinked films could be transferred onto commercially available support membranes. Unfortunately, the development of the morphology was strongly determined by the low surface tension of the first block, PB.

1.4. Block Copolymer Self-assembly in Solution

In selective solvents for one of the compartments, the immiscibility of block copolymer segments leads to the formation of micelles. The most typical micellar

structures obtained for linear AB diblock copolymers are star-like,^[57] crew-cut,^[58] cylindrical micelles,^[59] and vesicles.^[60] Aggregate formation strongly depends on the employed solvent, the solubility parameters according to the Flory-Huggins theory, the block sequence, the volume fractions, and the block lengths. If ABC block terpolymers are used, the micellar assemblies become more complex, in most cases core-shell-corona micelles are formed.^[61] For the analysis of such self-assembled structures, cryogenic transmission electron microscopy often is the method of choice. It allows high-resolution insight into complex fluids in a near *in-situ* state.^[62]

Besides their preparation and characterization, the crosslinking of block copolymer micelles is an interesting area of research. After fixation, the structures can be transferred into different, non-selective solvents, broadening the scope of possible applications for these systems. Amongst the reported methods were cold-vulcanization of polydiene systems,^[63] the use of multifunctional quaternization agents,^[64] and UV-irradiation.^[65] Another possibility for the modification of pre-formed micellar aggregates are sonication methods. Here, the size of, e.g., cylindrical micelles can be tuned in a precise and elegant way (Figure 1-10).^[63, 66]

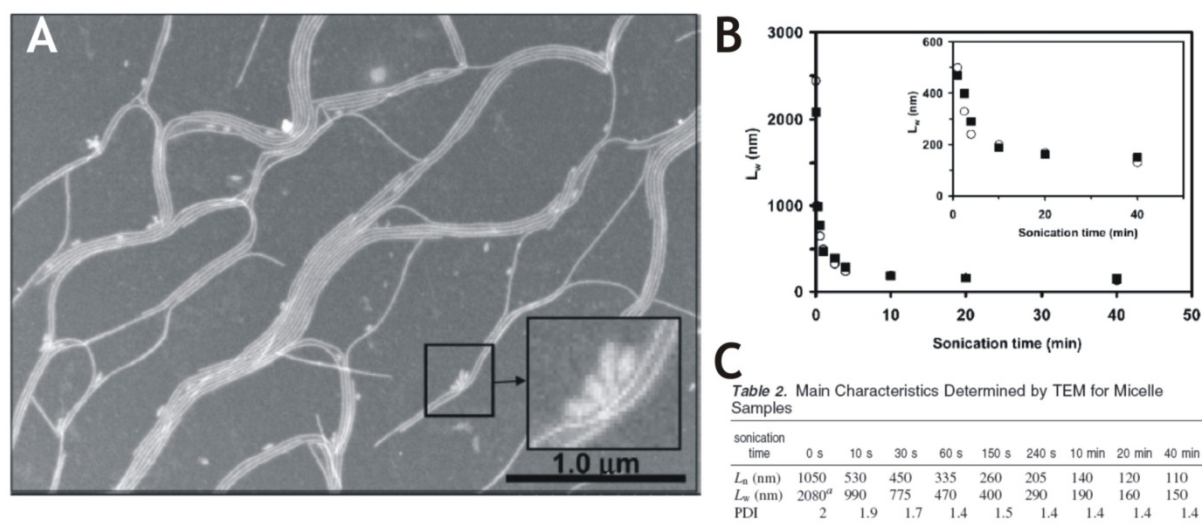


Figure 1-10: Dark-field TEM image showing fiber-like micelles of polyisoprene-*block*-poly(ferrocenyldimethylsilane) (PI-*b*-PFS) diblock copolymers (A); plot of the micelle weight-average length vs. sonication time (B); table summarizing the solution characteristics of the micelles obtained via TEM analysis (C).

1.4.1. Compartmentalized Polymeric Micelles

Multicompartiment systems are very promising candidates for future delivery applications. The storage of two different dyes in separate domains of micelles from μ -poly(ethylethylene)-*block*-poly(ethylene oxide)-*block*-poly(perfluoropropylene oxide) [μ -(PEE)(PEO)(PFPO)] miktoarm terpolymers has already been described by Hillmyer et al.^[67] Compartmentalized micelles are formed if one part of a micellar structure is further subdivided. In general, three different types of such multicompartiment systems have been reported so far: multicompartiment core,^[68] multicompartiment or patchy corona,^[69] and Janus-type systems.^[70]

There are different strategies for the formation of multicompartiment core micelles. One possibility is the use of two solvophobic blocks which exhibit a very high incompatibility among each other, e.g. the combination of hydrocarbon and fluorocarbon segments in aqueous media.^[68, 71] Other approaches are based on the kinetically induced rearrangement of polymeric micelles in response to changes in solvent quality or charge neutrality.^[72] The blending of different block copolymers and the subsequent fixation of the formed assemblies via crosslinking also lead to compartmentalized micellar systems.^[73] A short compendium of the mentioned pathways and the resulting structural motifs is shown in Figure 1-11 and 1-12.

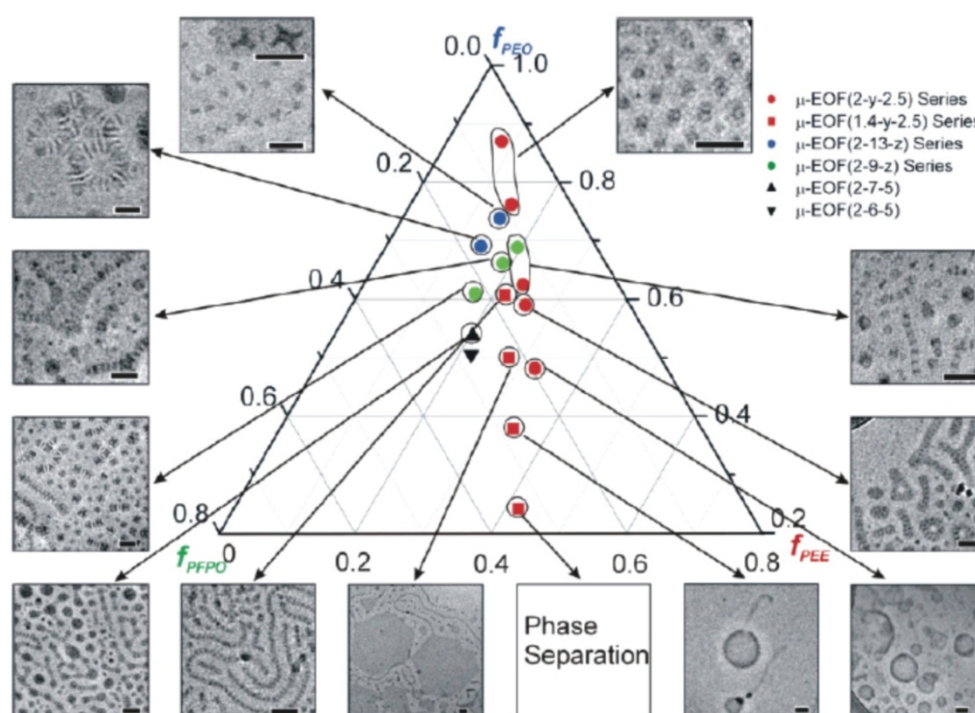


Figure 1-11: Phase diagram for the morphology of multicompartiment micelles formed by μ -EOF miktoarm terpolymers in dilute aqueous solution.^[68]

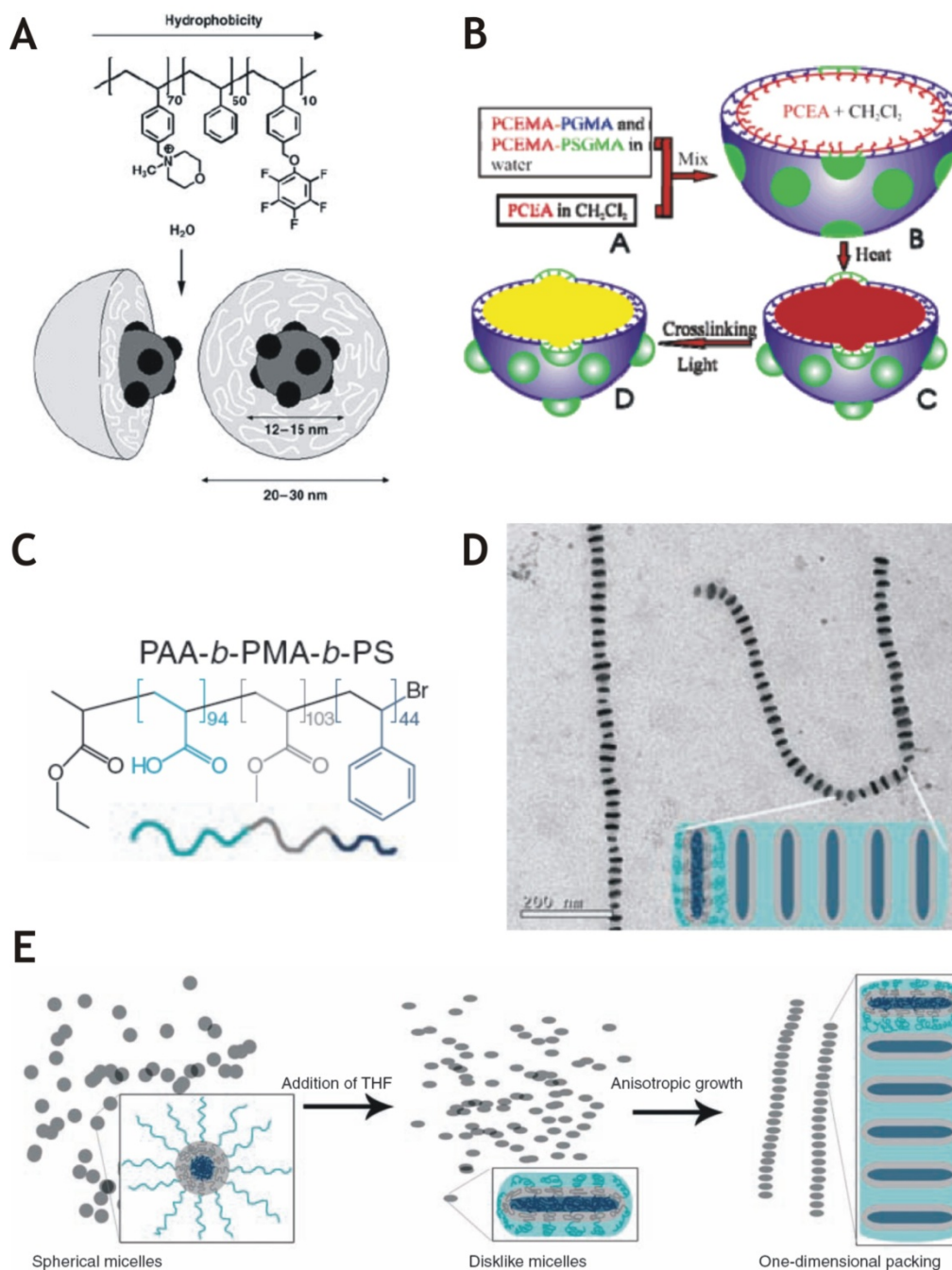


Figure 1-12: Self-assembly of a poly(4-methyl-4-(4-vinylbenzyl)morpholin-4-ium chloride)-*block*-polystyrene-*block*-poly(pentylfluorophenyl 4-vinylbenzyl ether) (PVBM-*b*-PS-*b*-PVBFP) block terpolymer (A);^[71] mixing of poly(2-cinnamoyloxyethyl methacrylate)-*block*-poly(glyceryl methacrylate) (PCEMA-*b*-PGMA) and the corresponding succinated diblock copolymer PCEMA-*b*-PSGMA in dichloromethane with subsequent crosslinking via UV irradiation (B);^[73] molecular structure of a poly(acrylic acid)-*block*-poly(methyl acrylate)-*block*-polystyrene (PAA-*b*-PMA-*b*-PS) block terpolymer (C); one-dimensional assembled structures of PAA-*b*-PMA-*b*-PS in mixtures of THF (67%) and water (33%) (D); formation mechanism proposed for the elongated multicompartiment cylinders (E).^[72]

Considerably fewer examples for a patchy or compartmentalized micellar corona are found in the literature. Recently, the thermo-reversible formation of

cylindrical micelles with a phase separated corona from polystyrene-*block*-polyethylene-*block*-poly(methyl methacrylate) (PS-*b*-PE-*b*-PMMA) block terpolymers has been reported.^[74] Here, the crystallization of the PE middle block was supposed to be the driving force for the formation of wormlike micelles. The micelles with a PE core and segregated PS and PMMA coronal chains are shown in Figure 1-13.

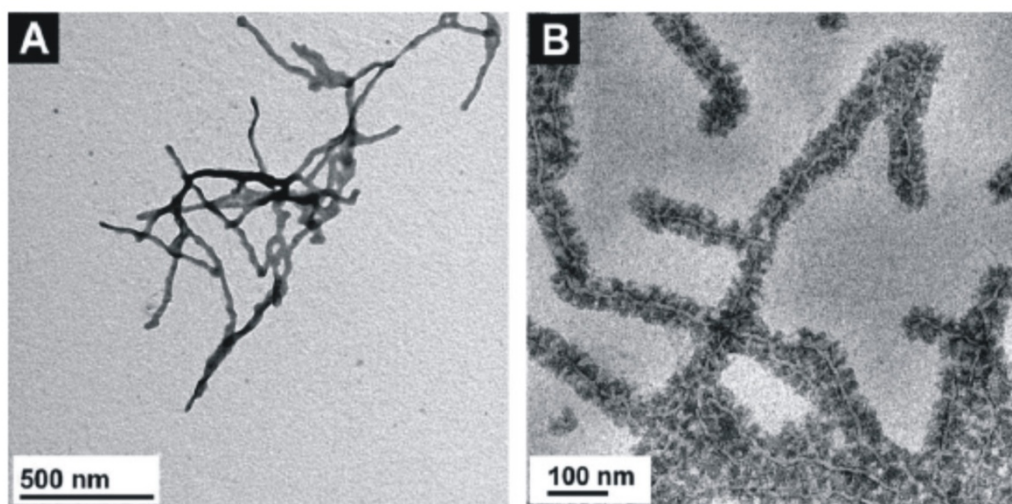


Figure 1-13: TEM micrographs of PS-*b*-PE-*b*-PMMA wormlike micelles drop-coated from acetone, a selective solvent for PMMA (A); drop-coated from toluene followed by selective staining of the PS domains with RuO₄ (B).^[74]

Janus systems are non-centrosymmetric, compartmentalized colloids exhibiting two sides of different chemistry or polarity. During the last decade, different synthetic pathways for the preparation of such structures evolved.^[70] Concerning block copolymers, Janus particles can be synthesized via the template-assisted pathway in a convenient manner and on the gram scale. Self-assembled suitable bulk morphologies of polystyrene-*block*-polybutadiene-*block*-poly(methyl methacrylate) (SBM) or polystyrene-*block*-polybutadiene-*block*-poly(*tert*-butyl methacrylate) (SBT) were crosslinked in the bulk and after re-dissolving and, eventually, sonication nicely dispersed Janus colloids were obtained. In that way, Janus micelles,^[75] cylinders,^[76] and discs^[63] could be prepared. The synthetic procedure is shown in Figure 1-14.

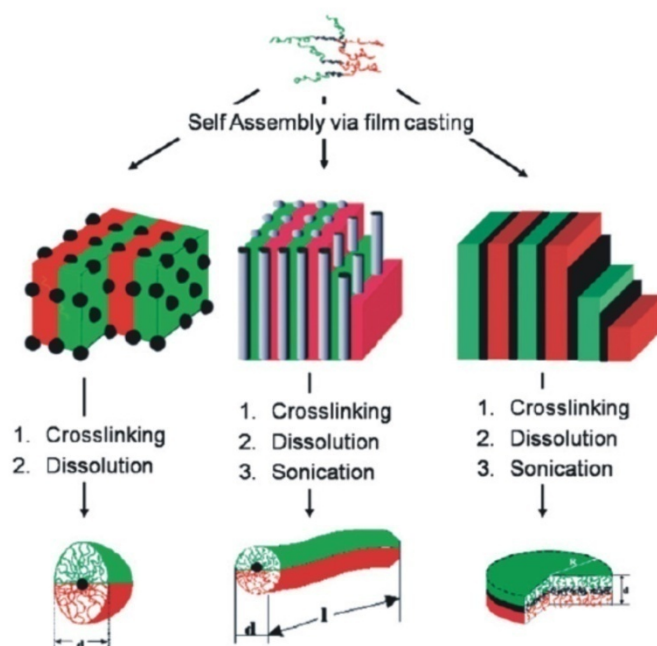


Figure 1-14: Template-assisted pathway for the fabrication of Janus micelles, cylinders, and discs.^[70]

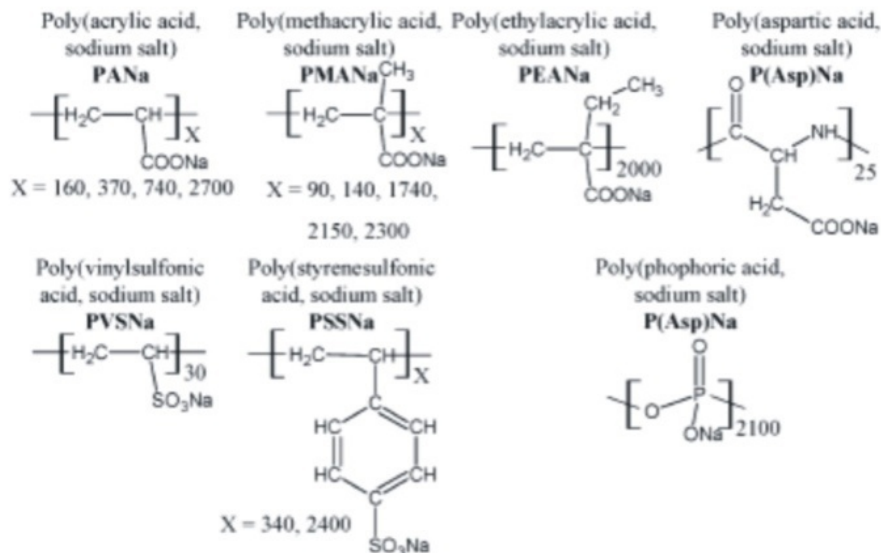
1.4.2. Interpolyelectrolyte Complexes

Interpolyelectrolyte complexes (IPECs) are formed if two oppositely charged polyelectrolytes, polymer chains bearing several charges, are mixed. Often, the charge ratio $Z (+/-)$ is used as a measure of the charge balance. For $Z (+/-) = 1$, the resulting material is uncharged and hydrophobic.^[77-79] There is a growing research interest in such complexes due to their dynamic and stimuli-responsive character. Such IPECs are capable of undergoing interpolyelectrolyte exchange reactions in aqueous media.^[80, 81] It could be shown by Kataoka et al. that even chain length recognition is possible. They investigated the core-shell supramolecular assembly of oppositely charged block copolymers and reported on extremely narrow micellar size distributions for systems where the polyelectrolyte chains matched exactly in length.^[82]

Polyelectrolytes are classified as either weak or strong cationic and anionic examples. The dissociation of weak polyelectrolytes typically depends on the surrounding conditions, like in the case of poly(methacrylic acid) (PMAA).^[79] Strong polyelectrolytes are permanently charged, a typical example is quaternized poly(1-

methyl-4-vinylpyridinium) bromide (PM4VP).^[79] An excerpt of commonly used linear polyelectrolytes is displayed in Figure 1-15.

Linear polyanions:



Linear polycations:

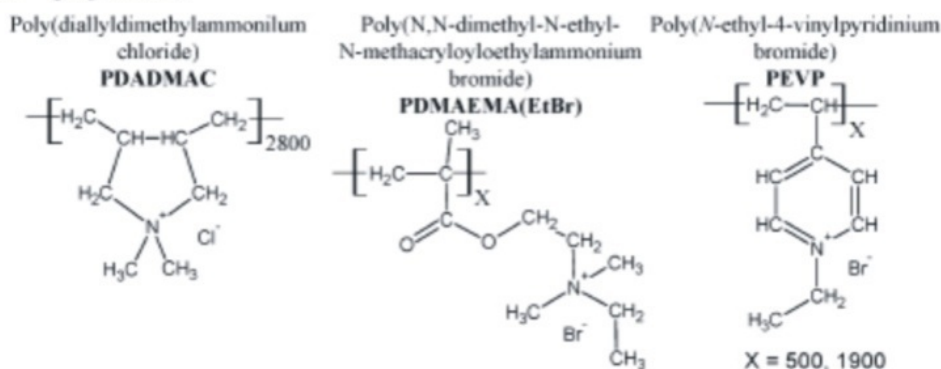


Figure 1-15: Commonly used weak and strong cationic and anionic linear polyelectrolytes.^[83]

The controlled formation of IPECs in solution provides a facile method for the stepwise building up of layered assemblies. Pergushov et al. successfully prepared core-shell-corona micelles through the complexation between negatively charged polyisobutylene-*block*-poly(methacrylic acid) (PIB-*b*-PMAA) micelles and positively charged PM4VP.^[77, 79] They also investigated the stability of these IPECs, depending on the charge ratio Z (+/-) (Figure 1-16).

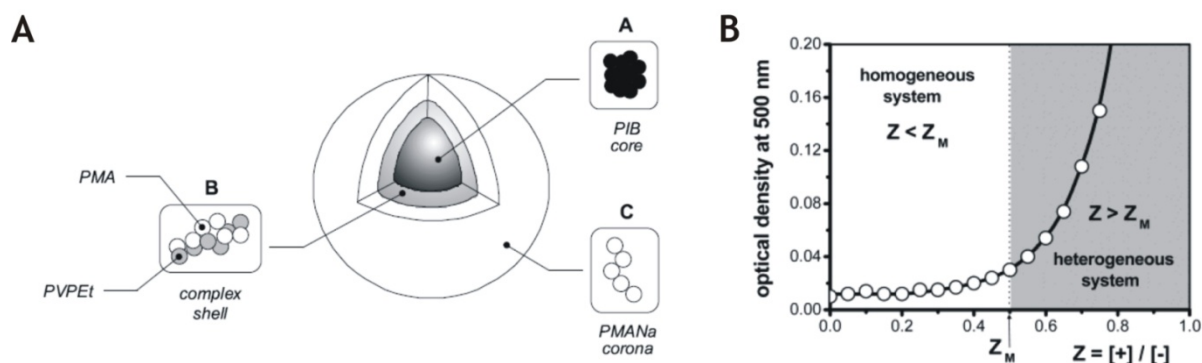


Figure 1-16: IPECs formed between PIB-*b*-PMAA micelles and PM4VP polyelectrolyte chains (A);^[79] IPEC stability depending on the Z (+/-) ratio (B).^[77]

Employing the same method, core-shell-corona IPECs were created via the electrostatically driven co-assembly of poly(ethylene oxide)-*block*-poly(4-vinylpyridine) (PEO-*b*-P4VP) and polystyrene-*block*-poly(acrylic acid) (PS-*b*-PAA).^[84]

Another remarkable feature of IPECs is that their formation is reversible. High salt concentrations are able to break up the complexes, resulting again in free polymer chains.^[85]

1.4.3. Hybrid Materials

Hybrid materials of polymers and inorganic nanoparticles (NPs) are supposed to combine the advantages of both components: superior mechanical properties and the processability of polymers and the advanced magnetic, optical, or catalytical characteristics of metals.^[86] Regarding the controlled preparation of such organic-inorganic hybrids, several methods have been described so far: the direct mixing of pre-synthesized metal nanoparticles and block copolymers,^[87] the in-situ generation of metal NPs in solution containing block copolymers, polymer brushes, or micellar aggregates,^[88-90] the covalent incorporation of metal atoms into polymer segments,^[91] or the selective deposition of metals onto pre-aligned polymeric substrates.^[92]

One attempt for the direct mixing of NPs and block copolymers has recently been described by Maria et al.^[93] Here, CdSe NPs were incorporated into semiconductor

polymers, containing a hole-conductor compartment carrying tetraphenylbenzidine units and P4VP as the second block. The resulting hybrid materials are promising candidates for the fabrication of novel polymer-based solar cells.

Schrinner et al. reported on a solution-based approach for the formation of noble metal nanoparticles stabilized by spherical polyelectrolyte brushes (SPBs).^[94, 95] Cationically charged SPBs with a PS core and grafted poly(2-aminoethyl methacrylate) chains were loaded with HAuCl_4 and subsequently reduced with NaBH_4 leading to stable, narrowly dispersed gold NPs located within the corona of the SPBs. Moreover, a double loading process with first Au and, afterwards, Pt yielded bimetallic nanoparticles (Figure 1-17).

If cylindrical polymer brushes (CPBs) are used as templates in a comparable manner, metal or semiconductor nanowires become feasible. Yuan et al. showed that CdSe,^[90] Tellurium,^[89] and Fe_3O_4 nanorods can be produced in this way (Figure 1-17).^[89]

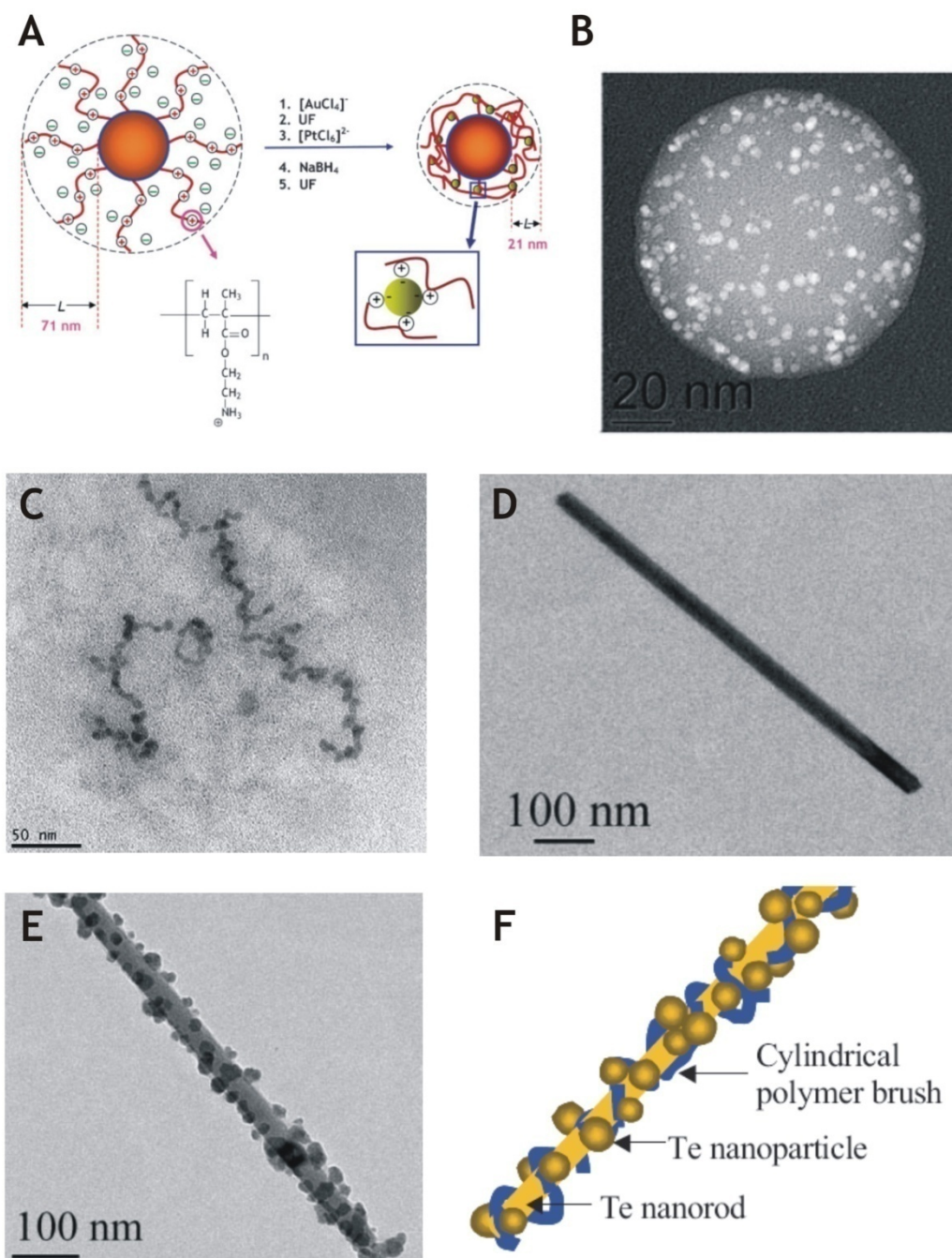


Figure 1-17: Two-step loading process for the formation of Au-Pt alloy NPs in the corona of cationic SPBs (A); HR-TEM micrograph of SPBs carrying bimetallic Au₅₅Pt₄₅ NPs (B);^[95] double loaded CdSe nanowires templated by core-shell CPBs (PAA-*b*-PnBA) (C);^[90] TEM micrograph of a single Tellurium nanorod (D); Tellurium nanowire with additionally attached Tellurium NPs (E); proposed structure of the CPB-Te hybrid particle (F).^[89]

The covalent incorporation of metal atoms into polymer chains basically is a synthetic approach involving both the synthesis of novel monomers and the exploitation of new or the modification of approved polymerization techniques.

This has already been partially described in a previous section of this introduction for anionic polymerization.

Atomic layer deposition (ALD) can be used to selectively deposit metal atoms in or onto specific compartments of self-assembled polymer microstructures. This has been demonstrated in the group of Oli Ikkala for PS-*b*-P4VP diblock copolymers.^[92] Here, continuous layers of Al₂O₃ were created on top of the P4VP shell of different block copolymer aggregates, being spherical or cylindrical in shape. Afterwards the polymer has been thermally decomposed, rendering hollow inorganic nanospheres and nanotubes (Figure 1-18).

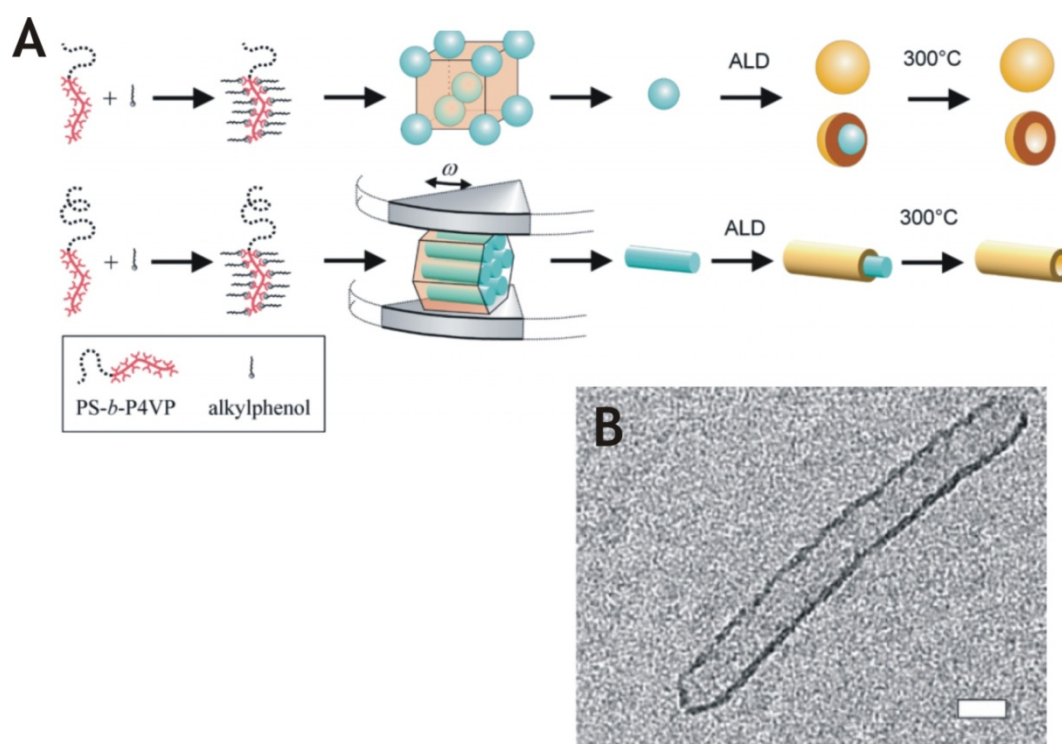


Figure 1-18: Preparation pathway for the fabrication of hollow inorganic nanospheres and nanotubes via first polymer self-assembly and subsequent ALD techniques (A); HR-TEM micrograph of a hollow Al₂O₃ nanotube (B).^[92]

In a different approach, Crossland et al. used double gyroidal structures formed by poly(4-fluorostyrene)-*block*-poly(D,L-lactide) (PFS-*b*-PLA) diblock copolymers for the preparation of hybrid solar cells.^[96] After film formation on pre-treated glass substrates, the PLA compartment was removed under basic conditions, yielding a porous gyroidal network. Afterwards, the structure was replicated electrochemically, generating an interpenetrating network of PFS and TiO₂. The polymer part has been removed and the resulting gyroidal TiO₂ network backfilled with a solid state hole transporting material. These bicontinuous bulk heterojunction solar cells exhibited promising characteristics and could serve as prototypes for novel polymer-based hybrid materials (Figure 1-19).

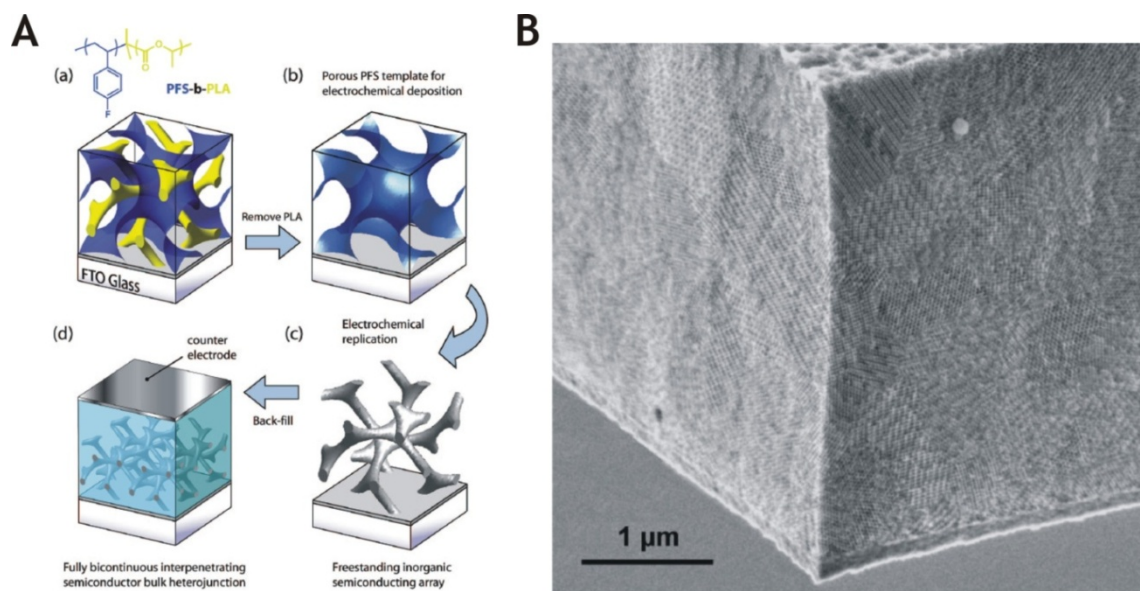


Figure 1-19: Fabrication of bicontinuous hybrid solar cells via the electrochemical replication of a gyroidal polymer microstructure (A); SEM fracture cross section image of a replicated TiO₂ porous array (B).^[96]

1.5. Objective of this Thesis

One focus of this thesis is the synthesis and the characterization of novel block co- and terpolymers via anionic polymerization techniques and their application to the preparation of stimuli-responsive membranes. Two pathways are to be explored: the polymeric thin-film based formation of composite membranes in close collaboration with the department of physical chemistry (A. Sperschneider) and the solution-assisted non-solvent induced phase separation (NIPS) route together with the department of technical chemistry at the University Duisburg-Essen. We aim at the successful fabrication of model systems for first investigations on membrane switchabilities in terms of pore size, separation quality, wettability, and overall water flux.

In addition to that, more general interest is devoted to the self-assembly of BVT block terpolymers in selective solvents for the first block, polybutadiene. Starting in organic solvents like acetone, the structure of the aggregates is to be determined and after crosslinking of the PB compartment the feasibility of the transfer of these aggregates into non-selective solvents like dioxane can be elucidated. Further modifications like the quaternization of the P2VP block or the hydrolysis of the P β BMA to PMAA then lead to water-soluble systems with one or two environmentally sensitive compartments. The aggregation behavior of those amphiphilic polymers will also be studied. Finally, first investigations concerning the formation of interpolyelectrolyte complexes of such PB-P2VP q -PMAA block terpolymer micelles with oppositely charged diblock copolymers will be carried out.

References

- [1] L. Leibler, *Macromolecules* **1980**, *13*, 1602.
- [2] T. Smart, H. Lomas, M. Massignani, M. V. Flores-Merino, L. Riuz Perez, G. Battaglia, *nanotoday* **2008**, *3*, 38.
- [3] A.-V. Ruzette, L. Leibler, *Nat Mater* **2005**, *4*, 19.
- [4] M. Lazzari, M. A. Lopez-Quintela, *Adv. Mater.* **2003**, *15*, 1583.
- [5] S. B. Darling, *Prog. Polym. Sci.* **2007**, *32*, 1152.
- [6] H.-A. Klok, S. Lecommandoux, *Adv. Mater.* **2001**, *13*, 1217.
- [7] T. Goldacker, V. Abetz, R. Stadler, I. Erukhimovich, L. Leibler, *Nature* **1999**, *398*, 137.
- [8] V. Abetz, T. Goldacker, *Macromol. Rapid. Commun.* **2000**, *21*, 16.
- [9] N. Nath, A. Chilkoti, *Adv. Mater.* **2002**, *14*, 1243.
- [10] Z. Nie, E. Kumacheva, *Nat Mater* **2008**, *7*, 277.
- [11] M. Yoshida, J. Lahann, *ACS Nano* **2008**, *2*, 1101.
- [12] S. Dai, P. Ravi, K.-C. Tam, *Soft Matter* **2008**, *4*, 435.
- [13] F. A. Plamper, A. Schmalz, M. Ballauf, A. H. E. Müller, *J. Am. Chem. Soc.* **2007**, *129*, 14538.
- [14] F. Plamper, A. Walther, A. H. E. Müller, M. Ballauff, *Nano Lett.* **2007**, *7*, 167.
- [15] H. Csetneki, G. Filipesei, M. Zrinyi, *J. Am Chem Soc.* **2006**.
- [16] P. Broz, S. Driamov, J. Ziegler, N. Ben-Haim, S. Marsch, W. Meier, P. Hunziker, *Nano Lett.* **2006**, *6*, 2349.
- [17] T. Breiner, K. Kreger, R. Hagen, M. Hackel, L. Kador, A. H. E. Müller, E. J. Kramer, H.-W. Schmidt, *Macromolecules* **2007**, *40*, 2100.
- [18] J. K. Bosworth, M. Y. Paik, R. Ruiz, E. L. Schwartz, J. Q. Huang, A. W. Ko, D.-M. Smilgies, C. T. Black, C. K. Ober, *ACS Nano* **2008**, *2*, 1396.
- [19] S. B. A. Ludwigs, A. Voronov, N. Rehse, R. Magerle, G. Krausch, *Nature materials* **2003**, *2*, 744.
- [20] M. Li, K. Douki, K. Goto, X. Li, C. Coenjarts, D. M. Smilgies, C. K. Ober, *Chem. Mater.* **2004**, *16*, 3800.
- [21] G. R. Whittell, I. Manners, *Advanced Materials* **2007**, *19*, 3439.
- [22] S. Z. D. A. R. I. M. G. C. W. James K. Li, *Advanced Materials* **2008**, *20*, 1989.
- [23] D. A. Rider, J. I. L. Chen, J.-C. Eloi, A. C. Arsenault, T. P. Russell, G. A. Ozin, I. Manners, *Macromolecules* **2008**, *41*, 2250.
- [24] D. A. Rider, K. A. Cavicchi, L. Vanderark, T. P. Russell, I. Manners, *Macromolecules* **2007**, *40*, 3790.
- [25] J.-C. Eloi, L. Chabanne, G. R. Whittell, I. Manners, *materialstoday* **2008**, *11*, 28.

- [26] M. Szwarc, *Nature* **1956**, *178*, 1168.
- [27] S. Ludwigs, A. Böker, V. Abetz, A. H. E. Müller, G. Krausch, *Polymer* **2003**, *44*, 6815.
- [28] A. Walther, A. Gödel, A. H. E. Müller, *Polymer* **2008**, *49*, 3217.
- [29] Z. Li, G. Liu, *Langmuir* **2003**, *19*, 10480.
- [30] J.-F. Gohy, S. Antoun, R. Jerome, *Macromolecules* **2001**, *34*, 7435.
- [31] S.-C. Chen, S.-W. Kuo, C.-S. Liao, F.-C. Chang, *Macromolecules* **2008**, *41*, 8865.
- [32] S. Jouenne, J. A. Gonzalez-Leon, A. V. Ruzette, P. Lodefier, S. Tence-Girault, L. Leibler, *Macromolecules* **2007**.
- [33] B. Schmitt, W. Stauf, A. H. E. Müller, *Macromolecules* **2001**, *34*, 1551.
- [34] T. Suzuki, J.-i. Kusakabe, T. Ishizone, *Macromolecules* **2008**, *41*, 1929.
- [35] H. Wang, M. A. Winnik, I. Manners, *Macromolecules* **2007**, *40*, 3784.
- [36] H. Hückstädt, A. Göpfert, V. Abetz, *Macromol. Chem. Phys.* **2000**, *201*, 296.
- [37] Z. Li, M. A. Hillmyer, T. Lodge, *Macromolecules* **2004**, *37*, 8933.
- [38] S. Nosov, H. Schmalz, A. H. E. Müller, *Polymer* **2006**, *47*, 4245.
- [39] Holger Schmalz, M. G. Lanzendörfer, V. Abetz, A. H. E. Müller, *Macromol. Chem. Phys.* **2003**, *204*, 1056.
- [40] A. A. Toy, S. Reinicke, A. H. E. Müller, H. Schmalz, *Macromolecules* **2007**, *40*, 5241.
- [41] M. Ulbricht, *Polymer* **2006**, *47*, 2217.
- [42] K. V. Peinemann, V. Abetz, P. F. W. Simon, *Nature mat.* **2007**, *6*, 992.
- [43] S. P. Nunes, K. V. Peinemann, *Membrane Technology*, 2nd ed., Wiley-VCH, Weinheim, **2006**.
- [44] P. van de Witte, P. J. Dijkstra, J. W. A. van den Berg, J. Feijen, *J. Membr. Sci.* **1996**, *117*, 1.
- [45] K. G. Neoh, L. Ying, G. Zhai, A. Y. Winata, E. T. Kang, *Journal of Colloid and Interface Science* **2003**, *265*, 396.
- [46] L. Ying, E. T. Kang, K. G. Neoh, *J. Membr. Sci.* **2003**, *224*, 93.
- [47] J. Xue, L. Chen, H. L. Wang, Z. B. Zhang, X. L. Zhu, E. T. Kang, K. G. Neoh, *Langmuir* **2008**, *24*, 14151.
- [48] F. Schacher, M. Ulbricht, A. H. E. Müller, *Adv. Funct. Mater.* **2008**, *accepted*.
- [49] F. Penacorada, A. Angelova, H. Kamusewitz, J. Reiche, L. Brehmer, *Langmuir* **1995**, *11*, 612.
- [50] H. H. Schwarz, K. Richau, D. R. Paul, *Polym. Bull.* **1991**, *25*, 95.
- [51] B. W. Boudouris, C. D. Frisbie, M. A. Hillmyer, *Macromolecules* **2008**, *41*, 67.
- [52] J. Bang, S. H. Kim, E. Drockenmuller, M. J. Misner, T. P. Russell, C. J. Hawker, *Journal of the American Chemical Society* **2006**, *128*, 7622.

- [53] S. Guo, J. Rzyayev, T. S. Bailey, A. S. Zalusky, R. Olayo-Valles, M. A. Hillmyer, *Chemistry of Materials* **2006**, *18*, 1719.
- [54] S. Y. Yang, J. Park, J. Yoon, M. Ree, S. K. Jang, J. K. Kim, *Advanced Functional Materials* **2008**, *18*, 1371.
- [55] S. Y. Yang, I. Ryu, H. Y. Kim, S. K. Jang, T. P. Russell, *Adv. Mater.* **2006**, *18*, 709.
- [56] A. Sperschneider, F. Schacher, M. Gawenda, L. Tsarkova, A. H. E. Müller, M. Ulbricht, G. Krausch, J. Köhler, *Small* **2007**, *3*, 1056.
- [57] M. Burkhardt, N. Martinez-Castro, S. Tea, M. Drechsler, I. Babin, I. Grishagin, R. Schweins, D. V. Pergushov, M. Gradzielski, A. B. Zezin, A. H. E. Müller, *Langmuir* **2007**, *23*, 12864.
- [58] X. André, M. Zhang, A. H. E. Müller, *Macromolecular Rapid Communications* **2005**, *26*, 558.
- [59] R. S. Yelamanchili, A. Walther, A. H. E. Müller, J. Brey, *Chem. Commun.* **2008**, 489.
- [60] P. Lim Soo, A. Eisenberg, *Journal of Polymer Science Part B: Polymer Physics* **2004**, *42*, 923.
- [61] C. A. Fustin, V. Abetz, J. F. Gohy, *Eur. Phys. J. E* **2005**.
- [62] H. Cui, T. K. Hodgdon, E. W. Kaler, L. Abezgauz, D. Danino, M. Lubovsky, Y. Talmon, D. J. Pochan, *Soft Matter* **2007**, *3*, 945.
- [63] A. Walther, X. Andre, M. Drechsler, V. Abetz, A. H. E. Müller, *Journal of the American Chemical Society* **2007**, *129*, 6187.
- [64] R. K. O'Reilly, C. Hawker, K. L. Wooley, *Chem. Soc. Rev.* **2006**, *35*, 1068.
- [65] X. Jiang, S. Luo, S. P. Armes, W. Shi, S. Liu, *Macromolecules* **2006**, *39*, 5987.
- [66] G. R. Guelrin, H. Wang, I. Manners, M. A. Winnik, *Journal of the American Chemical Society* **2008**, *130*, 14763.
- [67] T. Lodge, A. Rasdal, Z. Li, M. A. Hillmyer, *J. Am Chem Soc.* **2005**, *127*, 17608.
- [68] Z. Li, M. A. Hillmyer, T. Lodge, *Langmuir* **2006**, *22*, 9409.
- [69] J. Hu, G. Njikang, G. Liu, *Macromolecules* **2008**, *41*, 7993.
- [70] A. Walther, A. H. E. Müller, *Soft Matter* **2008**, *4*, 663.
- [71] S. Kubowicz, J.-F. Baussard, J.-F. Lutz, A. Thünemann, H. v. Berlepsch, A. Laschewsky, *Angew. Chem. int. Ed.* **2005**, *44*, 5262.
- [72] H. Cui, Z. Chen, S. Zhong, K. L. Wooley, D. J. Pochan, *Science* **2007**, *317*, 647.
- [73] R. Zheng, G. Liu, X. Yan, *J. Am Chem Soc.* **2005**, *127*, 15358.
- [74] H. Schmalz, J. Schmelz, M. Drechsler, J. Yuan, A. Walther, K. Schweimer, A. M. Mihut, *Macromolecules* **2008**, *41*, 3235.
- [75] R. Erhardt, A. Boker, H. Zettl, H. Kaya, W. Pyckhout-Hintzen, G. Krausch, V. Abetz, A. H. E. Müller, *Macromolecules* **2001**, *34*, 1069.

- [76] Y. Liu, V. Abetz, A. H. E. Müller, *Macromolecules* **2003**, *36*, 7894.
- [77] D. V. Pergushov, E. V. Remizova, J. Feldthusen, A. B. Zezin, A. H. E. Mueller, V. A. Kabanov, *J. Phys. Chem.* **2003**, *107*, 8093.
- [78] M. Burkhardt, M. Ruppel, S. Tea, M. Drechsler, R. Schweins, D. V. Pergushov, M. Gradzielski, A. B. Zezin, A. H. E. Müller, *Langmuir* **2008**, *24*, 1769.
- [79] D. V. Pergushov, E. V. Remizova, M. Gradzielski, P. Lindner, J. Feldthusen, A. B. Zezin, A. H. E. Müller, V. A. Kabanov, *Polymer* **2004**, *45*, 367.
- [80] K. N. Bakeev, V. A. Izumrudov, S. I. Kuchanov, A. B. Zezin, V. A. Kabanov, *Macromolecules* **1992**, *25*, 4249.
- [81] P. S. Chelushkin, E. A. Lysenko, T. K. Bronich, A. Eisenberg, V. A. Kabanov, A. V. Kabanov, *The Journal of Physical Chemistry B* **2008**, *112*, 7732.
- [82] A. Harada, K. Kataoka, *Science* **1999**, *283*, 65.
- [83] P. S. Chelushkin, E. A. Lysenko, T. K. Bronich, A. Eisenberg, V. A. Kabanov, A. V. Kabanov, *J. Phys. Chem. B* **2007**, *111*, 8419.
- [84] L. S. Z. J. M. K. W. Y. A. Wangqing Zhang, *Macromolecular Chemistry and Physics* **2005**, *206*, 2354.
- [85] H.-M. Buchhammer, G. Petzold, K. Lunkwitz, *Langmuir* **1999**, *15*, 4306.
- [86] S. Förster, M. Antonietti, *Adv. Mater.* **1998**, *10*, 195.
- [87] A. Haryono, W. H. Binder, *Small* **2006**, *2*, 600.
- [88] J. Shan, H. Tenhu, *Chem. Commun.* **2007**, 4580.
- [89] J. Yuan, H. Schmalz, Y. Xu, N. Miyajima, M. Drechsler, M. W. Möller, F. Schacher, A. H. E. Müller, *Advanced Materials* **2008**, *20*, 947.
- [90] J. Yuan, M. Drechsler, Y. Xu, M. Zhang, A. H. E. Müller, *Polymer* **2008**, *49*, 1547.
- [91] G. R. Whittell, I. Manners, *Advanced Materials* **2007**, *19*, 3439.
- [92] R. H. A. Ras, M. Kemell, J. de Wit, M. Ritala, G. ten Brinke, M. Leskelä, O. Ikkala, *Advanced Materials* **2007**, *19*, 102.
- [93] S. b. Maria, A. S. Susha, M. Sommer, D. V. Talapin, A. L. Rogach, M. Thelakkat, *Macromolecules* **2008**, *41*, 6081.
- [94] M. Schrunner, F. Polzer, Y. Mei, Y. Lu, B. Haupt, M. Ballauff, A. Gödel, M. Drechsler, J. Preussner, U. Glatzel, *Macromolecular Chemistry and Physics* **2007**, *208*, 1542.
- [95] M. Schrunner, S. Proch, Y. Mei, R. Kempe, N. Miyajima, M. Ballauff, *Advanced Materials* **2008**, *20*, 1928.
- [96] E. J. W. Crossland, M. Kamperman, M. Nedelcu, C. Ducati, U. Wiesner, D. M. Smilgies, G. E. S. Toombes, M. A. Hillmyer, S. Ludwigs, U. Steiner, H. J. Snaith, *Nano Letters*, ASAP.

Thesis Overview

This dissertation contains 8 publications, presented from chapter 3 to 10.

The main focus of this work was the application of well-defined block copolymers and their self-assembled structures for the generation of functional architectures with features in the nanometer size. These self-assembly studies involved solution based preparation pathways, thin films via spin coating onto different substrates, and equilibrium morphologies formed in the bulk. All block copolymers were synthesized via anionic polymerization procedures and characterized with SEC, ¹H-NMR, and MALDI-ToF mass spectrometry. The formed assemblies were further analyzed through scattering (SAXS, SLS, DLS), electron microscopic (TEM, SEM, cryo-TEM), and scanning force techniques (SFM).

Both thin film and bulk investigations aimed at the preparation of novel, stimuli-responsive membranes with advanced functionalities, e.g. separation properties that may be tuned through external stimuli like pH, temperature, or light. In the case of polymer thin films, controlled solvent annealing was utilized to enhance phase separation. Suitable films should then be transferred onto commercially available support membranes, generating composite structures. As an attractive alternative, self-supporting, asymmetric, and double stimuli-responsive membranes could be directly prepared via the non-solvent induced phase separation (NIPS) process from amphiphilic diblock copolymers.

Self-assembly in selective solvents was employed for different ABC block terpolymers, resulting in further compartmentalized micellar structures, pH- and salt-responsive systems, and dynamic interpolyelectrolyte complexes. Furthermore, different strategies for a controlled crosslinking of the micellar core were successfully tested.

The chapters can basically be subdivided into three topics. First, in chapters 3 and 4, the synthesis and characterization of BVT block terpolymers as well as their behavior in thin films on different substrates is described. The chapters 5 - 7 deal with the synthesis of diblock copolymers with a smart, hydrophilic second block, poly(N,N-dimethylaminoethyl methacrylate), and their application as stimuli-responsive asymmetric ultrafiltration membranes. Finally, chapters 8 - 10 specify

the results obtained for BVT block terpolymers in selective solvents, their modification, and their interpolyelectrolyte complexes.

Subsequently, a summary of the key results is presented for each individual chapter. For a complete description of a particular topic, the reader is referred to the respective chapter.

Synthesis, Characterization, and Bulk Crosslinking of Polybutadiene-*block*-poly(2-vinylpyridine)-*block*-poly(*tert*-butyl methacrylate) Block Terpolymers

Several BVT block terpolymers were synthesized via sequential living anionic polymerization in THF and their bulk morphology was investigated with SAXS and TEM. The diversity of the obtained structural patterns is shown in **Figure 2-1**.

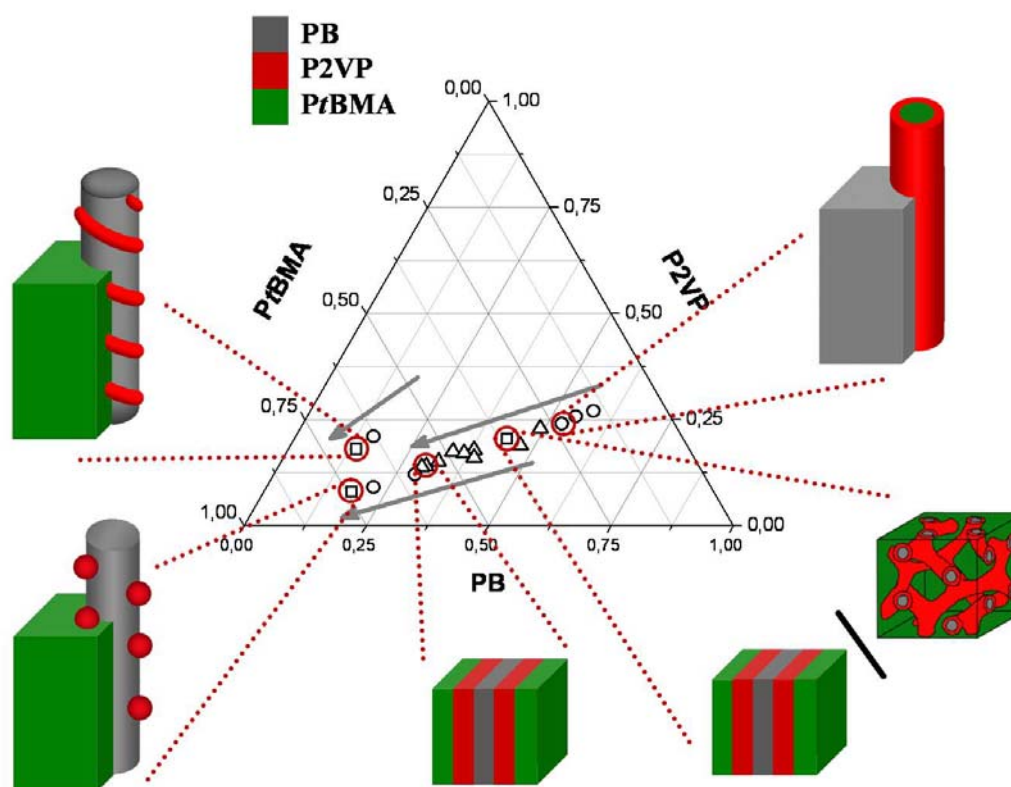


Figure 2-1: Ternary phase diagram obtained for several series of BVT block terpolymers, the grey phase resembles polybutadiene, the red phase poly(2-vinylpyridine), and the green phase poly(*tert*-butyl methacrylate; morphologies are lamellar (Δ), cylindrical (\circ), or either mixtures (lamellae coexisting with cylinders) or unusual structures (spheres on cylinders or helices on cylinders).

Among “classical” examples like lamellae or core-shell cylinders, also more complex patterns like spheres on cylinders or helices on cylinders could be found. We believe that the driving force for the formation of a non-continuous shell around the PB cylindrical core is the high incompatibility between PB and P2VP. To elucidate the use of such self-assembled structures as templates, e.g. for the site-specific generation of inorganic nanoparticles within the P2VP domain, the PB phase was crosslinked via addition of an UV-crosslinker. Afterwards, sonication-

assisted re-dissolution of the polymer films resulted in size-tunable, further compartmentalized polymeric cylinders. Exemplarily, this is highlighted for $B_{18}V_8T_{74}^{133}$ in Figure 2-2.

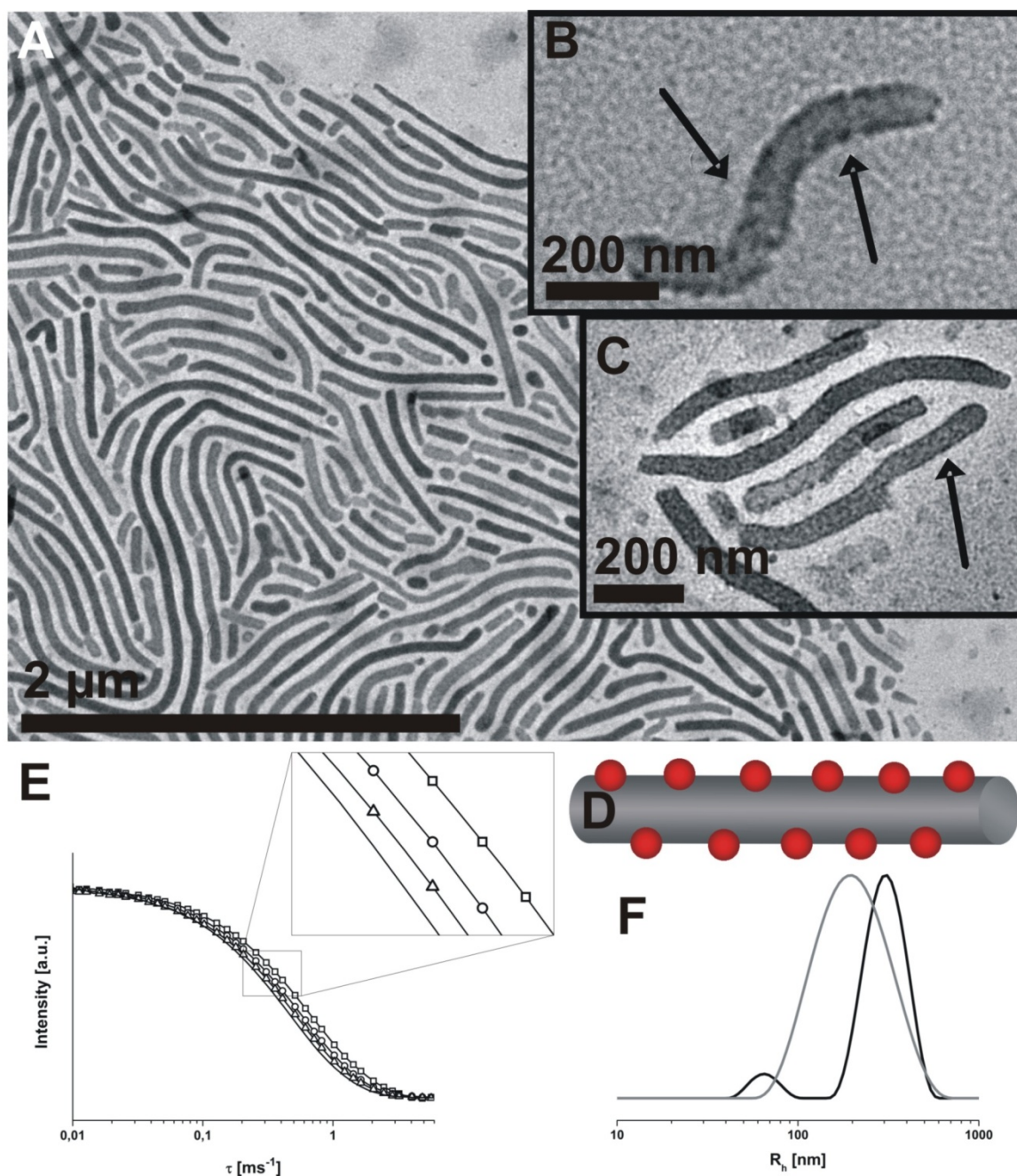


Figure 2-2: TEM micrograph for $B_{18}V_8T_{74}^{133}$ after 10 minutes sonication and drop-coating onto a TEM grid (A); enlargement of one single cylinder (B); enlargement of several cylinders after staining with iodine (C); schematic drawing of the proposed bulk structure, PB cylinder (grey) bearing P2VP spheres (red) embedded in a P β BMA matrix (D); DLS autocorrelation functions for $B_{18}V_8T_{74}^{133}$ after crosslinking in the bulk and subsequent sonication in THF for 1 (-□-), 3 (-○-), 5 (-Δ-), and 10 minutes (solid black line) (E), the inset shows a zoom of the relevant region; DLS CONTIN plots at $\Theta = 90^\circ$ for $B_{18}V_8T_{74}^{133}$ cylinders in THF after sonication for 1 (solid black line, $\langle R_h \rangle = 65$ and 310 nm) and 10 minutes (solid grey line, $\langle R_h \rangle = 185$ nm) (F).

Towards Nanoporous Membranes based on ABC Triblock Terpolymers

Thin films of two suitable BVT block terpolymers (synthesis and characterization is described in chapter 3) showing core-shell cylindrical patterns in the bulk were cast onto different substrates and the resulting morphologies compared to previously investigated SVT systems. Particular emphasis was put upon structures that could be further processed into porous membrane precursors through, e.g., the degradation of one of the compartments via UV treatment, in this case poly(*tert*-butyl methacrylate). Representative SEM micrographs for a SVT and a BVT system are shown in Figure 2-3.

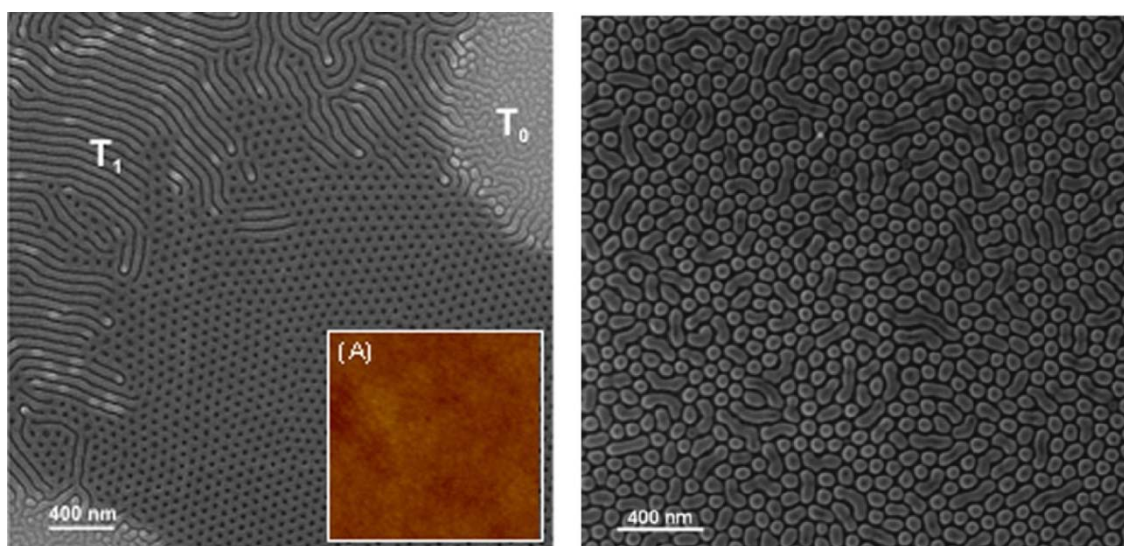


Figure 2-3: SEM image of a $S_{16}V_{21}T_{63}^{140}$ thin film after annealing in chloroform vapor ($p_{\text{CHCl}_3} = 0.8$ p₀; $t = 100$) with an acceleration voltage of 1.0 kV showing different morphologies in dependence of terrace height. Inset (A) SFM height image (size $1 \times 1 \mu\text{m}^2$). The sample surface is covered with a smooth rigid layer of P*t*BMA (left image); SEM image of a $B_{16}V_{21}T_{63}^{145}$ film, solely cylinders oriented perpendicular and parallel to the substrate surface (right image).

It turned out that the surface tension of the first blocks (PS, PB) played a major role for the final structure formation after solvent annealing with chloroform vapor. Although almost exactly the same molecular weights and compositions were used, hexagonally perforated lamellae were formed in the case of SVT terpolymers, whereas core-shell cylinders oriented either parallel or perpendicular to the substrate occurred for BVT samples. With longer annealing times, the fraction of perpendicular aligned cylinders could be dramatically increased. This could be explained through the distinctly lower surface tension of PB. For both systems, the P*t*BMA compartment could be degraded via UV irradiation, generating an

interconnected core-shell cylindrical network for SVT and freestanding arrays of PB core and P2VP cylinders for BVT block terpolymers. Both polymers were considered as attractive precursors for the fabrication of composite membranes. For BVT, this would require a further thin-film modification, e.g. ozonolysis to remove the PB core of the cylinders. Moreover, several very useful features with respect to the membrane technology have been identified, namely a similar equilibrium morphology on substrates with different wettability, the feasibility of a film transfer to another (porous) substrate and the stabilization of the films by internal cross-linking. This is exemplarily demonstrated for a thin-film of $B_{14}V_{18}T_{68}^{165}$ after spin casting onto a NaCl wafer, crosslinking via UV, and subsequent transfer onto a TEM grid (Figure 2-4).

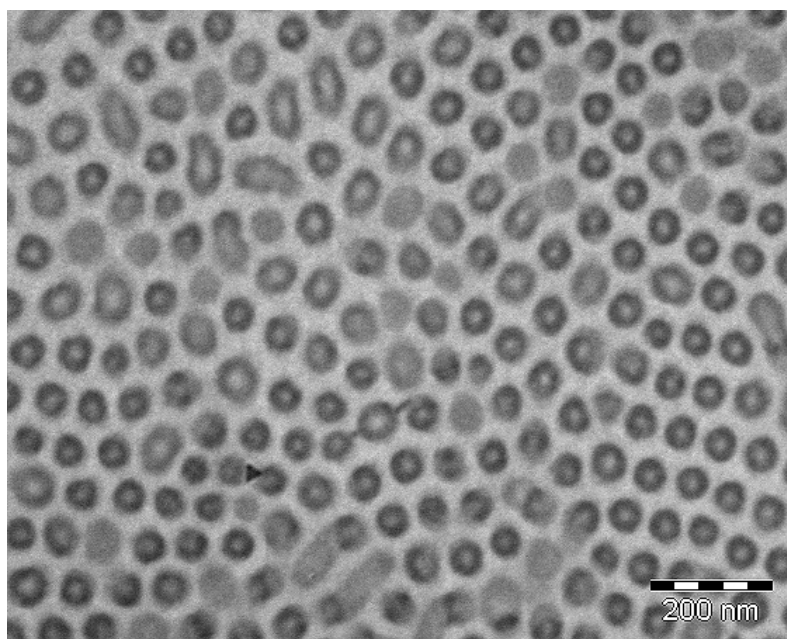


Figure 2-4: TEM image of a thin film of $B_{14}V_{18}T_{68}^{165}$ triblock terpolymer spin-cast onto a NaCl wafer from chloroform solution and transferred onto a TEM grid, revealing hexagonally packed core-shell cylinders: polybutadiene core and poly(2-vinyl pyridine) shell in a poly(*tert*-butyl methacrylate) matrix.

New Block Copolymers with Poly(N,N-dimethylaminoethyl methacrylate) as Double Stimuli-responsive Block

Novel, amphiphilic block copolymers with a narrow molecular weight distribution were synthesized via sequential anionic polymerization in THF: Polystyrene-*block*-poly(N,N-dimethylaminoethyl methacrylate) (PS-*b*-PDMAEMA), polybutadiene-*block*-poly(N,N-dimethylaminoethyl methacrylate) (PB-*b*-PDMAEMA), and poly(*p*-*tert*-butoxystyrene)-*block*-PDMAEMA. The corresponding SEC traces are shown in Figure 2-5.

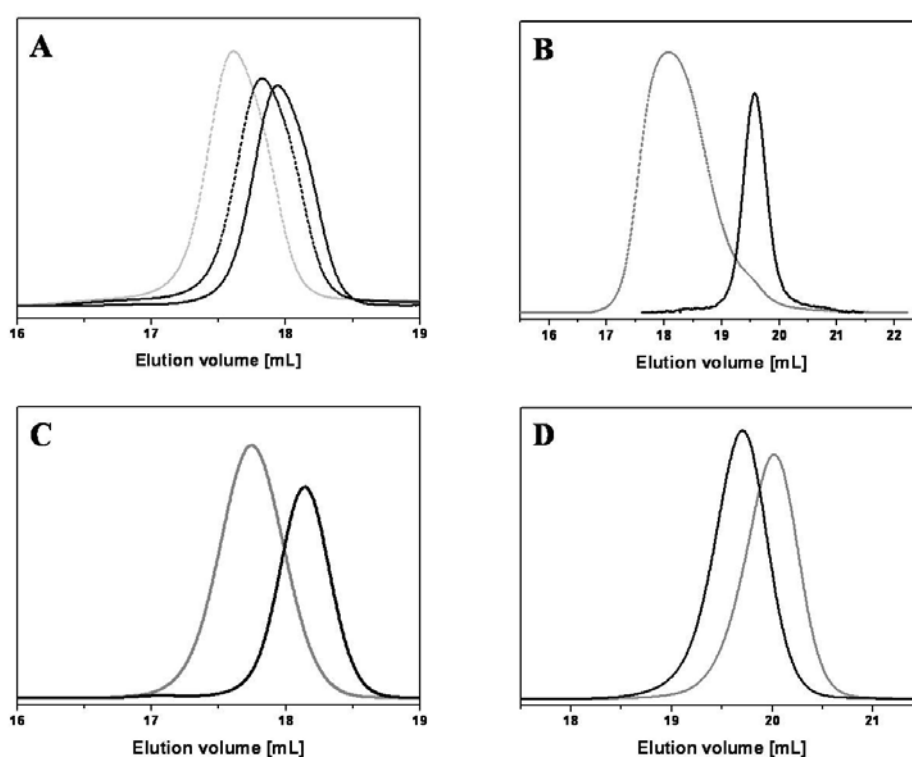


Figure 2-5: SEC elution traces (A) for P^tBS₄₅₀ (black solid line; PDI=1.02), P^tBS₄₅₀-*b*-PDMAEMA₁₁ (dashed black line; PDI=1.04) and P^tBS₄₅₀-*b*-PDMAEMA₄₉ (dashed grey line; PDI=1.04) in THF as eluent, (B) for B₂₉₀ (solid black line, PDI=1.02) and B₂₉₀-*b*-DMAEMA₂₄₀ (dashed grey line, PDI=1.07), (C) for B₈₁₀ (solid black line, PDI=1.02) and B₈₁₀-*b*-DMAEMA₆₅ (solid grey line, PDI=1.05), and (D) for PS₂₄₃ (solid grey line, PDI=1.02) and PS₂₄₃-*b*-DMAEMA₃₇ (solid black line, PDI=1.04) in THF and 0.25 wt. % TBAB as eluent.

Furthermore, a new strategy for the direct synthesis of poly(ethylene oxide)-*block*-PDMAEMA (PEO-*b*-PDMAEMA) diblock copolymers was exploited: using *sec*-BuLi as initiator in the presence of the *t*-BuP₄ phosphazene base, a facile changeover from an oxyanion to a carbanion could be performed. In this way PEO-*b*-PDMAEMA with a moderately narrow molecular weight distribution (PDI ≈ 1.40) was obtained.

Further investigations revealed that in this case slow initiation is taking place upon addition of DMAEMA to the reaction mixture. The reaction scheme is shown in Figure 2-6.

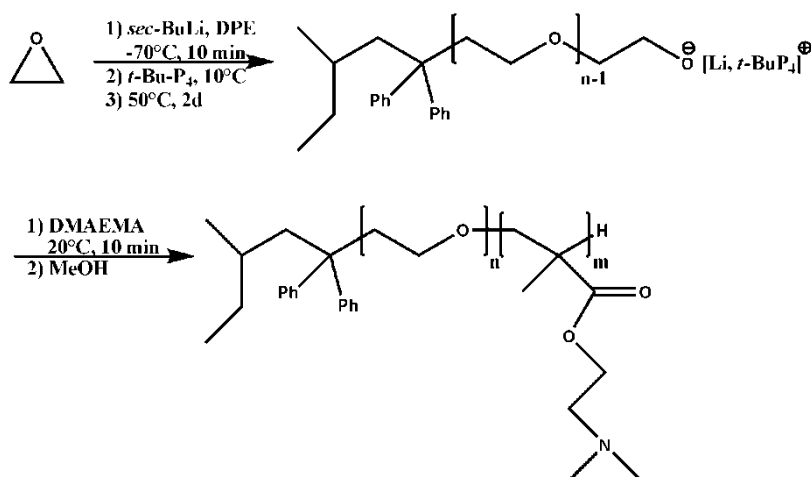


Figure 2-6: Synthesis of PEO-*b*-PDMAEMA diblock copolymers via sequential anionic polymerization in THF with Li⁺ counterion in the presence of *t*-BuP₄ phosphazene base.

All polymerizations were monitored using a NIR probe. In this way it could be shown that the addition of the phosphazene base causes a distinctly slower propagation rate for the DMAEMA block compared to the corresponding homopolymerization in the presence of alkoxides. Finally, the blocking efficiency of this approach (>95%) was compared to commercially available PEO macroinitiators with one single OH-function. After initial deprotonation with the same phosphazene base, polymerization of DMAEMA resulted in significantly lower blocking efficiencies (80%).

Self-supporting, Double Stimuli-responsive Porous Membranes from Polystyrene-*block*-poly(N,N-dimethylaminoethyl methacrylate) Diblock Copolymers

The non-solvent induced phase separation process was used to fabricate asymmetric membranes from amphiphilic PS-*b*-PDMAEMA diblock copolymers, which were synthesized and characterized in the previous chapter. Here, concentrated polymer solutions were applied onto polished glass substrates with a doctor blade and, after the so-called “open-time”, immersed into a non-solvent bath filled with water for coagulation and final film formation. These membranes exhibited a thin separation layer on top with pores in the nanometer-sized range and are supported from underneath by a macroporous volume structure. Two representative SEM micrographs are shown in **Figure 2-7**.

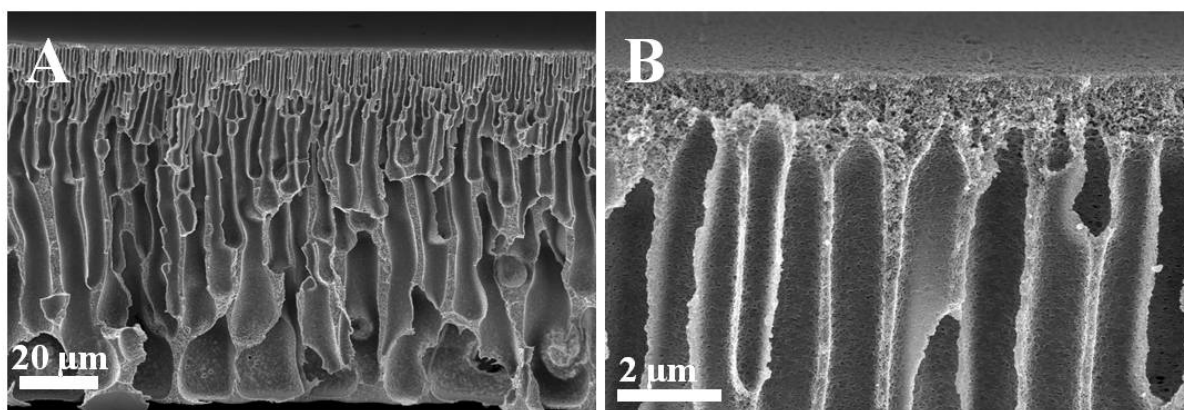


Figure 2-7: SEM micrographs of an asymmetric membrane prepared from $S_{81}D_{19}^{75}$ in a mixture of 50% THF and 50% DMF, “open-time” was 60 seconds; (A) cross section, (B) enlargement highlighting the top separation layer.

The high content of PS ensured an immediate precipitation upon contact with water. The hydrophilic PDMAEMA covered the pore walls and, due to the rapid demixing process, also was incorporated into the pore walls to a certain extent. Through the exploitation of the “smart” properties of PDMAEMA, response to pH and temperature, these membranes turned out to be double stimuli-responsive. The pH- and temperature-dependent water flux for such a system is shown in **Figure 2-8**.

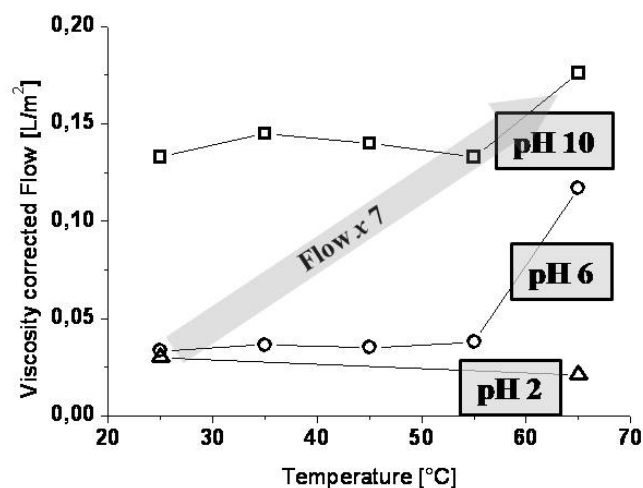


Figure 2-8: Water flux for $S_{81}D_{19}^{75}$ asymmetric membranes; depending on pH values and temperatures; the membranes were tempered at 65 °C for 120 minutes in both cases.

At low pH, PDMAEMA is fully protonated, almost swollen, and the lowest flux was obtained. No response to a rise in temperature could be detected. Upon elevating the pH to 6, PDMAEMA is less charged, the LCST was applicable and significantly higher flux values were achieved at 65 °C. At pH 10, the flux was already considerably higher at room temperature, attributed to uncharged and less extended PDMAEMA chains. Surprisingly, even under these conditions a further flux increase could be detected upon heating to 65 °C.

For a better estimation of the true pore size, pH-dependent filtrations were carried out with silica particles of different sizes. It turned out that under acidic conditions these membranes exhibited barrier pores in the separation layer with a size of about 15 - 30 nm. The inherent features of these systems were that they are defect-free on an area of several hundred μm^2 , high and tunable flux values, and a controllable pore size.

Double Stimuli-Responsive Ultrafiltration Membranes from Polystyrene-*block*-poly(N,N-dimethylaminoethyl methacrylate) Diblock Copolymers

After initial characterization and filtration tests carried out for $S_{81}D_{19}^{75}$, as described in the previous chapter, now the influence of the different variables during the membrane formation process was thoroughly investigated: solvent composition, “open-time”, initial film thickness, and pH- or temperature present in the coagulation bath. Moreover, all experiments were carried out for two different block copolymers, $S_{81}D_{19}^{75}$ and $S_{68}D_{32}^{100}$, to probe whether the content in hydrophilic PDMAEMA material plays an important role as well.

It turned out that for $S_{81}D_{19}^{75}$ the solvent composition for membrane casting was not crucial but both initial film thickness and “open-time” were, in terms of membrane structure. Contrary, for $S_{68}D_{32}^{100}$, the initial solvent composition strongly determined the resulting membrane morphology, whereas the effects of film height and “open time” induced certain changes, but by far not as pronounced as found for the other diblock copolymer. Exemplarily, the effect of the “open-time” on the membrane structure for $S_{68}D_{32}^{100}$ is shown in **Figure 2-9**.

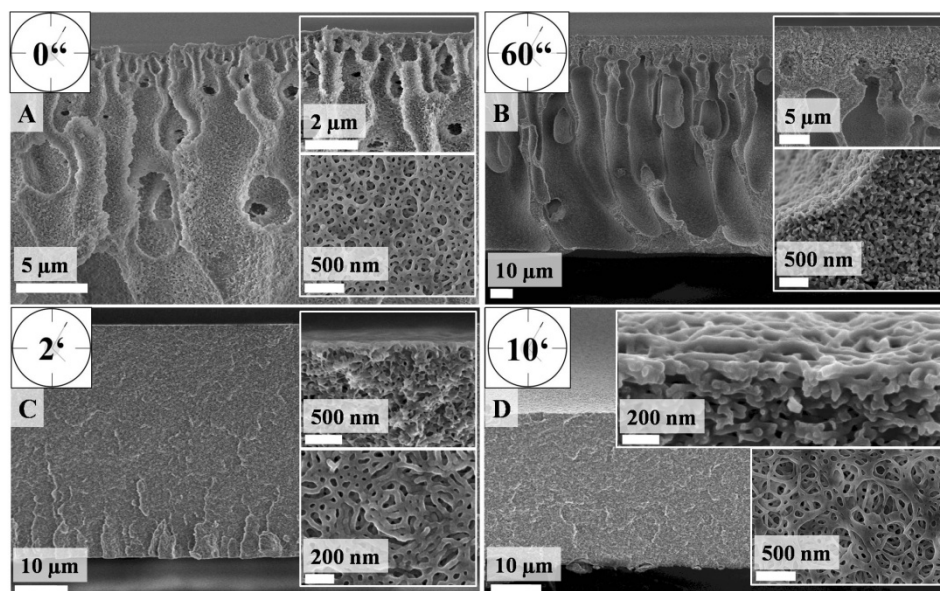


Figure 2-9: SEM micrographs for membranes from $S_{68}D_{32}^{100}$ cast from a mixture of THF (60%) and DMF (40%) after different “open-times”: 0 seconds (A), 60 seconds (B), 2 minutes (C), and 10 minutes (D); the upper insets show an enlargement of the respective separation layer, the lower insets display the morphology obtained at the bottom of the membrane.

It can be nicely seen that for an “open-time” exceeding 60 seconds a transition from an integrally asymmetric cross section towards a condensed, sponge-like membrane occurred. These findings were ascribed to the higher compatibility of $S_{68}D_{32}^{100}$ with the coagulation bath, water, caused by the higher content in hydrophilic material, PDMAEMA. This also resulted in more well-defined morphological features throughout the obtained membranes for $S_{68}D_{32}^{100}$ and can be explained by slower phase separation during coagulation compared to $S_{81}D_{19}^{75}$, where the PS content is more dominating.

Finally, pH- and temperature-dependent water flux measurements were carried out for representative membrane systems of both diblock copolymers. In all cases, double stimuli-responsive membrane systems could be obtained.

Multicompartment Core Micelles of ABC Block Terpolymers in Organic Media

The self-assembly of BVT block terpolymers in acetone as selective solvent for the first block, polybutadiene, was studied. Almost monodisperse, spherical micelles were formed. According to theory, these should consist of a PB core, a P2VP shell and a P*t*BMA corona. DLS CONTIN plots and the decay rate vs. q^2 are shown in **Figure 2-10**.

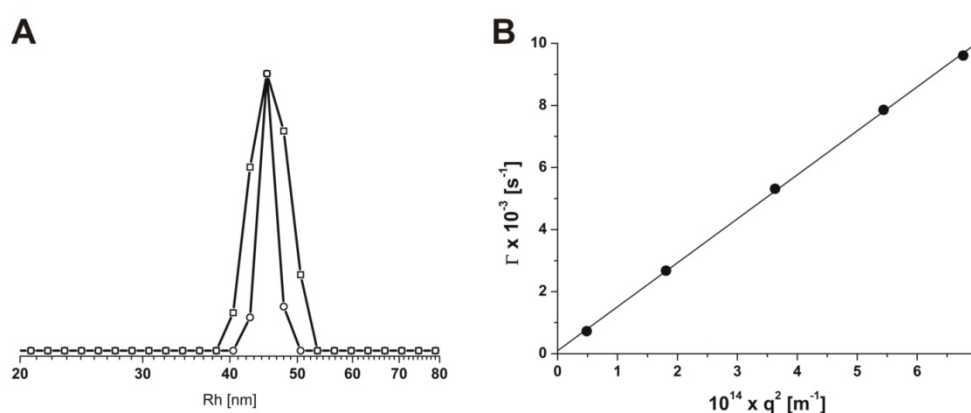


Figure 2-10: A: CONTIN plots (intensity weighted) for B₈₀₀V₁₉₀T₃₈₀ (grey line, $\langle R_h \rangle_z = 43\text{ nm}$) and B₈₀₀V₁₉₀T₅₅₀ (black line, $\langle R_h \rangle_z = 44\text{ nm}$) at $\Theta = 90^\circ$ in acetone solution (c = 1 g/L); B: Γ vs. q^2 for B₈₀₀V₁₉₀T₅₅₀.

As it turned out, the core of these micelles was further compartmentalized. P2VP formed spherical domains on the PB core, resulting in multicompartment core micelles. A possible explanation for this behavior is the high χ -interaction parameter for this particular system as P2VP is supposed to be soluble in acetone. A representative TEM micrograph and a schematic depiction of the proposed micellar structure are shown in **Figure 2-11**. To facilitate the transfer of these aggregates into different, non-selective solvents like dioxane or THF different core-crosslinking strategies were successfully carried out: either cold-vulcanization or UV-initiator assisted photopolymerization. Both methods resulted in well-defined, core-crosslinked micelles. Furthermore, the effect of reaction time and the amount of employed crosslinking agent were investigated. Crosslinking efficiencies were determined through a combination of ¹H-NMR and soxhlett extraction with THF.

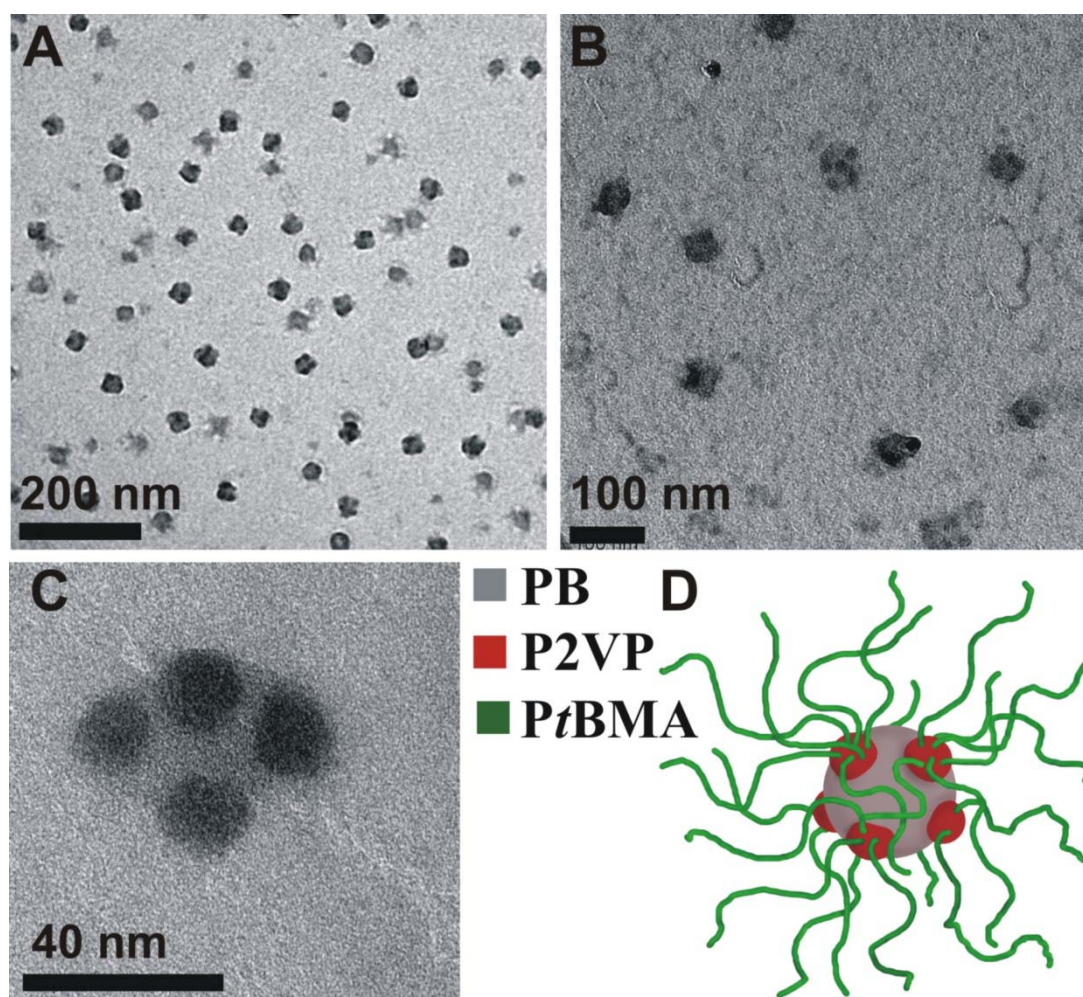


Figure 2-11: TEM images of multicompartiment micelles from $B_{800}V_{190}T_{550}$, drop-coated (A) and freeze-dried (B) from 0.1 g/L acetone solution onto carbon-coated gold TEM grids. C: single micelle at high magnification; D: proposed solution structure of the micelles.

Finally, the proposed micellar structure was proven through cryo-TEM measurements of core crosslinked aggregates after transfer to dioxane. This is shown in Figure 2-12.

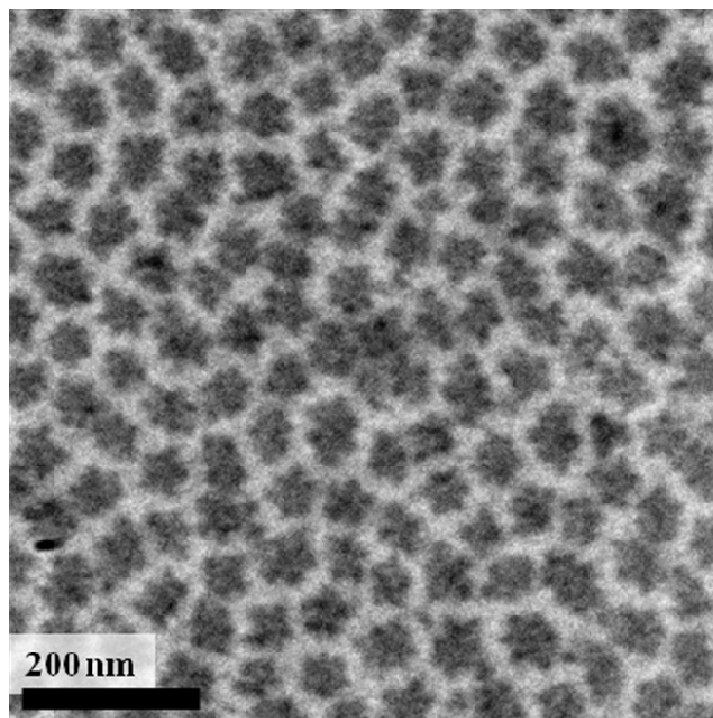


Figure 2-12: Cryo-TEM images of $B_{800}V_{190}T_{550}$ in dioxane after crosslinking of the polybutadiene core with 1 eq S_2Cl_2 in acetone and subsequent transfer of the aggregates into dioxane ($c = 0.2$ g/L); the scale bar corresponds to 100 nm.

Dynamic Multicompartment-Core Micelles in Aqueous Media

After the characterization of the aggregates of BVT block terpolymers in organic media (previous chapter), the focus was put on aqueous solutions. Therefore, $B_{800}V_{190}T_{550}$ was modified to render it amphiphilic. The middle block, P2VP, was quaternized and turned into a strong polyelectrolyte. Afterwards, the *Pt*BMA compartment was hydrolyzed, generating poly(methacrylic acid), a weak polyelectrolyte. For comparison, in one case only the *Pt*BMA block was modified to compare block terpolymers with one or two pH-dependent hydrophilic compartments. The reaction scheme for the polymer analogous treatment is shown in Figure 2-13.

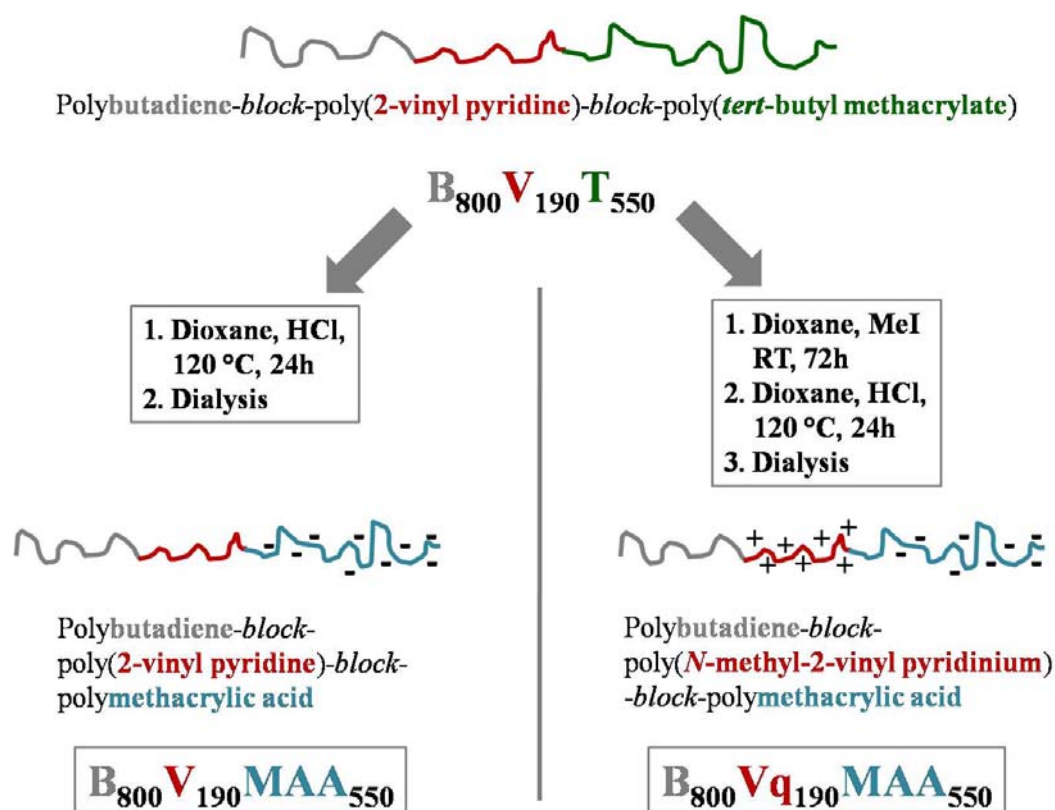


Figure 2-13: Schematic depiction of the two different pathways for the preparation of micellar solutions of B₈₀₀V₁₉₀MAA₅₅₀ in water.

After dialysis into aqueous solutions at high pH (10), different micellar aggregates were formed, depending on the previously carried out modification reactions. If only the P*t*BMA was hydrolyzed to PMAA, core-shell-corona micelles were formed, exhibiting a soft PB core, a P2VP shell, and a negatively charged PMAA corona. The proposed solution structure as well as cryo-TEM micrographs are shown in Figure 2-14. If P2VP was quaternized prior to hydrolysis of the P*t*BMA, the situation changed: now, under these conditions, the middle block was hydrophilic and positively charged whereas the PMAA still bears negative charges. Therefore, interpolyelectrolyte complexes between quaternized P2VP and PMAA were formed. As such structures become hydrophobic again, the IPECs collapsed and formed a patchy shell onto the soft PB core. This is shown in Figure 2-15. The difference in length between P2VP and PMAA ensured that the micelles were still water-soluble. We assume that after IPEC formation around 360 units of uncomplexed PMAA remained for each polymer chain.

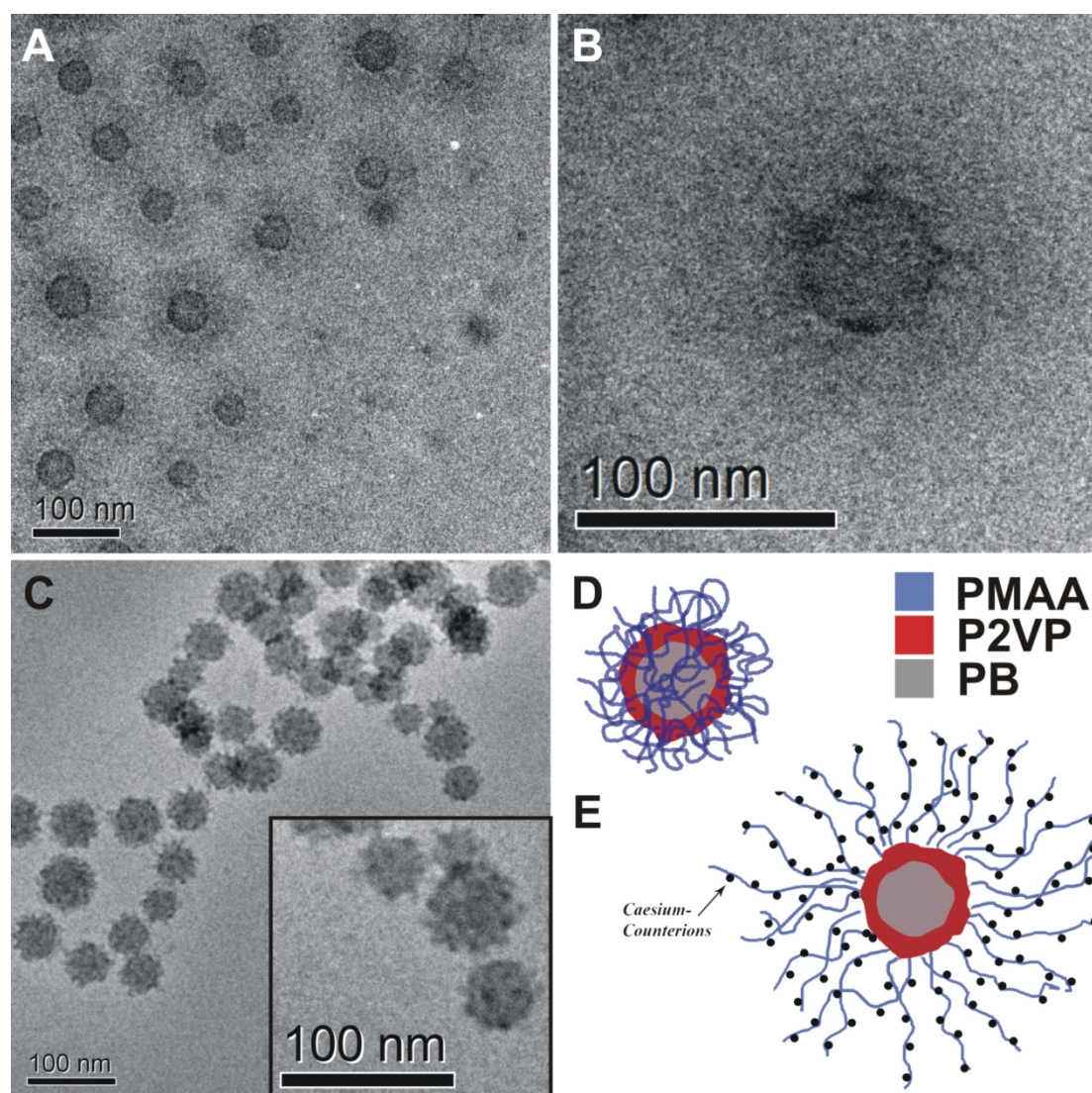


Figure 2-14: Cryo-TEM micrographs of $B_{800}V_{190}MAA_{550}$ in aqueous solution at pH 10 (0.05M CsCl, $c = 1$ g/L), Overview (A) and single core-shell-corona micelle (B; at pH 4 ($c = 1$ g/L) (C), the inset shows an enlargement; schematic depiction of the proposed solution structure of $B_{38}V_{18}MAA_{44}^{110}$ in solution depending on the pH; core-shell-corona structure with an expanded PMAA corona at pH 10 with additional CsCl (E) and a collapsed PMAA corona at pH 4 (D).

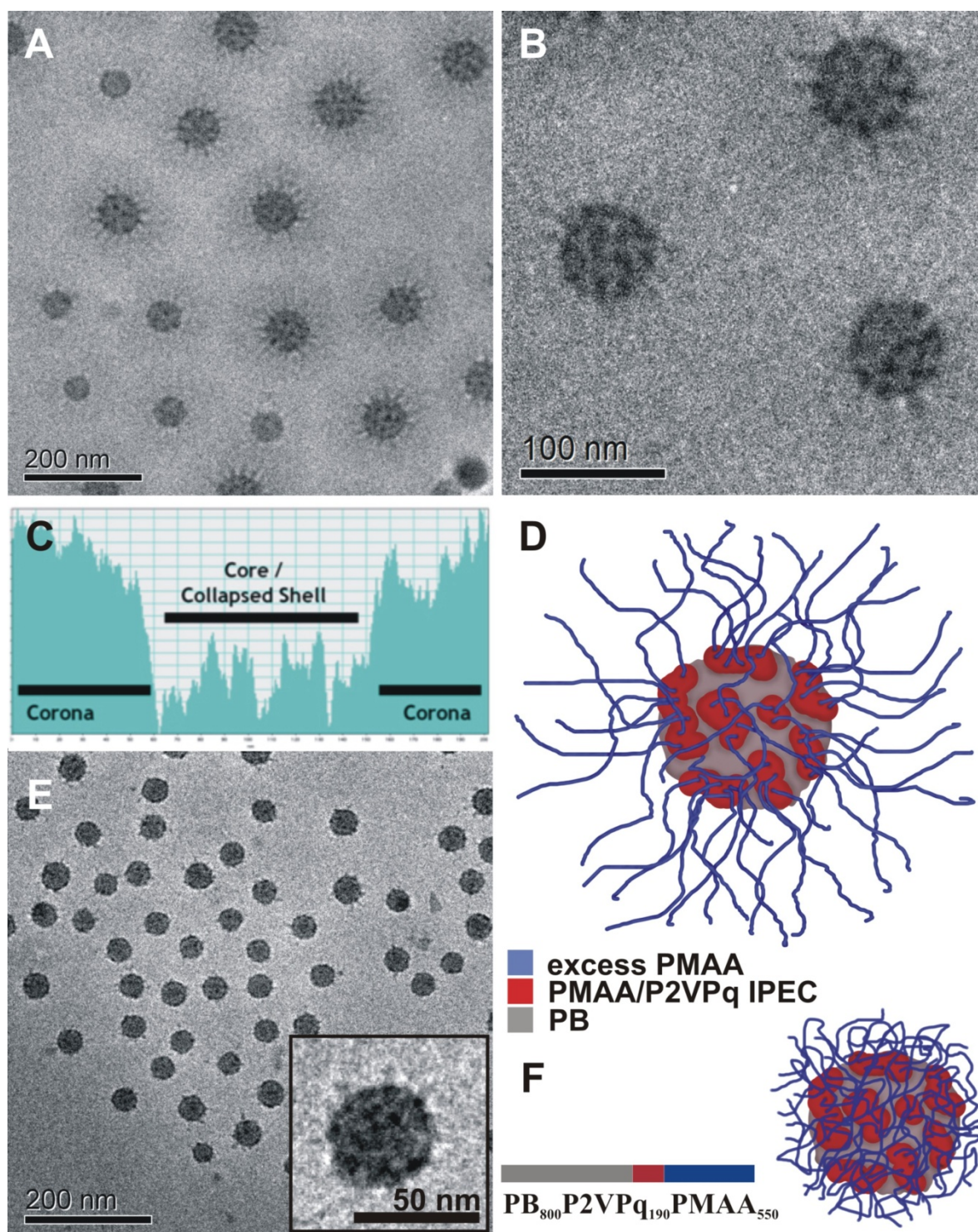


Figure 2-15: Cryo-TEM micrographs of $B_{800}Vq_{190}MAA_{550}$ in aqueous solution; (A+B) pH 10, ($c = 1$ g/L); (C) grey-scale analysis of a micellar cross-section; (D) proposed solution structure at pH 10, expanded PMAA corona; (E) cryo-TEM micrograph at pH 4, ($c = 1$ g/L), the inset shows a single micelle; (F) proposed solution structure at low pH, collapsed PMAA corona.

Both type of micellar aggregates showed response to changes in pH or salinity, rendering intelligent and dynamic colloids. These kinds of aggregates with intramicellar IPECs could serve as model systems for the control of charge and shape in polymeric micelles. The further complexation of the charged micellar aggregates with, for example, functional particles and block copolymers will be the subject of further studies.

Interpolyelectrolyte Complexes of Dynamic Multicompartmental Micelles

In the previous chapter the preparation and the characterization of polybutadiene-*block*-poly(*N*-methyl-2-vinylpyridinium)-*block*-poly(methacrylic acid) ($B_{800}Vq_{190}MAA_{550}$) block terpolymer micelles with a soft polybutadiene core, an interpolyelectrolyte complex (IPEC) shell made out of poly(*N*-methyl-2-vinylpyridinium) and poly(methacrylic acid), and a negatively charged PMAA corona was described. Now these micelles were mixed with positively charged poly(*N*-methyl-2-vinylpyridinium)-*block*-poly(ethylene oxide) (VqEO) diblock copolymers. Under these conditions, mixing resulted in the formation of a second IPEC shell onto the $B_{800}Vq_{190}MAA_{550}$ precursor micelles, surrounded by a PEO corona. The resulting multicompartmental IPECs exhibited dynamic behavior, highlighted through structural relaxation within a period of 10 days, followed by DLS, cryo-TEM, and SFM. The principle is shown in **Figure 2-16**.

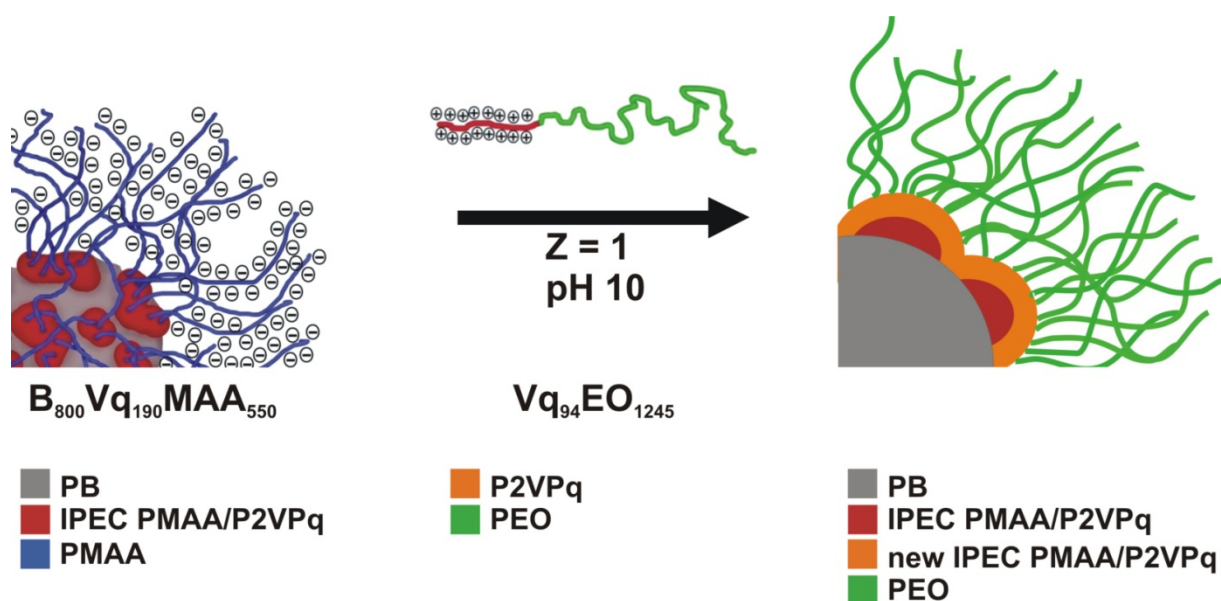


Figure 2-16: scheme for the formation of IPECs between negatively charged $B_{800}Vq_{190}MAA_{550}$ block terpolymer micelles and positively charged $Vq_{94}EO_{1245}$ diblock copolymers at charge neutrality ($Z = 1$);

Moreover, during the mixing of precursor micelles with oppositely charged diblock copolymers, a transition state could be identified. Here, the aggregates showed a rather star-like appearance, caused by the fast electrostatic attraction between stretched oppositely charged polymer chains and followed by a slow relaxation

towards the equilibrium structure. The intermediate state is displayed in **Figure 2-17**.

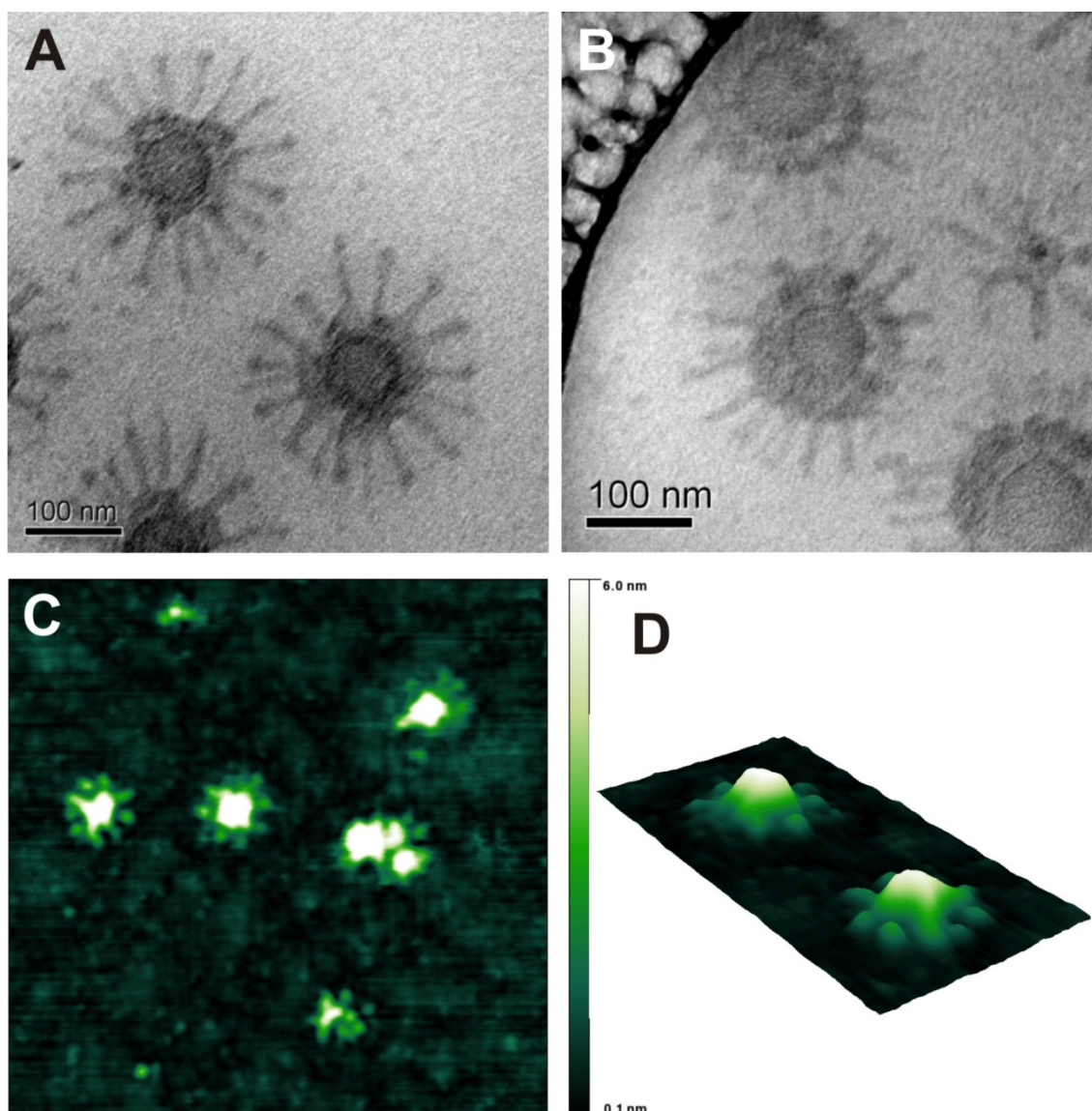


Figure 2-17: A, B: cryo-TEM micrograph of an IPEC at $Z = 1$ and pH 10 after 1h mixing time at different locations of the same sample; C, D: SFM images of an IPEC solution at $Z = 1$ and pH 10 after deposition on a carboncoated TEM grid, C displaying an enlargement of D.

Finally, the generation of hybrid structures through the in-situ formation of gold nanoparticles within the shell of both precursor micelles and equilibrated IPECs was investigated. For the $B_{800}Vq_{190}MAA_{550}$ micelles, uniform nanoparticles could be observed, almost exclusively located within the PMAA shell. As for the IPECs, Au nanoparticles could be synthesized within the block ionomer complex shell, further protected from the outside by the PEO shell. The results are shown in **Figure 2-18**.

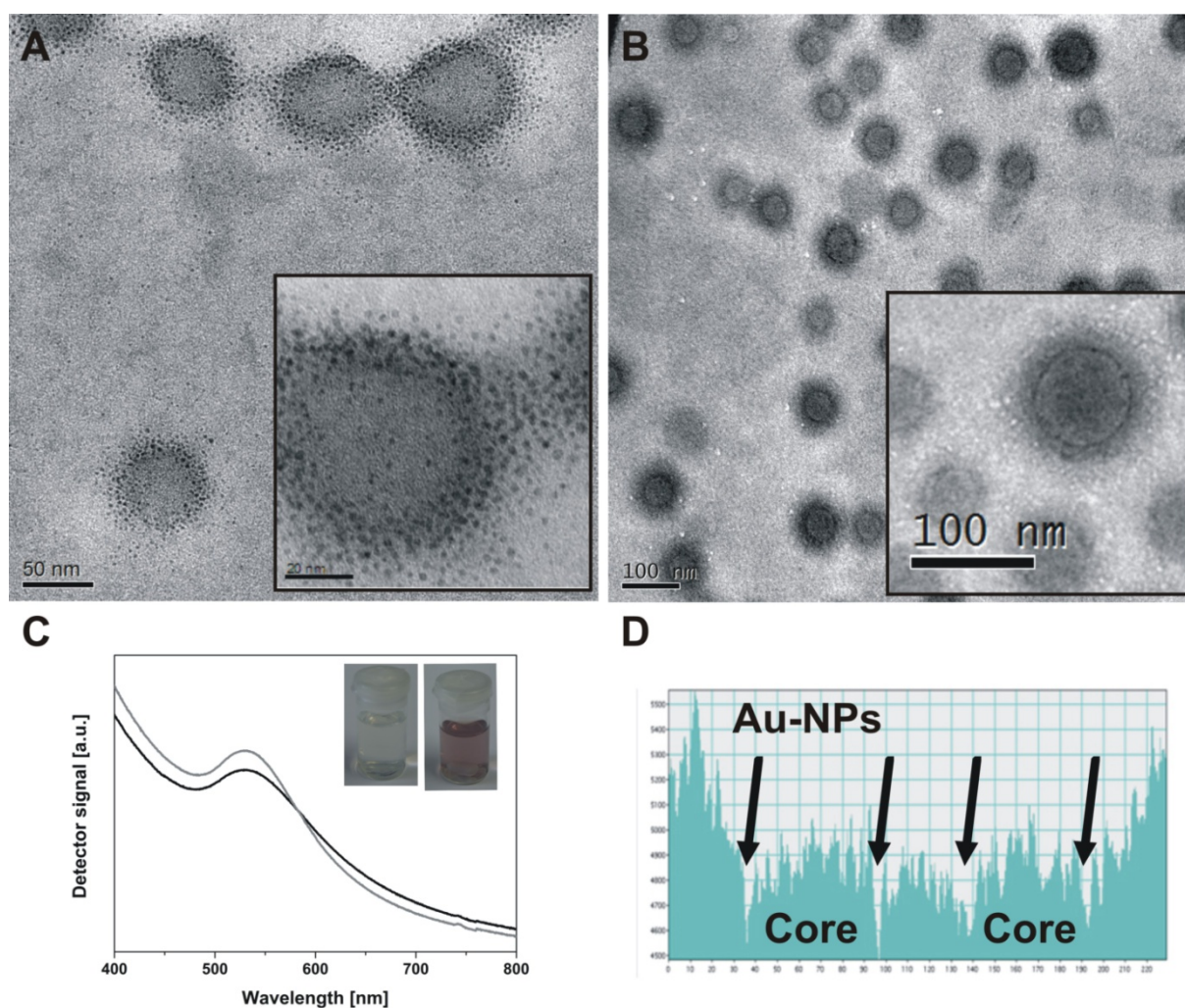


Figure 2-18: TEM micrograph of $B_{800}Vq_{190}MAA_{550}$ terpolymer micelles loaded with Au NPs on a carbon-coated copper grid (A), the inset displays an enlargement; cryo-TEM micrograph of the IPEC at $Z = 0.2$ loaded with Au NPs (B), the inset shows an enlargement; UV-VIS spectra of both the $B_{800}Vq_{190}MAA_{550}$ micelles (solid black line) and the IPEC (solid grey line) loaded with Au NPs (C), the inset are photos taken of the IPEC solutions before (left) and after (right) nanoparticles formation; grey-scale analysis of two adjacent IPECs in (B), highlighting the location of the nanoparticles inside the structure (D).

Individual Contributions to Joint Publications

The results presented in this dissertation were obtained in close collaboration with other people and published or submitted as indicated below. In the following, the contributions of all the coauthors to the different chapters will be specified. The asterisk denotes the corresponding author(s).

Chapter 3

This work has been submitted to *Polymer* under the title

“Synthesis, Characterization, and Bulk Crosslinking of Polybutadiene-*block*-poly(2-vinylpyridine)-*block*-poly(*tert*-butyl methacrylate) Block Terpolymers”
by F. Schacher*, J. Yuan, and A. H. E. Müller*.

I wrote the publication and performed most of the experiments.

J. Yuan performed some of the TEM measurements.

H. Schoberth and K. Schmidt performed most of the SAXS measurements.

A. Müller was involved in discussions and corrected the manuscript.

Chapter 4

This work is published in *Small* **2007**, 3, p. 1056 - 1063 under the title

“Towards Nanoporous Membranes based on ABC Triblock Terpolymers” by A. Sperschneider, F. Schacher, M. Gawenda, L. Tsarkova, M. Ulbricht, G. Krausch, J. Köhler, and A. H. E. Müller*.

A. Sperschneider and I wrote the publication.

I synthesized most of the polymers, performed the TEM experiments and was involved in all discussions.

A. Sperschneider performed the SEM and SFM measurements.

M. Gawenda, L. Tsarkova, M. Ulbricht, J. Köhler, and A. Müller were involved in discussions and corrected the manuscript.

Chapter 5

This work is published in *Macromol. Chem. Phys.* **2009**, 210, p. 256 - 263 under the title

“New Block Copolymers with Poly(N,N-dimethylaminoethyl methacrylate) as Double Stimuli-responsive Block” by F. Schacher*, M. Müllner, H. Schmalz, and A. H. E. Müller*.

I wrote the publication and performed most of the experiments.

M. Müllner synthesized part of the polymers during his advanced labcourse under my supervision.

H. Schmalz and A. Müller were involved in discussions and corrected the manuscript.

Chapter 6

This work is published in *Adv. Funct. Materials*, **2009**, 19, p. 1040 - 1045 under the title

“Self-supporting, Double Stimuli-responsive Membranes from Polystyrene-*block*-poly(N,N-dimethylaminoethyl methacrylate) Diblock Copolymers” by F. Schacher*, M. Ulbricht, and A. H. E. Müller*.

I wrote the publication and performed most of the experiments.

C. Schenk performed some of the water flux measurements.

T. Rudolph was involved in some of the filtration experiments under my guidance.

B. Goßler performed all the SEM measurements.

M. Ulbricht and A. Müller were involved in discussions and corrected the manuscript.

Chapter 7

This work is *in press* in *ACS Applied Materials & Interfaces* under the title

“Double Stimuli-responsive Ultrafiltration Membranes from Polystyrene-*block*-poly(N,N-dimethylaminoethyl methacrylate) Diblock Copolymers” by F. Schacher*, T. Rudolph, F. Wieberger, M. Ulbricht, and A. H. E. Müller*.

I wrote the publication and performed most of the experiments.

T. Rudolph was involved in membrane preparation, water flux measurements, and filtration tests under my guidance as a HiWi.

B. Goßler performed most of the SEM measurements.

F. Wieberger performed some of the SEM measurements and was involved in discussions.

M. Ulbricht and A. Müller were involved in discussions and corrected the manuscript.

Chapter 8

This work is published in *Macromolecules* **2009**, 42, p. 3540 - 3548 (cover article) under the title

“Multicompartment Core Micelles of ABC Block Terpolymers in Organic Media” by F. Schacher*, A. Walther, M. Ruppel, M. Drechsler, and A. H. E. Müller*.

I wrote the publication and performed most of the experiments.

A. Walther performed some of the cryo-TEM experiments and was involved in the discussions.

M. Drechsler performed some of the cryo-TEM experiments and was involved in the discussions.

M. Ruppel and A. Müller were involved in discussions and corrected the manuscript.

Chapter 9

This work is *in press* in *Langmuir* under the title

“Dynamic Multicompartment-Core Micelles in Aqueous Media” by F. Schacher*, A. Walther, and A. H. E. Müller*.

I wrote the publication and performed most of the experiments.

A. Walther performed the cryo-TEM experiments and was involved both in the corrections and the discussions.

A. Müller was involved in discussions and corrected the manuscript.

Chapter 10

This work has been submitted to *ACS Nano* under the title

“Interpolyelectrolyte Complexes of Dynamic Multicompartment Micelles” by F. Schacher*, E. Betthausen, A. Walther, H. Schmalz, D. Pergushov, and A. H. E. Müller*.

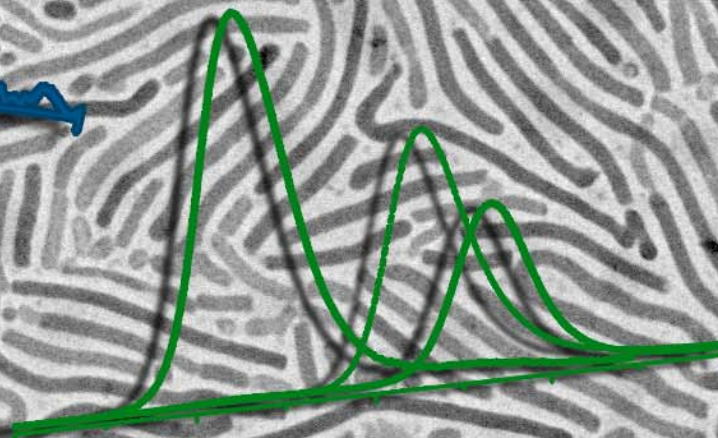
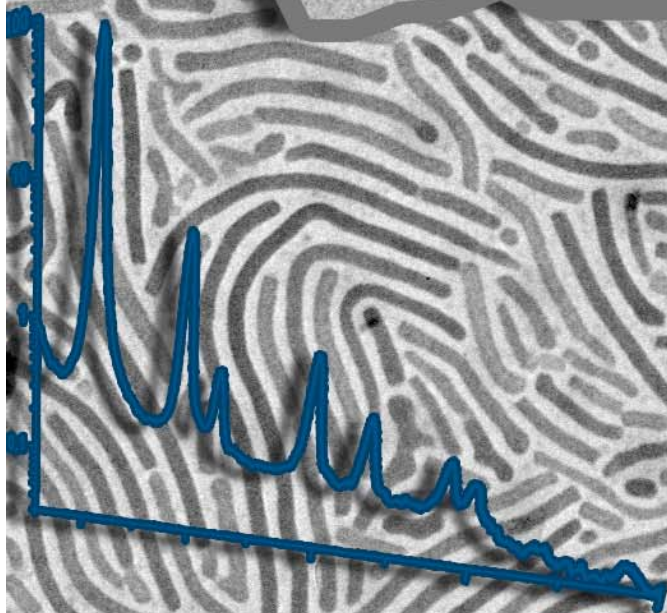
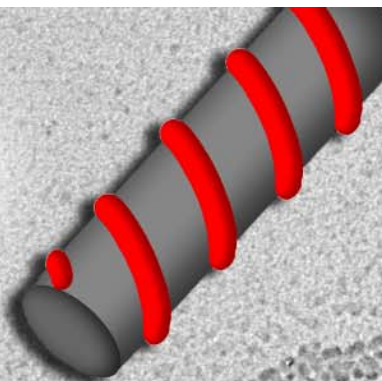
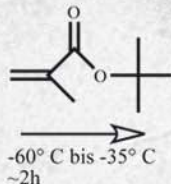
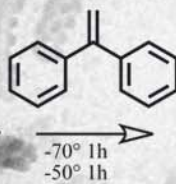
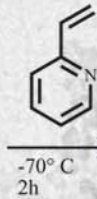
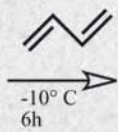
I wrote the publication and performed most of the experiments.

E. Betthausen performed some of the experiments during her advanced labcourse under my guidance.

A. Walther performed the cryo-TEM experiments and was involved in the discussions.

H. Schmalz, D. Pergushov, and A. Müller were involved in discussions and corrected the manuscript.

sec-BuLi
THF



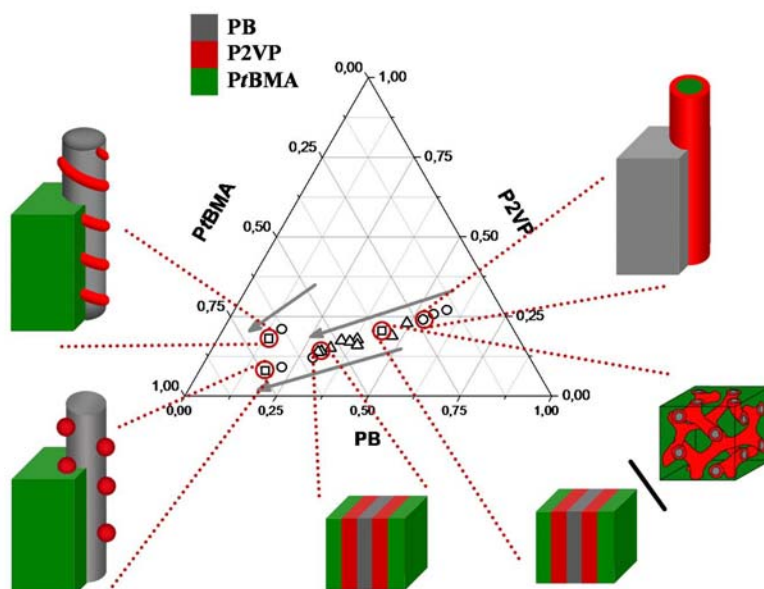
Synthesis, Characterization, and Bulk Crosslinking of Polybutadiene-*b*-poly(2-vinylpyridine)-*b*-poly(*tert*-butyl methacrylate) Block Terpolymers

Felix Schacher, Jiayin Yuan, and Axel H. E. Müller

Makromolekulare Chemie II and Bayreuther Zentrum für Kolloide und Grenzflächen,

Universität Bayreuth, 95440 Bayreuth, Germany

Email: Felix.schacher@uni-bayreuth.de; axel.mueller@uni-bayreuth.de



Abstract

We report on the synthesis and characterization of novel ABC triblock terpolymers, polybutadiene-*b*-poly(2-vinylpyridine)-*b*-poly(*tert*-butyl methacrylate) (BVT), via sequential living anionic polymerizations in THF at low temperatures using *sec*-butyl lithium as initiator. In this work, 18 BVT terpolymers were produced with volume fractions $\Phi_B : \Phi_V : \Phi_T$ in the range of 1 : 0.4 - 1.2 : 0.2 - 4.6. All polymers exhibit a very narrow molecular weight distribution ($PDI < 1.1$). They were characterized in terms of bulk morphology with small angle x-ray scattering and transmission electron microscopy, unveiling mostly lamellar patterns or hexagonally arranged cylindrical structures. $B_{44}V_{20}T_{36}^{98}$ displayed a partial gyroid structure coexisting with lamellar parts while $B_{18}V_8T_{74}^{133}$ exhibited cylinders with a non continuous shell around the PB core and could serve as an interesting template for the facile generation of multicompartmental self-assembled structures. Same accounts for $B_{14}V_{18}T_{68}^{165}$, here the middle block, P2VP, is forming a helix around the PB core. Crosslinking of the polybutadiene compartment of $B_{18}V_8T_{74}^{133}$ and $B_{14}V_{18}T_{68}^{165}$ with an UV-photoinitiator was performed at different ratios, followed by sonication assisted dissolution of the aggregates to elucidate further use of the terpolymers for the generation of soft polymeric nanoparticles with controlled functionality.

Keywords

Soft polymeric nanoparticles; Block Terpolymers; Anionic Polymerization; Crosslinking;

Introduction

Block copolymers are an interesting and versatile class of materials and their tailor-made properties, in particular thin-film and bulk morphology and domain spacing, render them suitable for the demand of smaller and smaller feature sizes in nanotechnology.^[1] Characteristic dimensions for the domain spacing of such microphase separated systems are in the range of 10 - 100 nm and the generation

of nanostructured assemblies with different chemical properties raises opportunities for applications in the fields of catalysis, membrane research, molecular templating or drug delivery.^[2, 3] The peculiar advantage of block copolymers here for are their intrinsic dimensions, the ease of synthesis and the facile control over architecture and chemical functionality, turning them into manageable nanoscale tools.^[4-7] In general, there are two possible ways for the use of block copolymer templates: either “as they are” or after the selective removal of one component through a chemical process like etching or photodegradation.^[8, 9]

In order to provide a sufficient control over domain spacing and topology, well-defined block copolymers are required. Usually, this is achieved by a variety of controlled / “living” polymerization methods, among them typically are anionic / cationic polymerization, atom transfer radical polymerization (ATRP), reversible addition-fragmentation polymerization (RAFT) and group transfer polymerization (GTP). Once obtained, block copolymers self-assemble into a large variety of morphologies, depending on composition, architecture, block sequence and molecular weight.^[10] Compared to AB diblock copolymers, considerably less work has been carried out on the synthesis and bulk properties of ABC block terpolymers.^[11] Here the resulting microphase separated structures are governed by several independent composition variables: the volume fractions (Φ_A , Φ_B , Φ_C), the three interaction parameters (χ_{AB} , χ_{BC} , χ_{AC}), the respective interfacial tensions (γ_{AB} , γ_{BC} , γ_{AC}) and previously mentioned factors like the chain topology.^[12-15] Stadler et al. studied the phase behavior of polystyrene-*b*-polybutadiene-*b*-poly(methyl methacrylate) (SBM) block terpolymers and among the classical morphologies obtained for ABC type terpolymers like lamellae, core-shell cylinders and core-shell spheres they also reported on more complex microphase separated structures featuring chiral assemblies,^[16] “knitting pattern” morphologies,^[17] and a new structural motif where two different cylindrical domains are formed instead of core-shell cylinders.^[18] In our group, the self-assembly of polystyrene-*b*-polybutadiene-*b*-poly(*tert*-butyl methacrylate) (SBT) and SBM block terpolymers is used to generate janus structures featuring nanometer-sized particles with two chemically different sides.^[19-21]

The aim of this work is the synthesis and characterization of polybutadiene-*b*-poly(2-vinylpyridine)-*b*-poly(*tert*-butyl methacrylate) (BVT) block terpolymers with

different ratios of the block segments. Well-defined terpolymers were obtained through sequential living anionic polymerization in THF at low temperatures using *sec*-butyl lithium as initiator. Different series of BVT terpolymers were produced with volume fractions $\Phi_A : \Phi_B : \Phi_C$ in the range of 1 : 0.4 - 1.2 : 0.2 - 4.6. All polymers exhibit a very narrow molecular weight distribution (below 1.1) as shown via size exclusion chromatography. Microphase separation of the BVT terpolymers was investigated in solution through small angle X-ray scattering in THF above the order-disorder transition and in the bulk via transmission electron microscopy. Phase allocation in the latter is accomplished through selective staining of either polybutadiene with OsO_4 [22] or poly(2-vinylpyridine) with iodine. [14] The strongest incompatibility here is between the first block, polybutadiene, and the second block, poly(2-vinylpyridine) ($x_{N, BV} = 0.325$). [23] Among the morphologies obtained are for the most part lamellae and core-shell cylinders with a polybutadiene or poly(*tert*-butylmethacrylate) core and a poly(2-vinylpyridine) shell. If the content of P2VP is kept low, the shell formed around the PB cylinders is not continuous any more, like in the case of $B_{18}V_8T_{74}^{133}$. In one case for $B_{44}V_{20}T_{36}^{98}$, (the subscripts refer to the weight fraction of the corresponding block and the superscript to the overall molecular weight in kg/mol.) a coexistence of lamellae and a gyroidal structure exists. For the terpolymers forming core-shell cylinders with a polybutadiene core in the bulk, in particular $B_{16}V_{21}T_{63}^{145}$, several useful features with respect to the membrane technology could be identified in thin films studied on different substrates after controlled annealing in solvent vapor, as already reported elsewhere. [24] It could further be shown that for $B_{14}V_{18}T_{68}^{165}$ the formation of a P2VP helix around the cylindrical PB core occurs in the bulk. $B_{30}V_{14}T_{56}^{141}$ was used to generate multicompartiment micelles either in organic solvents or in aqueous systems. [25]

Moreover, the polybutadiene compartment of the terpolymers is susceptible for crosslinking reactions. Fixation of the polymer morphologies after self-assembly was achieved through UV-light induced photo-polymerization of the cast polymer films after the incorporation of a suitable crosslinking agent, Lucirin-TPO® in this case. Films of block terpolymers showing bulk morphologies suitable for the generation of novel nanostructures, $B_{18}V_8T_{74}^{133}$ and $B_{14}V_{18}T_{68}^{165}$, were cast with additional crosslinking agent. After fixation of the self-assembled structures, these

were subjected to sonication procedures. In this way, multicompartmental polymeric nanoparticles could be prepared on a gram scale. Within the scope of this work, no effect of the crosslinking procedure on the bulk morphologies is observed for different amounts of crosslinking agent in the range of 1 - 10 wt. %.

Experimental

Synthesis

The linear BVT triblock terpolymers were synthesized via sequential living anionic polymerizations of butadiene, 2-vinylpyridine and *tert*-butyl methacrylate in THF at low temperatures using *sec*-butyl lithium as initiator.^[26] All polymerizations took place in the presence of alkoxides ($c = 0.013$ mol/L, typically this corresponds to a roughly 20-fold excess compared to the concentration of growing polymer chains). 1,3-butadiene was initiated at -70°C and polymerized for 5 hours at -10°C . Subsequently, 2-vinyl pyridine was added to the stirred tank reactor via ampoules. After polymerization of the second block, the living polybutadiene-*b*-poly(2-vinylpyridine) chain ends were endcapped with 1,1-diphenylethylene (DPE) in order to attenuate the nucleophilicity of the propagating species. In that way, transfer reactions upon addition of the third monomer, *t*BMA, due to too high nucleophilicity could be suppressed.^[27, 28] During the polymerizations of the P*t*BMA block, samples were taken after different reaction times and precipitated into degassed isopropanol. Therefore we could obtain several series of BVT block terpolymers with a constant ratio of first to second block and increasing P*t*BMA content. Overall, in this work we synthesized 18 polymers with volume fractions Φ_{B} : Φ_{V} : Φ_{T} in the range of 1 : 0.4 - 1.2 : 0.2 - 4.6.

Crosslinking

Crosslinking of the as-cast and annealed polymer films was carried out with a UV-lamp for 2h (Hoenle VG UVAHAND 250 GS, cut-off at 300 nm wavelength to avoid the polymerization of the methacrylic compartment).

Structural characterization

For structural characterization films of the BVT terpolymers were cast from THF by slow evaporation of the solvent over several days. The films were afterwards dried

under vacuum at room temperature first for 24h and at 50 °C thereafter for another 24h. Subsequent annealing at elevated temperatures above the glass transition of all three blocks (130 °C) under vacuum did not lead to any change in the microdomain structure of the samples except the polymer films with high polybutadiene content. For scattering experiments in solution the polymers were dissolved at concentrations above the order-disorder transition in THF over several days. Typically, the order-disorder transition (ODT) was in the range of 26 - 30 wt. % polymer.

Ultrathin (30 - 80 nm) samples for the transmission electron microscopy (TEM) were cut from the as-cast polymer films with a Reichert-Jung Ultracut E equipped with a diamond knife. For polymer samples with a higher polybutadiene content than 30 wt. %, microtome cutting at temperatures below the glass transition of PB (-16 °C) was performed. TEM micrographs were taken on either a Zeiss CEM 902 operating at 80 kV or a LEO 922 OMEGA operating at 200 kV, both in the bright field mode. In order to selectively enhance the electron density in one of the three compartments and therefore improve the contrast the samples were stained with either OsO₄ or iodine. The latter preferentially reacts with poly(2-vinylpyridine),^[14] forming a charge-transfer complex while OsO₄ attacks the polybutadiene segments.^[22] Thus, after iodine treatment the P2VP compartments should appear darker whereas PB comprises the same after OsO₄ staining. In both cases the P*t*BMA domains are not supposed to be affected. The methacrylic compound though is deteriorated through the electron beam and therefore considerable volume shrinkage of the respective microphase domain during the TEM measurement can lead to erroneous values.^[29] The electron densities calculated for the three different compartments are as follows: $\rho_e(\text{PB}) = 0.53 \text{ mol} / \text{cm}^3$ ^[30]; $\rho_e(\text{P2VP}) = 0.611 \text{ mol} / \text{cm}^3$ and $\rho_e(\text{P*t*BMA}) = 0.561 \text{ mol} / \text{cm}^3$.^[28]

Small Angle X-Ray Scattering (SAXS)

Small angle X-ray scattering (SAXS) measurements were performed on the ID2 beamline at the European Synchrotron Radiation Facility (ESRF, Grenoble, France). The typical photon flux obtained at the ID2 sample position is 8×10^{12} photons/s, the energy bandwidth is $\Delta E / E = 2 \times 10^{-4}$. All experiments were obtained at 12.5 keV corresponding to an X-ray wavelength of 0.1 nm. The scattering intensities

were detected via a CCD camera. The detector system is housed in a 10 m evacuated flight tube. The scattering patterns were corrected for the beam stop, the background, the used cuvettes, and the solvent prior to evaluations.

Size exclusion chromatography (SEC)

Size exclusion chromatography (SEC) with THF as eluent was performed on an apparatus equipped with PSS SDVgel columns (30 x 8 mm, 5 μm particle size) with 10^2 , 10^3 , 10^4 and 10^5 Å pore sizes using RI and UV detection ($\lambda = 254$ nm) at a flow rate of 1.0 mL / min ($T = 40^\circ\text{C}$). The calibration was based on polybutadiene standards.

Matrix assisted laser desorption ionization - time of flight mass spectrometry MALDI-ToF MS

The number-averaged molecular weight of the polybutadiene precursors in each case were determined with matrix assisted laser desorption ionization - time of flight mass spectrometry (MALDI-ToF) on a Bruker Reflex III equipped with a 337 nm N_2 laser in the linear mode and 20 kV acceleration voltage. Sodium trifluoroacetate (NaTFA, Fluka, 99.5 %) was used as salt for ion formation.

Nuclear magnetic resonance spectroscopy $^1\text{H-NMR}$

$^1\text{H-NMR}$ measurements were performed on a 250 MHz Bruker AC spectrometer using CDCl_3 or THF-d_8 as solvent and tetramethylsilane (TMS) as internal standard. The molecular weights of the P2VP and the P*t*BMA block were calculated from the number-averaged molecular weight of the precursor obtained through MALDI-ToF mass spectrometry and the ratio of characteristic NMR signals. The molecular characteristics of the BVT triblock terpolymers are summarized in **Table 1**.

Dynamic light scattering (DLS)

Dynamic light scattering (DLS) measurements were performed in sealed cylindrical scattering cells ($d = 10$ mm) at a scattering angle of 90° on an ALV DLS/SLS-SP 5022F equipment consisting of an ALV-SP 125 laser goniometer with an ALV 5000/E correlator and a He-Ne laser with the wavelength $\lambda = 632.8$ nm. The CONTIN algorithm was applied to analyze the obtained correlation functions. Apparent hydrodynamic radii were calculated according to the Stokes-Einstein equation.

Ultrasound sonication treatment

Sonication treatment was performed in solution in small glass vials. The used instrument was a Branson Digital Sonifier equipped with a tungsten tip. Amplitude was kept at 20% and typical sonication times were 1 second followed by a brake of 4 seconds. Total sonication times are always the summarized seconds of real sonication without breaks. Samples were always water cooled during the sonication procedure

Table 1: triblock terpolymer characteristics

Polymer ^a	Molecular weight distribution ^b	Volume fractions ^c $\Phi_A : \Phi_B : \Phi_C$	Bulk morphology ^d
B ₄₇ V ₁₉ T ₃₄ ⁶¹ (1) ^e	1.09	1 : 0.4 : 0.7	LL
B ₃₈ V ₁₆ T ₄₆ ⁸² (1)	1.09	1 : 0.4 : 1.1	LL
B ₂₉ V ₁₂ T ₅₉ ⁸⁶ (1)	1.08	1 : 0.4 : 1.9	CYL
B ₂₂ V ₉ T ₆₉ ¹⁰⁹ (1)	1.08	1 : 0.4 : 2.9	CYL
B ₁₈ V ₈ T ₇₄ ¹³³ (1)	1.08	1 : 0.4 : 3.9	CYL ^f
B ₅₅ V ₂₆ T ₁₉ ⁷⁷ (2)	1.04	1 : 0.4 : 0.3	CYL
B ₄₄ V ₂₀ T ₃₆ ⁹⁸ (2)	1.04	1 : 0.4 : 0.8	LL / GYR
B ₃₈ V ₁₈ T ₄₄ ¹¹² (2)	1.03	1 : 0.4 : 1.1	LL
B ₃₇ V ₁₇ T ₄₆ ¹¹⁷ (2)	1.03	1 : 0.4 : 1.2	LL
B ₃₂ V ₁₅ T ₅₃ ¹³² (2)	1.02	1 : 0.4 : 1.6	LL
B ₃₀ V ₁₄ T ₅₆ ¹⁴¹ (2)	1.02	1 : 0.4 : 1.8	LL
B ₂₉ V ₁₄ T ₅₇ ¹⁴⁵ (2)	1.02	1 : 0.4 : 1.8	LL
B ₃₄ V ₁₇ T ₄₉ ¹³⁶ (3)	1.02	1 : 0.5 : 1.4	LL
B ₁₆ V ₂₁ T ₆₃ ¹⁴⁵ (4)	1.02	1 : 1.2 : 3.7	CYL
B ₁₄ V ₁₈ T ₆₈ ¹⁶⁵ (4)	1.02	1 : 1.2 : 4.6	CYL ^g
B ₅₈ V ₂₇ T ₁₅ ⁷⁸ (5)	1.03	1 : 0.4 : 0.2	CYL
B ₅₃ V ₂₄ T ₂₃ ⁸⁴ (5)	1.02	1 : 0.4 : 0.4	CYL
B ₄₉ V ₂₃ T ₂₈ ⁸⁸ (5)	1.02	1 : 0.4 : 0.5	LL

a: subscripts denoting the weight fraction of the corresponding block in % and the superscript the overall molecular weight in kg/mol, determined through a combination of THF-SEC and ¹H-NMR measurements; b: determined via THF-SEC, calibrated with 1,4-polybutadiene standards; c: calculated according to the density of the different blocks in combination with the finally

determined composition; d: determined via a combination of SAXS and TEM measurements; LL lamellar morphology; CYL hexagonally packed core-shell cylinders; GYR gyroidal motif, core-shell; e: polymers with the same number in brackets were synthesized within the same series; f: a non-continuous shell was observed for the polymer with the lowest P2VP content, $B_{18}V_8T_{74}^{133}$; g: butadiene cylinders which exhibit a P2VP helix around the core were found to be hexagonally arranged in a *P*/BMA matrix;

Results and discussion

Synthesis and characterization of the block terpolymers

All polymers were synthesized via sequential anionic polymerization in THF in the presence of alkoxides and exhibit very low molecular weight distributions. Some exemplarily THF-SEC traces for $B_{34}V_{17}T_{49}^{136}$ including the precursors and the series of $B_{58}V_{27}T_{15}^{78}$, $B_{53}V_{24}T_{23}^{84}$, and $B_{49}V_{23}T_{28}^{88}$ are shown in **Figure 1**. All obtained elution traces are monomodal. Furthermore, Figure 1C displays a MALDI-ToF MS spectrum of $B_{34}V_{17}T_{49}^{136}$.

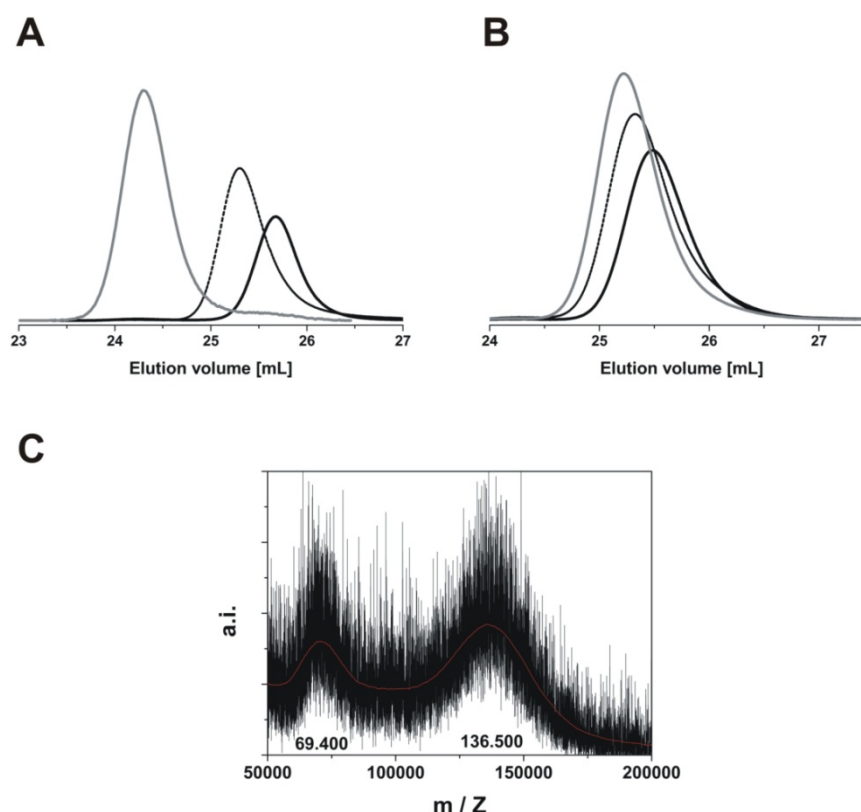


Figure 1: THF-SEC elution traces for B_{46} (solid black line), $B_{66}V_{34}^{69}$ (dashed black line) and $B_{34}V_{17}T_{49}^{136}$ (solid grey line) (A); THF-SEC elution traces for $B_{58}V_{27}T_{15}^{78}$ (solid black line), $B_{53}V_{24}T_{23}^{84}$ (dashed black line), and $B_{49}V_{23}T_{28}^{88}$ (solid grey line) (B); MALDI-ToF MS spectrum for $B_{34}V_{17}T_{49}^{136}$, the red line is a smoothed curve and a guide to the eye.

Two populations are observed in the MALDI-ToF mass spectrum. The main peak with 136.500 g/mol is the block terpolymer, the second one with 69.400 g/mol almost half and, hence, double ionized block terpolymer. Please note that mass spectrometry of block copolymers, especially at molecular weights exceeding 100.000 g/mol, is a challenging task.^[31] Double ionization most probably occurs due to the middle block, P2VP.

Structural characterization

The following chapter summarizes the results obtained for the microphase separated bulk morphologies of the synthesized BVT block terpolymers by slow casting from THF solutions. For the most samples, either lamellae or hexagonally arranged core-shell cylinders could be identified, barely $B_{44}V_{20}T_{36}$ ⁹⁸ showed coexisting lamellae and gyroidal parts. This composition in combination with examples for lamellae, $B_{30}V_{14}T_{56}$ ¹⁴¹, and hexagonally arranged helical cylinders, $B_{14}V_{18}T_{68}$ ¹⁶⁵ with B core, V helix winding around the cylindrical core, and T matrix or $B_{53}V_{24}T_{23}$ ⁸⁴ with T core, V shell, and B matrix, are discussed here in more detail. Furthermore, the block terpolymer with the lowest content of P2VP, $B_{18}V_8T_{74}$ ¹³³, is forming an incontinuous shell of P2VP around the PB core in the bulk state, rendering it interesting for the generation of multicompartiment polymeric nanoparticles. For $B_{18}V_8T_{74}$ ¹³³ and $B_{14}V_{18}T_{68}$ ¹⁶⁵, also the aggregates present in solution after crosslinking of the as-cast bulk films and subsequent sonication assisted dissolution are investigated and shown in detail. The rest of the synthesized block terpolymers mentioned in Table 1 appears only to present a complete view. It is noteworthy that $B_{44}V_{20}T_{36}$ ⁹⁸ and $B_{30}V_{14}T_{56}$ ¹⁴¹ are from the same polymer series and in an analogous way, $B_{16}V_{21}T_{63}$ ¹⁴⁵ and $B_{14}V_{18}T_{68}$ ¹⁶⁵ originate from another series as indicated by the numbers in brackets (cf. Table 1).

B₄₄V₂₀T₃₆⁹⁸: coexistence of lamellae / gyroid

According to TEM, B₄₄V₂₀T₃₆⁹⁸ shows a coexistence of two morphologies (Figure 2). Most parts of the sample, however, show lamellae, as depicted in Figure 2A. A partial gyroidal structure is shown in Figure 2B. In both cases, the dark phase corresponds to the polybutadiene compartment due to OsO₄ staining prior to the TEM measurements.

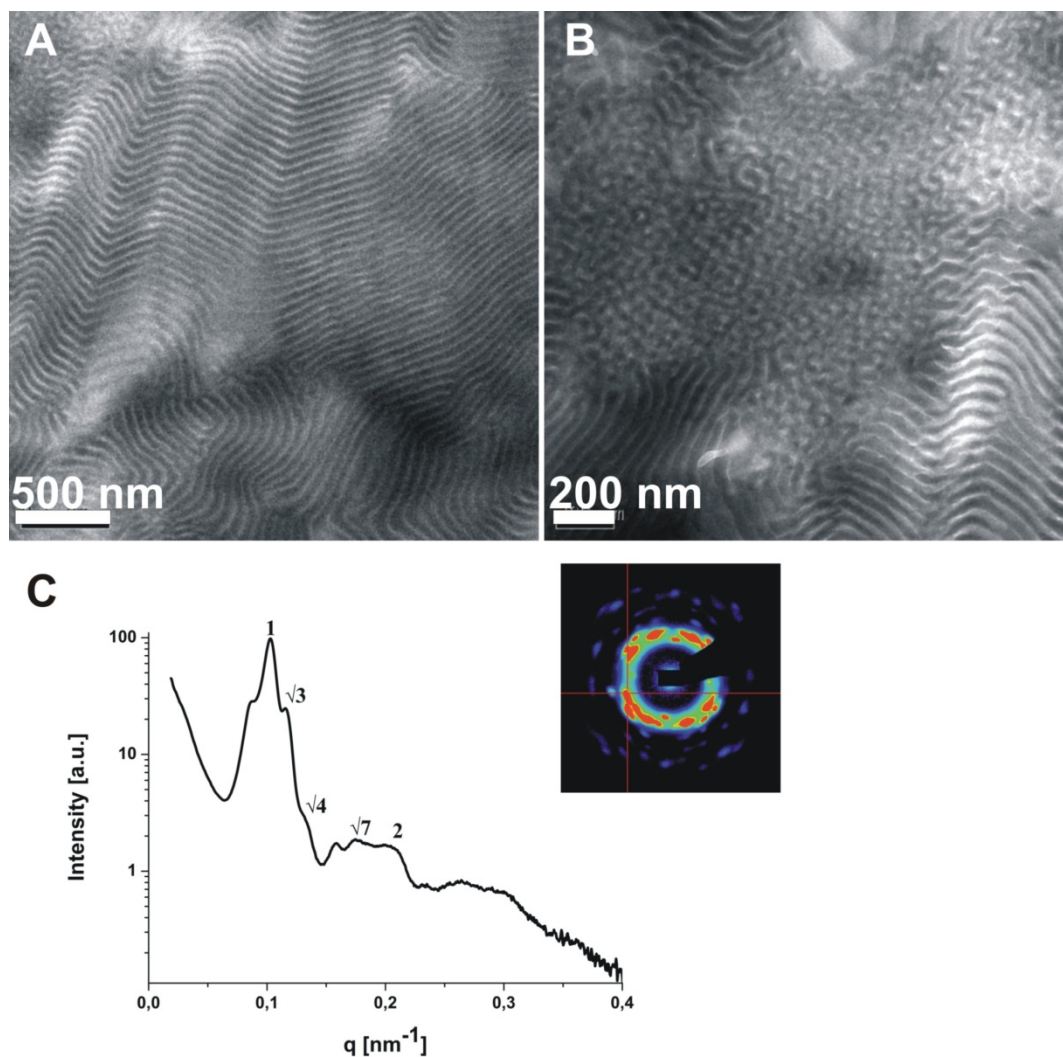


Figure 2: TEM micrographs of B₄₄V₂₀T₃₆⁹⁸ cast from THF after staining with OsO₄ (A, B); the black part corresponds to polybutadiene; SAXS pattern of B₄₄V₂₀T₃₆⁹⁸ at 35 wt.% in THF (C), the inset shows the intensity profile obtained at the detector.

Figure 2A illustrates the lamellar structure. In the upper left corner of the same TEM micrograph the transition from the lamellar into the gyroid structure is visible. A comparable location is enlarged in Figure 2B. In Figure 2C the corresponding SAXS

pattern in THF (35 wt. %) is shown, the inset shows the intensity profile obtained at the detector. It is rather complex and seems to contain reflexes of at least two miscellaneous structural motifs. The two maxima with the relative positions 1:2 are typical for a lamellar structure (reflections [001]; [002]). Besides, the reflexes with the relative positions $\sqrt{3} : \sqrt{4} : \sqrt{7}$ could be assigned to a gyroidal motif assuming that the peak at the relative position of $\sqrt{3}$ corresponds to the [211] reflection. According to the literature, the relative ratios of the maxima for a scattering pattern of a gyroidal morphology are $\sqrt{3} : \sqrt{4} : \sqrt{7} : \sqrt{10} : \sqrt{11}$ as discussed before.^[32, 33] The long period for the lamellar structure can be calculated to $d_{\text{SAXS}} = 61 \text{ nm}$ (Eq. 1). Through the assignment of the [211] reflection one can deduce the lattice pattern parameter for the gyroidal structure, $a_{\text{SAXS}} = 71 \text{ nm}$ (Eq. 2).

$$(1) d_{\text{SAXS}} = \frac{2n\pi}{q_{\text{SAXS}}} \quad (2) a_{\text{SAXS}} = \frac{2\pi\sqrt{x}}{q_{\text{SAXS}}}$$

With n being the peak order ($n = 1$ for the first peak of the lamellar pattern), q_{SAXS} being the peak value obtained from the SAXS measurement (0.102 nm^{-1} for [100] and 0.116 nm^{-1} for [211]), and x the order of the peak from the gyroid pattern, in this case $x = \sqrt{3}$ due to $hkl = [211]$. It is well-known that the interpretation of SAXS patterns from ABC triblock terpolymers bears much more complexity than for simple AB diblock copolymers. Here, the relative electron densities affect both scattering contrast and the relative scattering intensities, producing SAXS patterns where certain reflexes can be nearly extinguished.^[34] Hence, the pattern shown in Figure 2C for $B_{44}V_{20}T_{36}$ ⁹⁸ may not exhibit all the relevant reflexes necessary for a complete assignment of a gyroidal motif. Unfortunately, the signal to noise ratio in Figure 2C strongly diminishes at $q > 0.3 \text{ nm}^{-1}$, making it difficult to assign any further peaks. According to the volume / weight fractions of the three building blocks, we assume a poly(2-vinylpyridine) core with a poly(*tert*-butyl methacrylate) shell for the gyroidal motif embedded in a polybutadiene matrix.

B₃₀V₁₄T₅₆¹⁴¹: lamellae

An increase of the P*t*BMA volume fraction within this terpolymer series to $\Phi_B : \Phi_V : \Phi_T = 1 : 0.4 : 1.8$ leads to a complete lamellae formation in the bulk. This is illustrated in Figure 3. The TEM micrograph (Figure 3A) depicts uniformly aligned lamellae in a micron sized range. The dark part (central lamella) in Figure 3B corresponds to the polybutadiene compartment, stained through the treatment with OsO₄ and flanked by smaller grey poly(2-vinylpyridine) microdomains on each side. The light parts represent the poly(*tert*-butyl methacrylate). As mentioned earlier, the microdomain dimensions from TEM do not necessarily coincide with the calculated volume fractions, caused through the electron beam damage of the methacrylic phase. Hence, the P*t*BMA domains are not significantly larger than the PB compartments, although the volume fraction is almost the double. It has been reported that methacrylic domains may shrink to less than half of the expected value in that way.^[35]

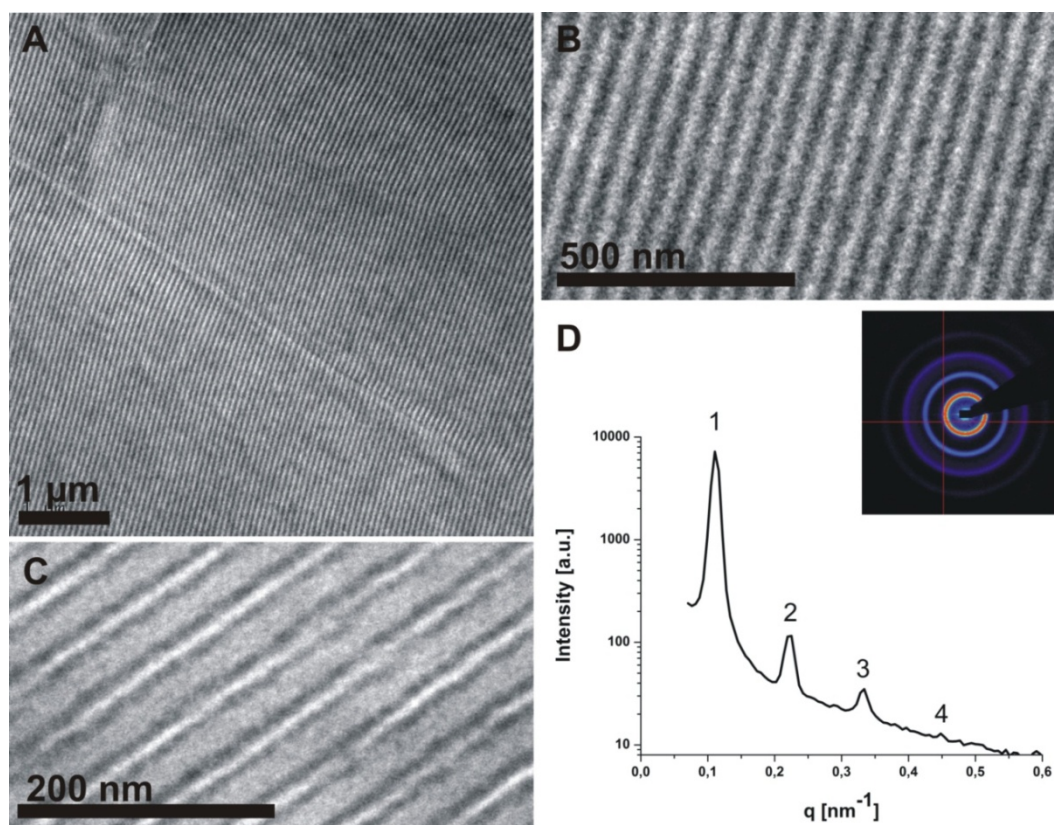


Figure 3: TEM micrographs of B₃₀V₁₄T₅₆¹⁴¹ cast from THF after staining with OsO₄ (A, B); the black phase resemble polybutadiene; after staining with iodine, the dark parts resemble P2VP (C), scale bar corresponds to 200 nm; SAXS pattern of B₃₀V₁₄T₅₆¹⁴¹ at 35 wt.% in THF (C), the inset shows the intensity profile obtained at the detector.

Figure 3C shows a TEM micrograph after staining with iodine. Here, the dark domains correspond to P2VP. The ll morphology can be nicely seen. Two parallel dark P2VP domains are adjacent to a lighter PB lamella. The lightest parts again are P*t*BMA, which is not at all affected through the staining procedure. The long periods obtained from TEM are around 60 nm in both cases. In Figure 3D the SAXS pattern in solution (35 wt. % in THF) is depicted, the inset shows the intensity profile at the detector of the beamline. The lamellar morphology is again confirmed and the characteristic peaks for such structural motifs at integer multiples of the first order peak are visible. The relative reflex positions 1 : 2 : 3 : 4 are related to the [100] : [200] : [300] : [400] reflections. From the SAXS measurements, the long period was calculated to $d_{\text{SAXS}} = 57 \text{ nm}$ (cf. Eq. 1 above, with $q_{\text{SAXS}} = 0.111 \text{ nm}^{-1}$ for [100]) and is in good agreement with the results obtained from TEM.

$\text{B}_{18}\text{V}_8\text{T}_{74}^{133}$: core shell cylinders with a non continuous shell

The terpolymer with the lowest content of P2VP, 8 %, exhibits a core-shell cylindrical morphology. The hexagonal arrangement, although slightly distorted, is shown in **Figure 4A**, the corresponding FFT pattern in the inset, **Figure 4B**. In the enlargement, **Figure 4C**, it can be seen that the cylinders are slightly ill-shaped. To our opinion, the low content of P2VP results in the formation of a non-continuous shell around the PB core. This then results in the generation of an additional interface between PB and P*t*BMA, although, according to the block sequence, these compartments are not directly interconnected. In **Figure 4D** the microtome cut has been stained with iodine, enhancing the electron density in the P2VP phase. Here, the disrupted nature of the P2VP shell is more evident, as it appears darker. Several, unconnected black dots are surrounding the PB cylindrical core.

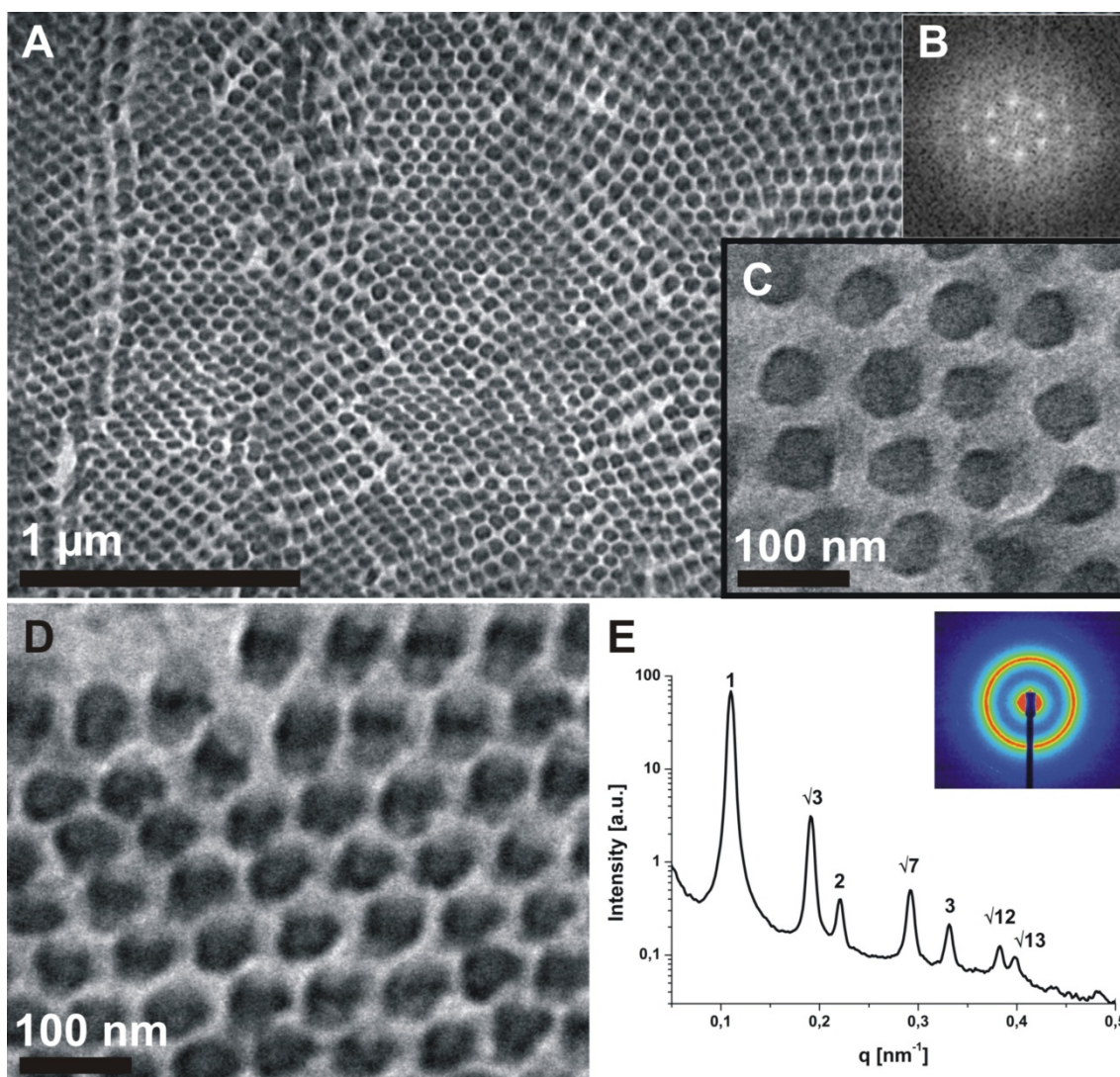


Figure 4: TEM micrographs of $B_{18}V_8T_{74}^{133}$ cast from THF after staining with OsO_4 (A); the black phase resembles PB; the inset (B) shows a FFT pattern obtained from A; enlargement from A (C); TEM micrograph of $B_{18}V_8T_{74}^{133}$ cast from THF after staining with iodine (D), the black phase shows P2VP; SAXS pattern of $B_{18}V_8T_{74}^{133}$ at 35 wt.% in THF (E), the inset shows the intensity profile obtained at the detector.

The formation of an additional interface between first and end-block of block terpolymers upon drastically reducing the volume fraction of the middle block has already been reported before.^[36] If the x-parameters for the BVT block terpolymers are compared, $x_{BT} = 0.01$, $x_{BV} = 0.13-0.26$, and $x_{BV} = 0.325$,^[37, 38] PB and P*t*BMA are supposed to show the lowest incompatibility. Moreover, PB and P2VP should avoid each other most. Therefore, it seems possible that the breaking up of an existing continuous P2VP shell reduces the interfacial tension of the whole system even though a new interface between PB and P*t*BMA is generated. The SAXS pattern of

$B_{18}V_8T_{74}^{133}$ in THF (35 wt. %) is shown in Figure 4E. The inset displays the intensity profile obtained at the detector. All important reflections for hexagonally arranged cylinders are present and could be successfully assigned, [100], [110], [200], [210], [300], [220], and [310]. Calculation of the long period from the SAXS pattern results in $d_{SAXS} = 67$ nm (Eq. 3).

$$(3) L = \frac{d_{SAXS}}{\sin(60^\circ)} = \frac{2}{\sqrt{3}} d_{SAXS}$$

With d_{SAXS} calculated according to Eq. 1. A further evaluation gives rise to the cylinder radius, $R_{Cyl} = 20$ nm. From TEM, the cylinder radius was estimated to be slightly larger, $R_{Cyl} = 25$ nm, probably due to distortion of the structure occurring during the microtome cutting. Besides that, both TEM and SAXS confirm the formation of a hexagonally packed cylindrical structure.

To further elucidate the structure of this P2VP shell, the PB core of the cylinders was crosslinked in the bulk. Therefore, films with up to 10% UV crosslinking agent, Lucirin-TPO®, were cast from THF and exposed to UV-light for 2h afterwards. Subsequent swelling and further sonication of the polymer films in THF lead to dissolution of the self-assembled structures. Soxhlett extraction of the crosslinked polymer samples with THF was used to estimate the degree of crosslinking, around 75 % in this case. These were then drop-coated onto carbon-coated grids and analyzed via TEM. Also dynamic light scattering (DLS) was performed to assess the average size of the particles in dependence of the sonication time. The results are shown in **Figure 5**.

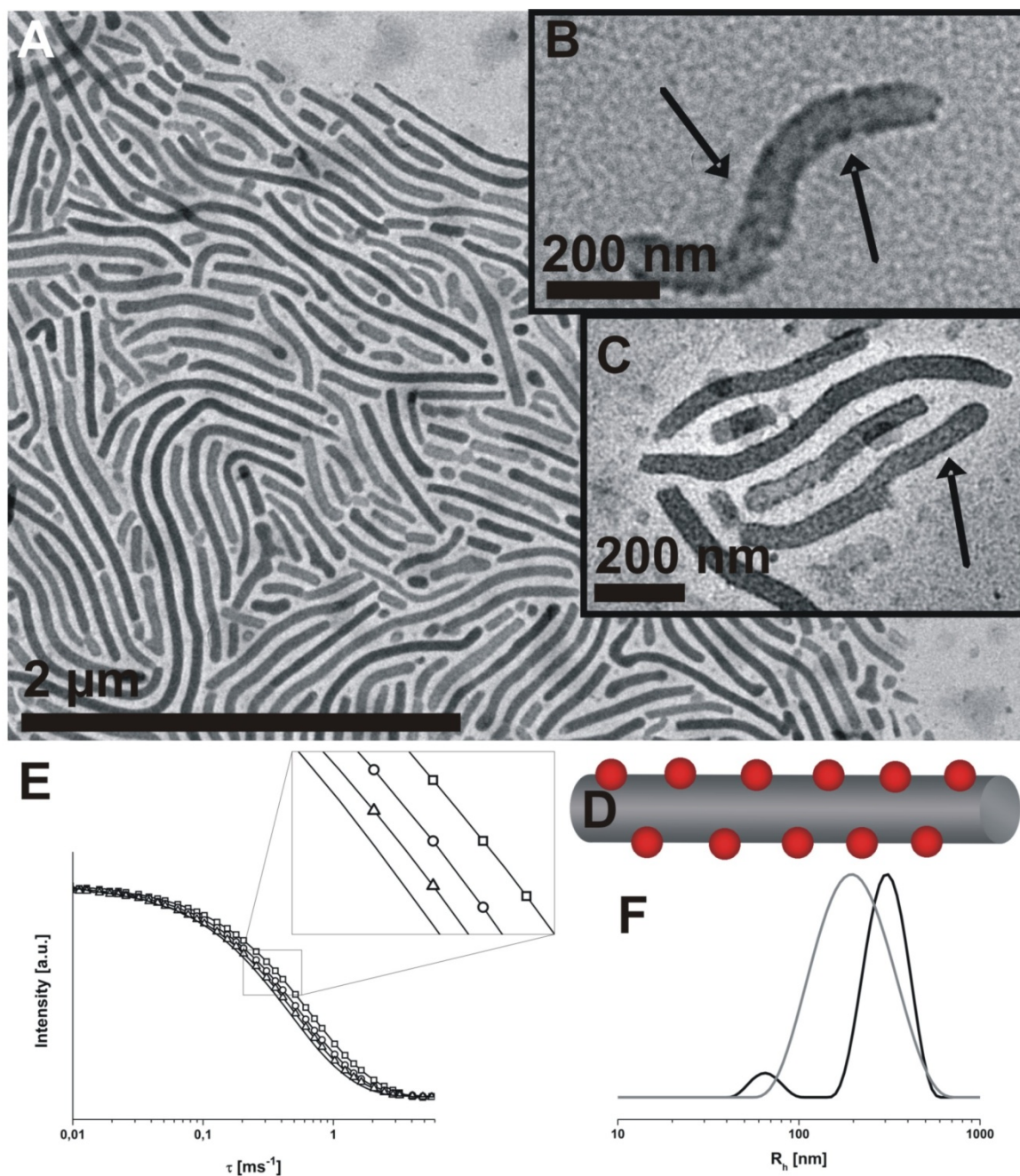


Figure 5: TEM micrograph for $B_{18}V_8T_{74}^{133}$ after 10 minutes sonication and drop-coating onto a TEM grid (A); enlargement of one single cylinder (B); enlargement of several cylinders after staining with iodine (C); schematic drawing of the proposed bulk structure, PB cylinder (grey) bearing P2VP spheres (red) embedded in a P β BMA matrix (D); DLS autocorrelation functions for $B_{18}V_8T_{74}^{133}$ after crosslinking in the bulk and subsequent sonication in THF for 1 (-□-), 3 (-○-), 5 (-△-), and 10 minutes (solid black line) (E), the inset shows a zoom of the relevant region; DLS CONTIN plots at $\Theta = 90^\circ$ for $B_{18}V_8T_{74}^{133}$ cylinders in THF after sonication for 1 (solid black line, $\langle R_h \rangle_z = 65$ and 310 nm) and 10 minutes (solid grey line, $\langle R_h \rangle_z = 185$ nm) (F).

In Figure 5A a TEM micrograph of $B_{18}V_8T_{74}^{133}$ cylinders deposited from THF solution after 10 minutes sonication is depicted. The cylinders are very uniform in diameter but show a rather large length distribution due to the sonication process. The

diameter measured via TEM in this case is around 75 nm, significantly larger than via calculation from d_{SAXS} . This is due to swelling of the partially crosslinked structure in THF, a good solvent for all the three blocks. In Figure 5B and C enlargements of the same sample are displayed. Here, the non-continuous P2VP shell is more evident. Especially in Figure 5B, a rather random distribution of small black dots along the cylinder can be seen. We suppose that these are spherical P2VP domains located on the PB cylinder. Through the dissolution in THF, P2VP also swells and, in some cases, this may lead to a partially continuous corona and a tubular appearance of the polymeric cylinders, as displayed in Figure 5C, despite the low volume fraction of the middle block. Together with the results presented in Figure 4, we propose the following bulk morphology for $B_{18}V_8T_{74}^{133}$, depicted in Figure 5D: hexagonally arranged PB cylinders (grey) covered by P2VP spheres (red) embedded in a *Pt*BMA matrix. Figure 5E shows the DLS autocorrelation functions after different sonication times. A clear shift with increasing sonication towards lower decay times is observable. The corresponding CONTIN plots at $\Theta = 90^\circ$ for 1 (solid black line) and 10 minutes (solid grey line) are displayed in Figure 5F. In the beginning, after 1 minute sonication, hydrodynamic radii of 65 and 310 nm are observed. After 10 minutes sonication this is decreasing to a single, although far broadened, peak at $\langle R_h \rangle_z = 185$ nm. The broadening can be explained through the rather harsh sonication treatment.

$B_{14}V_{18}T_{68}^{165}$: P2VP helix around hexagonally arranged PB cylinders

The terpolymer with a rather high content of *Pt*BMA, $\Phi_B : \Phi_V : \Phi_T = 1 : 1.2 : 4.6$, also exhibits a core-shell cylindrical morphology, as illustrated in Figure 6. The dark phase represents polybutadiene, the core of the cylinders, due to the OsO_4 staining (Figure 6A). The grey compartments correspond to the surrounding poly(2-vinylpyridine) shell and the light parts show poly(*tert*-butyl methacrylate), the matrix. As for the other BVT terpolymer morphologies discussed here, the *Pt*BMA compartment suffers from considerable shrinkage caused through radiation damage. The inset, Figure 6B, shows a FFT pattern from Figure 6A, confirming the hexagonal arrangement of the cylinders. Figure 6C presents an “on-top” view onto

the cylinders heads, being slightly distorted. Here, the microtome cut has been stained with iodine, which enhances the electron density in the P2VP shell.

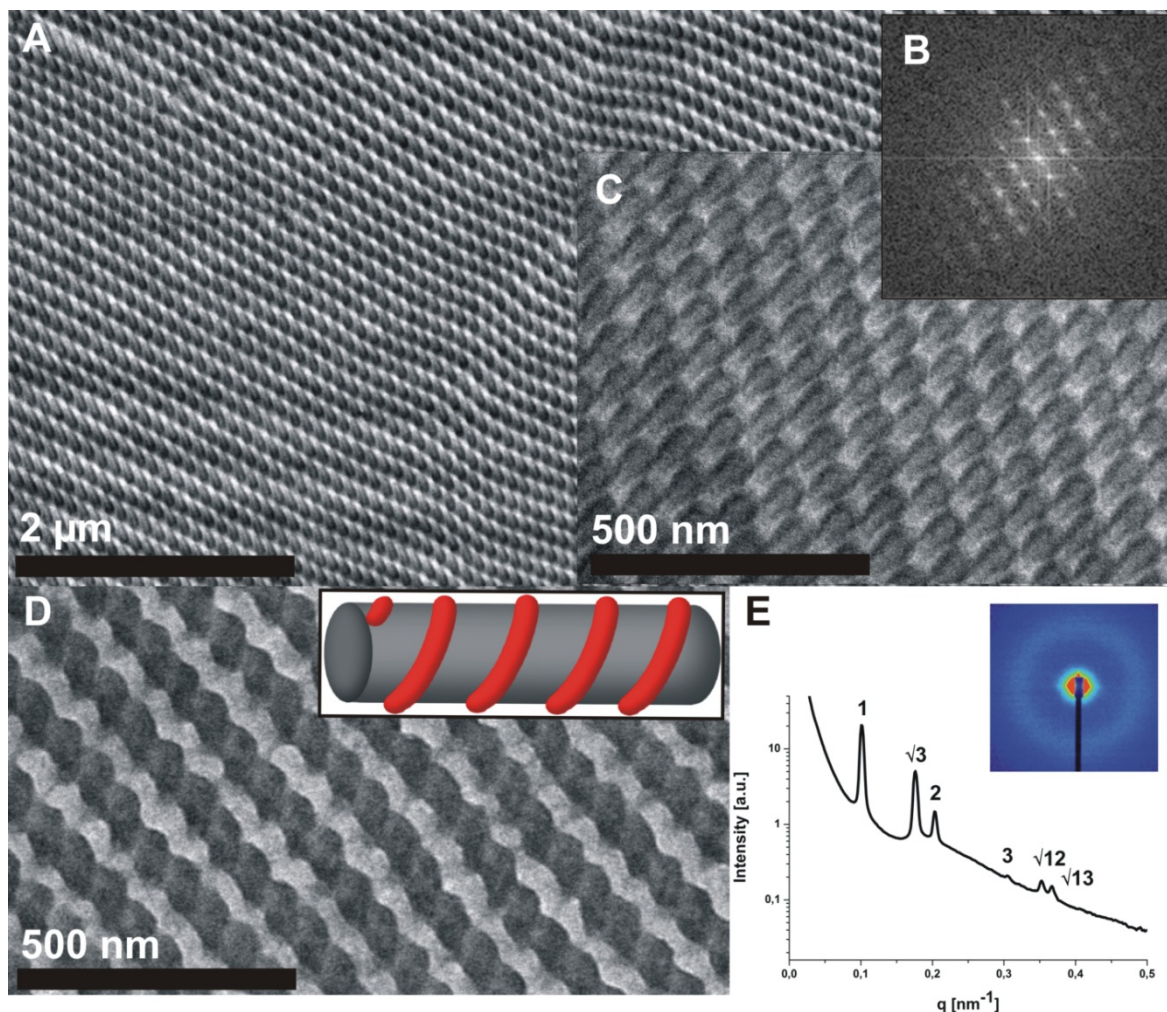


Figure 6: TEM micrographs of $B_{14}V_{18}T_{68}^{165}$ cast from THF after staining with OsO_4 (A); the black phase resembles PB; the inset (B) shows a FFT pattern obtained from A; TEM micrograph of $B_{14}V_{18}T_{68}^{165}$ cast from THF after staining with iodine (C), the black phase shows P2VP; Side-view onto the cylinders, the inset depicts what we suppose is the bulk morphology, PB cylinders (grey) carrying a P2VP helix (red) embedded in a *Pt*BMA matrix (D); SAXS pattern of $B_{14}V_{18}T_{68}^{165}$ at 35 wt.% in THF (E), the inset shows the intensity profile obtained at the detector.

A dark grey “horse-shoe” around each of the PB cylinders is observed in Figure 6C. Surprisingly, the P2VP shell is not continuous, which would result in the formation of a complete ring around the PB compartment. In Figure 6D a side-view of the cylinders is presented, also stained with iodine for a better visualization of the P2VP part. Clearly, the formation of a P2VP helix can be seen. Although, from this image, all presented helices seem to be right-handed, typically a mixture of both left- and right-handed species was found. The finding of a non-continuous shell around the PB core and therefore the generation of an additional interface

between PB and P*t*BMA can be explained like before (3.2.3.). The difference here is that the P2VP block is somewhat longer, resulting in a higher volume fraction. Helical or chiral morphologies have been reported before for SBM block terpolymers.^[36, 39] Here, a double-helical morphology containing PS cylinders with a PB helix around them embedded in a PMMA matrix were observed. The inset in Figure 6D displays the proposed bulk structure in this case, a grey PB cylinder coated with a red P2VP helix. The SAXS pattern from THF solution (35 wt. %) is shown in Figure 6E. The scattering maxima appear at relative positions of $1 : \sqrt{3} : 2 : 3 : \sqrt{12} : \sqrt{13}$ which correspond to the [100], [110], [200], [300], [220] and [310] reflections of a hexagonal cylindrical structure. The [210] peak is missing. Calculation of the long period from the SAXS pattern (cf. 3.2.3.) results in $d_{\text{SAXS}} = 72$ nm. A further evaluation gives rise to the cylinder diameter, $R_{\text{Cyl}} = 21$ nm (cf. Equation 3). From TEM, the cylinder radius was estimated to be slightly larger, $R_{\text{Cyl}} = 25$ nm.

To further elucidate the structure of these cylinders in the bulk, the PB core of the cylinders was crosslinked like shown before for $B_{18}V_8T_{74}^{133}$. Again, films were cast with additional 10% UV crosslinking agent, Lucirin-TPO®, from THF and exposed to UV-light for 2h afterwards. **Figure 7** summarizes the DLS and TEM results.

In Figure 7A a TEM micrograph of $B_{14}V_{18}T_{68}^{165}$ cylinders deposited from THF solution after crosslinking with 10% TPO and subsequent sonication for 5 minutes is shown. Again, the cylinders are rather uniform in diameter but show a rather large length distribution. The helical morphology cannot be definitely confirmed, although the cylinders do not exhibit an homogeneous surface. Here, the diameter measured via TEM is around 100 nm, almost deviating by a factor of 2 from the SAXS results. This can be attributed to the swelling of the partially crosslinked cylindrical core in THF. Figure 7B shows the DLS autocorrelation functions after different sonication times. The decay times shift with increasing sonication towards lower values. The corresponding CONTIN plots at $\Theta = 90^\circ$ for 5 (-□-), 10 (-○-), and 15 minutes (-Δ-) are displayed in Figure 7C. After 5 minutes sonication a value for $\langle R_h \rangle_z$ of 205 nm was obtained. Surprisingly, the population shows a quite narrow distribution ($\text{PDI}_{\text{DLS}} = 1.08$). After 10 minutes sonication, $\langle R_h \rangle_z = 145$ nm, and after 15 minutes $\langle R_h \rangle_z = 130$ nm were measured. Again, sonication results in a certain broadening of the CONTIN plots.

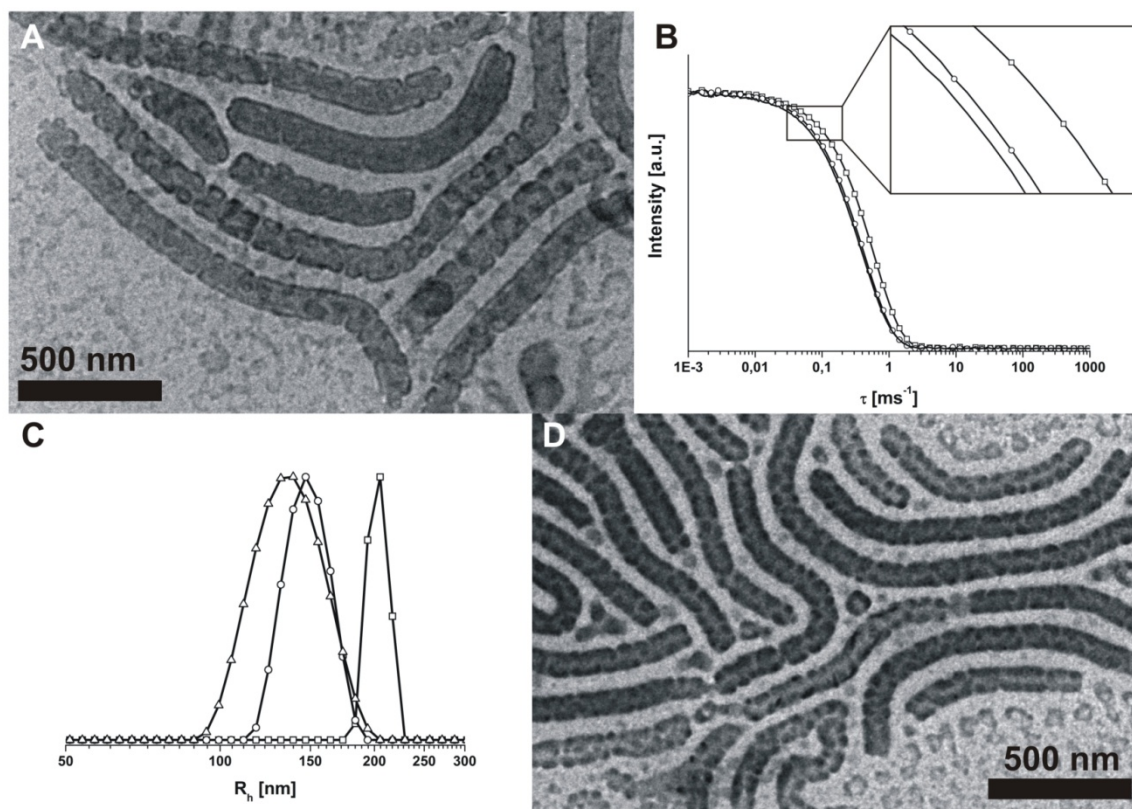


Figure 7: TEM micrograph for $B_{14}V_{18}T_{68}^{165}$ after 5 minutes sonication and drop-coating onto a TEM grid (A); DLS autocorrelation functions for $B_{14}V_{18}T_{68}^{165}$ after crosslinking in the bulk and subsequent sonication in THF for 5 (-□-), 10 (-○-), and 15 minutes (solid black line) (B), the inset shows a zoom of the relevant region; DLS CONTIN plots at $\Theta = 90^\circ$ for $B_{14}V_{18}T_{68}^{165}$ cylinders in THF after sonication for 5 (-□-, $\langle R_h \rangle_z = 205$ nm), 10 (-○-, $\langle R_h \rangle_z = 145$ nm), and 15 minutes (-△-, $\langle R_h \rangle_z = 130$ nm) (C); TEM micrograph for the same sample as (A) after staining with iodine (D).

Figure 7D shows basically the same sample like Figure 7A after staining with iodine. Dark, round spots with a diameter of approximately 15-20 nm are present on the PB core of the cylinders, representing the P2VP compartments. Obviously, upon contact with THF, a good solvent for P2VP, the helices swell and upon deposition of the cylinders onto the TEM grid the polymer chains collapse again into spherical domains. Nevertheless, these cylindrical nanoparticles could serve as interesting multicompartamental templates for the generation of hybrid structures.

$B_{58}V_{27}T_{15}^{78}$: inverted core shell cylinders

The previously discussed terpolymer, $B_{14}V_{18}T_{68}^{165}$, was also tested as a precursor for the fabrication of thin-film composite membranes.^[24] Nicely ordered arrays of core-shell cylinders aligned perpendicular to the surface on various substrates could be produced. However, the removal of the polybutadiene core of these thin-film structures to generate porous structures is not so straightforward. It is therefore of

interest to invert the structure, resulting in a polybutadiene matrix with embedded cylinders consisting of a P*t*BMA core and a P2VP shell. The genuine advantage would be that the cylinder cores could be easily removed through UV-induced depolymerization of the P*t*BMA, giving access to porous materials with pH-responsive (P2VP) pore walls. Thus, a polymer series with volume fractions $\Phi_B : \Phi_V : \Phi_T = 1 : 0.4 : 0.2 - 0.5$ has been synthesized. As mentioned in Table 1, both $B_{58}V_{27}T_{15}^{78}$ and $B_{53}V_{24}T_{23}^{84}$ show hexagonally packed cylinders with a P*t*BMA core although only $B_{58}V_{27}T_{15}^{78}$ is discussed here in more detail. TEM images for this block terpolymer cast from THF and stained with iodine as well as SAXS data are shown in Figure 8.

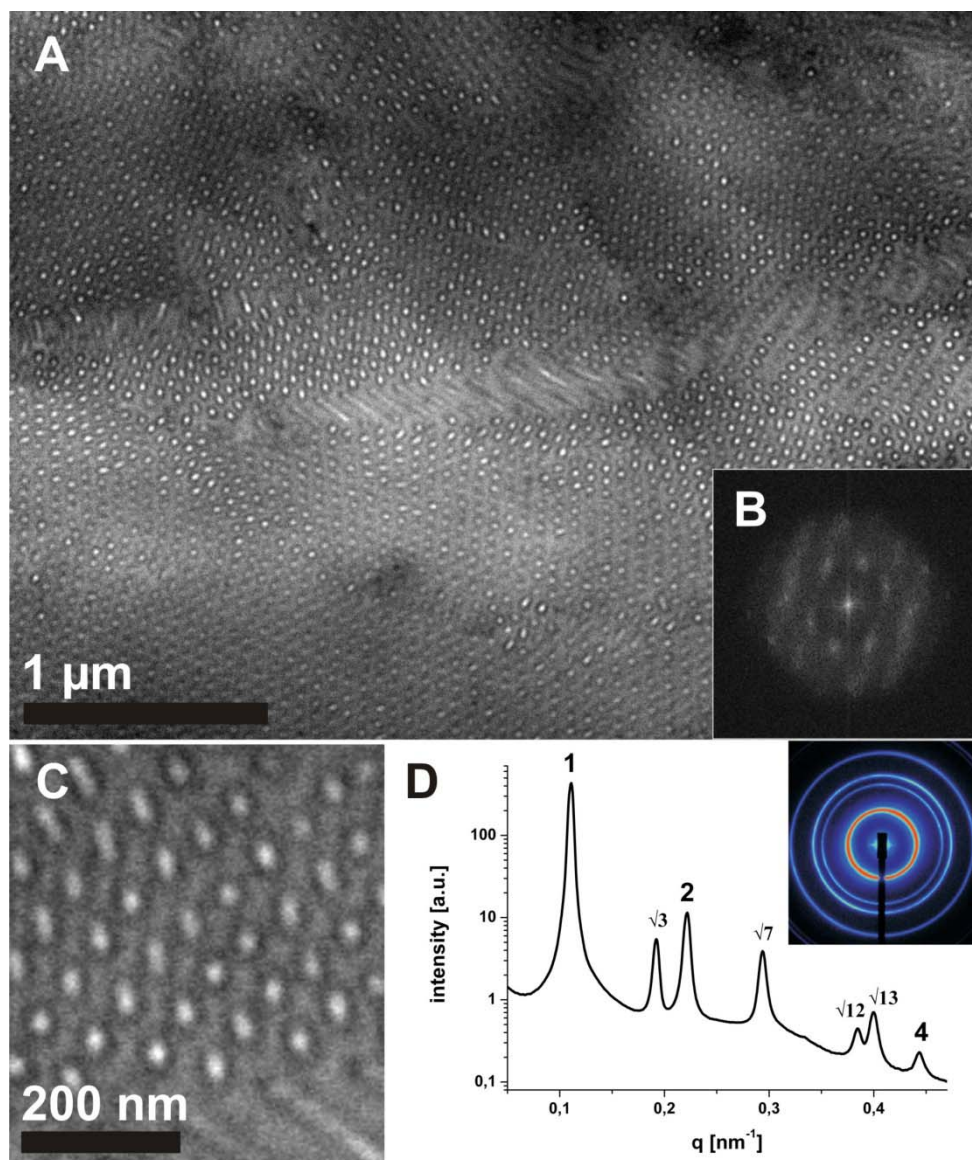


Figure 8: TEM micrographs of $B_{58}V_{27}T_{15}^{78}$ cast from THF after staining with iodine (A, C); the black phase resembles P2VP; scale bar corresponds to 1 μm (A) and 200 nm (C); the inset (B) shows a FFT pattern obtained from A; SAXS pattern obtained from $B_{58}V_{27}T_{15}^{78}$ at 30 wt. % in THF (D), the inset shows the intensity profile at the detector.

In Figure 8A an “on-top” view onto the cylinders is shown. Clearly, a hexagonal pattern can be observed. This is highlighted in the FFT in Figure 8B. Figure 8C displays an enlargement where the cylinder fine structure can be seen. The light core of the cylinders is P*t*BMA, already deteriorated through the incident electron beam. The dark ring resembles the P2VP shell, darkened through the staining treatment with iodine, surrounded by the grey PB matrix. If measured via TEM, the long period for this hexagonally packed morphology is 55 nm and the average cylinder diameter is 40 nm (20 nm for the P*t*BMA core and 2 x 10 nm for the P2VP shell). It is apparent that the as-cut films are rather strongly bended and distorted as a result of the high polybutadiene content. Microtome cutting had to be performed at low temperatures (-30 °C) to reduce the softness of the material. The SAXS pattern from THF solution (30 wt. %) is shown in Figure 8D. The scattering maxima appear at relative positions of 1 : $\sqrt{3}$: 2 : $\sqrt{7}$: $\sqrt{12}$: $\sqrt{13}$: 4 which correspond to the [100], [110], [200], [210], [220], [310] and [400] reflections of a hexagonal cylindrical structure. Calculation of the long period from the SAXS pattern results in $d_{\text{SAXS}} = 64$ nm (Eq. 3) and is in good agreement with the values obtained via TEM measurements.

Phase Diagram for BVT Block Terpolymers

The results from the previous chapters are summarized in a ternary phase diagram (Figure 9). The terpolymers discussed within the scope of this manuscript are highlighted (red circles) and their proposed bulk morphologies are schematically depicted around the phase diagram. Within each polymer series the grey arrow indicates an increasing volume fraction of P*t*BMA.

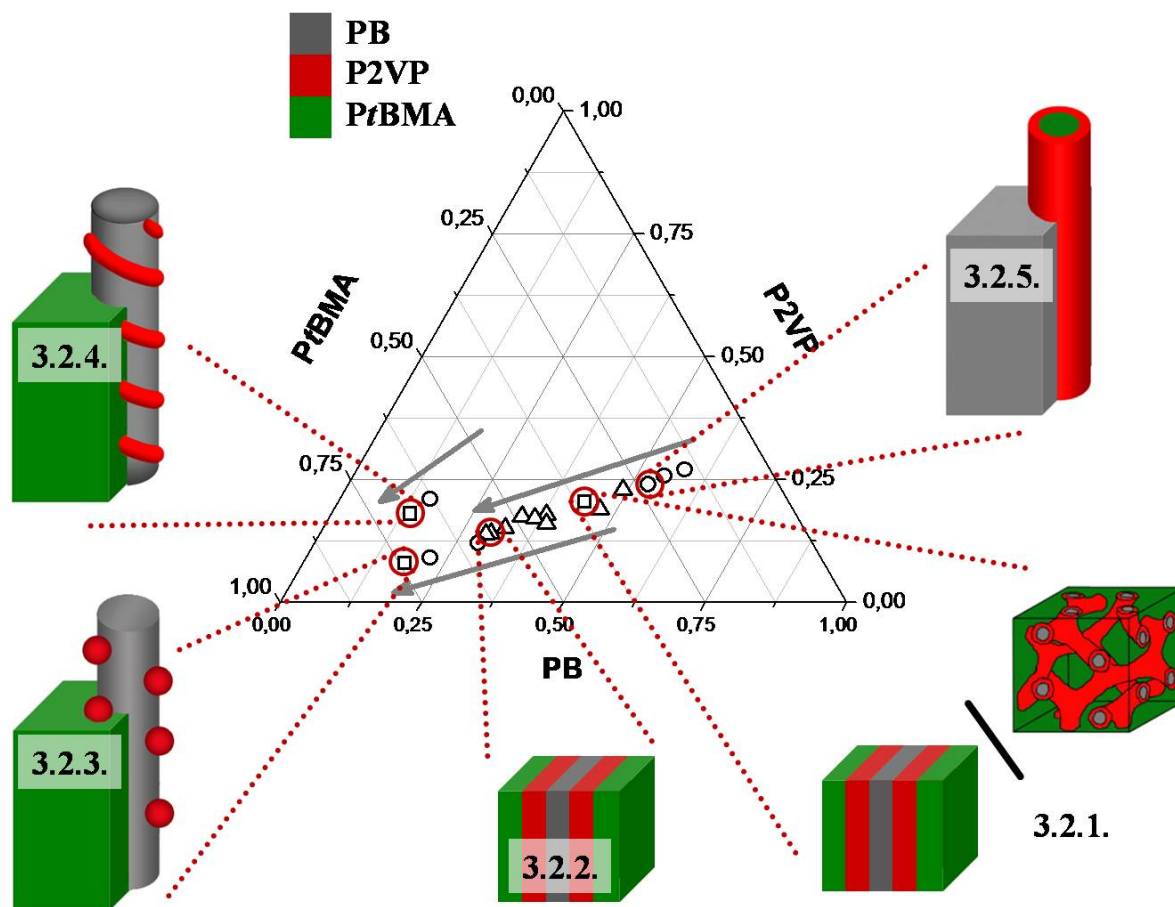


Figure 9: Ternary phase diagram obtained for several series of BVT block terpolymers, the grey phase resembles polybutadiene, the red phase poly(2-vinylpyridine), and the green phase poly(*tert*-butyl methacrylate; morphologies are lamellar (Δ), cylindrical (\circ), or either mixtures (3.2.1.) or unusual structures (spheres on cylinders 3.2.3. or helices on cylinders 3.2.4.).

Open spheres resemble cylindrical morphologies, open triangles lamellar structures. All non-typical examples are represented by open rectangles: the helical morphology for $B_{14}V_{18}T_{68}^{165}$ (3.2.5.), the cylinders with a non-continuous shell for $B_{18}V_8T_{74}^{133}$ (3.2.4.), and the coexisting between lamellae and gyroid for $B_{44}V_{20}T_{36}^{98}$ (3.2.1.). In Table 1 the different block terpolymers of one series are marked by the numbers in brackets. Within series 1, the morphology changes from LL for $B_{47}V_{19}T_{34}^{61}$ and $B_{38}V_{16}T_{46}^{82}$ to hexagonally arranged core-shell cylinders, PB core and P2VP shell for $B_{29}V_{12}T_{59}^{86}$, $B_{22}V_9T_{69}^{109}$, and $B_{18}V_8T_{74}^{133}$. The content of P2VP for $B_{29}V_{12}T_{59}^{86}$ and $B_{22}V_9T_{69}^{109}$ is still high enough to form a continuous shell. For $B_{18}V_8T_{74}^{133}$, this is not the case. The lowest content of P2VP, 8 wt. %, results in the formation of spherical domains situated on the PB core of the cylinder. For series

2, the high butadiene content of $B_{55}V_{26}T_{19}$ ⁷⁷ leads to the formation of P*t*BMA cylinders with a P2VP shell in a PB matrix. With increasing P*t*BMA content, a mixed volume structure consisting of lamellae and a gyroidal motif was found for $B_{44}V_{20}T_{36}$ ⁹⁸ (3.2.1.). Higher volume fractions of P*t*BMA resulted in the formation of purely lamellar morphologies for $B_{38}V_{18}T_{44}$ ¹¹², $B_{37}V_{17}T_{46}$ ¹¹⁷, $B_{32}V_{15}T_{53}$ ¹³², $B_{30}V_{14}T_{56}$ ¹⁴¹ (3.2.2.), and $B_{29}V_{14}T_{57}$ ¹⁴⁵. Same accounts for the only block terpolymer of series 3, $B_{34}V_{17}T_{49}$ ¹³⁶. For series 4, hexagonally arranged core-shell cylinders with a PB core and a P2VP shell are obtained for $B_{16}V_{21}T_{63}$ ¹⁴⁵. The cylindrical arrangement of the PB segments is also present in the case of $B_{14}V_{18}T_{68}$ ¹⁶⁵ although here the middle block forms a helix along the PB cylinders. For the last series, 5, inverted core shell cylinders with a P*t*BMA core and a P2VP shell are obtained for $B_{58}V_{27}T_{15}$ ⁷⁸ and $B_{53}V_{24}T_{23}$ ⁸⁴. Upon further increasing the P*t*BMA volume fraction, a lamellar morphology is found for $B_{49}V_{23}T_{28}$ ⁸⁸.

Conclusion

Several series of polybutadiene-*block*-poly(2-vinylpyridine)-*block*-poly(*tert*-butylmethacrylate) (BVT) block terpolymers have been synthesized and exhaustively characterized. Among the morphologies obtained are lamellar (LL), cylindrical (C \perp), a mixture of gyroidal and lamellar (GYR/LL), and cylindrical morphologies with a noncontinuous P2VP shell (spheres on cylinders for $B_{18}V_8T_{74}$ ¹³³ and helices on cylinders for $B_{14}V_{18}T_{68}$ ¹⁶⁵). Especially the latter two block terpolymers were shown to be very interesting precursors for the generation of novel multicompartmental core-crosslinked polymeric cylindrical polymeric nanoparticles. For this, a sonication-assisted pathway developed in our group has been adopted and it could be demonstrated that the size of the generated nanoparticles can be tuned by the sonication time in a fashionable way. The results presented here in combination with earlier work nicely show that the BVT system provides a suitable platform for the preparation of advanced and sophisticated nanostructured systems in the bulk, in solution, and in thin films.

Acknowledgements

The authors would like to thank Dr. Holger Schmalz and Denise Danz for help during the synthesis of the polymers and for MALDI-ToF measurements. Dr. Kristin Schmidt and Heiko Schoberth are acknowledged for SAXS measurements on beamline ID2 in Grenoble. We thank Markus Drechsler for some TEM measurements and Katharina and Benjamin Schatz for help with the illustrations. We also thank Sabine Wunder for performing SEC measurements. Financial support was received from the Volkswagen foundation in the framework of the “complex materials” programme. The crosslinking agent, Lucirin-TPO®, was kindly provided by BASF.

References:

- [1] M. Lazzari, M. A. Lopez-Quintela, *Adv. Mater.* **2003**, *15*, 1583.
- [2] N. Hadjichristides, S. Pispas, *Adv. Polym. Sci.* **2006**, *200*, 37.
- [3] M. A. Hillmyer, *Nanoporous materials from block copolymer precursors*, Vol. 189, Springer-Verlag Berlin Heidelberg, **2005**.
- [4] H. Li, W. T. S. Huck, *Curr. Opin. Solid State Mater. Sci.* **2002**, *6*, 3.
- [5] K. Ishizu, K. Tsubaki, A. Mori, S. Uchida, *Prog. Polym. Sci.* **2003**, *28*, 27.
- [6] R. Francis, B. Lepoittevin, D. Taton, Y. Gnanou, *Macromolecules* **2002**, *35*, 9001.
- [7] H.-A. Klok, S. Lecommandoux, *Adv. Mater.* **2001**, *13*, 1217.
- [8] G. Liu, J. Ding, S. Stewart, *Angew. Chem. int. Ed.* **1999**, *38*, 835.
- [9] J. D. Guojun Liu, T. Hashimoto, K. Kimishima, F. M. Winnik, S. Nigam, *Chem. Mater.* **1999**, *11*, 2233.
- [10] V. Abetz, P. F. W. Simon, *Phase Behavior and morphologies of block copolymers*, Vol. 189, Springer-Verlag Berlin Heidelberg, **2005**.
- [11] N. Hadjichristidis, M. Pitsikalis, H. Iatrou, *Synthesis of block copolymers*, Vol. 189, Springer-Verlag Berlin Heidelberg, **2005**.
- [12] K. Jung, V. Abetz, R. Stadler, *Macromolecules* **1996**, *29*, 1076.
- [13] R. Stadler, C. Auschra, J. Beckmann, U. Krappe, I. Voigt-Martin, L. Leibler, *Macromolecules* **1995**, *28*, 3080.
- [14] H. Hückstädt, A. Göpfert, V. Abetz, *Macromol. Chem. Phys.* **2000**, *201*, 296.
- [15] H. Hückstädt, A. Göpfert, V. Abetz, *Polymer* **2000**, *41*, 9089.
- [16] U. Krappe, R. Stadler, I. Voigt-martin, *Macromolecules* **1995**, *28*, 4558.
- [17] U. Breiner, U. Krappe, E. L. Thomas, R. Stadler, *Macromolecules* **1998**, *31*, 135.
- [18] S. Brinkmann, R. Stadler, E. L. Thomas, *Macromolecules* **1998**, *31*, 6566.
- [19] Y. Liu, V. Abetz, A. H. E. Müller, *Macromolecules* **2003**, *36*, 7894.
- [20] R. Erhardt, A. Boker, H. Zettl, H. Kaya, W. Pyckhout-Hintzen, G. Krausch, V. Abetz, A. H. E. Müller, *Macromolecules* **2001**, *34*, 1069.
- [21] A. Walther, X. Andre, M. Drechsler, V. Abetz, A. H. E. Müller, *J. Am. Chem. Soc.* **2007**, *129*, 6187.
- [22] K. Kato, *J. Polym. Sci. Polymer Letters* **1966**, *4*, 35.
- [23] A. F. Barton, *CRC Handbook of Polymer Liquid Interaction Parameters and Solubility Parameters*, CRC Press, Boca Raton, **1990**.
- [24] A. Sperschneider, F. Schacher, M. Gawenda, L. Tsarkova, A. H. E. Müller, M. Ulbricht, G. Krausch, J. Köhler, *Small* **2007**, *3*, 1056.
- [25] F. Schacher, A. Walther, M. Ruppel, A. H. E. Müller, *Macromolecules* **2009**, submitted.

- [26] E. Giebeler, R. Stadler, *Macromol. Chem. Phys.* **1997**, *198*, 3815.
- [27] D. Freyss, P. Rempp, H. Benoît, *Polym. Lett.* **1964**, *2*, 217.
- [28] S. Ludwigs, A. Böker, V. Abetz, A. H. E. Mueller, G. Krausch, *Polymer* **2003**, *44*, 6815.
- [29] L. C. Sawyer, D. T. Grubb, *Polymer microscopy*, Chapman & Hall, London, **1996**.
- [30] T. Goldacker, Diss. thesis, Dissertation (Bayreuth), **1999**.
- [31] G. Montaudo, F. Samperi, M. S. Montaudo, *Progress in Polymer Science* **2006**, *31*, 277.
- [32] M. W. Matsen, *J. Chem. Phys.* **1998**, *108*, 785.
- [33] P. Garstecki, R. Holyst, *Phys. Rev. E* **2001**, *64*, 021501.
- [34] Y. Mogi, M. Nomura, H. Kotsuji, K. Ohnishi, Y. Matsushita, I. Noda, *Macromolecules* **1994**, *27*, 6755.
- [35] V. Abetz, T. Goldacker, *Macromol. Rapid Comm.* **2000**, *21*, 16.
- [36] U. Krappe, R. Stadler, I. Voigt-martin, *Macromolecules* **1995**, *28*, 4558.
- [37] J. E. Mark, *Physical Properties of Polymers Handbook*, American Institute of Physics press, Woodbury, **1996**.
- [38] D. W. Schubert, M. Stamm, A. H. E. Müller, *Polymer Eng. & Science* **1999**, *39*, 1501.
- [39] U. Breiner, U. Krappe, V. Abetz, R. Stadler, *Macromol. Chem. Phys.* **1997**, *198*, 1051.

Towards Nanoporous Membranes based on Linear ABC Triblock Terpolymers

Alexandra Sperschneider¹, Felix Schacher¹, Marcel Gawenda³, Larisa Tsarkova²,
Axel H.E. Müller^{1,*}, Mathias Ulbricht³, Jürgen Köhler⁴, and Georg Krausch²

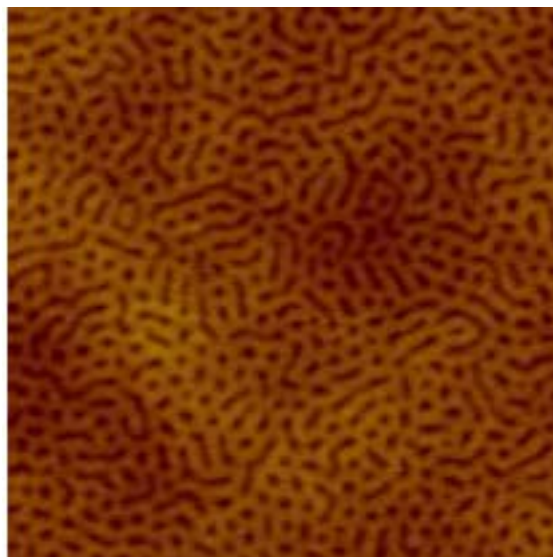
¹ Makromolekulare Chemie II, Universität Bayreuth, D-95440 Bayreuth, Germany

² Physikalische Chemie II, Universität Bayreuth, D-95440 Bayreuth, Germany

³ Technische Chemie II, Universität Duisburg-Essen, D-45117 Essen, Germany

⁴ Experimentalphysik IV, Universität Bayreuth, D-95440 Bayreuth, Germany

Email: Axel.Mueller@uni-bayreuth.de



Abstract

Block copolymers represent an exciting class of complex materials as they self-assemble into highly regular structures of nanoscopic dimensions. When prepared in thin films, such structures can be used for a variety of applications including lithographic masks or nanoporous membranes. In this contribution we report about nanostructures in thin films of structurally analogous polybutadiene-*block*-poly(2-vinyl pyridine)-*block*-poly(*tert*-butyl methacrylate) (BVT) and polystyrene-*block*-poly(2-vinyl pyridine)-*block*-poly(*tert*-butyl methacrylate) (SVT) triblock terpolymers which were synthesized via sequential living anionic polymerization. The morphological behavior of annealed SVT and BVT films was investigated by scanning force and scanning electron microscopies. We demonstrate that the difference in the terpolymer composition results in the formation of ordered perforated lamella phase in SVT films and of hexagonally packed core-shell cylinders in BVT films. Further, the BVT films show high potential for the fabrication of composite membranes using track-etched poly(ethylene terephthalate) macroporous filters as a support.

Keywords: triblock terpolymer, composite membranes, anionic polymerization, thin film morphology, self-assembly

Introduction

The development of synthetic membranes has always been inspired by nature, in particular by the fact that the selective transport through biological membranes is enabled by highly specialized macro- and supramolecular assemblies based on and involved in molecular recognition. The success of membrane technology has already been impressively demonstrated for the first large-scale industrial processes, water purification by reverse osmosis and blood detoxification by dialysis or ultrafiltration. The search for novel synthetic membranes, in particular those with higher transport selectivity, is still a challenge of outstanding relevance for the field. Currently, most of the technically used membranes are produced from organic polymers via phase inversion methods, i.e. a

controlled phase separation of polymer solutions induced by non-solvent addition, solvent evaporation or temperature change.^[1, 2] Many scientifically interesting, technically challenging, and commercially attractive separation problems cannot be solved with membranes according to the state-of-the-art. Novel membranes with a higher chemical selectivity, e.g. for isomers, enantiomers or larger biomolecules, or with a selectivity which can be switched by an external stimulus or which can adapt to the environment / process conditions are required. In addition, minimizing the thickness of the membrane barrier layer is essential. Approaches to develop synthetic membranes of the “next generation” have been reviewed recently.^[3]

The potential of block copolymers with incompatible blocks for nanotechnology applications has been realized in the past decade and a considerable number of examples has been described in the literature.^[4] Nanoporous materials may be generated by the selective removal of one of the components from a self-assembled block copolymer. Through adjusting chain length, composition, and molecular architecture, these materials are able to exhibit pore sizes and topology of parent structures and they can therefore be employed as nanolithographic masks, templates or even separation membranes. The first group reporting about a porous membrane-like structure from an ordered block copolymer precursor was Lee *et al.*^[5] Porous films generated in that way were then characterized employing adsorption measurements as well as gravimetric and spectroscopic methods. Three years later Smith and Meier were the first ones to show that ozonolysis can effectively remove the polydiene component in polystyrene-*block*-polybutadiene (PS-BB) or polystyrene-*block*-polyisoprene (PS-PI) diblock copolymers without altering the structure of the uncrosslinked PS domains.^[6] In 2003, Sidorenko *et al.* used a mixture of a polystyrene-*block*-poly(4-vinyl pyridine) (PS-P4VP) diblock copolymer and 2-(4-hydroxybenzene-azo)benzoic acid (HABA). Depending on the casting conditions, the annealing solvent and polymer-analogous reactions thin films with pores perpendicular to the surface could be generated.^[7] An elegant way to nanoporous materials without the need of cross-linking or degradation steps was shown by Zalusky *et*

al.^[8] Mesoporous polystyrene monoliths were prepared by hydrolytical removal of the polylactide block from a polystyrene-*block*-polylactide (PS-PLA) diblock copolymer. Pore sizes within this system were adjustable via the molecular weight of the diblock copolymer. They also presented rather simple methods for alignment of the PLA cylinders.^[9] Nanoporous PS generated in this way has the solubility and thermal characteristics of bulk polystyrene homopolymer and any potential application of these materials that requires pore structure stability must work within these limitations.

A different approach was published by Ndoni *et al.* in 2003.^[10] Here the polydiene component of a diblock copolymer was not removed through ozonolysis but kept as matrix material. They report on the synthesis and radical cross-linking of polybutadiene-*block*-poly(dimethylsilane) (PB-PDMS) followed by removal of the silane compound through HF etching. Unfortunately, the morphology was strongly affected by the rather rigorous cross-linking conditions. When replacing polybutadiene by polyisoprene and performing the etching step with tetrabutylammonium fluoride (TBAF) instead of HF, Cavicchi *et al.* received better results.^[11] They reported on the formation of porous PI monoliths from ordered, aligned and crosslinked PI-PDMS. Structures and porosity were investigated with SEM and SAXS measurements after removal of the silyl component with TBAF in THF. These experiments showed that nanoporous rubbers may be generated, having potential as functionalizable porous materials through the remaining double bonds.

It was shown earlier that the microdomain structures in thin films of SVT triblock terpolymer show pronounced dependence on the film thickness.^[12] Among those, the perforated lamella morphology (PL) is the most suitable for the fabrication of novel composite membranes. It was demonstrated in experiments,^[13-16] and in computational simulations,^[17] that in thin films of cylinder-forming block copolymers the PL phase is stabilized by the strong surface fields. Moreover, the PL structure was successfully converted into a pH-responsive layer through the hydrolysis of the ester moiety of the P*t*BMA component.^[18] Furthermore, additional morphologies such as short standing cylinders or complex

gyroid structures, which provide a complex but regular channel geometry, are potentially of high interest.

Despite the impressive microscopic, spectroscopic and other characterization studies of the ordered porous morphologies based on di- or triblock copolymers, a direct demonstration of the membrane function, i.e. permeability measurements or even a selective permeation controlled by the nanoporosity of the polymer film, is yet to be accomplished.

Here we demonstrate the effect of the triblock terpolymer composition on the resulting complex morphology in thin films of polystyrene-*block*-poly(2-vinyl pyridine)-*block*-poly(*tert*-butyl methacrylate) (SVT) and of polybutadiene-*block*-poly(2-vinyl pyridine)-*block*-poly(*tert*-butyl methacrylate) (BVT) triblock terpolymers. Additionally, we varied the nature of the substrate, the molecular weight of the BVT terpolymer and the annealing conditions. By replacing the rather brittle polystyrene block in the SVT terpolymer through rubbery polybutadiene, we optimize the matrix properties, yielding a more flexible system. Furthermore, cross-linking of the polybutadiene compartment enhances the thin film stability. The morphological behavior of annealed SVT and BVT films was investigated by scanning force microscopy (SFM), transmission electron microscopy (TEM) and scanning electron microscopy (SEM). The strategic aim of this work is to explore the potential of the fabrication of composite membranes from thin nanoporous blockcopolymer films on macroporous filters as supports.

Experimental

Synthesis of Block Terpolymers. The synthesis and characterization of the linear SVT triblock terpolymers have already been described.^[19] The BVT triblock terpolymers were synthesized via sequential living anionic polymerization in THF using *sec*-butyl lithium as initiator. After polymerization of butadiene and 2-vinyl pyridine at -10 °C and -70 °C respectively, 1,1-diphenylethylene was added to reduce the nucleophilicity of the living chain ends. During the polymerization of the P*t*BMA block at -35 °C, samples were taken from the reactor after different polymerization times and were precipitated into degassed me-

thanol. The number-average molecular weight of the polybutadiene precursor and the molecular weight distributions of the triblock terpolymers were determined by gel permeation chromatography (GPC). All polymers exhibit a narrow molecular weight distribution characterized by polydispersity indices between 1.01 and 1.05. Additionally, ^1H NMR spectra were acquired using CDCl_3 as solvent and tetramethylsilane (TMS) as internal standard. The molecular weights of the P2VP and the PtBMA blocks were calculated using the terpolymer composition determined by NMR and the polystyrene molecular weights from GPC. The molecular parameters of the triblock terpolymers are listed in **Table 1** and GPC eluograms of BVT terpolymers are shown in **Figure 1**.

Size Exclusion Chromatography (SEC) measurements were performed on a set of 30 cm SDV-gel columns of 5 μm particle size having nominal pore sizes of 10^5 , 10^4 , 10^3 and 10^2 Å with refractive index and UV ($\lambda=254$ nm) detection. An elution rate of 1 ml/min with THF as solvent was used.

^1H -Nuclear Magnetic Resonance Spectroscopy (NMR). ^1H NMR spectra were recorded on a Bruker 250 AC spectrometer using either CDCl_3 or THF-d_8 as solvent and tetramethylsilane (TMS) as internal standard.

Table 1: Molecular Characteristics of Triblock Terpolymer

Polymer ^a	M_w/M_n ^b	$\Phi_{\text{PS/PB}} : \Phi_{\text{P2VP}} : \Phi_{\text{PtBMA}}$ ^c
$\text{S}_{16}\text{V}_{21}\text{T}_{63}^{140}$	1.03	1 : 1.3 : 3.90
$\text{B}_{16}\text{V}_{21}\text{T}_{63}^{145}$	1.02	1 : 1.3 : 3.90
$\text{B}_{14}\text{V}_{18}\text{T}_{68}^{165}$	1.02	1 : 1.3 : 4.85

^a subscripts represent the weight fractions of the respective block (in weight %); the superscript denotes the total weight-average molecular weight in kg/mol

^b polydispersity determined by GPC

^c relative volume fractions of blocks

Thin Film Preparation. SVT and BVT polymer thin films were prepared by spin-casting 5 g/L solutions in chloroform onto polished silicon wafers and NaCl surfaces, respectively. In order to improve the chain mobility and equilibrate

the microdomains, the thin films were annealed under controlled solvent vapor pressure. Subsequently, the samples were quenched by a flow of pure dried air in order to freeze the developed morphologies. The fast quenching procedure ensures reproducibility.

For cross-linking of the polybutadiene block in BVT thin films, 3 wt.-% of the photoinitiator Lucirin-TPO (BASF) was added to a 5 g/L polymer solution. After spin-casting onto NaCl (crysTec GmbH, Germany) and annealing in controlled solvent vapor, the samples were subsequently exposed to UV light with a cutoff at 300 nm for 60 minutes leaving the PtBMA block undamaged.

Scanning Force Microscopy (SFM). Microdomain structures and film thickness were investigated with SFM (Dimension 3100, Veeco Metrology) operated in Tapping Mode. The spring constant of the silicon cantilevers was in the range between 35-92 nN/m. The corresponding resonance frequency varies between 285 and 385 kHz. Phase images were recorded at free amplitudes of about 30-50 nm at a setpoint of 90 % of the free cantilever amplitude. Height measurements were performed by scratching the polymer films with a scalpel (see also [20]) and measuring the height of the polymer film surface with respect to the underlying substrate. The phase contrast was resolved due to the different physical properties of the components. Polybutadiene is liquid at room temperature whereas poly(*tert*-butyl methacrylate) and poly(2-vinyl pyridine) are in a glassy state at temperatures below 100 °C.

Field-Emission Scanning Electron Microscopy (SEM). We used SEM (LEO 1530, Zeiss) for further characterization of the polymer thin films. Due to the depolymerization of the PtBMA matrix phase by the electron beam, new insights into the morphology were gained [21]. Applying the InLens detector with a slow acceleration voltage of 0.5 kV, we received a sufficient material contrast between the two remaining polymer phases without staining or sputtering,

Transmission Electron Microscopy (TEM). For creating new polymer composite membranes, it is essential to remove the triblock terpolymers from the substrates enabling the transfer to template membranes. For this end we prepared thin films of $B_{14}V_{18}T_{68}^{165}$ on NaCl substrates (as explained above). After solvent

annealing, the NaCl plates were dissolved in bidistilled water and the free-floating film was picked up with carbon-coated copper grids (Plano, Wetzlar). Subsequently, the samples were checked with TEM (CEM 902, Zeiss, 80 kV) looking for defects caused by the transfer.

Results and Discussion

In order to induce long-range order of microstructures of block copolymer thin films, typically thermal or solvent annealing procedures are applied. The assembly of microdomains on a microscale is accompanied by the surface roughening on a macroscale, i.e. the formation of terraces (coexisting flat regions with equilibrium film thickness) and of dewetting patterns. These two other dynamic processes are considered to affect pronouncedly and destructively (in case of dewetting) thin films from block copolymers with a relatively low total molecular weight. Thin polymer films consisting of comparatively long chains (with a total molecular weight of above 100 kg/mol) are relatively stable towards dewetting^[22] on an experimental timescale. In addition, in thin films of high molecular weight block copolymers, such as presented in this study, the terrace formation is considerably retarded due to the high viscosity of the polymers.^[23]

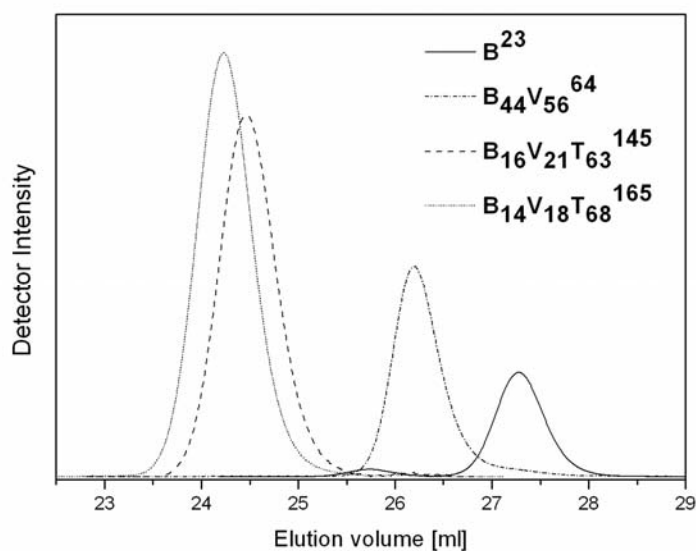


Figure 1: GPC eluograms of polybutadiene, polybutadiene-*b*-poly(2-vinyl pyridine), and two BVT triblock terpolymers.

Thin Film Phase Behavior of $S_{16}V_{21}T_{63}^{140}$. After spin-casting from a chloroform solution, the samples were annealed for 100 h in chloroform vapor ($p_{\text{CHCl}_3} = 0.8 p_0$, with p_0 representing the vapor pressure of chloroform at 295 K). Under these annealing conditions the polymer volume fraction in swollen films is $\phi = 0.36 \pm 0.04$. Due to the polymer swelling, the chain mobility is considerably increased, facilitating the diffusion-driven transport and the development of the equilibrium macro- and microstructures.

The annealed $S_{16}V_{21}T_{63}^{140}$ samples show macrostructures (terraces) on a scale of tens of μm (visible in optical microscopy). Large-scan SFM height images (not shown here) reveal coexisting terraces with the heights of $T_0 = 16 \pm 3$ nm and $T_1 = 36 \pm 2$ nm with characteristic microstructures in each terrace, which can only be visualized in SEM measurements (**Figure 2**). On a μm scale the SFM height and phase images show no lateral structure (inset in Figure 2A). The whole polymer surface is covered with a smooth, stiff layer of one component. In contrast, in SEM measurements the surface layer turned out to be unstable during the electron beam exposure despite of a low acceleration voltage of 0.5 kV. Comparing all three polymer components, poly(*tert*-butyl methacrylate) (PtBMA) is the only block which is depolymerized via photolysis during UV or electron beam exposure.^[24] In addition, PtBMA represents the phase with the lowest surface tension (see **Table 2**) which is expected to form a glassy ($T_{g,(\text{PtBMA})} = 135^\circ\text{C}$) continuous cover layer which then minimizes the interfacial tension between the polymer film and air^[25, 26]. The other two components, polystyrene ($\gamma_{\text{PS}}=41$ mN/m^[27]) and poly(2-vinyl pyridine) ($\gamma_{\text{P2VP}}=40$ mN/m^[28]) remain underneath this surface layer independent of the resulting morphology.

Table 2: Surface Tensions of used Polymer Components

polymer	surface tension [mN/m]
polystyrene (PS)	41.0 ^[27]
polybutadiene (PB)	24.5 - 32.0 ^[29, 30]
poly(2-vinyl pyridine) (P2VP)	40.0 ^[28]
poly(<i>tert</i> -butyl methacrylate) (P <i>t</i> BMA)	30.5 ^[27]

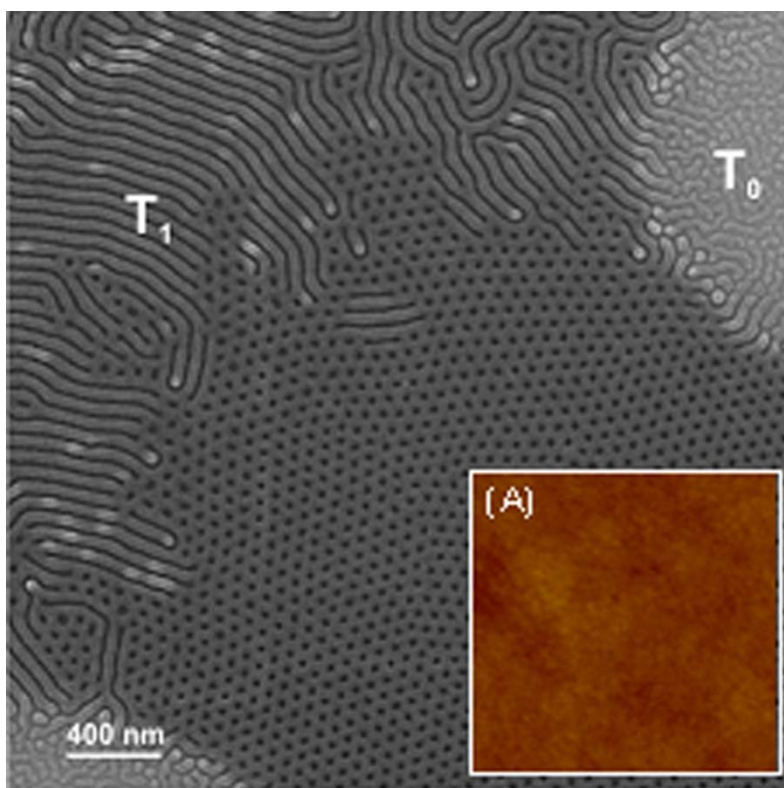


Figure 2: SEM image of a $S_{16}V_{21}T_{63}^{140}$ thin film after annealing in chloroform vapor ($p_{\text{CHCl}_3} = 0.8 p_0$; $t = 100$) with an acceleration voltage of 1.0 kV showing different morphologies in dependence of terrace height. The scale bar corresponds to 400 nm. Inset (A) SFM height image (size $1 \times 1 \mu\text{m}^2$; height scale $\Delta z = 0\text{-}20$ nm). The sample surface is covered with a smooth rigid layer of P*t*BMA.

We now describe in more detail the microdomain structures as revealed by the SEM measurements. The thinnest part of the film (T_0 in Figure 2) is often referred to as a disordered phase or wetting layer. With increasing film thickness,

T_0 transforms into cylinders orientated parallel to the substrate which form the first terrace, T_1 . Moreover, with further increase of the film thickness to 47 ± 2 nm the cylindrical structure changes to PL morphology resembling a typical filter or membrane surface. The associated changes in height within one terrace may be due to different characteristic spacings of cylinder and PL morphology.^[14] The molecular architecture of SVT suggests that a PL unit cell consists of a polystyrene core surrounded by a poly(2-vinyl pyridine) shell and penetrated by well-defined P β BMA pores (for further information see also ^[12, 13, 31]). The SEM image of a $S_{16}V_{21}T_{63}^{140}$ thin film in **Figure 3A** indicates the formation of the PL phase over macroscopically large areas. The hexagonal order of perforations (pores) with an average diameter of 35 ± 3 nm is confirmed by the Fourier transformation (inset in Figure3B). The estimated porosity of such nanostructure is about 21%.

We note that the observed microstructures and terrace heights are in agreement with the combinatorial studies of Ludwigs *et al.*^[31]

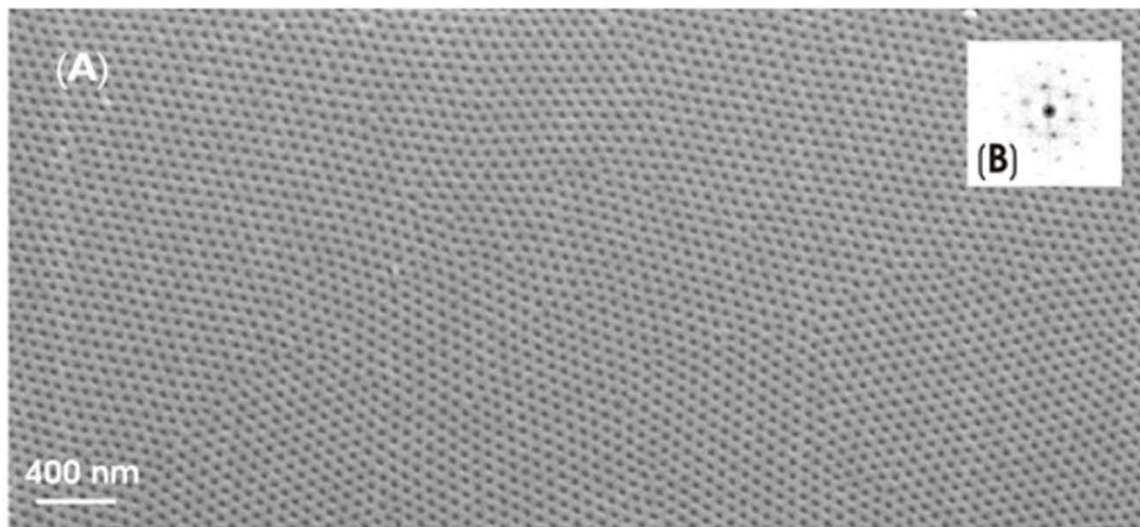


Figure 3: (A) Typical SEM image of a $S_{16}V_{21}T_{63}^{140}$ triblock terpolymer thin film after spin-casting from chloroform solution and solvent annealing for 100 h; acceleration voltage 1.0 kV. The scalebar corresponds to 400 nm; (B) Fourier transformation confirms the hexagonally arranged PL structure.

Thin Film Phase Behavior of $B_{16}V_{21}T_{63}^{145}$. Spin-casted 30 ± 2 nm thick films were annealed in chloroform vapor under the same conditions as described for $S_{16}V_{21}T_{63}^{140}$. SFM height measurements reveal a macroscopically smooth surface of the film with no terraces formed upon the annealing procedure. On a smaller scale, the lateral nanostructures become visible.

SFM height image in **Figure 4A** reveals coexisting morphology represented by channels (dark and white stripes) and by wells (dark dots) surrounded by mesh-like walls (bright color). In the corresponding phase image (Figure 4B) two phases with different mechanical properties are clearly distinguished. The dark color in the phase image corresponds to the PB block which is the only soft component in the presented system. The mesh-like hard matrix is presumably composed of the two other glassy components, i.e. P2VP and P*t*BMA. We note that in contrast to the $S_{16}V_{21}T_{63}^{140}$ films, in this case the PL morphology was not observed.

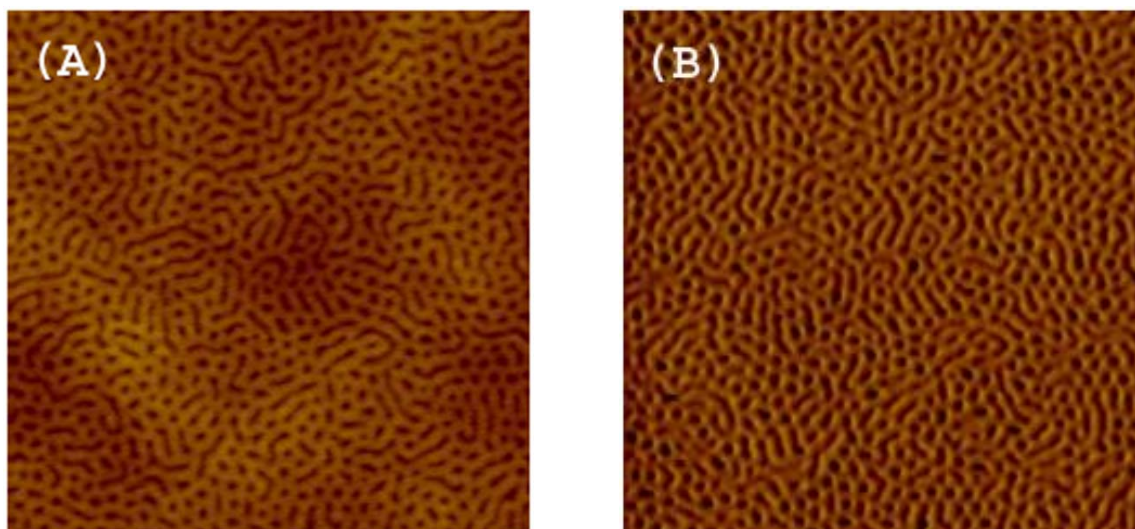


Figure 4: (A) Typical SFM height image of a $B_{16}V_{21}T_{63}^{145}$ triblock terpolymer thin film spin-cast from chloroform solution after annealing for 100 h in chloroform vapor (image size $2.5 \times 2.5 \mu\text{m}^2$; height scale $\Delta z = 0\text{-}20$ nm) showing coexisting morphologies. The low, dark areas correspond to the soft PB compartment which is distorted due to strong SFM tapping conditions. The higher, brighter mesh-like matrix around is presumably composed of the other two rigid polymer compartments P2VP and P*t*BMA. The contrast differences in the corresponding phase image (B) confirm this observation (image size $2.5 \times 2.5 \mu\text{m}^2$; phase contrast 30°).

The nanostructured free surface of $B_{16}V_{21}T_{63}^{145}$ films, as revealed by SFM measurements, indicates that P*t*BMA does not form the continuous surface layer that was detected for $S_{16}V_{21}T_{63}^{140}$ films (inset to Figure 1). This effect can be explained by the modified polymer composition, the consequential changes in the glass-transition temperature and the surface tension (Table 2) of the BVT components. Both, PB and P*t*BMA blocks show comparable surface tension enabling both components to segregate to the free surface. Therefore, the lateral nanopattern can be resolved in solvent annealed films by SFM measurements.

Additional information concerning the composition of the mesh-like hard matrix was obtained in SEM measurements. **Figure 5** displays microdomain pattern in the $B_{16}V_{21}T_{63}^{145}$ film, which was described above (Figure 4). The structure is represented by core-shell stripes and dots, which we identify with the core-shell cylinders oriented parallel and perpendicular to the film surface, respectively, with an average diameter of 67.8 ± 9.0 nm (Figure 5). The mesh-like hard matrix, which was clearly visualized in SFM images (Figure 4), is decomposed upon electron-beam-exposure, which points to its composition of P*t*BMA compartment.

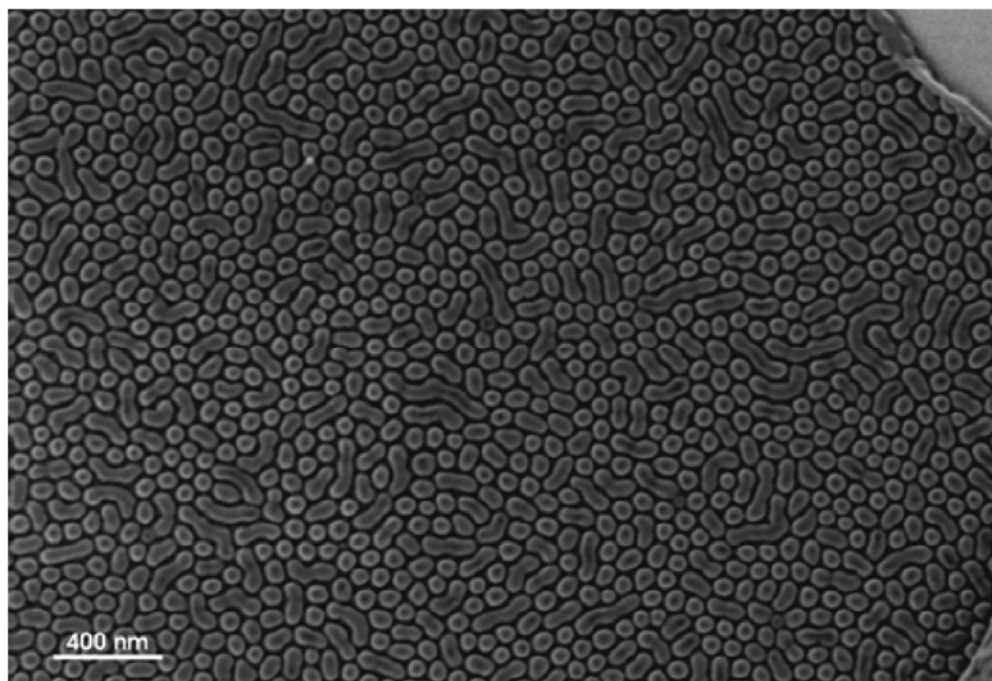


Figure 5: SEM image of the $B_{16}V_{21}T_{63}^{145}$ film shown in Figure 2 (acceleration voltage 0.5 kV). Solely cylinders oriented perpendicular and parallel to the substrate surface are found whereas the surrounding matrix phase, which was clearly resolved in the SFM height measurements (Figure 2), is depolymerized by the electron beam. The scalebar corresponds to 400 nm.

The stripes and distorted dots, which appear as defects in the hexagonally ordered structure of perpendicular cylinders, annihilate with increasing the time of equilibration. By step-wise annealing, we followed the evolution of lying cylinders into cylinders oriented perpendicular to the substrate. The TEM image in Figure 6 displays the mechanism of such transformation via interfacial undulations along the lying cylinder axis and the resulting break-up into spherical domains.^[32]

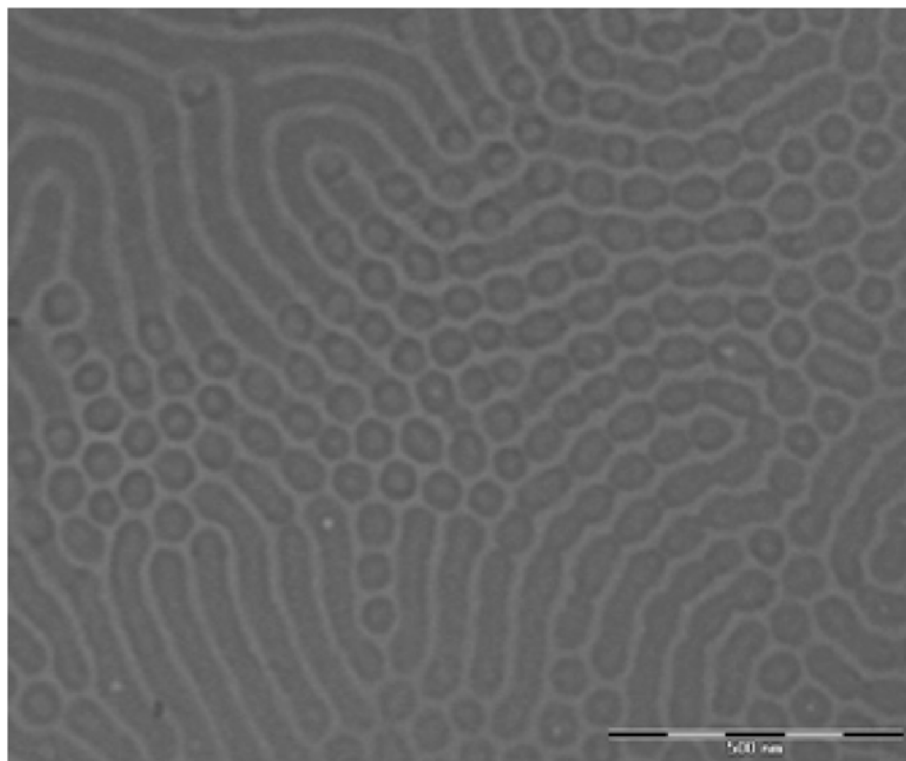


Figure 6: TEM image of a $B_{16}V_{21}T_{63}^{145}$ thin film successfully transferred after controlled solvent annealing for two hours reveals an intermediate stage in the cylinder transformation mechanism. The cylinders orientated parallel to the substrate show a rather undulated shape resulting in a break-up into spherical domains. The scalebar corresponds to 500 nm.

Thin Film Phase Behavior of $B_{14}V_{18}T_{68}^{165}$. For further investigation of the molecular architecture effects on the resulting morphology and long-range order, we studied a BVT terpolymer with increased total molecular weight. A 39 ± 3 nm thick film was prepared under the conditions described above. SFM height measurements revealed a smooth film surface on a macroscale (no terrace development).

SEM measurements (not shown) reveal vertically oriented core-shell cylinders with an average diameter of 64 ± 5 nm which look similar to the structures described above for $B_{16}V_{21}T_{63}^{145}$ films (Figure 5). In order to get close insight into microdomain structure, we performed SFM measurements of the BVT films after exposure to the electron beam in SEM.

SFM height and phase images in **Figure 7** clearly confirm the core-shell morphology. We note that due to removal of the P*t*BMA block, the film surface appears in the height image rough with an averaged roughness of 6 ± 1 nm.

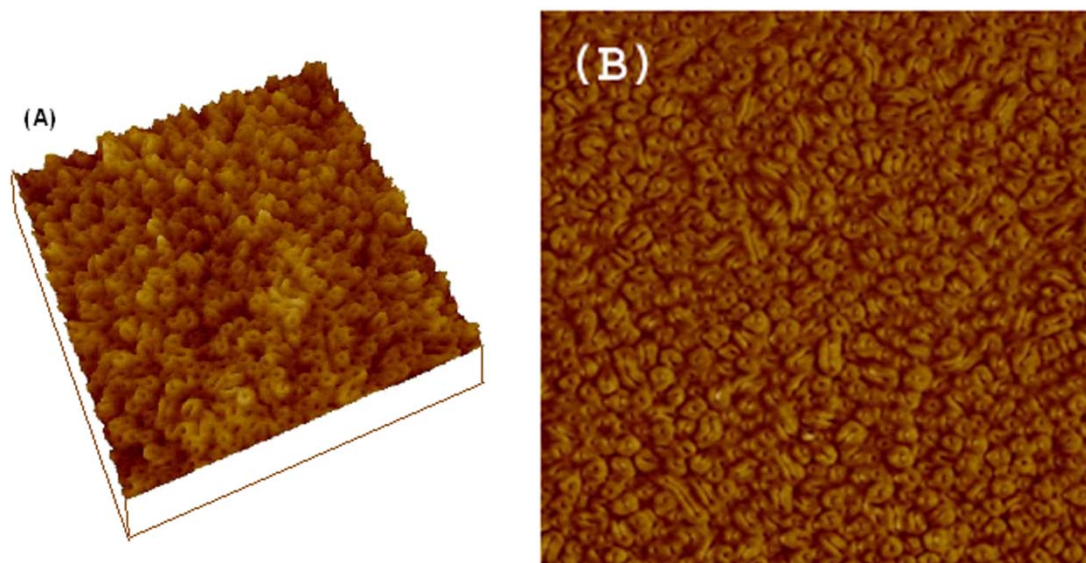
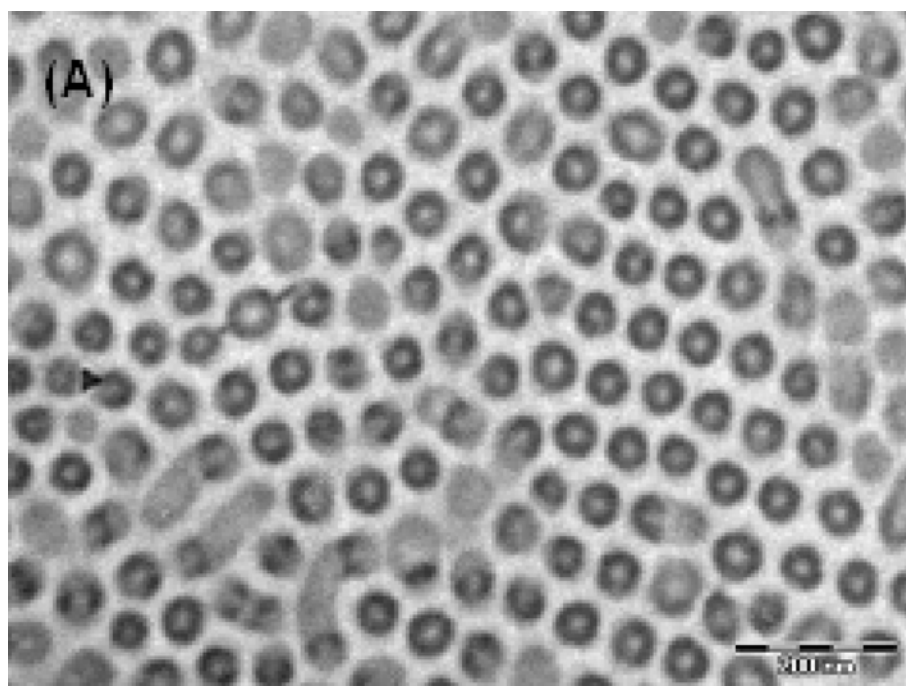


Figure 7: (A) Typical 3D-SFM height image (image size $2.5 \times 2.5 \mu\text{m}^2$; height scale $\Delta z = 0\text{-}20$ nm) of a $B_{14}V_{18}T_{68}^{165}$ triblock terpolymer (spin-cast from chloroform solution, solvent annealed for 100 h) after electron beam exposure. The resulting morphology of vertical cylinders can be easily observed. The corresponding phase image (B) confirms the structure of core-shell cylinders whereas the soft PB compartment forms the core (black color) and the stiff P2VP compartment equals the surrounding shell (bright color) (image size $2.5 \times 2.5 \mu\text{m}^2$; phase contrast = 20°).

In order to probe the prospective of BVT nanostructures in membrane technology, we replaced the silicon oxide substrate by the crystalline sodium chloride (NaCl) surface, which makes the transformation of the polymer film from the solid substrate for the further analysis and usage more feasible. Immediately after annealing on NaCl substrate, BVT films were transferred onto carbon-coated TEM grids. Carbon coating enhances film stability during the electron-beam-exposure. The TEM image in **Figure 8A** clearly reveals the core-shell morphology which confirms the successful film transfer. A further step towards optimization of the mechanical properties and chemical stability of the membrane prototypes was achieved by selective cross-linking of the PB component via UV-initiator. The above procedure considerably improves physical properties of the polymer films and facilitates the film transfer to the technologically approved substrates. Importantly, the desired film nanostructure is perfectly preserved after the cross-linking (Figure 8B).



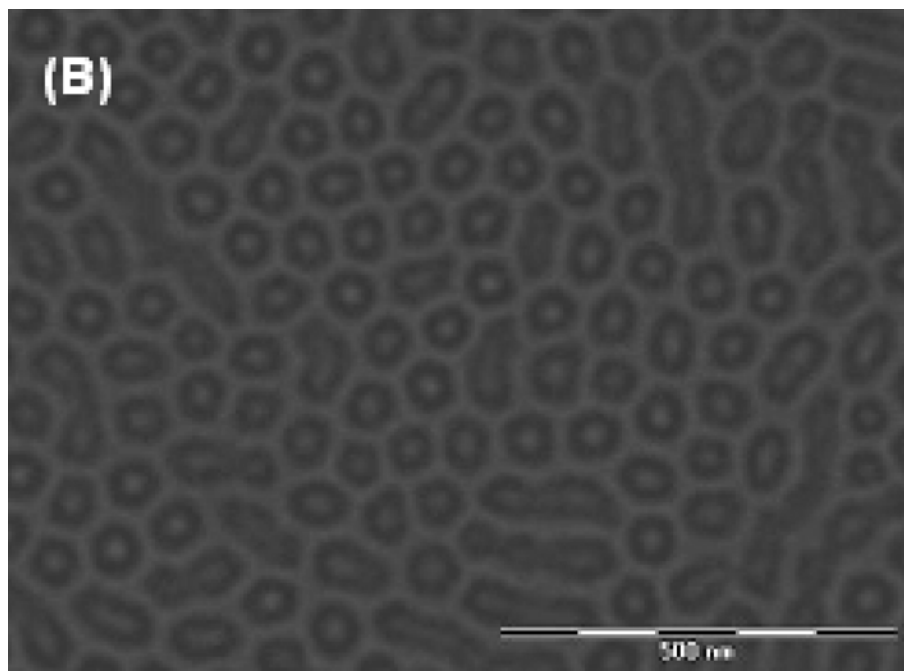


Figure 8: (A) TEM image of a thin film of $B_{14}V_{18}T_{68}^{165}$ triblock terpolymer spin-cast onto a NaCl wafer from chloroform solution and transferred onto a TEM grid, revealing hexagonally packed core-shell cylinders: polybutadiene core and poly(2-vinyl pyridine) shell in a poly(*tert*-butyl methacrylate) matrix. The scalebar corresponds to 200 nm. (B) TEM image of a cross-linked $B_{14}V_{18}T_{68}^{165}$ thin film displaying comparable structures as shown in (A). The scalebar corresponds to 500 nm.

In order to characterize and probe the size/charge-based permeation selectivity of block copolymer nanostructures, thin polymer films must be transformed onto suitable substrates providing sufficient mechanical stability of a potential membrane. Considering the diameters of the pore precursors identified in this work (~ 35 nm; SVT), moderately thick (membrane) filters with pore diameters between ~ 0.2 and ~ 5 μm are suitable base materials for the fabrication of block copolymer thin-film composite membranes. Surface-functionalized track-etched PET membranes, which had already been well established as model systems for selective and stimuli-responsive transport through well-defined pores in the nano- and micrometer range,^[3, 33] are the first choice. The transfer to other supports, for example to silicon nitride-based microsieves,^[34] is another perspective. The results of our study demonstrate that upon annealing under sufficient solvent vapour pressure, the resulting microdomain structure is not

sensitive to the chemical nature of the substrate (NaCl or silicon oxide) due to the strong screening effect of the solvent. On the other side, the transfer of the polymer films to the supporting membranes is considerably facilitated by the improved mechanical properties of the films.

Conclusion

SFM, TEM and SEM reveal the nanostructures in thin films of structurally analogous polybutadiene-*block*-poly(2-vinyl pyridine)-*block*-poly(*tert*-butyl methacrylate) (BVT) and polystyrene-*block*-poly(2-vinyl pyridine)-*block*-poly(*tert*-butyl methacrylate) (SVT) triblock terpolymers. The difference in the terpolymer composition results in the formation of ordered perforated lamella phase in SVT films and of hexagonally packed core-shell cylinders in BVT films. Both morphologies are considered to be attractive precursors for nanoporous separation membranes. This requires further processing of the films via selective degradation of one component in order to “open” the pores.

For the novel BVT terpolymers, several very useful features with respect to the membrane technology have been identified, namely a similar equilibrium morphology on substrates with different wettability, the feasibility of film transfer to another (porous) substrate and the stabilization of the films by internal cross-linking. Thin SVT films demonstrated membrane-suitable morphology and feasibility of their transfer to support membranes. Further processing of terpolymers microstructures towards nanoporous separation membranes is currently under investigation.

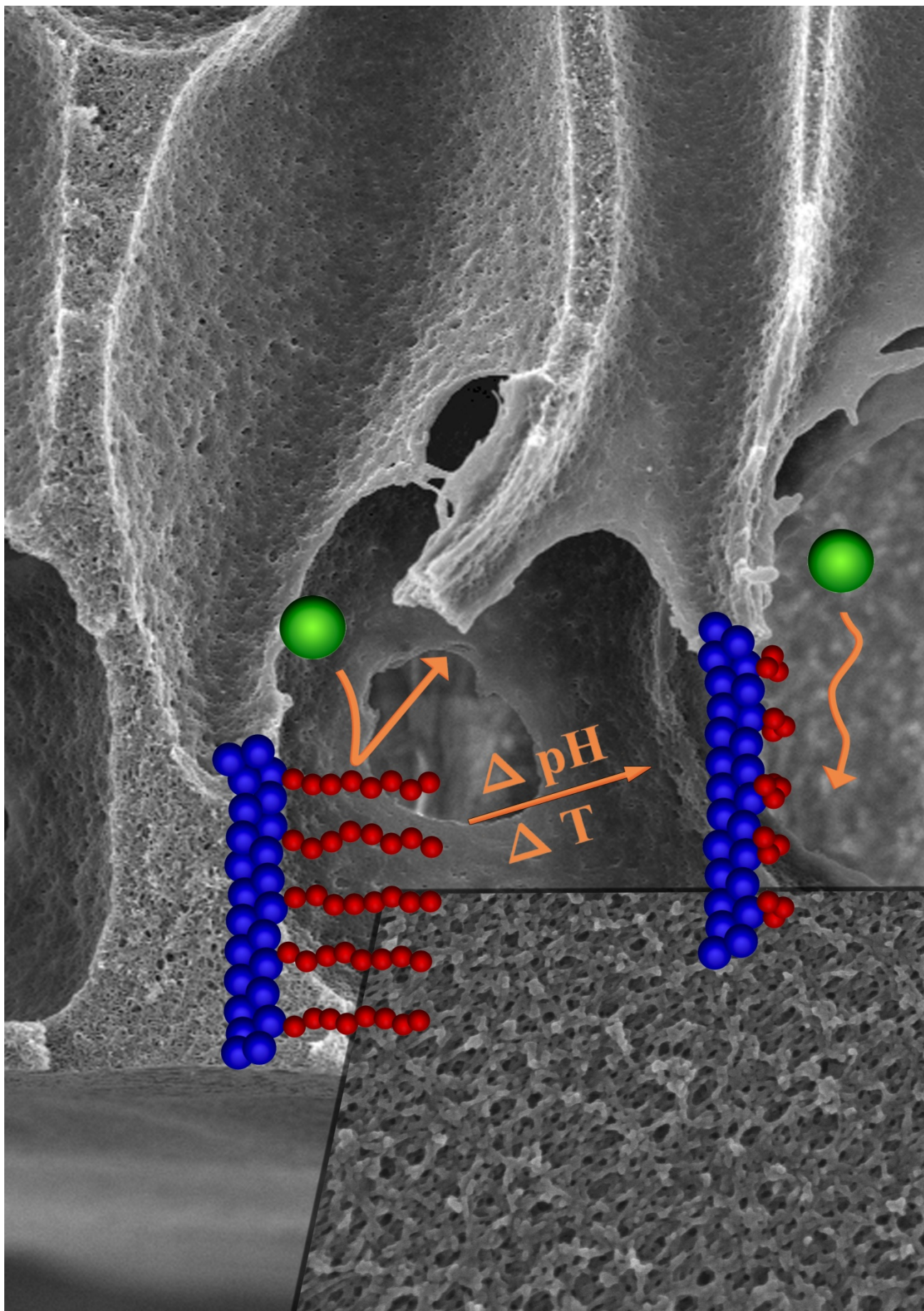
Acknowledgements

This research is supported by the VolkswagenStiftung. We thank Carmen Kunert for the TEM measurements.

References

- [1] M. Mulder, *Basic principles of membrane technology, Vol. 2*, Kluwer academic publishers, Dordrecht, **1996**.
- [2] P. van de witte, P. J. Dijkstra, J. W. A. van den berg, J. Feijen, *J. Memb. Sci.* **1996**, *117*, 1.
- [3] M. Ulbricht, *Polymer* **2006**, *47*, 2217.
- [4] M. A. Hillmyer, *Nanoporous materials from block copolymer precursors, Vol. 189*, Springer-Verlag Berlin Heidelberg, **2005**.
- [5] J. S. Lee, A. Hirao, S. Nakahama, *Macromolecules* **1988**, *21*, 274.
- [6] D. R. Smith, D. J. Meier, *Polymer* **1992**, *33*, 3777.
- [7] A. Sidorenko, I. Tokarev, S. Minko, M. Stamm, *J. Am Chem. Soc.* **2003**, *125*, 12211.
- [8] A. S. Zalusky, R. Olayo, C. J. Taylor, M. A. Hillmyer, *J. Am. Chem. Soc.* **2001**, *123*, 1519.
- [9] A. S. Zalusky, R. Olayo, J. H. Wolf, M. A. Hillmyer, *J. Am. Chem. Soc.* **2002**, *124*.
- [10] S. Ndoni, M. Vigild, R. H. Berg, *J. Am. Chem. Soc.* **2003**, *125*, 13366.
- [11] K. A. Cavicchi, A. S. Zalusky, M. A. Hillmyer, T. P. Lodge, *Macromol. Rapid Commun.* **2004**, *25*, 704.
- [12] S. Ludwigs, G. Krausch, R. Magerle, A. V. Zvelindovsky, G. J. A. Sevink, *Macromolecules* **2005**, *38*, 1859.
- [13] S. Ludwigs, A. Böker, N. Rehse, A. Voronov, R. Magerle, G. Krausch, *Nat. Mater.* **2003**, *2*, 744.
- [14] L. Tsarkova, A. Knoll, G. Krausch, R. Magerle, *Macromolecules* **2006**, *39*, 3608.
- [15] I. Park, S. Park, H. W. Park, T. Chang, H. Yang, C. Y. Ryu, *Macromolecules* **2006**, *39*, 315.
- [16] A. Knoll, A. Horvat, K. S. Lyakhova, G. Krausch, G. J. A. Sevink, A. V. Zvelindovsky, R. Magerle, *Phys. Rev. Lett.* **2002**, *89*, 035501.
- [17] D. A. Hajduk, *Macromolecules* **1997**, *30*, 3788.
- [18] S. Ludwigs, K. Schmidt, G. Krausch, *Macromolecules* **2005**, *38*, 2376.
- [19] S. Ludwigs, A. Böker, V. Abetz, A. H. E. Mueller, G. Krausch, *Polymer* **2003**, *44*, 6815.
- [20] L. Tsarkova, A. Knoll, G. Krausch, R. Magerle, *Macromolecules* **2006**, *39*, 3608.

- [21] L. C. Sawyer, D. T. Grubb, *Polymer microscopy*, Chapman & Hall, London, **1996**.
- [22] M. Geoghegan, G. Krausch, *Progress in Polymer Science* **2002**, *28*, 261.
- [23] L. Tsarkova, in *Nanostructured Soft Matter: Experiment, Theory, Simulation and Perspectives* (Ed.: A. V. Zvelindovsky), Springer Verlag, Heidelberg, **2007**.
- [24] N. Grassie, G. Scott, *Polymer Degradation and Stabilisation*, Cambridge University Press, Cambridge, **1988**.
- [25] S. H. Anastasiadis, T. P. Russell, S. K. Satija, C. F. Majkrzak, *Phys. Rev. Lett.* **1989**, *62*, 1852.
- [26] H. Hasegawa, K. Hashimoto, *Macromolecules* **1985**, *18*, 589.
- [27] J. E. Mark, *Physical properties of polymers handbook*, American institute of physics press, Woodbury, **1996**.
- [28] K. Ishizu, Y. Yamada, T. Fukutomi, *Polymer* **1990**, *31*, 2047.
- [29] A. Turturro, E. Gattiglia, P. Vacca, G. T. Viola, *Polymer* **1995**, *36*, 3987.
- [30] L. H. Lee, *J. Polym. Sci. A-2* **1967**, *5*, 1103.
- [31] S. Ludwigs, K. Schmidt, C. M. Stafford, E. J. Amis, M. J. Fasolka, A. Karim, R. Magerle, G. Krausch, *Macromolecules* **2005**, *38*, 1850.
- [32] L. Tsarkova, A. Knoll, R. Magerle, *Nano Letters* **2006**, *6*, 1574.
- [33] C. Geismann, A. Yaroshchuk, M. Ulbricht, *Langmuir* **2006**, *in press* ([doi:10.1021/la0603774](https://doi.org/10.1021/la0603774)).
- [34] C. J. M. Van Rijn, *Nano and Microengineered Membrane Technology*, Elsevier Science, Amsterdam, **2004**.

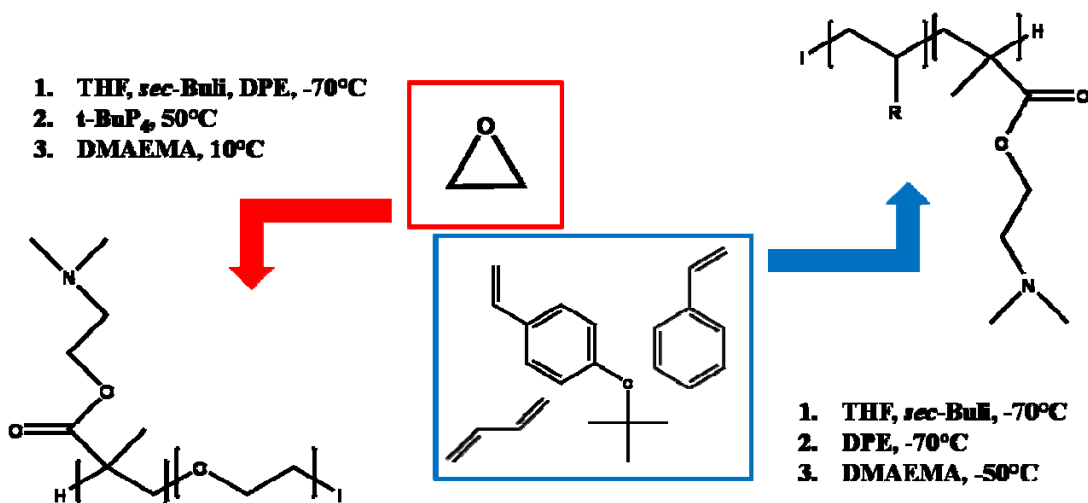


New Block Copolymers with Poly(*N,N*-dimethylaminoethyl methacrylate) as Double Stimuli-responsive Block

Felix Schacher, Markus Müllner, Holger Schmalz*, and Axel H. E. Müller*

Makromolekulare Chemie II, and Bayreuther Zentrum für Kolloide und Grenzflächen,
Universität Bayreuth, D-95440 Bayreuth, Germany

Email: Holger.Schmalz@uni-bayreuth.de; Axel.Mueller@uni-bayreuth.de;



Abstract

The synthesis of several diblock copolymers with *N,N*-dimethylaminoethyl methacrylate (DMAEMA) via anionic polymerization is presented; PS-*b*-PDMAEMA, PB-*b*-PDMAEMA, poly(*p*-*tert*-butoxystyrene)-*b*-PDMAEMA and PEO-*b*-PDMAEMA. The latter was synthesized using *sec*-butyllithium as initiator in presence of the phosphazene base *t*-BuP₄, enabling a facile changeover from an oxyanion to a carbanion. All reactions resulted in narrowly distributed block copolymers (PDI < 1.1). For PEO-*b*-PDMAEMA, diblock copolymers with a high blocking efficiency and a near-narrow molecular weight distribution (PDI < 1.40) could be prepared. The advantage of the presented one-pot synthesis is a significantly higher blocking efficiency compared to commercially available PEO macroinitiators under similar conditions.

Introduction

Living anionic polymerization is a demanding but nevertheless versatile tool for the preparation of well-defined polymers. Since Szwarc's pioneering work in 1956,^[1, 2] the number of polymers prepared via this technique is huge, especially in the field of block copolymers. In particular, amphiphilic block copolymers have attracted strong interest due to their usability in aqueous systems and therewith a certain number of potential applications.^[3, 4] The interest in stimuli-responsive ("smart") polymers, i.e. polymers whose properties change in response to environmental changes, has increased tremendously.^[5]

N,N-Dimethylaminoethyl methacrylate (DMAEMA) is known to be a both pH- and temperature-sensitive polymer.^[6] The LCST of PDMAEMA is strongly pH-dependent but may also be tuned by molecular weight or polymer architecture. By choosing the right mono- or multivalent counterions even UCST behavior has been reported.^[7-10] Quaternization leads to a strong polyelectrolyte.

Synthesis of block copolymers with DMAEMA as a "smart" block has been achieved via reversible addition-fragmentation chain transfer (RAFT) polymerization,^[11] by atom transfer radical polymerization (ATRP),^[6, 7, 10, 12] group transfer polymerization (GTP)^[13-15] and anionic polymerization. For the latter, selection of an appropriate initiating system plays an important role, e.g., carbanion,^[16] nitranion,^[17] ester enolate,^[18] and alkoxide^[18-20] initiated anionic polymerizations have been re-

ported. However, the number of anionically prepared well defined block copolymers with DMAEMA is still rather limited. Jérôme and his coworkers^[18, 21] used anionic polymerization to synthesize block copolymers of DMAEMA with methyl methacrylate, *tert*-butyl methacrylate, styrene, α -methylstyrene, and 2-vinyl pyridine with narrow molecular weight distributions. However, the molecular weights of the PDMAEMA part were always below 15,000 g/mol. More often, block copolymers with PDMAEMA are made by a block extension of modified macroinitiators by means of RAFT and ATRP.^[19, 20] Drawbacks here often are either incomplete end-functionalization of the macroinitiator or low blocking efficiencies upon polymerization of the second block resulting in unreacted initiating species leftover in the product. Therefore, one-pot reactions yielding well-defined block copolymers with DMAEMA segments are of great interest, especially if the polymerization of the other monomer is only achievable under certain conditions. This is the case for poly(ethylene oxide) (PEO), accessible only via ionic ring-opening polymerization.

In this communication we describe the synthesis and characterization of several diblock copolymers with DMAEMA as second block and molecular weights for the PDMAEMA ranging up to 38,000 g/mol or, in terms of repeating units, 240. First, polystyrene-*block*-PDMAEMA, poly(1,2-butadiene)-*block*-PDMAEMA, and poly(*p*-*tert*-butoxystyrene)-*block*-PDMAEMA, were synthesized via sequential anionic polymerization in THF at low temperatures with *sec*-butyllithium as initiator in the presence of lithium alkoxides. The amphiphilic diblock copolymers PB-*b*-PDMAEMA and *P**t*BS-*b*-PDMAEMA have not been reported before. The latter may be further modified through the removal of the *tert*-butoxy protecting group under acidic conditions in order to render poly(*p*-vinylphenol)-*block*-PDMAEMA (*Pp*V*P*-*b*-PDMAEMA) diblock copolymers with narrow molecular weight distributions. *Pp*V*P* is a pH-responsive polymer, becoming water-soluble at high pH through deprotonation.^[22] The homopolymer has been used in photoresists.^[22-24]

The first successful block copolymerization of ethylene oxide (EO) and methacrylic monomers was performed by Ulbricht et al. using potassium as counterion.^[25, 26] However, the polydispersities reported were rather high. The polymerization of *N,N*-diethylaminoethyl methacrylate (DEAEMA) with potassium alkoxide initiation at temperatures from 0 to +50 °C was first reported by Nagasaki et al.^[27] They ascribed the successful reaction to possible complexation of the potassium counter-

tion by the tertiary amino moiety of the monomer and therefore an increased reactivity of the oxyanion. The polydispersities were in the range of 1.1-1.5, however, initiator efficiencies could not be precisely determined due to lack of a suitable SEC calibration. In our case, the synthesis of PEO-*b*-PDMAEMA proceeded with Li⁺ as counterion in the presence of the *t*-BuP₄ phosphazene base. This initiator/ligand combination has been shown earlier to enable the ring-opening polymerization of EO and derivatives without the use of potassium or caesium counterions.^[28-30] Our approach for PEO-*b*-PDMAEMA presents a novel and convenient way to such type of block copolymers because the one-pot synthesis provides a manageable and facile changeover from an oxyanion to a carbanion without noticeable side reactions and leads to a blocking efficiency close to 100%.

Experimental

Materials. Tetrahydrofuran (Merck, p.a.) was purified by successive distillation over CaH₂ and potassium and kept under dry nitrogen before usage. Ethylene oxide (Linde, 3.0) was condensed onto CaH₂ and stirred at 0 °C for 3 h before being transferred into glass ampoules for storage. Prior to use ethylene oxide was additionally purified over *n*-BuLi and condensed into a sampling ampoule. *Tert*-butoxystyrene was distilled twice using a high vacuum line (10⁻⁴ - 10⁻⁵ mbar); first over CaH₂ and then after stirring with Bu₂Mg. Styrene (BASF) and DMAEMA (Aldrich, p.a.) were degassed three times via freeze-pump-thaw cycles. After degassing, styrene was stirred over Bu₂Mg and condensed under high vacuum into storage ampoules and kept frozen under N₂ until use whereas DMAEMA was stirred with Oct₃Al prior to condensation. Butadiene (Messer-Griesheim) was passed through columns filled with molecular sieves (4Å) and basic aluminum oxide. Afterwards it was condensed into a glass reactor and stored over dibutylmagnesium. Prior to polymerization the calculated amount of monomer was condensed into a pre-cooled burette. 1,1-Diphenylethylene (Aldrich, 97%) was purified by stirring with *sec*-BuLi under N₂ followed by distillation. The phosphazene base *t*-BuP₄ (Fluka, 1 M in hexane), *sec*-BuLi (Acros, 1.3 M in cyclohexane/hexane: 92/8), *n*-BuLi (Acros, 1.6 M in hexane), Bu₂Mg (Aldrich, 1 M in heptane), Et₃Al (Aldrich, 1 M in hexanes) were used as received.

Polymerizations. Polymerizations were carried out in a thermostated laboratory autoclave (Büchi) under dry nitrogen atmosphere. The synthesis of all block copolymers except PEO-*b*-PDMAEMA was accomplished in THF (500 mL) by sequential anionic polymerization of the corresponding monomers using *sec*-BuLi as initiator. At -70 °C *sec*-BuLi was added to THF followed by fast addition of the first monomer. The conversion of the first monomer was always monitored via the NIR probe. After a reaction time of 1 hour (S, *t*BS) at -70 °C or 10 hours at -10 °C (B), 2 eq 1,1-diphenylethylene were added via syringe to end cap the living chain ends. After 1h, DMAEMA was added to the reaction mixture via syringe and stirred for two hours at -50 °C. The polymer was purified by precipitation in water. For a typical example, 24 g styrene (26.4 ml, 0.23 mol), 6 g DMAEMA (6.45 ml, 0.038 mol), 0.7 ml *sec*-BuLi (1 mmol, [P] = 0.5 mmol / L), and 0.36 g DPE (0.36 ml, 2 mmol) were employed.

PEO-*b*-PDMAEMA was prepared in THF using 1,1-diphenyl-3-methylpentyllithium (DPMPLi) as initiator. DPMPLi was prepared in-situ by the reaction of *sec*-BuLi with 1,1-diphenylethylene ([*sec*-BuLi]/[DPE] = 1/1.1) in THF at -70 °C. After addition of EO the reaction was kept at -70 °C for 1 h. Subsequently, the temperature was increased stepwise (1 h at -30 °C, -10°C, and 30 min at 0 °C) to 10 °C in order to avoid side reactions. Then the phosphazene base *t*-BuP₄ ([DPMPLi]/[*t*-BuP₄] = 1/0.95) was added to start the polymerization of EO. Complete conversion of EO at 50 °C was achieved after 2 days. Afterwards, the temperature was lowered to 10 °C and DMAEMA was added via syringe. After the polymerization of the second block was complete, the living chain ends were terminated with degassed isopropanol. The polymer was precipitated in cold hexane (-20°C).

Online FT-NIR Spectroscopy. NIR spectra were recorded with a Nicolet Magna 560 FT-IR optical bench equipped with a white light source and a PbS detector. Online monitoring was accomplished using a laboratory autoclave (Büchi) equipped with an all-glass low-temperature immersion transmission probe (Hellma) with an optical path length of 10 mm and connected to the spectrometer via 2 m fiber-optical cables. The probe was fed through a port in the stainless steel top plate of the reactor and immersed into the reaction mixture. Data processing was performed with Nicolet's OMNIC software. Each spectrum was accumulated from 16 scans with a resolution of 4 cm⁻¹. The total collection time per spectrum was about 10 s. Conversions, x_p , were calculated using the following equation (1):

$$X_p = \frac{A_0 - A_t}{A_0 - A_\infty} \quad (1)$$

Where A_t is the absorbance at time t , A_0 = initial absorbance, and A_∞ = absorbance at full conversion. The apparent rate constants of propagation were extracted from the linear regime in the corresponding first-order time-conversion plots, $-\ln(1-x_p)$ versus time, by the slope of the linear fit at values of $1 \leq -(\ln(1-x_p)) \leq 2$.

Matrix-Assisted Laser Desorption Ionization Time-of-Flight Mass Spectrometry (MALDI-ToF MS) was performed on a Bruker Reflex III with a UV laser operating at 337 nm and an accelerating voltage of 20 kV. 1,8,9-trihydroxyanthracene (dithranol) and silver triflate as cationizing agent were used for the PS and PB homopolymers. Samples were dissolved in THF (10 mg/mL) and mixed with matrix (20 mg/mL in THF) and salt (10 mg/mL in THF) at a mixing ratio of 20 : 5 : 1 (v/v, matrix : analyte : salt). 1 μ L of this mixture was spotted onto the target and allowed to dry. 200 - 500 laser shots were accumulated for a spectrum.

Size Exclusion Chromatography (SEC) experiments were performed on a Waters instrument calibrated with narrowly distributed PEO standards for the PEO homopolymer, PS standards for the PS homopolymer and 1,4-PB standards for the PB homopolymer at 40 °C. Four PSS-SDV gel columns (5 μ m) with a porosity range from 10^2 to 10^5 Å (PSS, Mainz, Germany) were used together with a differential refractometer and a UV detector at 254 nm. Measurements were performed in THF with a flow rate of 1 mL/min using toluene as internal standard.

SEC experiments for the block copolymers containing DMAEMA were performed on a Waters instrument calibrated with narrowly distributed polystyrene standards. Four PSS-SDV gel columns (5 μ m) with a porosity range from 10^2 to 10^4 Å (PSS, Mainz, Germany) were used together with a differential refractometer and a UV detector at 254 nm. Measurements were performed in THF with additional 0.25-wt% tetrabutylammonium bromide (TBAB) as eluent and 0.5 ml/min as flow rate.

The absolute number-average molecular weights, M_n , of the synthesized block copolymers were determined by $^1\text{H-NMR}$ in CDCl_3 (Bruker AC 250 spectrometer) using the M_n of the first block, as determined by MALDI-ToF MS or SEC, and suitable NMR signal areas of the corresponding blocks.

Results and Discussion

The results presented in this report will be divided into two parts; first, a brief overview is given on the PS-*b*-PDMAEMA, PB-*b*-PDMAEMA and P*t*BS-*b*-PDMAEMA diblock copolymers and in the second part the results concerning PEO-*b*-PDMAEMA are discussed.

PS-*b*-PDMAEMA, PB-*b*-PDMAEMA and P*t*BS-*b*-PDMAEMA diblock copolymers were synthesized via sequential living anionic polymerization in THF at low temperatures using *sec*-BuLi as initiator. The first monomer was polymerized at -70 °C for 30 minutes (styrene), -10 °C for 10 hours (butadiene) or -70 °C for 1 hour (*p*-*tert*-butoxystyrene). The conversion of the first monomer was always monitored via the NIR probe. The reaction times were chosen to assure complete conversion of the first monomer. Subsequently, the living chain ends were capped with 1,1-diphenylethylene at -70 °C for one hour in order to reduce the nucleophilicity and to enable a smooth start of the second methacrylic monomer.^[31, 32] Afterwards, DMAEMA was added and the reaction was allowed to slowly warm up to -50 °C. DMAEMA was allowed to polymerize for one hour, followed by termination with 2-propanol. The THF-SEC traces for the P*t*BS₄₅₀ precursor, P*t*BS₄₅₀-*b*-PDMAEMA₁₁ and P*t*BS₄₅₀-*b*-PDMAEMA₄₉ diblock copolymers (subscripts denote the degree of polymerization) are shown in Figure 1A, indicating the living nature of the reaction. Figure 1B displays the SEC traces for the B₂₉₀ precursor and B₂₉₀DMAEMA₂₄₀ with THF and 0.25 wt. % TBAB as eluent. Please note that for B₂₉₀DMAEMA₂₄₀ a noticeable amount of termination (12%, calculated via a combination of SEC and ¹H-NMR) occurred. We believe that in this case a small amount of residual butadiene monomer prevailed. This may have added again to the DPE chain end, leading to a nucleophilic attack of the ester group upon addition of DMAEMA. Figure 1C shows the SEC traces for B₈₁₀ and B₈₁₀-*b*-DMAEMA₆₅. No side-reactions were observed in this case. Finally, Figure 1D displays the results obtained for PS₂₄₃ and PS₂₄₃-*b*-DMAEMA₃₇. The obtained results for all PS-*b*-PDMAEMA, PB-*b*-PDMAEMA and P*t*BS-*b*-PDMAEMA diblock copolymers are summarized in Table 1. As can be seen, the polymerizations resulted in narrowly distributed block copolymers (PDI < 1.1).

Table 1. Molecular characterization of the synthesized block copolymers.

sample ^a	$10^{-3} M_n$ (precursor) [g/mol]	$10^{-3} M_n$ (copolymer) ^b [g/mol]	M_w/M_n
$S_{243}DMAEMA_{37}$	24.3 ^c	30.0	1.04 ^c
$B_{810}DMAEMA_{65}$	43.7 ^d	54.0	1.05 ^c
$B_{290}DMAEMA_{240}$	15.7 ^d	53.5	1.07 ^c
$tBS_{450}DMAEMA_{11}$	80.1 ^e	82.0	1.04 ^f
$tBS_{450}DMAEMA_{49}$	80.1 ^e	88.0	1.04 ^f

- a) The subscripts denote the degree of polymerization of the corresponding block;
b) Calculated from 1H -NMR spectra in $CDCl_3$ using the absolute M_n of the first block;
c) Determined by SEC in THF with additional 0.25 wt. % TBAB calibrated with PS standards;
d) Determined by MALDI-ToF MS spectrometry;
e) Determined by SEC in THF equipped with a MALLS detector;
f) Determined by SEC in THF calibrated with PS standards.

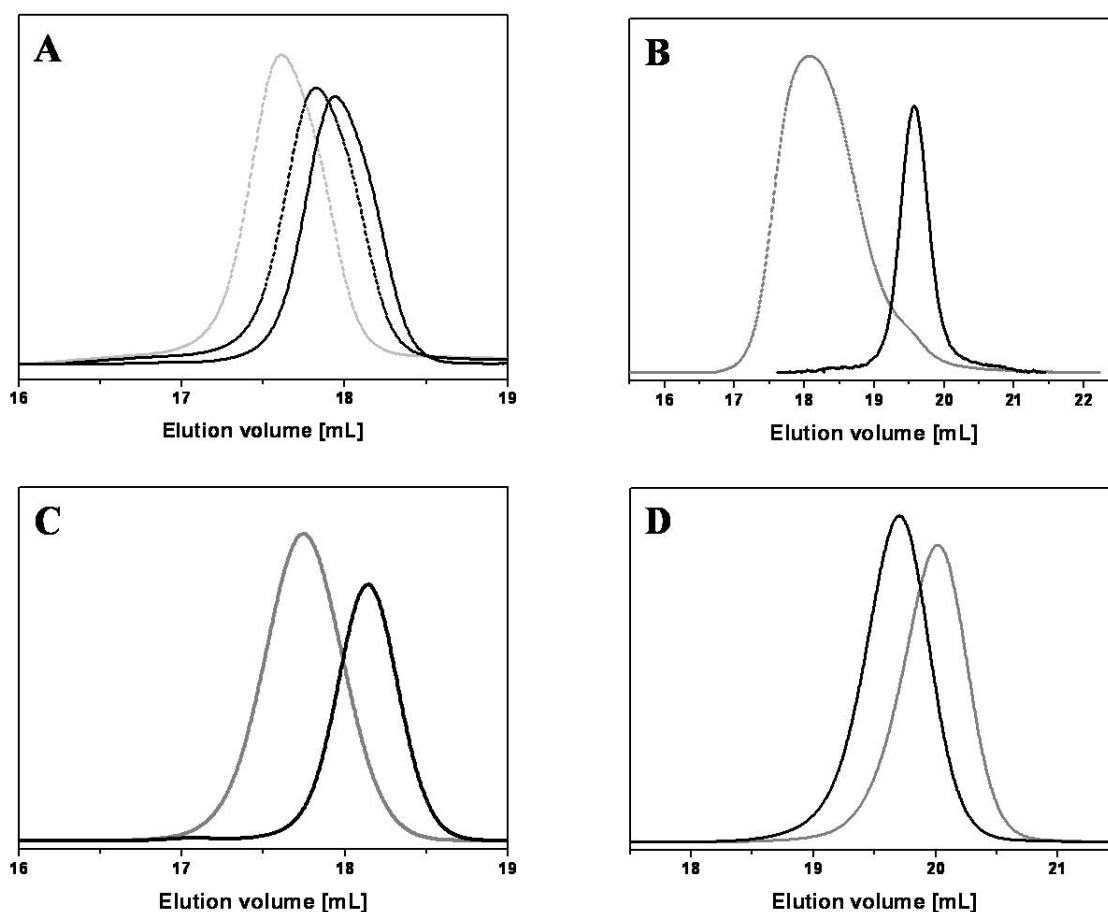


Figure 1: SEC elution traces (A) for $PtBS_{450}$ (black solid line; PDI=1.02), $PtBS_{450}$ - b -PDMAEMA₁₁ (dashed black line; PDI=1.04) and $PtBS_{450}$ - b -PDMAEMA₄₉ (dashed grey line; PDI=1.04) in THF as eluent, (B) for B_{290} (solid black line, PDI=1.02) and B_{290} - b -DMAEMA₂₄₀ (dashed grey line, PDI=1.07), (C) for B_{810} (solid black line, PDI=1.02) and B_{810} - b -DMAEMA₆₅ (solid grey line, PDI=1.05), and (D) for PS_{243} (solid grey line, PDI=1.02) and PS_{243} - b -DMAEMA₃₇ (solid black line, PDI=1.04) in THF and 0.25 wt. % TBAB as eluent.

PEO-*b*-PDMAEMA was synthesized via sequential anionic polymerization in THF with 1,1-diphenyl-3-methylpentyllithium (DPMP-Li) as initiator as depicted in Scheme 1. DPMP-Li was formed in situ at $-70\text{ }^{\circ}\text{C}$ through the addition of 1,1-diphenyl ethylene and *sec*-BuLi. After stirring for 10 minutes at this temperature, ethylene oxide (EO) was added and the reaction mixture was stirred at $-70\text{ }^{\circ}\text{C}$ for one hour. Subsequently, the temperature was raised slowly to $10\text{ }^{\circ}\text{C}$, followed by addition of the phosphazene base *t*-BuP₄ in order to promote polymerization of EO, which was conducted at $50\text{ }^{\circ}\text{C}$ for 2 days. The ratio of [*sec*-BuLi]/[*t*-BuP₄] was kept at 1/0.95. After complete conversion of the first monomer the temperature was lowered to $10\text{ }^{\circ}\text{C}$ (below this value the living PEO chains start to crystallize in THF) and DMAEMA was added. The reaction was terminated after 30 minutes with degassed methanol.

Scheme 1: Synthesis of PEO-*b*-PDMAEMA diblock copolymers via sequential anionic polymerization in THF with Li⁺ counterion in the presence of *t*-BuP₄ phosphazene base.

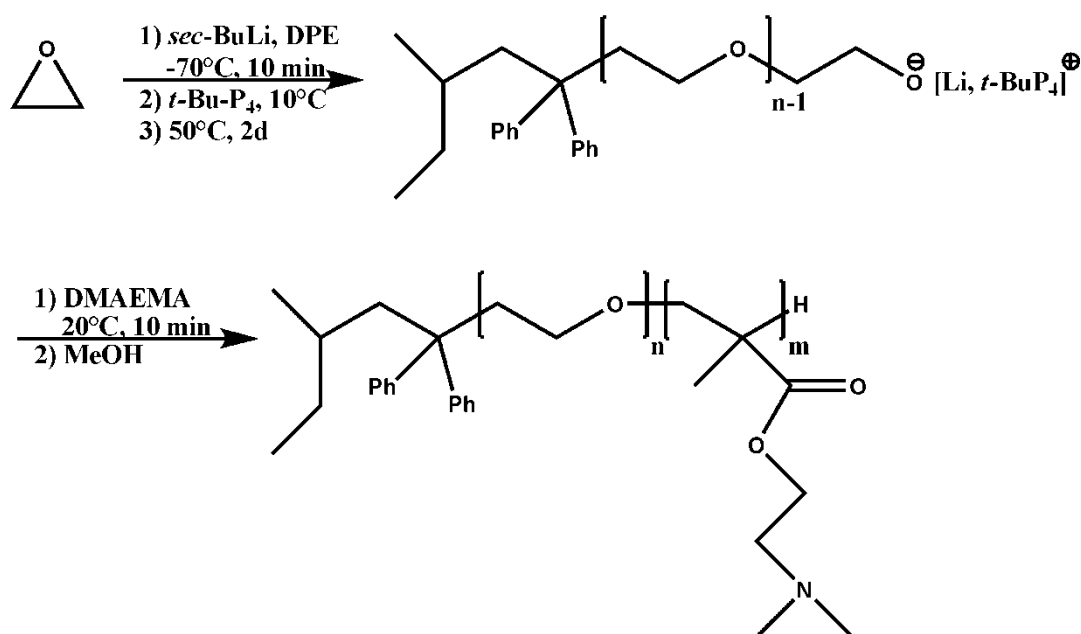


Table 2: Molecular characterization of the synthesized PEO-*b*-PDMAEMA block copolymers.

sample ^a	initiating system	$10^{-3} M_n$ (precursor) [g/mol]	$10^{-3} M_n$ (copolymer) [g/mol] ^b	M_w/M_n ^c	f^d
EO ₃₂₅ DMAEMA ₁₅₇	PEO [Li, <i>t</i> -BuP ₄] ⁺ , 10 °C ^e	14.3 ^f	40.5	1.40	96.6%
EO ₄₅ DMAEMA ₅₁ ^g	PEO ₄₅ -OH, <i>t</i> -BuP ₄ , 20 °C	2.0 ^f	10.9	1.70	80%
EO ₄₅ DMAEMA ₅₁ ^g	PEO ₄₅ -OH, <i>t</i> -BuP ₄ , 5 °C	2.0 ^f	11.0	1.60	80%

^{a)} The subscripts denote the degree of polymerization of the corresponding block;

^{b)} Determined via a combination of SEC and ¹H-NMR measurements;

^{c)} Determined by SEC in THF with additional 0.25 wt. % TBAB calibrated with PS standards;

^{d)} the initiation efficiency was calculated from ¹H-NMR spectra in CDCl₃ using the absolute M_n of the first block for calibration;

^{e)} DMAEMA added according to scheme 1; sequential living anionic polymerization;

^{f)} Determined by MALDI-ToF MS;

^{g)} Theoretical composition calculated for 100% macroinitiator efficiency.

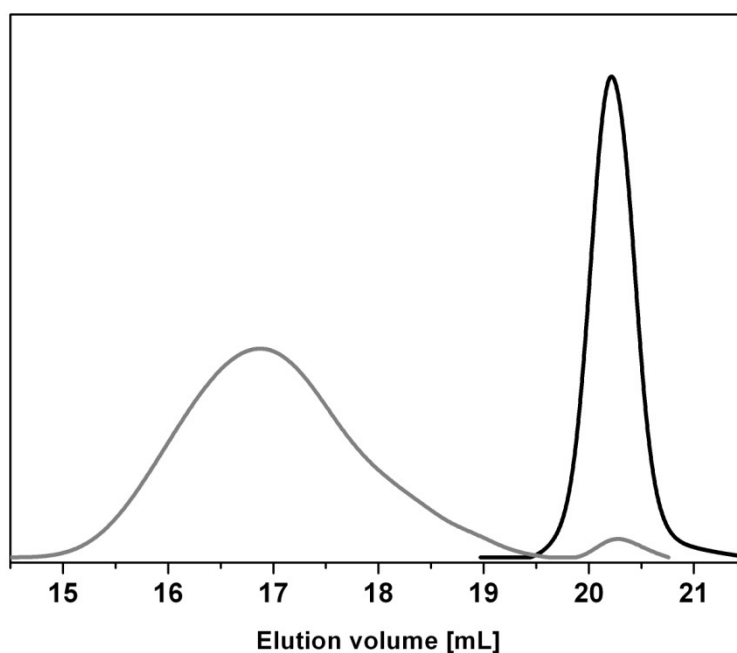


Figure 2: SEC elution traces of PEO₃₂₅ (solid black line; PDI=1.02) and PEO₃₂₅-*b*-PDMAEMA₁₅₇ (solid grey line; PDI=1.40) with THF and additional 0.25 wt. % *t*BAB as eluent.

The advantage of this synthetic approach is the possibility of a one-pot synthesis. Alternatively, the polymerization technique has to be changed from anionic to a controlled radical technique, potentially coupled with a considerable loss of macroinitiator. Furthermore, ABC triblock terpolymers with PEO as a water-soluble middle block and methacrylic monomers as endblock become feasible. The additional advantage of anionic polymerization is the control of the resulting microstructure, like in the case of butadiene or isoprene. The SEC traces in THF with 0.25 wt. % tetrabutylammonium bromide (TBAB) of PEO₃₂₅ and PEO₃₂₅-*b*-PDMAEMA₁₅₇ are given in Figure 2. The molecular characteristics of the PEO₃₂₅-*b*-PDMAEMA₁₅₇ diblock copolymer are shown in Table 2. The well-controlled nature of the polymerization is demonstrated by the PEO₃₂₅ precursor with a PDI of 1.02. As can be seen, a small amount of precursor is left in the SEC trace of PEO₃₂₅-*b*-PDMAEMA₁₅₇, but this corresponds to below 4 mol %, calculated by integration of the SEC eluograms, normalized by the molecular weights of the precursor and block copolymer, obtained via MALDI-ToF MS and ¹H-NMR, respectively. The molecular weight distribution is much broader (PDI = 1.40, PS calibration). To investigate the polymerization kinetics, NIR spectra were recorded during the polymerization and after solvent subtraction the vinylic =C-H overtone vibration of DMAEMA at 6162 cm⁻¹ was used for the calculation of the conversion. The results are shown in Figure 3A.

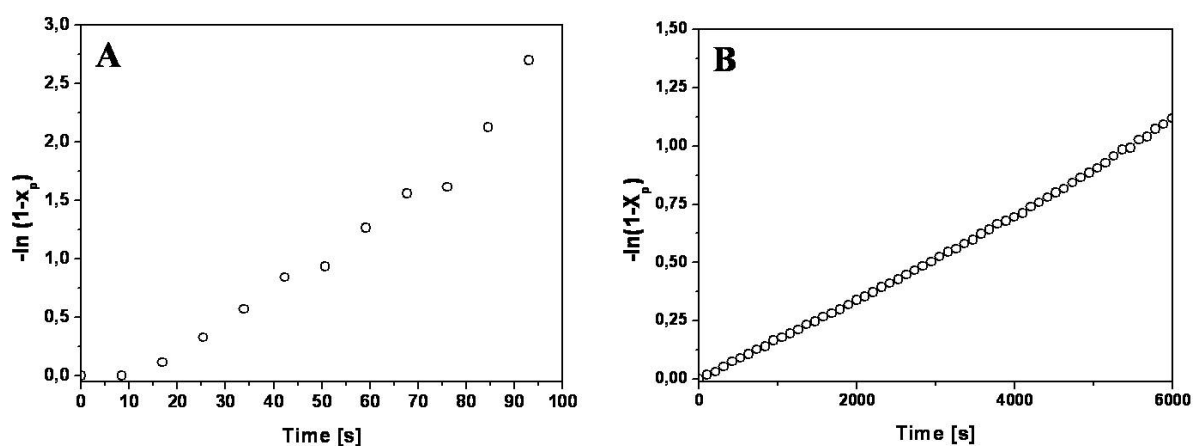


Figure 3: First-order plot of the kinetics of DMAEMA polymerization initiated by PEO-Li/*t*-BuP₄ in THF at 10 °C (A), first-order plot of the kinetics of the DMAEMA polymerization initiated by DPMPLi in THF at -70 °C (B).

Figure 3 clearly shows that slow initiation occurs upon addition of DMAEMA to the living PEO chain ends. This is expected since alkoxide anions are much less reactive than ester enolate ones. After ca. 20 s (ca. 20% monomer conversion), the first-order plot becomes linear (slope, $k_{\text{app}} = 0.031 \text{ s}^{-1}$), indicating a living polymerization. Taking into account the concentration of active chain ends, $[P^*] = 9.24 \times 10^{-4} \text{ mol/L}$, results a rate constant, $k_p = 33.5 \text{ L mol}^{-1} \text{ s}^{-1}$. Given the elevated temperature, the obtained polymerization rate is very low. In contrast, the homopolymerization of DMAEMA at $-70 \text{ }^\circ\text{C}$ initiated by DPHLi in the absence of phosphazene base but in presence of an excess of alkoxides (0.013 mmol/L) yielded a rate constant of $k_p = 60.8 \text{ L mol}^{-1} \text{ s}^{-1}$ (Figure 3B). Apparently, the phosphazene base dramatically decreases the reactivity of the PDMAEMA-Li chain end. According to theory,^[33] slow initiation should result in a maximum PDI of 1.33, explaining the obtained results for PEO-*b*-PDMAEMA with a PDI of ca. 1.40. The slightly higher value could be due to partial adsorption on the column during the SEC measurements as the copolymer has a rather long PDMAEMA block compared to most of the other block copolymers presented here. We suppose that with increasing content of PDMAEMA the effect of salt addition to the SEC eluent, which should prevent adsorption to the column, diminishes. A similar effect can be seen in the SEC traces for B₂₉₀DMAEMA₂₄₀ (Figure 1B). To further evaluate the distribution of the PEO₃₂₅-*b*-PDMAEMA₁₅₇ diblock copolymer MALDI-ToF mass spectrometry was performed. The results are depicted in Figure 4. The lower trace shows the PEO₃₂₅ precursor with a peak maximum at $M_n = 14\,300 \text{ g/mol}$ whereas the upper curve corresponds to the PEO₃₂₅-*b*-PDMAEMA₁₅₇ diblock copolymer. The residual amount of PEO₃₂₅ precursor is clearly visible, although easily overestimated due to the fact that ionization discriminates different polymers and that shorter chains are more easily ionized. For the diblock copolymer, MALDI results in a molecular weight of $M_n = 39\,100 \text{ g/mol}$ and a polydispersity of 1.02. It is known that MALDI rather underestimates polydispersities, so the true value for the molecular weight distribution of PEO₃₂₅-*b*-PDMAEMA₁₅₇ should be situated between the SEC and MALDI results.^[34] The molecular weight for PEO₃₂₅-*b*-PDMAEMA₁₅₇, though, is in quite good accordance with ¹H-NMR ($M_n = 40\,500 \text{ g/mol}$, Table 2).

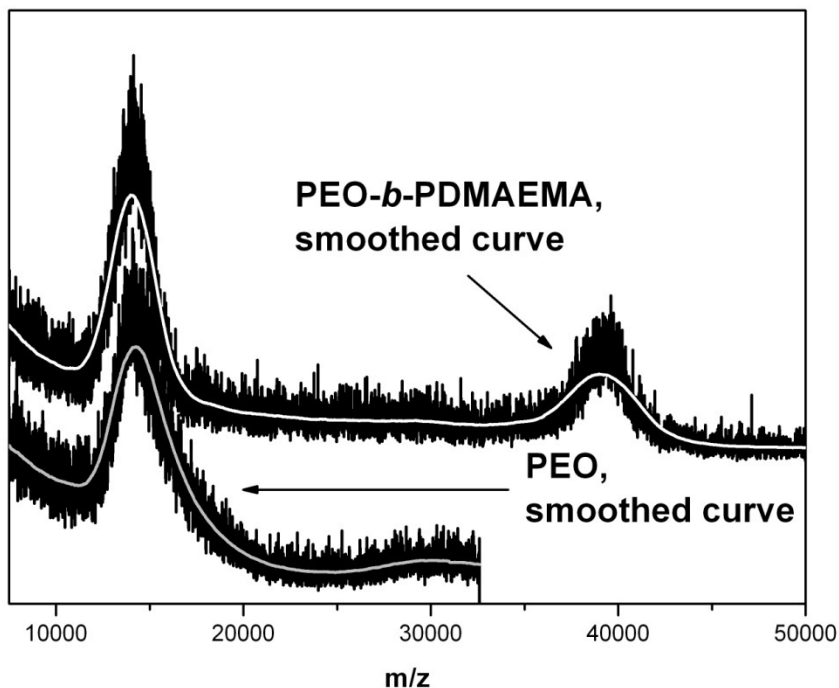


Figure 4: MALDI-ToF mass spectra of PEO₃₂₅ (lower curve, smoothed curve depicted in light gray; $M_{\text{peak}}=14300$ g/mol; matrix (DHB): salt (AgTFA): polymer = 10:1:1) and PEO₃₂₅-*b*-PDMAEMA₁₅₇ (upper curve, smoothed curve displayed in white; $M_{\text{peak}}=39100$ g/mol; matrix (DCTB): salt (KTFA): polymer = 10:1:1).

To point out the advantages of the one-pot synthesis presented here, comparable anionic polymerizations were performed employing a commercially available monofunctional PEO-OH as a macroinitiator with a molecular weight of 2 000 g/mol (EO₄₅-OH) and a polydispersity index of 1.03. The polymer was purified through repeated precipitation in methanol and afterwards dried over night on a high vacuum line at 50 °C. Then it was dissolved in dry THF and cooled to 5 °C. Below this value, the polymer starts to crystallize; the temperature is lower compared to PEO₃₂₅ due to its lower molecular weight. Afterwards, *t*-BuP₄ phosphazene base (1 eq) was added and the reaction mixture was stirred for one hour to ensure complete deprotonation of PEO-OH. Then DMAEMA was added and after 30 minutes the polymerization was terminated with methanol. The results are shown in Table 2. SEC traces (THF with 0.25 wt.-% TBAB as eluent) are provided in Figure 5. The remaining unreacted macroinitiator can be clearly seen underneath the precursor. The two different polymerization temperatures (5 °C and 25 °C) do not seem to affect the reaction significantly. In both cases, blocking efficiency was around 80mol% (de-

terminated through a combination of SEC and $^1\text{H-NMR}$), i.e. significantly lower compared to that of the one-pot synthesis.

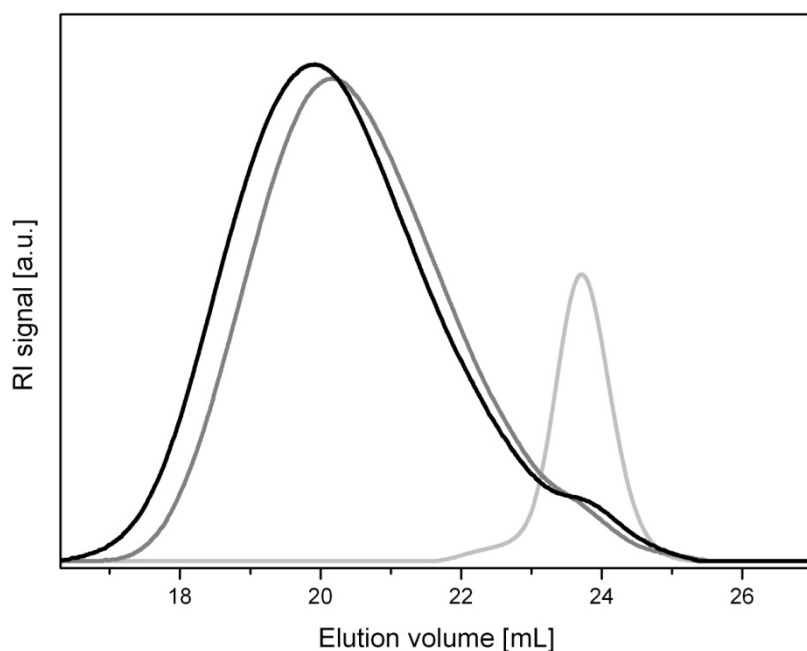


Figure 5: SEC elution traces of PEO_{45} (light grey line) and $\text{PEO}_{45}\text{-}b\text{-PDMAEMA}_{51}$ (grey and black line) with THF and additional 0.25 wt. % TBAB as eluent; the difference between both $\text{PEO}_{45}\text{-}b\text{-PDMAEMA}_{51}$ samples is the polymerization temperature (25°C for (grey line) and 5°C for (black line)); blocking efficiency is comparable and around 80 mol%.

Conclusions

Several diblock copolymers with DMAEMA as a second “smart” block were successfully synthesized. $\text{PS-}b\text{-PDMAEMA}$, $\text{PB-}b\text{-PDMAEMA}$ and $\text{P}t\text{BS-}b\text{-PDMAEMA}$ were adequately characterized and their behavior in the bulk as well as in solution as building block for self-organized nanostructures will be reported in the near future. $\text{PS-}b\text{-PDMAEMA}$ diblock copolymers show potential in the field of stimuli-responsive membranes.^[35] In the case of $\text{PEO-}b\text{-PDMAEMA}$, the characterization is still not absolutely conclusive, but a living manner of the polymerization is definitely indicated. Online FT-NIR measurements indicate a slow initiation taking place and, thus, polydispersities in the range of 1.3 are to be expected. It will now be the subject of further research to extend these results to ABC triblock terpolymers with PEO as middle block and PDMAEMA as end block and also their possible application as, e.g. stimuli-responsive polymeric hydrogels.

Acknowledgment

The authors thank Manuela Schumacher and Jeannine Rockser for the MALDI-ToF MS measurements and Sabine Wunder, Michael Sommer and Andreas Walther for the SEC measurements. Financial support from the VolkswagenStiftung and German Science Foundation (priority program 1259) is gratefully appreciated.

References:

- [1] M. Szwarc, M. Levy, R. Milkovich, *J. Am. Chem. Soc.* 1956, 78, 2656.
- [2] M. Szwarc, *Nature (London)* 1956, 178, 1168.
- [3] S. Förster, M. Antonietti, *Adv. Mater.* 1998, 10, 195.
- [4] M. A. Cohen Stuart, B. Hofs, I. K. Voets, A. de Keizer, *Curr. Opin. Colloid Interface Sci.* 2005, 10, 30.
- [5] C. Schilli, M. Zhang, A. H. E. Müller, *Macromolecules* 2004, 37, 7861.
- [6] F. A. Plamper, A. Schmalz, E. Penott-Chang, M. Drechsler, A. Jusufi, M. Ballauff, A. H. E. Müller, *Macromolecules* 2007, 40, 5689.
- [7] F. A. Plamper, A. Schmalz, M. Ballauff, A. H. E. Müller, *J. Am. Chem. Soc.* 2007, 129, 14538.
- [8] F. Plamper, A. Walther, A. H. E. Müller, M. Ballauff, *Nano Lett.* 2007, 7, 167.
- [9] F. Plamper, M. Ruppel, A. Schmalz, O. Borisov, M. Ballauff, A. H. E. Müller, *Macromolecules* 2007, 40, 8361.
- [10] Y. Xu, S. Bolisetty, M. Drechsler, B. Fang, J. Yuan, M. Ballauff, A. H. E. Müller, *Polymer* 2008, 49, 3957.
- [11] D. Fournier, R. Hoogenboom, L. Thijs, R. M. Paulus, U. S. Schubert, *Macromolecules* 2007, 40, 915.
- [12] E. Rakhmatullina, T. Braun, M. Chami, V. Malinova, W. Meier, *Langmuir* 2007, 23, 12371-12379.
- [13] C. S. Patrickios, A. B. Lowe, S. P. Armes, N. C. Billingham, *J. Polym. Sci., Part A: Polym. Chem.* 1998, 36, 617.
- [14] T. C. Krasia, C. S. Patrickios, *Polymer* 2002, 43, 2917.
- [15] A. I. Triftaridou, S. C. Hadjiyannakou, M. Vamvakaki, C. S. Patrickios, *Macromolecules* 2002, 35, 2506.
- [16] S. Antoun, P. Teyssié, R. Jérôme, *Macromolecules* 1997, 30, 1556.
- [17] L. Qiongqiong, Y. Zhangqing, N. Peihong, *Colloid Polym. Sci.* 2004, 387.
- [18] S. Creutz, P. Teyssié, R. Jérôme, *Macromolecules* 1997, 30, 6.

- [19] S. Liu, J. V. M. Weaver, Y. Tang, N. C. Billingham, S. P. Armes, K. Tribe, *Macromolecules* 2002, *35*, 6121.
- [20] M. Vamvakaki, N. C. Billingham, S. P. Armes, *Macromolecules* 1999, *32*, 2088.
- [21] J.-F. Gohy, S. Antoun, R. Jerome, *Macromolecules* 2001, *34*, 7435.
- [22] P.-H. Tung, S.-W. Kuo, S.-C. Chen, C.-L. Lin, F.-C. Chang, *Polymer* 2007, *48*, 3192.
- [23] M. Li, K. Douki, K. Goto, X. Li, C. Coenjarts, D. M. Smilgies, C. K. Ober, *Chem. Mater.* 2004, *16*, 3800.
- [24] T. Higashimura, K. Kojima, M. Sawamoto, *Makromol. Chem.* 1989, *15*, 127.
- [25] G. Dinesh, S. Höring, J. Ulbricht, *Makromol. Chem., Rapid Comm.* 1984, *5*, 615.
- [26] H. Reuter, I. V. Berlinova, S. Höring, J. Ulbricht, *Eur. Polym. J.* 1991, *27*, 673.
- [27] Y. Nagasaki, Y. Sato, M. Kato, *Macromol. Rapid Commun.* 1997, *18*, 827.
- [28] A. Ah Toy, S. Reinicke, A. H. E. Müller, H. Schmalz, *Macromolecules* 2007, *40*, 5241.
- [29] B. Esswein, A. Molenberg, M. Möller, *Macromol. Symp.* 1996, *107*, 331.
- [30] H. Schmalz, M. G. Lanzendörfer, V. Abetz, A. H. E. Müller, *Macromol. Chem. Phys.* 2003, *204*, 1056.
- [31] D. Freyss, P. Rempp, H. Benoît, *Polym. Lett.* 1964, *2*, 217.
- [32] R. P. Quirk, T. Yoo, Y. Lee, J. Kim, B. Lee, *Adv. Polym. Sci.* 2000, *153*, 67.
- [33] L. Gold, *J. Chem. Phys.* 1958, *28*, 91.
- [34] G. Montaudo, F. Samperi, M. S. Montaudo, *Progress in Polymer Science* 2006, *31*, 277.
- [35] F. Schacher, M. Ulbricht, A. H. E. Müller, *submitted* 2008.

Self-Supporting, Double Stimuli-Responsive Porous Membranes from Polystyrene-*block*-poly(N,N-dimethylaminoethyl methacrylate) Diblock Copolymers*

Felix Schacher*, Mathias Ulbricht, and Axel H. E. Müller*

[*] Prof. Axel H. E. Müller, Felix Schacher

Makromolekulare Chemie II, Universität Bayreuth

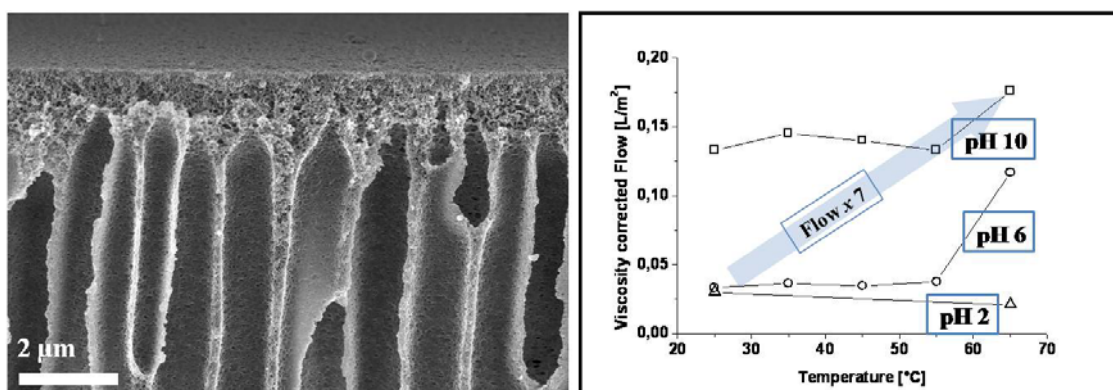
Universitätsstrasse 30, D-95440 Bayreuth

E-mail: axel.mueller@uni-bayreuth.de; felix.schacher@uni-bayreuth.de;

Prof. Mathias Ulbricht

Technische Chemie II, Universität Duisburg-Essen

Universitätsstr. 2, D-45117 Essen



Abstract

Asymmetric membranes are prepared via the non-solvent induced phase separation (NIPS) process from a polystyrene-*block*-poly(N,N-dimethylaminoethyl methacrylate) (PS-PDMAEMA) block copolymer. The polymer was prepared via sequential living anionic polymerization. Membrane surface and volume structures were characterized by scanning electron microscopy. Due to their asymmetric character, resulting in a thin separation layer with pores below 100 nm on top and a macroporous volume structure, the membranes are self-supporting. Furthermore, they exhibit a defect-free surface over several hundred μm^2 . Polystyrene serves as the membrane matrix, whereas the pH- and temperature-sensitive minority block, PDMAEMA, renders the material double stimuli-responsive. Therefore, in terms of water flux, the membranes are able to react on two independently applicable stimuli, pH and temperature. Compared to the conditions where the lowest water flux is obtained, low temperature and pH, activation of both triggers results in a 7-fold permeability increase. The pore-size distribution and the separation properties of the obtained membranes were tested through the pH-dependent filtration of silica particles with sizes of 12-100 nm.

Introduction

Block copolymers represent an ambitious class of materials as their scope of applicability is still rising. Mostly, this is due to their inimitable self-assembling properties, rendering them suitable for applications in solution,^[1] in thin films^[2, 3] or as components of porous composite membranes.^[4, 5] Also in the field of industrially important membrane production processes, in particular via controlled phase separation (“phase-inversion”) of polymer solutions, block copolymers are becoming more and more popular. This is mainly attributed to the constantly increasing number of processes in which the desired separation problem cannot be solved with state-of-the-art membranes.^[6] Characteristic problems are uneven pore size distributions or insufficient long-term stability, especially due to membrane fouling. A very important issue is also the additional functionalization of membrane materials.^[6] Often, membrane surfaces are post-functionalized through “grafting-to”,^[7] “grafting-from”^[8] or reactive coating with polymers.^[9]

An alternative are additives to the membrane polymer, and special graft or block copolymers have already been found to be rather efficient in rendering the surface of porous membranes from standard engineering polymers such as poly(vinylidene fluoride) or polyethersulfone more hydrophilic and less susceptible to fouling.^[10, 11]

One of the key features of block copolymers is the facile implementation of “smart” materials, containing compartments with the ability to change conformation or properties upon application of environmental stimuli like pH, temperature or light^[12]. Hence, in combination with their ability to create well-defined patterns on a mesoscopic length scale, block copolymers embody promising candidates for the fabrication of stimuli-responsive functional membranes with high selectivity, tunable properties and narrowly distributed pores.

Non-solvent-induced phase separation (NIPS) is the most important industrial process for the fabrication of “asymmetric” membranes, having a very thin “skin” layer supported by a macroporous substructure.^[13] Recently, this process has been applied for the first time to well-defined block copolymers, polystyrene-*block*-poly(4-vinylpyridine) (PS-*b*-P4VP).^[14] Asymmetric membranes with a narrow pore size distribution in a ~250 nm thin separation layer could be obtained. Here, P4VP should act as a weak polyelectrolyte and therefore a pH-sensitive block; however the stimuli-responsive transport through the membranes was not reported in that work. Other attempts use stimuli-responsive polymeric additives in already established NIPS processes in order to enhance the properties of the resulting membranes through co-precipitation.^[15, 16] However, the reported procedures generate membranes which can react to a single stimulus only.

Here we present the formation of double stimuli-responsive membranes for the possible applications in ultrafiltration or microfiltration. These materials combine a rather narrow pore-size distribution with mechanical stability and high water flux. The membranes were prepared via NIPS from amphiphilic polystyrene-*block*-poly(*N,N*-dimethylaminoethyl methacrylate) (PS-*b*-PDMAEMA) diblock copolymers in THF/DMF mixtures. The resulting structures are self-supporting and defect-free over several hundred μm^2 . The advantage of using PDMAEMA as the hydrophilic block is that its solubility in aqueous solution can be triggered by two stimuli, pH and temperature.^[17-19] Temperature response is related to a lower critical solution temperature (LCST). The corresponding phase transition temperature (cloud point,

T_{cl}) strongly depends on solution pH, the cloud point can get close to room temperature at $\text{pH} \geq 10$ for high molecular weights. The polymer is completely soluble over the whole accessible temperature range below $\text{pH} 6$ due to partial or full protonation. In presence of small amounts of multivalent counterions, in addition to the LCST, even an upper critical solution temperature (UCST) can be obtained for such systems.^[19] There have been attempts to incorporate PDMAEMA into ultrafiltration membranes through random copolymerization with acrylonitrile,^[20] but the content of switchable material was rather low, and the recovery of the PDMAEMA conformation after stimuli-response was hampered.^[21]

Experimental

Materials

sec-Butyllithium (Acros) was used as delivered. THF (Fluka) was distilled from CaH_2 and K. Afterwards, the solvent was directly transferred into the stirred glass reactor. Styrene was kindly provided by BASF and was stirred over Bu_2Mg and afterwards condensed on a vacuum line into glass ampoules. N,N-dimethylaminoethyl methacrylate (Aldrich) was stirred with tri-octylaluminium and afterwards condensed on a vacuum line. 1,1-diphenylethylen (Aldrich) was distilled from *sec*-butyllithium. The 12 nm particles were purchased from Aldrich (LUDOX AM-30, suspension in water). The particles with 22, 36, 60, and 104 nm were synthesized using the Stöber method.^[24]

Synthesis

Polystyrene-*block*-poly(2-dimethylaminoethyl methacrylate) was synthesized via sequential living anionic polymerization in THF (500 ml) at low temperatures in the presence of alkoxides to stabilize the living chain end.^[25] First, styrene (25 g, 0.24 mol) was initiated with *sec*-butyllithium (0.35 ml, 0.49 mmol) at -70°C . Afterwards, the reaction was allowed to proceed at -70°C for 30 minutes. For polymerization of the second block, the polystyrene chains were end-capped with 1,1-diphenyl ethylene (0.18 ml, 1 mmol) at -50°C in order to attenuate the reactivity of the anions. Otherwise, attack of the ester moiety would occur upon addition of 2-dimethylaminoethyl methacrylate. The latter (5.86 g, 37.3 mmol) was injected via syringe into the reaction vessel and was polymerized for 1 h at -40°C . Finally, the

reaction was stopped through addition of 3 ml of degassed isopropanol, and the polymer was purified through dialysis against THF and dioxane and freeze-dried.

Membrane preparation

Membranes were prepared via the NIPS process. 200 μm thick films were cast from a solution of PS-*b*-PDMAEMA (1.5 g, 15 wt. %), DMF (4.25 g, 42.5 wt. %) and THF (4.25 g, 42.5 wt. %) with a doctor blade onto polished glass substrates. After 60 seconds exposure to air (relative humidity was 30-40% and temperature was $\sim 20^\circ\text{C}$), the as-cast films were immersed into a bath containing de-ionized water for final formation of the membrane morphology. During the next 60 minutes, the films started to lift off the glass surface. After 12 hours, the membranes were taken out of the water bath, stored in de-ionized water until used and characterized as follows.

Water flux measurements

Water flux measurements were carried out in a stirred ultrafiltration test cell (Amicon 8010, Millipore, effective membrane diameter 22 mm) connected to a water reservoir at a constant height of the water column of 25 cm, providing a trans-membrane pressure of 0.025 bar. The membrane was placed in this cell which was immersed in a water bath kept at constant temperature. pH was adjusted through dilute solutions of NaOH and HCl in deionized water; after each change in pH a time span of 2 hours under flow-through was used to allow equilibration. Temperature ramps were performed through keeping the whole ultrafiltration cell in a tempered water bath. Steps were 10 K, equilibration time in between two points was 1 hours, except for the highest temperature (65°C : 2 hours).

Filtration of silica particles

Filtrations of colloidal silica particles were carried out in the same ultrafiltration cell as described above, but at a pressure of 0.1 - 0.2 bar supplied by nitrogen. The feed solutions were prepared through diluting the particle stock solutions with de-ionized water and adjusting the pH with NaOH or HCl. Typically, 10 ml of the feed solutions were filled into the Amicon cell. After the filtration of 8 ml, the remaining 2 ml were kept as retentate solution. Upon changing the particle size, the cell was rinsed 5 times with de-ionized water, and afterwards 50 ml were passed through the membrane to remove adsorbed silica particles.

Characterization

NMR

^1H -NMR measurements were performed on a Bruker 250 MHz AC spectrometer in CDCl_3 as solvent. The block copolymer composition was determined through the integral ratio between the styrene protons (5H, $\delta \sim 7.2$ ppm) and the CH_2 protons adjacent to the tertiary amino group of DMAEMA (2H, $\delta = 4.1$ ppm).

Size exclusion chromatography

Gel permeation chromatography (GPC) measurements were performed on a set of 30 cm SDV-gel columns of 5 mm particle size having a pore size of 10^5 , 10^4 , 10^3 and 10^2 Å with refractive index and UV ($\lambda = 254$ nm) detection. GPC was measured at an elution rate of 1 ml/min with THF containing 0.25 wt.% TBAB as eluent.

Scanning electron microscopy

SEM was carried out on a Leo Gemini 1530. The specimens were dried under vacuum over night and coated with approximately 2 nm Pd. For cross section, a piece of the sample was frozen together with the sample holder and broken afterwards.

Dynamic light scattering

Dynamic light scattering (DLS) measurements were performed in sealed cylindrical scattering cells ($d = 10$ mm) at a scattering angle of 90° on an ALV DLS/SLS-SP 5022F equipment consisting of an ALV-SP 125 laser goniometer with an ALV 5000/E correlator and a He-Ne laser with the wavelength $\lambda = 632.8$ nm. The CONTIN algorithm was applied to analyze the obtained correlation functions. Apparent hydrodynamic radii were calculated according to the Stokes-Einstein equation.

Results and Discussion

Synthesis and Characterization

The selected block copolymer was synthesized via sequential living anionic polymerization has a number average molecular weight of 75,000 g/mol and exhibits a narrow molecular weight distribution with $M_w/M_n = 1.04$. The final composition was determined as $PS_{81}PDMAEMA_{19}^{75}$. The subscripts denote the weight fractions in % and the superscript the molecular weight in kg/mol. The corresponding degrees of polymerization are 607 for polystyrene and 92 for PDMAEMA. The SEC traces with THF and additional 0.25 % tetrabutylammonium bromide (TBAB) as eluent are shown in Figure 1. The molecular weight of the PS block was determined via a PS calibration curve. For the second block, PDMAEMA, the 1H -NMR integral ratios between characteristic signals of the two blocks (PS: 5H, $\delta = 6.8 - 7.3$ ppm; PDMAEMA: 2H, -CH₂-, $\delta \approx 4$ ppm) were compared.

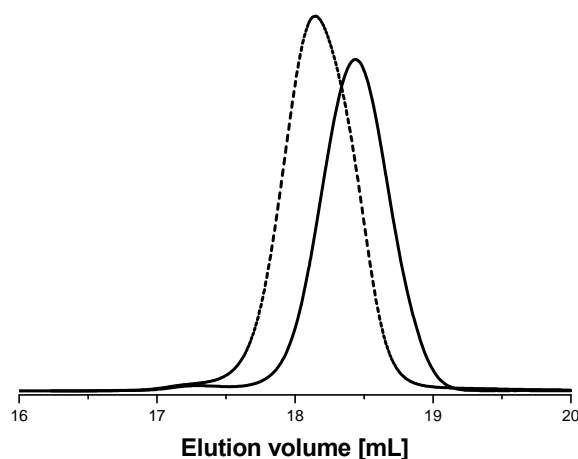


Figure 1: SEC traces for the PS precursor (solid line) and the $S_{81}D_{19}^{75}$ diblock copolymer (dashed line).

Membrane Preparation via Phase Inversion

The NIPS process is a straightforward and fast one-step procedure. Membranes formed by this preparation process usually exhibit an integrally anisotropic cross-section and are classical examples for high-performance materials for pressure-driven separation processes like ultrafiltration, nanofiltration or reverse osmosis.^[6] An intrinsic feature is the thin separation layer on top (thickness ~50 nm up to sev-

eral μm), supported from underneath through the main macroporous part of the membrane. Typically, polymer solutions of about 10-20 wt. % in organic solvents or solvent mixtures that are miscible with water are cast on a substrate, e.g. glass, using a doctor blade, and afterwards they are immersed in a non-solvent bath for coagulation and final film formation. We used a mixture of THF (50%) as a highly volatile solvent with DMF (50%). After film-casting, the solvent was allowed to evaporate for 60 seconds before the whole substrate was immersed into a non-solvent bath filled with de-ionized water ($\text{pH} \approx 6$). During the time before immersion, mostly THF evaporates, the polymer enriches at the polymer-air interface and presumably phase separation starts in the top layer of the “proto-membrane”. We suppose that this step is crucial for the formation of the pores of the separation layer. Generally, PDMAEMA is water-soluble at ambient temperature but the high content of hydrophobic polystyrene in PS-*b*-PDMAEMA assured immediate precipitation upon contact with water. This is even more pronounced as THF is the better solvent for polystyrene, and the composition of the solvent mixture in the top layer region is strongly shifted towards DMF already before non-solvent contact. After immersion in the precipitation bath, final solvent exchange and solid film formation take place. The membranes were taken out of the water bath after 12 hours and dried in vacuum for scanning electron microscopy (SEM) analysis. The resulting micrographs are shown in **Figure 2**.

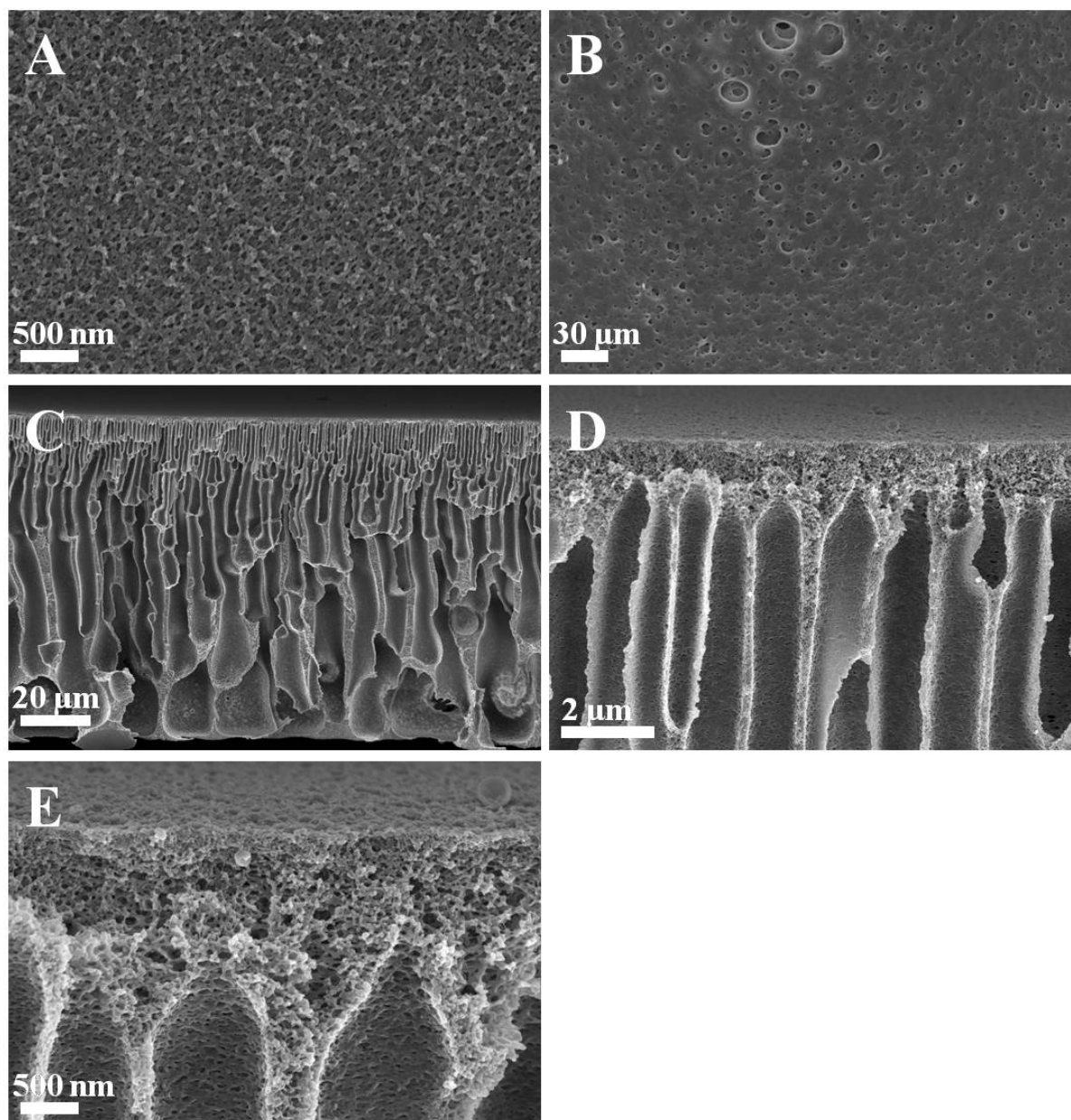


Figure 2: SEM micrographs of the membranes prepared via phase inversion (NIPS); A: on-top view onto the membrane surface; B: view onto the bottom of the membrane; C-E: cross sections at different magnifications.

Figure 2A presents a view onto the outer membrane surface at high magnification. The structure does not seem to be well-ordered; the appearance is rather sponge-like without any long-range order. We ascribe this to the rapid precipitation occurring upon the immersion of the “proto”-membrane into the non-solvent bath. The pore size is in the range of 20-80 nm, positioning this membrane at the borderline between ultra- and microfiltration.^[6] However, no larger pores or defects are present; the membrane exhibits a regular porous surface over several hundred μm^2 . Figure 2B is the view onto the bottom surface, formerly in contact with the glass

substrate. Here, the membrane exhibits larger pore sizes up to 1 μm . This is not undesirable because larger pores in the supporting sublayer are the precondition for a high flux. Figures 2C, D and E show cross-sectional cuts of the asymmetric membrane at different magnifications. Clearly, a distinguished separation layer is obtained on the top with a thickness of around 1 μm (E). Beneath this fragment, broader channels appear with an evident arrangement perpendicular towards the former glass substrate (C). These are the so-called macrovoids, developed during the immersion and final film formation in the water bath. This cross-section structure is typical for polymer membranes obtained by NIPS with rapid precipitation (“instantaneous demixing”), the anisotropy is due to the time delay and changing compositions during non-solvent / solvent exchange over film thickness.^[22] The reason for instantaneous demixing is the incompatibility of the PS blocks in PS-*b*-PDMAEMA with water. Membrane thickness as determined via SEM or a dial gauge was $85 \pm 10 \mu\text{m}$. Unfortunately, the sponge-like morphology of the membrane top layer prohibited the calculation of the effective membrane porosity and therefore, neither Hagen-Poiseuille’s law^[14] nor the Guerout-Elford-Ferry equation^[23] could be employed for the estimation of an average pore diameter.

Water Flux Measurements

The water flux through the membrane was measured as function of the applied transmembrane pressure. At 0.5 bar and 25°C, a flux of 560 L/m²h could be obtained. Compared to the values reported for the PS-*b*-P4VP asymmetric membranes (20 L/m²h),^[14] the flux is considerably higher. This could probably be explained by a smaller effective pore size of the membranes from this previous work. The dependence of flux on pressure is shown in **Figure 3A**, and as expected for a stable porous membrane, flux increases in a linear manner.

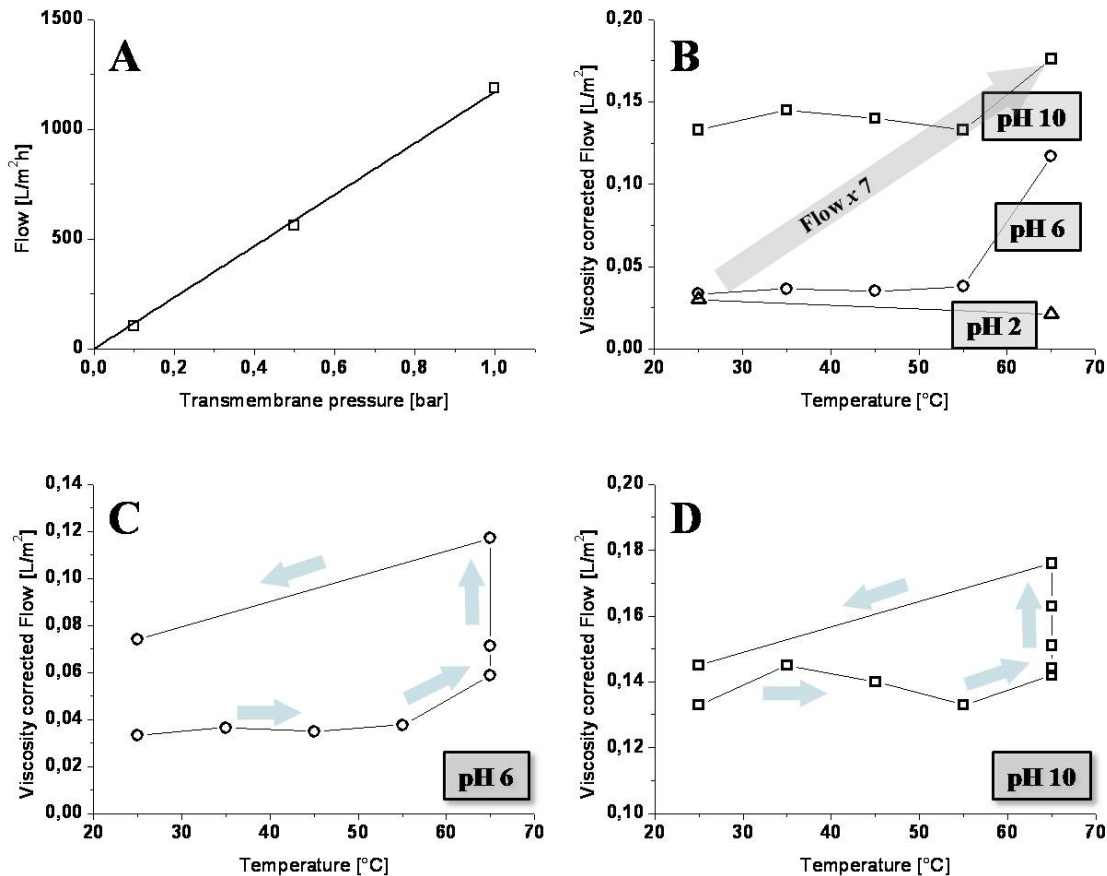


Figure 3: Water flux for $S_{81}D_{19}^{75}$ asymmetric membranes; depending on the applied transmembrane pressure and linear regression (A); for different pH values and temperatures (B, overview); for pH 6 (C) and pH 10 (D) depending on the temperature; the membranes were tempered at 65 $^{\circ}C$ for 120 minutes in both cases; the black lines in B, C, and D are just a guide to the eye; please note that the decrease of flux to a new constant value upon decrease of temperature from 65 to 25 $^{\circ}C$ occurs within 2 h at pH 10 and 12 h at pH 6.

Next, environmental conditions were varied to trigger the two possible stimuli for PDMAEMA. To reach a new equilibrium state under flow-through conditions, each change in pH was performed over a time span of 2 hours. The waiting time in between two temperature segments was 1 hour (except for 65 $^{\circ}C$: 2 hours). Figure 3B provides an overview over all the performed steps. All flux values except those in Figure 3A are corrected with respect to viscosity. Figure 4 shows a schematic depiction of our conclusion with respect to the membrane pore walls at the different stages of the experiment.

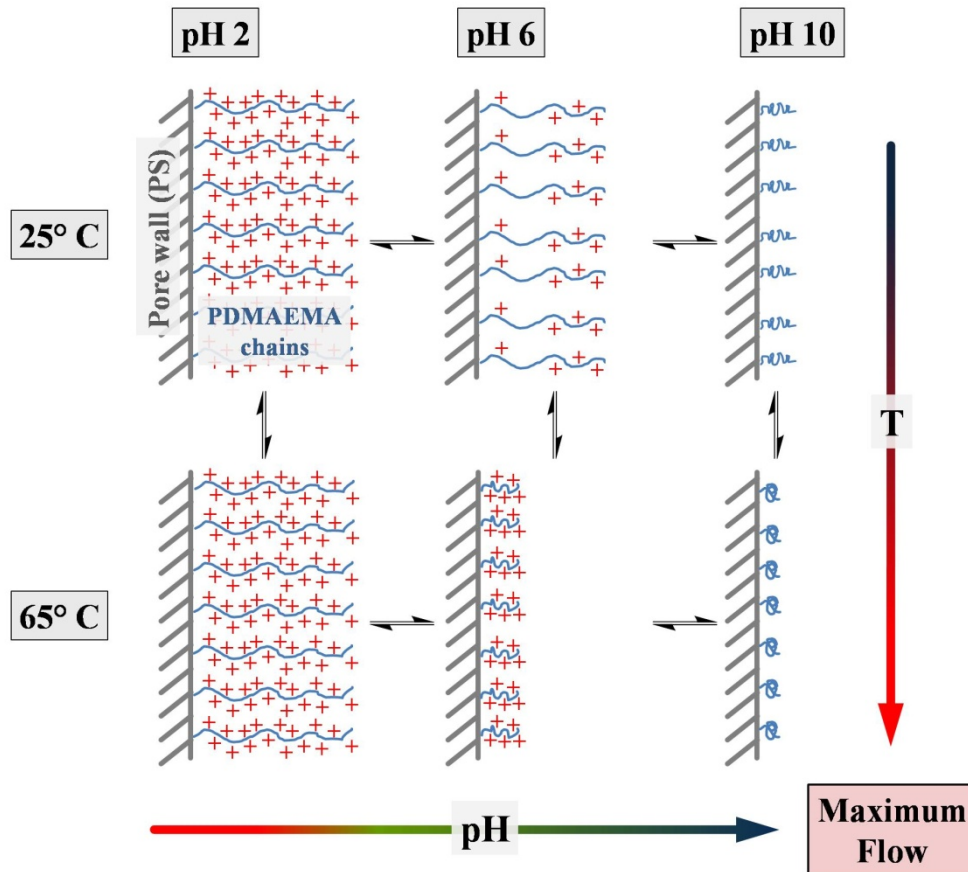


Figure 4: Schematic depiction of the different states of the inner part of membrane pores for $S_{81}D_{19}^{75}$ depending on pH and temperature; idealized illustration as PDMAEMA also is incorporated into the pore walls.

At pH 2 and ambient temperature, a viscosity-corrected flux value of 0.025 L/m^2 was obtained. No flux increase could be detected upon raising the temperature to 65°C . This is due to full protonation of the PDMAEMA segments, keeping the charged polymer chains extended at all temperatures (Figure 3, left hand part). At pH 6, PDMAEMA is still partially protonated ($\text{pK}_b = 7.78^{[17]}$). The measured flux at room temperature is not significantly higher and does not change until 55°C (Figure 4, upper middle part). However, at 65°C , flux increased by a factor of 4. Here, the charge density along the polymer chain segments is considerably lower than at pH 2, resulting in a certain collapse upon heating above the phase transition temperature. Though, some charge is present and hence the chains cannot completely collapse (Figure 4, lower middle part). Therefore, the transmembrane flux does not reach its maximum value. At pH 10 and 25°C , the flux is already high. At this pH, the polymer chains are uncharged and less extended (Figure 4, upper right part). At 65°C the flux further increased, indicating a further collapse of the PDMAEMA

segments (Figure 4, lower right part). To fortify our conclusions drawn in Figure 4, the relative change in flux should be higher for pH 6 than for pH 10. Indeed, whereas flux increases by a factor of 4 for pH 6, heating to 65 °C at pH 10 alters the water flux by a factor of 1.6. If the flux at pH 2 and 25 °C is compared to the final value at pH 10 and 65 °C, permeability increases by a factor of 7. Assuming standard pore flow models (cf. above), this corresponds to a change in effective pore radius by a factor of 2 to 3. Former work in our group compared the LCST behavior of linear and star-shaped PDMAEMA depending on molecular weight, concentration, and pH.^[17] Here, the cloud point for a PDMAEMA with a degree of polymerization of 108 (similar to that of the PDMAEMA in our block copolymer) was determined $T_{cl} = 76$ °C at pH 6 and 39 °C at pH 10. For the case reported here, no difference could be seen between the phase transition temperatures at pH 6 and pH 10. For pH 6, the phase transition temperatures are comparable to our former work. Note that the situation for an asymmetric membrane is distinct from a dissolved linear polymer chain. A more appropriate model would be a polymer brush confined on the pore surface.

Please note that Figure 4 is drawn in an idealized way. As the block copolymer does not undergo complete phase separation it is very likely that PDMAEMA is not only covering the pore walls but is also incorporated into them. Compared to the membranes of Peinemann et al.,^[14] the phase-separated morphology of the $S_{81}D_{19}^{75}$, especially in the separation layer is less developed. If responsive chain segments are part of the pore walls the “switching” of PDMAEMA should include two steps: first, the collapse of the freely mobile expanded chains inside the pores and, second, a certain “de-swelling” of chains buried in the wall material consisting mainly of polystyrene. Indeed, the novel membranes require a certain time until the increase or decrease in permeability is finished. This is highlighted in Figure 3C for pH 6 and 3D for pH 10. In both cases, the filtration cell was kept at 65 °C for 2 hours and the flux development was monitored. After this time span, no further increase in permeability could be detected. Furthermore, the flux at both pH 6 and 10 shows a certain hysteresis after cooling down to 25 °C; again, less pronounced for the latter case. The responsive chain segments do not seem to be able to fully recover their original state under conditions where they are partially deswollen. It is noteworthy, that the partial recovery of PDMAEMA chain conformation after cooling down to 25 °C is somewhat faster for pH 10 (2 h) than for pH 6 (12 h). This further amplifies

the impression we try to give in Figure 4. The chain segment collapse resulting from the application of the LCST is more pronounced at pH 6. At higher pH, the polymer chains are already far less stretched in solution. Also, the relative gain in permeability is higher for pH 6. However, if the pH is changed to 2, the initial flux value can be fully recovered within 2 hours. This is due to complete protonation of PDMAEMA, leading to increased mobility for free and wall-buried chain segments.

Filtration of Silica particles

To evaluate the actual pore size distribution of the membranes filtration experiments with synthetic silica colloids at different pH-values were carried out. To minimize adsorption to the membrane, the concentrations were kept low (0.1 - 0.2 %) in all cases. Silica particles with diameters of 12, 22, 36, 60, and 104 nm were used. The silica particles with 12 nm were the only ones being stable under acidic conditions, in all the other cases the particles started to aggregate. The particle solutions were filtered at a pressure of 0.2 bar. Retention was determined by the comparison of the count rate obtained via dynamic light scattering (DLS) for feed, retentate and permeate solutions. Silica colloids with 22, 36, 60, and 104 nm diameter were filtered at pH 6 and pH 10, the colloids with 12 nm diameter at pH values of 2, 6 and 10. The results are shown in Figure 5.

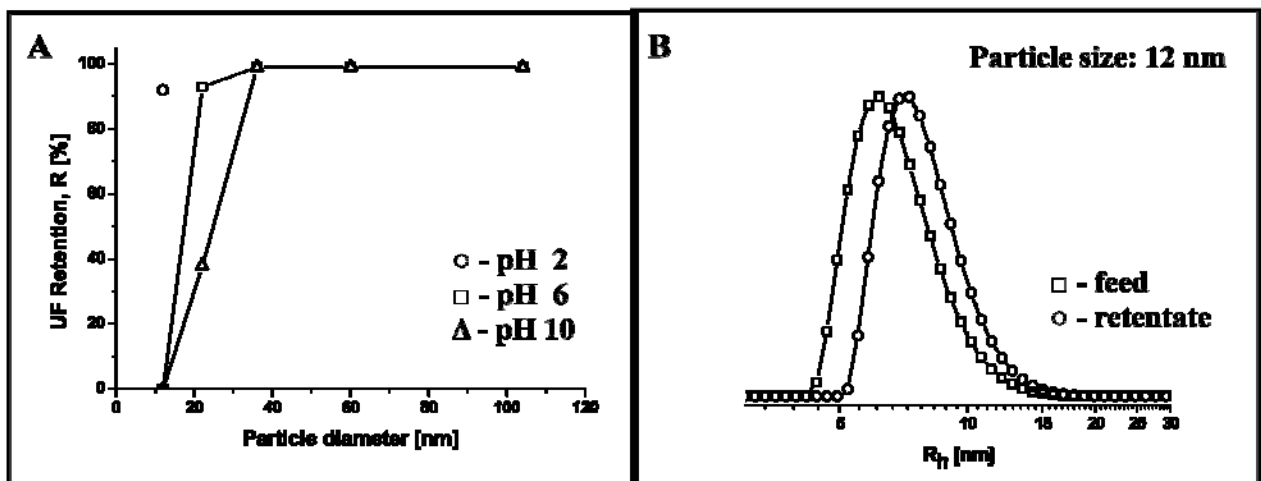


Figure 5: Retention of the $S_{81}D_{19}^{75}$ membrane for silica colloids with 12, 22, 36, 60, and 104 nm at pH 2 (○-○), pH 6 (□-□) and pH 10 (△-△) (A); intensity weighted CONTIN plots for the particle size distributions of the 12 nm feed solution before (□-□) and the retentate solution (○-○) after filtration (B) at pH 2.

As depicted in Figure 5A, at pH 6 almost no silica particles are able to pass the membrane. This is due to the swelling of the PDMAEMA chains covering the pore walls at this pH (cf. Figure 4). Even for the particles with a diameter of 22 nm more than 95 % are rejected. This situation changes upon increasing the pH. At pH 10, again, the silica colloids with 36, 60, and 104 nm are not able to pass the membrane. The particles with 22 nm, however, now can pass through the pores. The amount of rejected particles in this case was measured to be 37 %. This can be explained by the collapse of the PDMAEMA chains under these conditions. Thus, the membrane pores are more “opened”, enabling a significantly less hindered permeation of the 22 nm silica particles through the pore channels.

As shown in Figure 3 and 4, at pH 6 the PDMAEMA chains are partially protonated and the pore interior of the membranes is swollen. Nevertheless, a considerable water flux can be detected. The lowest flux was measured at pH 2, with fully protonated and, thus, at most extended PDMAEMA chains inside the pores. Therefore, silica particles with a diameter of 12 nm and with an improved stability under acidic conditions were used for ultrafiltration at all three pH values. However, despite the low concentration, adsorption occurs onto the pore surface of the membrane. This results in an initial apparent rejection of around 50% even for pH 6. However, after two filtration cycles, the PDMAEMA chains are saturated with the silica particles, and for the following filtrations no rejection can be seen. This is analogous to the breakthrough behavior of membrane adsorbers with weak anion-exchange groups.^{5,6} Attempts to quantify the desorption from the membranes with water were unsuccessful because the count rate obtained by DLS was too low to give reliable values. Therefore, at least five filtration cycles were carried out in each case. The effective rejection was calculated by the average of the last three filtration cycles. At both pH 6 and pH 10 all particles passed the membrane, no rejection could be detected. However, at pH 2, only about 7 % of the particles could be detected in the permeate. This, in combination with the polydispersity of silica particles (PDI = 1.2, determined by DLS for the feed solution) gives a convenient measure for the effective pore diameter under these conditions. If feed and retentate solutions are compared via DLS, as shown in Figure 5B, the hydrodynamic radius increases ($\langle R_h \rangle_{z, \text{feed}} = 6 \text{ nm}$ and $\langle R_h \rangle_{z, \text{retentate}} = 7.5 \text{ nm}$; the concentration of the permeate solution was too low to determine R_h with sufficient accuracy). Thus, we conclude that at pH 2 only particles with a diameter of less than 15 nm are able to

pass the membrane. Since the membrane barrier has a positive charge under these conditions (cf. Figure 4), and the colloids have no positive surface charge, a Donnan exclusion mechanism⁵ can be excluded, and the membrane selectivity is based on their stimuli-responsive pore size.

Conclusion

We successfully prepared double stimuli-responsive porous membranes via the non-solvent induced phase separation method from an amphiphilic diblock copolymer. The structures exhibit a thin separation layer with pores in the range of 20-80 nm and a thickness of around 1 μm . Both stimuli could be reversibly applied. Triggering the LCST of the membranes takes place within 60-120 minutes, presumably due to incorporation of “smart” PDMAEMA material both into pore interior and pore walls. After pH-response, acidic conditions have to be adopted in order to ensure complete recovery of the most swollen conformation leading to smallest effective pore sizes. The inherent features of these membranes besides two independently executable switches are constant and reproducible flux values, absence of noticeable defects on a scale of several hundred μm^2 and their ability to form self-supported mechanically stable films. An initial evaluation of the pore size depending on the pH at 25°C showed that under acidic conditions silica particles with a diameter of 15 nm or larger were fully rejected while the same particles could completely pass the membranes at pH 6 to 10. At pH 10, even particles with a diameter of 22 were able to pass the membrane. Therefore, the novel functional materials are ultrafiltration membranes with tunable cut-off pore size. It will now be the subject of further investigations to evaluate the usefulness of these novel materials in areas like the filtration or removal of viruses, bacteria and other particles. Besides the different size selectivity as function of different combinations of pH and temperature, additional effects of pore charge on selectivity will also be investigated. Rejection of positively charged particles should be much higher at low pH than at high pH, or the “switchable” ion-exchange adsorber properties towards negatively charged particles could be exploited as well.

Acknowledgement

The authors would like to thank Benjamin Gossler for the SEM measurements, Tobias Rudolph for help during film-casting, and Sabine Wunder, Christina Löffler and Robin Pettau for SEC measurements (all University of Bayreuth). Claudia Schenk, Marcel Gawenda and Dr. Heru Susanto are acknowledged for their help during the stay of FS at University Duisburg-Essen. Markus Retsch (Max Planck Institut für Polymerforschung, Mainz) kindly provided the silica particles with 22, 36, 60, and 104 nm. Funding was received from the VolkswagenStiftung within the framework “Complex Materials”. (Supporting Information is available online from Wiley InterScience or from the author).

References

- [1] H. Cui, Z. Chen, S. Zhong, K. L. Wooley, D. J. Pochan, *Science* **2007**, *317*, 647-650.
- [2] S. B. A. Ludwigs, A. Voronov, N. Rehse, R. Magerle, G. Krausch, *Nat. Mater.* **2003**, *2*, 744-747.
- [3] A. Sperschneider, F. Schacher, M. Gawenda, L. Tsarkova, A. H. E. Müller, M. Ulbricht, G. Krausch, J. Köhler, *Small* **2007**, *3*, 1056-1063.
- [4] S. Y. Yang, I. Ryu, H. Y. Kim, S. K. Jang, T. P. Russell, *Adv. Mater.* **2006**, *18*, 709-712.
- [5] S. Y. Yang, J. Park, J. Yoon, M. Ree, S. K. Jang, J. K. Kim, *Adv. Funct. Mater.* **2008**, *18*, 1371.
- [6] M. Ulbricht, *Polymer* **2006**, *47*, 2217-2262.
- [7] E. J. Klein, *J. Membr. Sci.* **2000**, *179*, 1.
- [8] M. Ulbricht, H. Yang, *Chem. Mater.* **2005**, *17*, 2622-2631.
- [9] S. P. Nunes, M. L. Sforca, K. V. Peinemann, *J. Membr. Sci.* **1995**, *106*, 49.
- [10] J. F. Hester, P. Banerjee, Y. Y. Won, A. Akthakul, M. H. Acar, A. M. Mayes, *Macromolecules* **2002**, *35*, 7652-7661.
- [11] Y. Q. Wang, T. Wang, Y. L. Su, F. B. Peng, H. Wu, Z. Y. Jiang, *Langmuir* **2005**, *21*, 11856-11862.
- [12] S. Dai, P. Ravi, K.-C. Tam, *Soft Matter* **2008**, *4*, 435-449.

- [13] S. P. Nunes, K. V. Peinemann, *Membrane Technology in the Chemical Industry*, 2nd ed., Wiley-VCH, Weinheim, **2006**.
- [14] K. V. Peinemann, V. Abetz, P. F. W. Simon, *Nat. Mater.* **2007**, *6*, 992-996.
- [15] S. H. Yoo, J. H. Kim, J. Y. Jho, J. Won, Y. S. Kang, *J. Membr. Sci.* **2004**, *236*, 203-207.
- [16] Y. -H. Zhao, Y. -L. Qian, B. -K. Zhu, Y. -Y. Xu, *J. Membr. Sci.* **2008**, *310*, 567-576.
- [17] F. Plamper, M. Ruppel, A. Schmalz, O. Borisov, M. Ballauff, A. H. E. Müller, *Macromolecules* **2007**, *40*, 8361-8366.
- [18] F. Plamper, A. Walther, A. H. E. Müller, M. Ballauff, *Nano Lett.* **2007**, *7*, 167-171.
- [19] F. A. Plamper, A. Schmalz, M. Ballauf, A. H. E. Müller, *J. Am. Chem. Soc.* **2007**, *129*, 14538-14539.
- [20] Y. -L. Su, C. Li, *J. Membr. Sci.* **2007**, *305*, 271-278.
- [21] Y. -L. Su, C. Li, *J. Colloid Interface Sci.* **2007**, *316*, 344-349.
- [22] P. van de Witte, P. J. Dijkstra, J. W. A. van den Berg, J. Feijen, *J. Membr. Sci.* **1996**, *117*, 1-31.
- [23] C. Feng, B. Shi, G. Li, Y. Wu, *J. Membr. Sci.* **2004**, *237*, 15-24.
- [24] W. Stöber, A. Fink, E. Bohn, *J. Coll. Interf. Sci.* **1968**, *26*, 62-69.
- [25] F. Schacher, M. Müllner, H. Schmalz, A. H. E. Müller, *Macromol. Chem. Phys.*, *accepted*

Double Stimuli-Responsive Ultrafiltration Membranes from Polystyrene-*block*-poly(N,N-dimethylaminoethyl methacrylate) Diblock Copolymers*

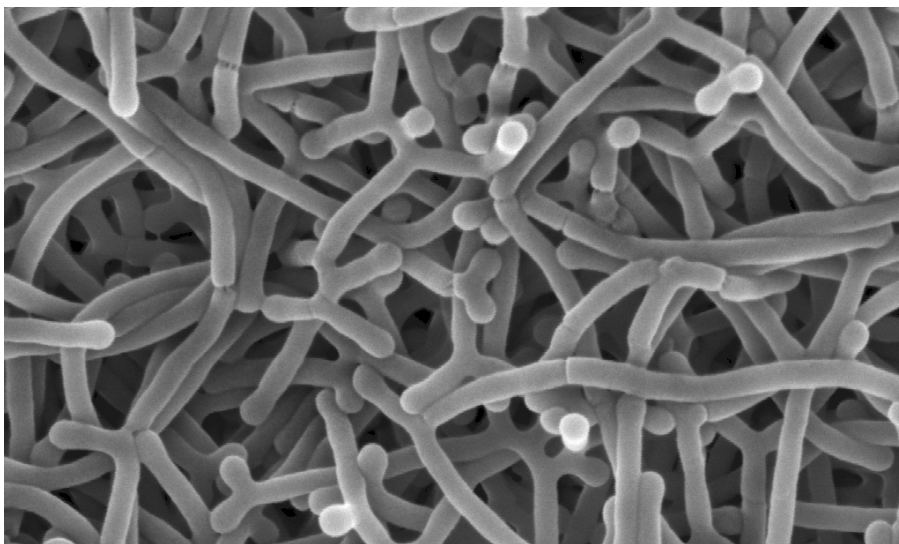
Felix Schacher^{1*}, Tobias Rudolph¹, Florian Wieberger², Mathias Ulbricht³, and Axel H. E. Müller^{1*}

¹Makromolekulare Chemie II, Universität Bayreuth, D-95440 Bayreuth, Germany

²Makromolekulare Chemie I, Universität Bayreuth, D-95440 Bayreuth, Germany

³Technische Chemie II, Universität Duisburg-Essen, D-45117 Essen, Germany

E-mail: axel.mueller@uni-bayreuth.de; felix.schacher@uni-bayreuth.de;
mathias.ulbricht@uni-due.de



Abstract

We report on the formation of self-supporting, double stimuli-responsive ultrafiltration membranes via the nonsolvent induced phase separation (NIPS) process. The polymers, polystyrene-*block*-poly(N,N-dimethylaminoethyl methacrylate) (PS-*b*-PDMAEMA), were synthesized via living anionic polymerization in THF using *sec*-butyllithium as initiator. Two amphiphilic diblock copolymers were used, $S_{81}D_{19}^{75}$ and $S_{68}D_{32}^{100}$. The membranes were cast from mixtures of THF and DMF. The influence of the solvent composition, the “open-time” before immersion into the coagulation bath, and the casting film thickness onto the membrane morphology were thoroughly investigated and flux values obtained for the different membrane systems were compared. The higher content in hydrophilic polymer for $S_{68}D_{32}^{100}$ resulted in a better compatibility with the non-solvent bath consisting of water, leading to a slower precipitation and, thus, an improved control of the phase separation occurring. Under certain conditions, ordered microphase separated porous morphologies were observed in parts of the membrane cross-section. Further, the “smart” properties of those novel materials are shown for two representative systems. It could be demonstrated that both stimuli for PDMAEMA, pH and temperature, can be reversibly and independently applied in order to significantly change the transmembrane water flux.

Introduction

In the last decade, membrane separations have gained high technical relevance in a wide range of applications, from water purification to medical applications.¹ Increasing complexity in modern separation processes is accompanied by demanding and further specialized requirements for a suitable membrane, by far exceeding commonly known properties like chemical inertness, thermal and mechanical stability, and mechanical strength. Especially when it comes to new technically challenging or commercially attractive separation problems, many state-of-the-art membranes are facing their limitations.

Polymers are by far the most important membrane materials, especially because of the relative ease and flexibility to manufacture a large diversity of effective barrier structures for different membrane processes. Possible pathways towards the design of novel membranes are the modification of already established membrane structures, an alteration of the preparation techniques, or the use of new building blocks with improved functionalities. Furthermore, attempts have been made to blend hydrophobic and hydrophilic compounds, mainly focusing on the improvement of both fouling characteristics and membrane morphology.² The activities in this field have been reviewed recently.³ Main challenges for the development of novel ultrafiltration membranes are a narrow and adjustable pore size distribution and a thin barrier layer so that the tradeoff between high selectivity and high flux could be overcome.⁴ In addition, the fouling tendency should be minimized.

Using block copolymers as building blocks represents a facile and straightforward methodology for the simple incorporation of different structural or chemical features into bulk materials. Junctions between two compartments are covalent and therefore thermodynamically, chemically, and mechanically stable.^{5, 6} Especially amphiphilic block copolymers have received considerable interest concerning their synthesis via living⁷ or controlled polymerization techniques⁸ and their self-assembly in the bulk,⁹⁻¹¹ in thin-films,¹² or in solution.¹³ Through recent advances, block copolymer dimensions on the nanoscale and resulting morphologies become more and more predictable. In that way block copolymers are able to combine superior mechanical properties of hydrophobic and the wettability and

surface chemistry of hydrophilic materials. Moreover, smart polymeric materials render these structures sensitive to external stimuli like pH,¹⁴ temperature,¹⁵ or light¹⁶ and broaden the scope of possible applications of such systems. First attempts had been made to prepare ultrafiltration membranes from diblock copolymers by using one block as pore template: after film formation, an annealing step was crucial to obtain well-defined micro phase-separated morphologies in the bulk of the polymer film, then a selective dissolution or etching step had to be performed.^{17, 18}

One of the most important industrial processes for the fabrication of integrally anisotropic (“asymmetric”) polymer membranes is non-solvent-induced phase separation (NIPS) where a casted film of a polymer solution is immersed in a precipitation bath.¹⁹ This is a straightforward and fast one-step procedure. Membrane morphology and barrier structure can be controlled by a range of parameters; most important are the mutual interactions between membrane polymer and solvent (or solvent mixture) on the one hand, and between polymer and non-solvent on the other hand (polymer solvent and non-solvent must be miscible). In addition to the thermodynamic boundary conditions, the kinetics of mass-transfer and phase separation can have a decisive influence.²⁰ The obtained materials typically exhibit a very thin “skin” layer which strongly determines the separation properties and is mechanically supported by a macroporous substructure.²⁰ Such “asymmetric” membranes find their applications in pressure-driven separation processes such as ultrafiltration, nanofiltration or reverse osmosis. If water is used as non-solvent, phase separation of amphiphilic block copolymers should result in a hydrophobic matrix featuring pores which are coated with the hydrophilic compartment. Recently, this has been demonstrated for well-defined block copolymers, polystyrene-*block*-poly(4-vinylpyridine).²¹ Here, poly(4-vinylpyridine) should cover the pore interior and serve as a weak polyelectrolyte, rendering the membranes pH-sensitive - this, however, had not been studied. Other attempts towards stimuli-responsive membranes via immersion precipitation are based on statistical²² or grafted²³ block copolymers with smart properties. In our groups, a well-defined polystyrene-*block*-poly(*N,N*-dimethylaminoethyl methacrylate) (PS-*b*-PDMAEMA) block copolymer was shown to form self-supporting asymmetric membranes via the NIPS process from solvent mixtures of THF and

DMF.²⁴ This polymer, $S_{81}D_{19}^{75}$, was synthesized via sequential anionic polymerization techniques.⁷ Note that the subscripts correspond to the weight fractions of the corresponding blocks and the superscript is the absolute molecular weight in kg/mol. We could show that these membranes are able to react onto two independently addressable stimuli, pH and temperature, in terms of water flux and effective pore-size, attributed to the smart properties of the hydrophilic block, PDMAEMA.¹⁵

Within this contribution we considerably extend our earlier work. A block copolymer comprising a higher content of hydrophilic material, $S_{68}D_{32}^{100}$, was synthesized in an analogous way and also used for the fabrication of stimuli-responsive asymmetric membranes. The parameters of the membrane casting process, NIPS, were systemically varied for both $S_{81}D_{19}^{75}$ and $S_{68}D_{32}^{100}$. First, the influence of the composition of the solvent mixture (THF and DMF) for the casting solution on the resulting membrane morphology and performance is thoroughly investigated. Further, the influences of different “open-times” in between film casting and the immersion into the coagulation bath as well as of varied casted film thickness were studied. All obtained membrane structures were analyzed with scanning electron microscopic techniques, and the corresponding water fluxes were determined. Finally, the double stimuli-responsive character for one representative membrane of each polymer is demonstrated through pH- and temperature dependent flux measurements. Although not all parameters which have influence on membrane structure for the presented system consisting of block copolymer, THF, DMF, and water are exhaustively addressed, we are able to point out important tendencies, and the results can be interpreted in a conclusive way. Please note that we are dealing with a combination of two ternary phase diagrams, polymer, solvent, and non-solvent for each of the two blocks, providing a complex multi-parameter space.

Experimental

Materials

sec-Butyllithium (Acros) was used as delivered. THF (Fluka) was distilled from CaH₂ and K. Afterwards, the solvent was directly transferred into the stirred glass reactor. Styrene was kindly provided by BASF and was stirred over Bu₂Mg (Aldrich) and afterwards condensed on a vacuum line into glass ampoules. N,N-dimethylaminoethyl methacrylate (Aldrich) was stirred with tri-octylaluminium (Aldrich) and afterwards condensed on a vacuum line. 1,1-diphenylethylene (Aldrich) was distilled from *sec*-butyllithium and stored under nitrogen.

Synthesis

Polystyrene-*block*-poly(N,N-dimethylaminoethyl methacrylate) was synthesized via sequential living anionic polymerization in THF (500 ml) at low temperatures in the presence of alkoxides to stabilize the living chain end. The detailed procedure has already been described.⁷ For S₆₈D₃₂¹⁰⁰, first styrene (68 g, 0.65 mol) was initiated with *sec*-butyllithium (1.3 ml, 0.99 mmol) at -70 °C. Afterwards, the reaction was allowed to proceed at -70 °C for 30 minutes. For polymerization of the second block, the polystyrene chains were end-capped with 1,1-diphenylethylene (0.36 ml, 2 mmol) at -50 °C in order to attenuate the reactivity of the anions.^{25, 26} Otherwise, attack of the ester moiety would occur upon addition of N,N-dimethylaminoethyl methacrylate. The latter (32 g, 0.21 mol) was injected via syringe into the reaction vessel and was polymerized for 1 h at -40 °C. Finally, the reaction was stopped through addition of 3 ml of degassed isopropanol, and the polymer was purified through dialysis against THF and dioxane and freeze-dried. S₈₁D₁₉⁷⁵ has been prepared in an analogous way, employing both monomers in the appropriate ratio.

Membrane preparation

Membranes were prepared via the NIPS process. 200 µm thick films were cast from a solution of PS-*b*-PDMAEMA (1.5 g, 15 wt. %), and a mixture of DMF and THF with a doctor blade onto polished glass substrates. After the so-called “open-time” in contact with air (relative humidity was 30-40% and temperature was ~20 °C), the as-cast films were immersed into a bath containing de-ionized water for final

formation of the membrane morphology. During the next 60 minutes, the films started to lift off the glass surface. After 12 hours, the membranes were taken out of the water bath and stored in de-ionized water until used for water flux measurements.

Water flux measurements

Water flux measurements were carried out in a stirred ultrafiltration test cell (Amicon 8010, Millipore, effective membrane diameter 22 mm) connected to a water reservoir at a constant height of the water column of 25 cm, providing a transmembrane pressure of 0.025 bar. Values provided in Table 1A and 1B were obtained through averaging the obtained water fluxes for 3 membranes. Deviations in between membranes of the same cast film were in the range of 15 %. The membrane was placed in this cell which was immersed in a water bath kept at constant temperature. pH was adjusted through dilute solutions of NaOH and HCl in deionized water; after each change in pH a time span of 2 hours under flow-through was used to allow equilibration. Temperature ramps were performed through keeping the whole ultrafiltration cell in a tempered water bath. Steps were 10 °C, equilibration time in between two points was 1 hour, except for the highest temperature (65 °C: 2 hours).

Characterization

NMR

¹H-NMR measurements were performed on a Bruker 250 MHz AC spectrometer in CDCl₃ as solvent. The block copolymer composition was determined through the integral ratio between the styrene protons (5H, δ = 6.3-7.2 ppm) and the CH₂ protons adjacent to the ester group group of DMAEMA (2H, δ = 4.1 ppm).

Size exclusion chromatography

Size exclusion chromatography (SEC) measurements were performed on a set of 30 cm SDV-gel columns of 5 mm particle size having a pore size of 10⁵, 10⁴, 10³ and 10² Å with refractive index and UV (λ = 254 nm) detection. SEC was measured at an elution rate of 1 ml/min with THF containing 0.25 wt.% tetra-butylammoniumbromide (TBAB) as eluent.

Scanning electron microscopy

SEM was carried out on a Leo Gemini 1530. The specimens were dried under vacuum over night and coated with approximately 2 nm Pd. For the cross sections, a piece of the sample was frozen together with the sample holder and broken afterwards.

Transmission electron microscopy

TEM micrographs were taken on a Zeiss CEM 902 operating at 80 kV.

Dynamic light scattering

Dynamic light scattering (DLS) measurements were performed in sealed cylindrical scattering cells ($d = 10$ mm) at a scattering angle of 90° on an ALV DLS/SLS-SP 5022F equipment consisting of an ALV-SP 125 laser goniometer with an ALV 5000/E correlator and a He-Ne laser with the wavelength $\lambda = 632.8$ nm. The CONTIN algorithm was applied to analyze the obtained correlation functions. Apparent hydrodynamic radii were calculated according to the Stokes-Einstein equation.

Results and Discussion

Synthesis of the PS-*b*-PDMAEMA block copolymers

Two amphiphilic block copolymers were synthesized via sequential anionic polymerization in THF. After purification, they were characterized through a combination of $^1\text{H-NMR}$ and SEC. The final composition was determined to be $S_{81}D_{19}^{75}$ and $S_{68}D_{32}^{100}$. Note that the subscripts refer to the weight fraction of the corresponding block and the superscript to the absolute molecular weight in kg/mol. The degrees of polymerization were $S_{600}D_{90}$ ($S_{81}D_{19}^{75}$) and $S_{650}D_{205}$ ($S_{68}D_{32}^{100}$). Both polymers exhibited a very narrow molecular weight distribution (polydispersity index (PDI) = 1.03 for $S_{81}D_{19}^{75}$ and 1.08 for $S_{68}D_{32}^{100}$). The SEC traces with THF and additional 0.25 % TBAB as eluent and the $^1\text{H-NMR}$ spectrum for $S_{68}D_{32}^{100}$ are shown in Figure 1.

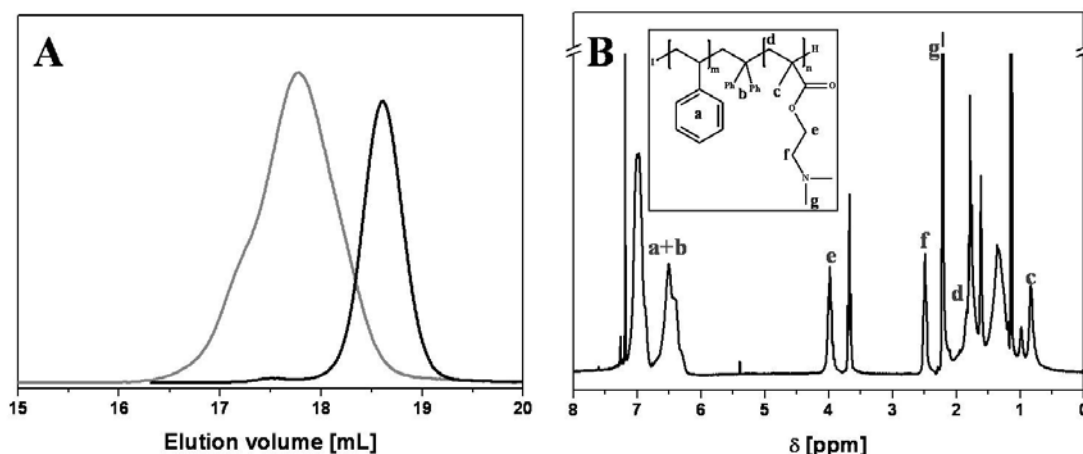


Figure 1: SEC traces for the S_{68} precursor (solid black line) and $S_{68}D_{32}^{100}$ (solid grey line) with THF and additional 0.25 wt. % TBAB as eluent (A); $^1\text{H-NMR}$ spectrum in CDCl_3 for $S_{68}D_{32}^{100}$, the inset shows the chemical structure of the AB diblock copolymer and the assignment of the important NMR-signals (B).

During the polymerization of $S_{68}D_{32}^{100}$, a small amount of recombination occurred, as visible in the SEC trace in Figure 1A. That also explains the slightly increased PDI. The molecular weight of the first block, polystyrene, was determined with a PS calibration curve. The NMR in Figure 1B was used to determine the length of the second block, PDMAEMA, via the comparison of the styrenic protons (a, 5H, $\delta = 6.2$

- 7.3 ppm) and the methylene group of DMAEMA adjacent to the ester moiety (e, 2H, $\delta = 4.1$ ppm). The contribution from the single 1,1-diphenylethylene used for endcapping of the living PS chains for the NMR integral of the PS protons was negligible.

Membrane preparation and characterization

All membranes were prepared via the NIPS process. Mixtures of THF and DMF which are supposed to mix ideally and are both miscible with water in the coagulation bath were selected as solvent for the block copolymers. THF is supposed to be the better solvent for PS, DMF for PDMAEMA. Polymer solutions of 15 wt. % in THF/DMF mixtures were cast on a pre-cleaned planar glass substrate using a doctor blade with different step heights (50 - 200 μm). After film-casting, the solvent was allowed to evaporate for a certain amount of time (up to 10 minutes) before the whole substrate was immersed into the non-solvent bath. This is the so-called “open-time”. During this step, mostly the higher volatile solvent (here THF) evaporates, the polymer enriches at the polymer-air interface and eventually phase separation could even start in the top layer of the “proto-membrane”. We suppose that this step is crucial for the formation of the pores of the separation layer as well as the overall porous membrane structure. After immersion in the precipitation bath, final solvent exchange and solid film formation took place.

In an earlier work, we had shown that for a mixture of THF (50%) and DMF (50%), a polymer concentration of 15 wt. %, a doctor blade step height of 200 μm , an “open-time” of 60 seconds, and deionized water as the coagulation bath double stimuli-responsive membranes with addressable effective pore size could be obtained for $S_{81}D_{19}^{75,24}$. These asymmetric membranes exhibited two independently addressable stimuli, pH and temperature, attributed to the smart properties of the second block, PDMAEMA. We now extend this work to another polymer, $S_{68}D_{32}^{100}$. The higher content of the second block, PDMAEMA, should have an influence on the membrane morphology under similar casting/NIPS conditions as the hydrophilic-to-hydrophobic balance of the diblock copolymer is altered. A higher content of DMAEMA should increase the compatibility with the coagulation bath and therefore result in a slower, more controlled precipitation or phase separation.

The aggregation behavior of PS-*b*-PDMAEMA in dilute aqueous solution under the same conditions was studied. Solutions with a polymer concentration of 1-5 g/L were prepared in a mixture of THF (50%) and DMF (50%), and the solvent was then exchanged against deionized water via dialysis. Both polymers formed spherical core-corona micelles in water at pH 6 with $\langle R_h \rangle_z = 35$ nm ($S_{81}D_{19}^{75}$, $DP_{PDMAEMA} = 90$) and $\langle R_h \rangle_z = 45$ nm ($S_{68}D_{32}^{100}$, $DP_{PDMAEMA} = 205$) as revealed via dynamic light scattering and transmission electron microscopic techniques (DLS and TEM results are not shown here). The size difference can be tentatively explained through the block length of the corresponding PDMAEMA compartment. Under these conditions, the polymer chains are protonated and moderately stretched. In both cases, the length of the PS block is comparable. The details of the phase diagram of such block copolymers in the bulk are not known, but according to their composition and volume fractions, the equilibrated materials should form cylindrical morphologies. We estimated the chi-parameter for this system by using the solubility parameters for PS (9.1 (cal/cm³)^{1/2}) and PDMAEMA (9.21 (cal/cm³)^{1/2}).²⁷ This resulted in a value of 0.024, which is rather small. If the corresponding degrees of polymerization are used ($600 + 90$ for $S_{81}D_{19}^{75}$ and $650 + 205$ for $S_{68}D_{32}^{100}$), $\chi \cdot N$ has a value of 16.8 and 20.5, indicating phase separation of the two blocks taking place. One may, of course, speculate about the applicability of this method for a system where the solubility parameters are rather close.

In the following, first a detailed description of one representative membrane structure is given. Thereafter, the influences of solvent composition, “open time”, and casted film thickness are discussed in separate sections.

Asymmetric membrane structure

The NIPS process typically generates membranes with an anisotropic cross section. We obtained this for several combinations of the varied parameters. Exemplarily, the structure obtained for a mixture of THF (60%) and DMF (40%), an “open-time” of 60 seconds, and a casted film thickness of 200 μ m is shown in Figure 2.

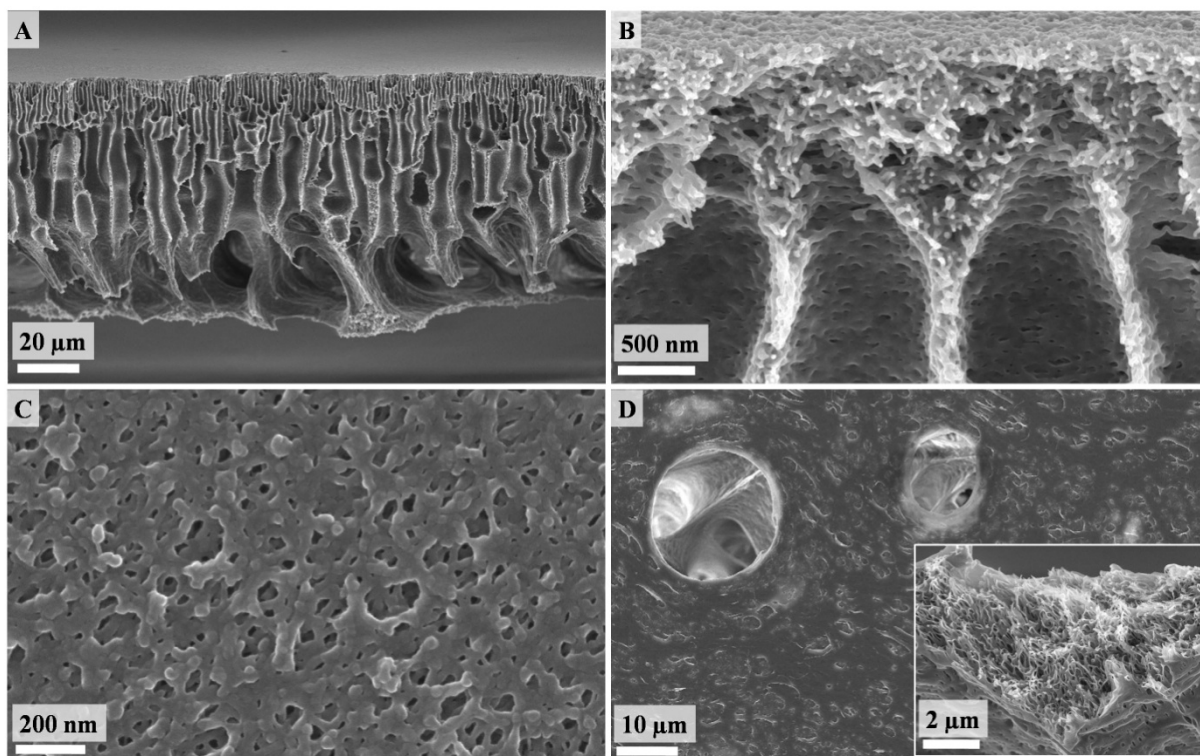


Figure 2: SEM micrographs of a $S_{81}D_{19}^{75}$ membrane prepared via the NIPS process (60% THF / 40% DMF, 200 μm ; 60 sec); A, B: cross sections at different magnifications; C: on-top view onto the membrane surface; D: view onto the bottom surface of the membrane, the inset shows the structure obtained in the proximity of the bottom surface.

Figure 2A displays a cross section of the membrane. The membrane thickness as determined via SEM was $80 \pm 10 \mu\text{m}$, and the anisotropic nature is evident. A thin separation layer with a thickness of around $1 \mu\text{m}$ and a compact sponge-like structure was obtained at the surface formerly in contact with air (Figure 2B). Beneath the top layer, broader “finger-like” channels appeared, the so-called “macrovoids”. These develop during the immersion in the coagulation bath. Membrane structures like this are typical for systems which show “instantaneous demixing” during the NIPS process.^{20, 28} Here, the rapid precipitation upon contact with water was attributed to the PS part of the PS-*b*-PDMAEMA block copolymers. The anisotropy then results from both time delay and an uneven composition distribution throughout the whole film during the solvent / non-solvent exchange. Macrovoids like obtained in this case are acceptable for “medium pressure” applications like ultra- or microfiltration. Figure 2C presents an on-top view onto the membrane surface. The structure is not well-ordered, no long-range order could be seen. The appearance was rather sponge-like. Although the pore sizes obtained via SEM were in the range of 20-80 nm, the effective barrier pore size for a comparable structure was shown to be in the range of 10-30 nm.²⁴ This would

position the membrane at the borderline between ultra- and microfiltration.³ The bottom surface which has been in contact with the glass substrate is shown in Figure 2D. Large pores with sizes up to 20 μm were present. All observed features of the membrane pore structure should yield high water fluxes. The inset in Figure 2D highlights the structure obtained in close proximity to the bottom of the membrane, e.g. on an edge originating from the cross section preparation. Wormlike, interconnecting objects could be seen. Apparently, the time delay for demixing between top and bottom surface of the casted film lead to a more controlled phase separation and resulted in structural features which are different from those for precipitated standard membrane polymers. This will be discussed in more detail in the following sections.

Influence of the solvent composition

The choice of the polymer solvent is a crucial parameter for the NIPS process. Here, mixtures of THF and DMF were used, and the compositions varied from 25% / 75% to 75% / 25% for both $S_{81}D_{19}^{75}$ and $S_{68}D_{32}^{100}$. The two compartments, PS and PDMAEMA, are inherently different in their chemical nature. While PDMAEMA is soluble in water, PS is completely insoluble. Further, THF is supposed to be the better solvent for PS, and DMF for PDMAEMA. As THF is more volatile than DMF, during the “open-time” mostly THF evaporates in the top-layer of the “proto-membrane”. This, in combination with the hydrophobicity of the PS block, ensured immediate precipitation upon contact of the film with the coagulation bath. To investigate the effect of the solvent composition on the final membrane morphology and performance, both $S_{81}D_{19}^{75}$ and $S_{68}D_{32}^{100}$ membranes were cast from solutions of 75% THF / 25% DMF, 60% THF / 40% DMF, 50% THF / 50% DMF, 40% THF / 60% DMF, and 25% THF / 75% DMF. In all cases, the “open-time” was 60 seconds, and the casted film thickness was 200 μm . SEM micrographs for all prepared samples are shown in Figure 3. The insets in the SEM micrographs show enlargements of the cross section (upper inset) and the membrane morphology on the bottom of the membrane (lower inset), if found different from that of the top section. The grey bars on the right hand side of Figure 3 display the solvent composition used for the fabrication of the respective two membranes: dark grey corresponds to the THF, lighter grey to the DMF content.

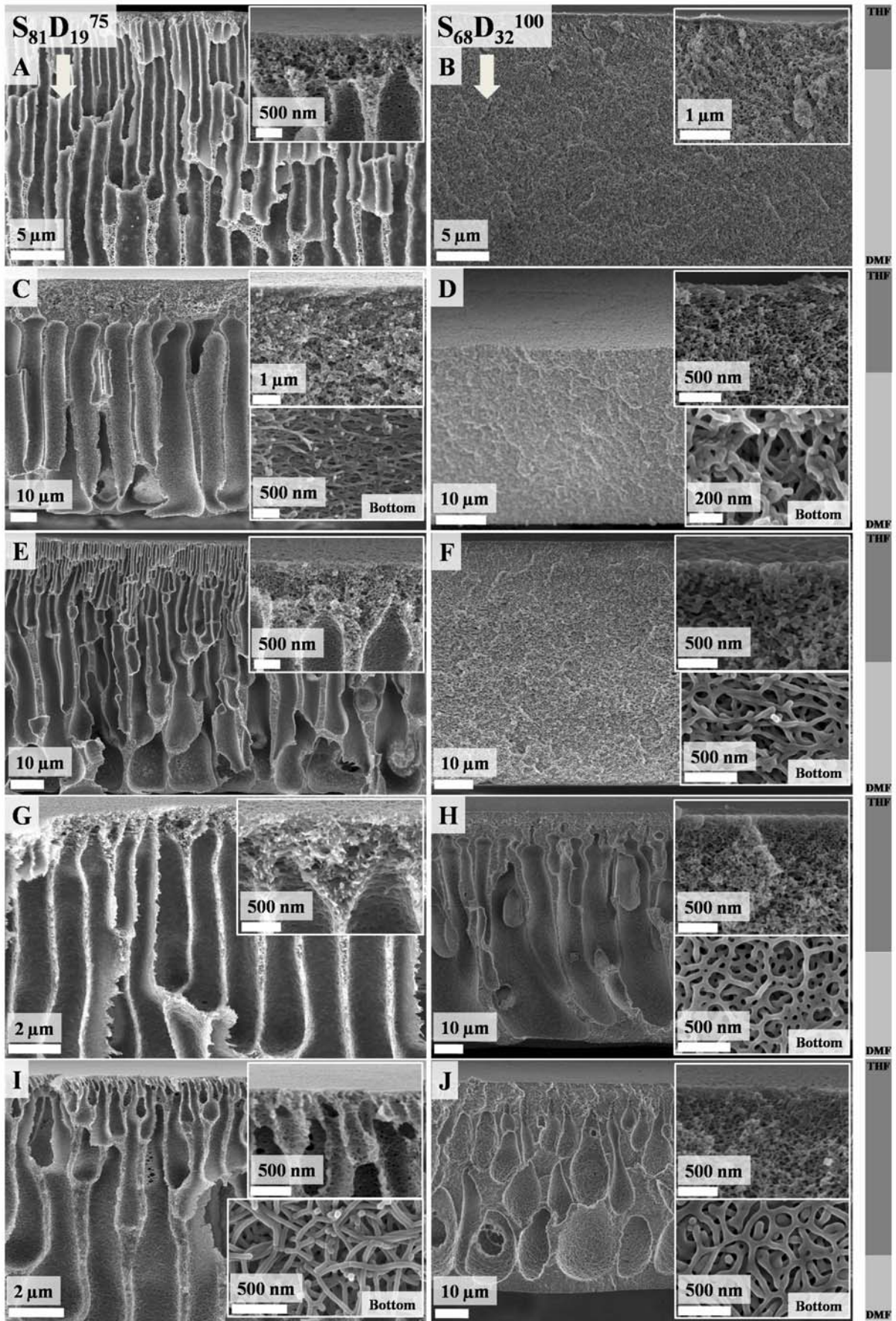


Figure 3: SEM micrographs for $S_{81}D_{19}^{75}$ and $S_{68}D_{32}^{100}$ membranes cast from different solvent mixtures: the left column shows $S_{81}D_{19}^{75}$, the right column $S_{68}D_{32}^{100}$, the grey bars to the right correspond to the solvent composition (dark grey - THF, lighter grey - DMF); the solvent composition was 25% THF / 75% DMF (A, B), 40% THF / 60% DMF (C, D), 50% THF / 50% DMF (E, F), 60% THF / 40% DMF (G, H), and 75% THF / 25% DMF (I, J); the insets show enlargements of the respective cross section (upper inset) and the membrane morphology at the bottom of the structure (lower inset), if found to be different from the top layer.

First, the influence of the solvent composition will be described for each polymer separately. Afterwards, both polymers will be compared. The left column shows the obtained structures for $S_{81}D_{19}^{75}$ (Figure 3A, C, E, G, I). At first glance, all the membranes exhibited similar morphologies. A thin, compact separation layer was formed on top of a macroporous support with “finger-like” macrovoids oriented perpendicular to the glass substrate. The membrane thickness also was comparable in all cases and in the range of 80-90 μm , as determined via cross sectional SEM. The upper inset in each micrograph presents an enlargement of the separation layer. Typically, this part had a thickness of around 1 μm , except for a casting solution of 40% THF / 60% DMF (Figure 3C). Here the top layer was around 15-20 μm thick. Apart from that, both structure and porosity of the skin layer seemed to be independent from the solvent mixture used for film casting. Contrary, as shown in the lower inset in Figure 3C, at the bottom surface of the membrane wormlike structures were formed with a thickness of 60-70 nm and a length of up to several μm . In some cases, even interconnecting networks of such worms could be found. Obviously, the mechanism for the structure formation here strongly differs from that of the top layer. This may result from a different solvent composition present at the bottom of the polymer film following the immersion into the water bath. Surprisingly, such wormlike objects were not found for lower or for slightly higher THF contents of the casting solution (note that the membrane from 40% THF / 60% DMF had also a different “skin” layer thickness). However, upon increasing the amount of THF to 75%, similar observations could be made (Figure 3I, lower inset). Here, the cylindrical aggregates seemed to be far more developed, visible through the even appearance of the surface. They are better defined concerning the average diameter. Moreover, less junctions are formed, the cylinders merely entangle.

The situation was different if the same experiments were carried out for the polymer with the higher content of hydrophilic material, $S_{68}D_{32}^{100}$ (Figure 3B, D, F, H, J). For the lowest content of THF (25%), the whole membrane cross section

exhibited a sponge-like morphology, as seen before for the separation layer on top exclusively (Figure 3B). With raising THF content, the structure became less compact (Figure 3D, upper inset, 40% THF) and, like seen for $S_{81}D_{19}^{75}$, wormlike structures were again developed at the bottom surface (Figure 3D, lower inset). This got even more pronounced for a THF content of 50% (Figure 3F, lower inset). Also here, the cylindrical structures appeared further developed, with less branches and a higher aspect ratio. Along with the apparent higher porosity, the overall film thickness increased as well. For 25% and 40% THF, films with around 40-45 μm were obtained whereas for $\geq 50\%$ THF a thickness of 65 μm could be determined via SEM. If 60% THF were used in the casting solution, a transition in the membrane structure could be seen. Figure 3H displays an asymmetric structure again, as found for $S_{81}D_{19}^{75}$ before (Figure 2). Clearly, a compact barrier layer was formed on top of the membrane (Figure 3H, upper inset) with a thickness of 5-10 μm . The macrovoids here were not “finger-like”, instead they were “pear-shaped”. This could also be attributed to the increased PDMAEMA content and the better compatibility between polymer and non-solvent, altering the kinetics of the phase separation.²⁰ The bottom view (Figure 3H, lower inset) presents a rather packed network of branched cylindrical structures. After casting with the highest THF content, 75%, the overall membrane morphology was comparable (Figure 3J). Here, the “pear-shaped” appearance of the macrovoids was even more pronounced. Also, different layers of macrovoids were present, scarcely one example penetrating from separation layer to the bottom was found. The structure within the top layer did not show any difference (Figure 3J, upper inset), whereas the branching tendency within the bottom surface increased (Figure 3J, lower inset).

Irrespective of the polymer, the variation of the solvent mixture composition has two consequences: with increasing THF content, the compatibility between solvent and non-solvent slightly decreases whereas the viscosity decreases considerably; both, thermodynamic and kinetic, effects should lead to faster overall phase separation. However, if compared, the solvent composition of the casting solution did not have a drastic effect on the obtained membrane structures for $S_{81}D_{19}^{75}$. Depending on the THF content, slight variations in the thickness of the separation layer on top of the membranes were observed. Furthermore, at certain compositions a more controlled phase separation of the block copolymer was

promoted in close proximity to the glass substrate, resulting in cylindrical structures. This could be explained by the composition gradient throughout the polymer film which develops following immersion of the “proto membrane” into the water bath leading to a delayed precipitation so that defined block copolymer aggregation could take place before. In contrast, for $S_{68}D_{32}^{100}$, the solvent composition played an important role. Up to 50% THF in the initial casting solution, membranes with an isotropic cross section were obtained. First, this could be explained through the higher compatibility of the used block copolymer with the coagulation bath caused by the higher content in hydrophilic material, PDMAEMA. Second, during the “open-time”, mostly THF evaporates and the DMF content increased in the as-cast polymer film. As DMF is supposed to be the better solvent for PDMAEMA this further enhances the described effect. In combination, both shifted the system away from rapid demixing and resulted in a more compact membrane structure. If a sufficiently high THF content was used for film casting, the same “open-time” caused enough solvent depletion so that, upon immersion in the water bath, rapid demixing also occurred for this polymer. In this case, 60% THF have proven to be enough, as shown in Figure 3H. To our opinion, the structures obtained at the bottom surface fortify the drawn conclusions. The higher compatibility of $S_{68}D_{32}^{100}$ with water resulted in a slower precipitation and, for all solvent compositions except 25% THF, in well-defined cylindrical aggregates. At the same time, the increasing overall content of the good solvent for PS (THF) also favored the delayed precipitation as precondition for the formation of defined aggregates of the block copolymer. Up to now, no absolutely conclusive explanation could be given for the amount of branching observed for these structures. The tendency for $S_{68}D_{32}^{100}$, however, seemed to increase with the THF content, as shown in the lower insets of Figure 3D, F, H, and J. Overall, the block copolymer and its composition had a decisive influence on the porous membrane morphology resulting from the NIPS process, and for $S_{68}D_{32}^{100}$ the selective solvent properties for the two blocks could be used to change the pore structure (while viscosity is of less importance). The morphological features obtained at the bottom of the membranes, unfortunately, could scarcely be compared with solution-based aggregation experiments (cf. above) as the actual solvent composition at the point of immersion was hard to determine.

Influence of the “open time”

As described earlier, asymmetric cross-section structures were desired for high-flux membranes. Hence, the solvent compositions taken for the investigation of the “open-time” were 50% THF / 50% DMF in the case of $S_{81}D_{19}^{75}$ and 60% THF / 40% DMF for $S_{68}D_{32}^{100}$. The casted film thickness was 200 μm in all cases. For both polymers, experiments were carried out with “open-times” between 0 seconds and 10 minutes. To avoid any misinterpretation, we clearly state that 0 seconds corresponded to an immediate immersion of the as-cast film into the water bath. Nevertheless, a delay of a few seconds due to the removal of the doctor blade and, of course, the casting process itself, could not be avoided. First, results for both polymers are described separately and are afterwards compared.

$S_{81}D_{19}^{75}$

Membranes were cast from solutions of $S_{81}D_{19}^{75}$ with “open-times” of 0, 30, 60, 90 seconds, 2, and 3 minutes. For times exceeding 90 seconds, no further difference in the membrane structure could be found. SEM micrographs of membrane cross sections obtained for different “open-times” are shown in Figure 4. The upper insets show an enlargement of the structure at the separation layer on top of the membranes. In one case, an on-top view onto the membrane surface in contact with air is shown in the lower inset. Figure 4A shows a cross section obtained after 0 seconds. Clearly, the asymmetric nature of the membrane could be seen. The top layer (Figure 4A, inset), however, appears far more dense and does not show any pores. Obviously, the very short “open-time” prevented the system from the formation of a porous top layer. Indeed, the membrane did not exhibit any measurable water flux (cf. below), hinting to a non-porous top layer. However, this will be discussed in more detail later. Beneath, “finger-like” macrovoids were obtained, attributed again to the rapid demixing process.

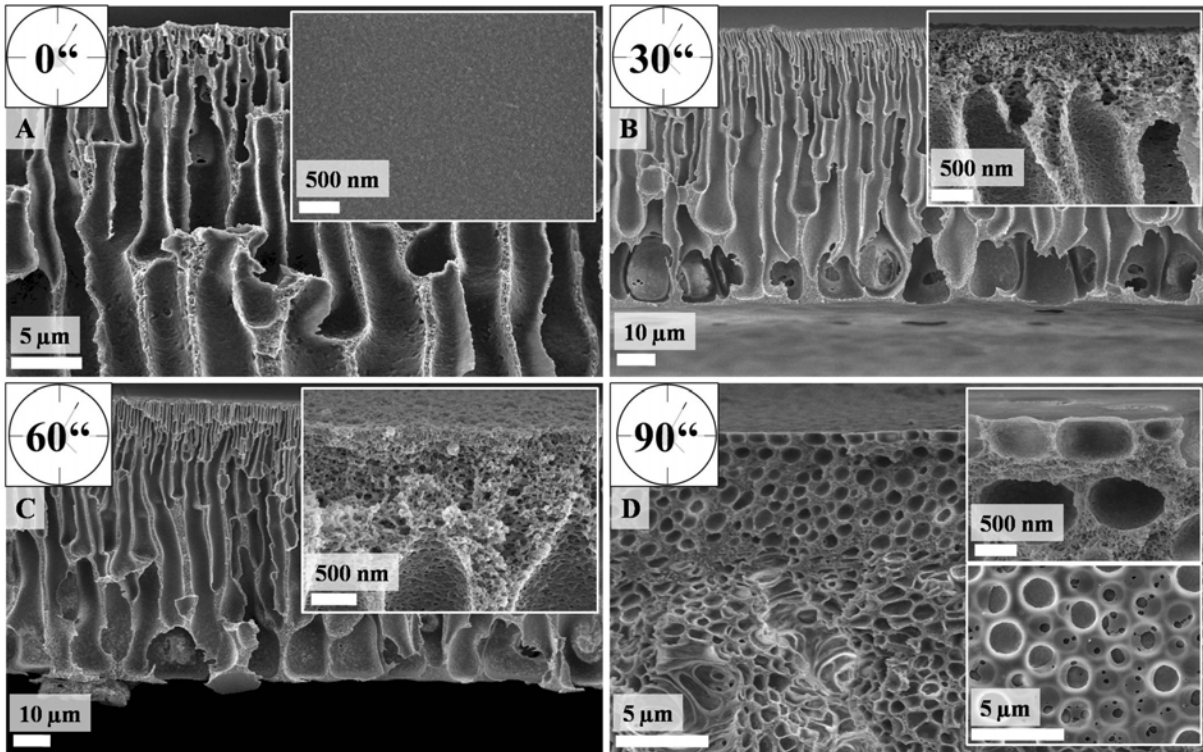


Figure 4: SEM micrographs for membranes from $S_{81}D_{19}^{75}$ cast from a mixture of THF (50%) and DMF (50%) after different “open-times”: 0 seconds (A), 30 seconds (B), 60 seconds (C), and 90 seconds (D); the upper insets show the membrane top surface (A), or an enlargement of the respective separation layer (B, C), the lower inset displays an on-top view onto the top layer.

After 30 seconds “open-time”, the formation of a porous top layer was already evident, as shown in Figure 4B. This separation layer exhibited a thickness of around 1 μm . After 60 seconds, almost no difference in the membrane structure was obtained (Figure 4C). The top layer increased slightly in thickness. This situation changed if the “open-time” was increased to 90 seconds. Here, the membrane no longer showed an asymmetric cross section (Figure 4D). Instead, a sponge-like morphology was obtained throughout the whole film. Obviously, through the solvent evaporation during these 90 seconds a too high polymer concentration was reached and phase separation occurred even before the immersion into the water bath. In the lower inset of Figure 4D an on-top view onto the membrane top layer is shown. Comparable to the cross section, spherical holes in the range of 2-5 μm could be seen. Similar observations were made if the “open-time” was increased beyond 90 seconds, but the macropore dimensions did not further increase with time.

$S_{68}D_{32}^{100}$

Membranes were cast from solutions of $S_{68}D_{32}^{100}$ with “open-times” of 0, 30, 60, 90 seconds, 2, 3, and 10 minutes. SEM micrographs of the membranes cross sections obtained for different “open-times” are shown in Figure 5.

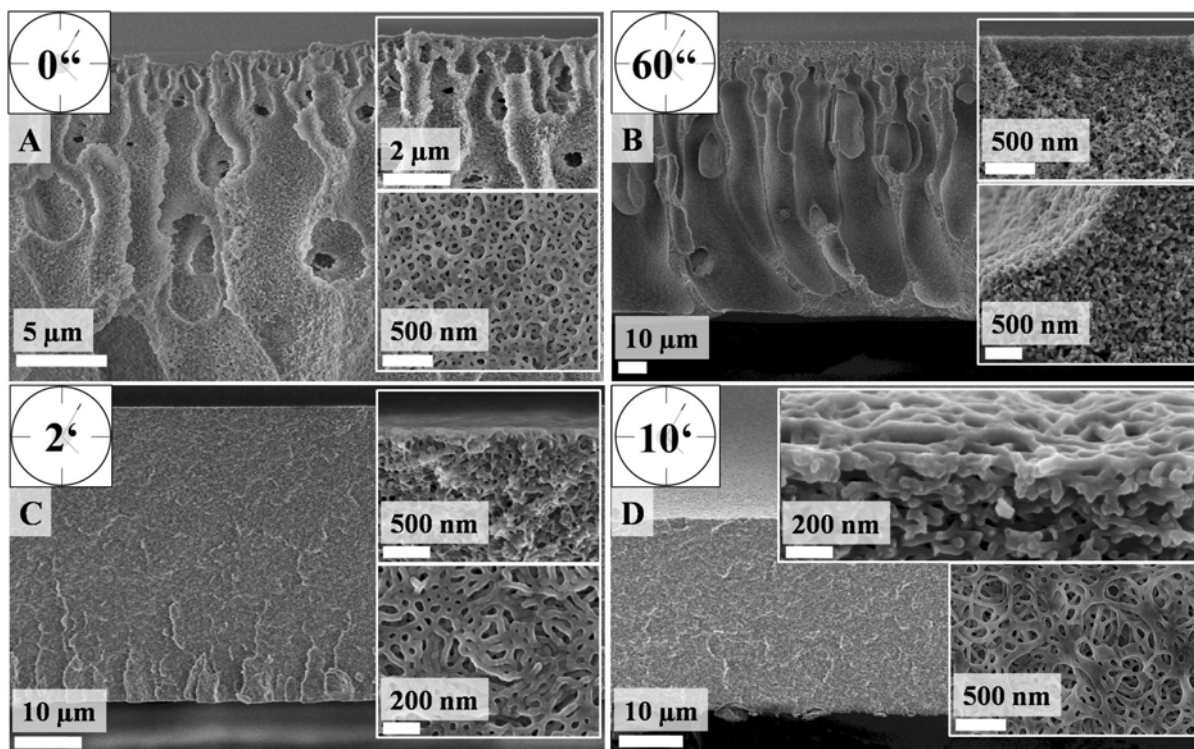


Figure 5: SEM micrographs for membranes from $S_{68}D_{32}^{100}$ cast from a mixture of THF (60%) and DMF (40%) after different “open-times”: 0 seconds (A), 60 seconds (B), 2 minutes (C), and 10 minutes (D); the upper insets show an enlargement of the respective separation layer, the lower insets display the morphology obtained at the bottom of the membrane.

If the as-cast film was immersed into the coagulation bath immediately, both separation layer and the volume structure were less developed (Figure 5A). The top layer, like observed for $S_{81}D_{19}^{75}$, exhibited a thickness below 500 nm and showed no pores (Figure 5A, upper inset). Also here, no water flux could be obtained (cf. below). The macrovoids beneath were rather broad and ill-defined. At the bottom surface, interconnecting wormlike objects were observed (Figure 5A, lower inset). After 60 seconds, the membrane structure was as already described in the previous chapter. A compact separation layer with a thickness of around 10 μm is formed, supported from underneath by “pear-shaped” macrovoids. If longer “open-times” were used, the membrane morphology changed. After 2 minutes, an isotropic cross section was obtained (Figure 5C), comparable to the structures obtained for 60 seconds and a lower THF content in the casting solution (cf. Figure 3B, D, F). A

possible explanation is that the long “open-time” resulted again in a depletion of the polymer film from THF, leading to phase separation occurring before the immersion step. Contrary to $S_{81}D_{19}^{75}$, where a sponge-like structure with features in the region of 2-5 μm was formed, for $S_{68}D_{32}^{100}$ a densely packed sponge-like structure could be seen. Again, the altered block copolymer composition played an important role. As DMF is the better solvent for PDMAEMA, its higher content improved the solubility of the block copolymer even at higher concentrations in the remaining solvent mixture, now mainly consisting of DMF. As a direct result, more defined structures could be obtained for $S_{68}D_{32}^{100}$ even for long “open-times”. This could also be seen in the lower inset of Figure 5C, where wormlike structures are shown at the bottom surface of the membrane. To further elucidate this statement, an as-cast polymer film was left for 10 minutes prior to immersion. In this particular case, all THF should have been evaporated and the “proto-membrane” should only consist of polymer and DMF. Clearly, the obtained membrane (Figure 5D) exhibits a similar structure as the one formed after 2 minutes. If combined with the results discussed for different solvent compositions, the tendency for the formation of branches for the cylindrical structures at the bottom surface of the membranes seems to increase with the “open-time”. For 10 minutes, scarcely single, unconnected cylinders can be seen (Figure 5D, lower inset).

Comparison of both block copolymers

An increase in “open-time” over a certain critical value resulted in macrophase separation taking place prior to the immersion into the coagulation bath for both block copolymers investigated. This critical value was determined through both the content in hydrophilic material, PDMAEMA, and THF. Due to the high volatility of THF, the amount of THF in the casting solution determined the actual polymer concentration at comparable “open-times”. For the polymer with the lower content of DMAEMA, $S_{81}D_{19}^{75}$, the critical value was reached after 90 seconds. Here, the polymer already precipitated in the as-cast film, as could be observed by transition to a turbid film. After immersion in the coagulation bath, an isotropic cross section with a comb-like morphology had formed. The longer PDMAEMA block of $S_{68}D_{32}^{100}$ yielded a higher compatibility with the water bath and also kept the block copolymer soluble at higher concentrations. Thus, even for an “open-time”

of 10 minutes, more developed microphase separated porous features could be obtained as displayed in Figure 5D.

Influence of casted film thickness

After the discussion on the role of the solvent composition of the casting solution and the “open-time”, the next important parameter was the step height used for film casting. A thicker film contains more solvent and, due to mass transfer over the same area, should slower deplete with respect to the THF content. The influence of the casted film thickness was investigated for $S_{81}D_{19}^{75}$. Films with 50, 100, 150, and 200 μm thickness were cast like described before. The solvent composition was 50% THF and 50% DMF. The “open-time” was kept at 60 seconds. The resulting SEM micrographs are shown in Figure 6. Note that only cross sections for 50, 100, and 150 μm initial film thicknesses are shown here, for 200 μm the reader is referred to Figure 3C or Figure 4C.

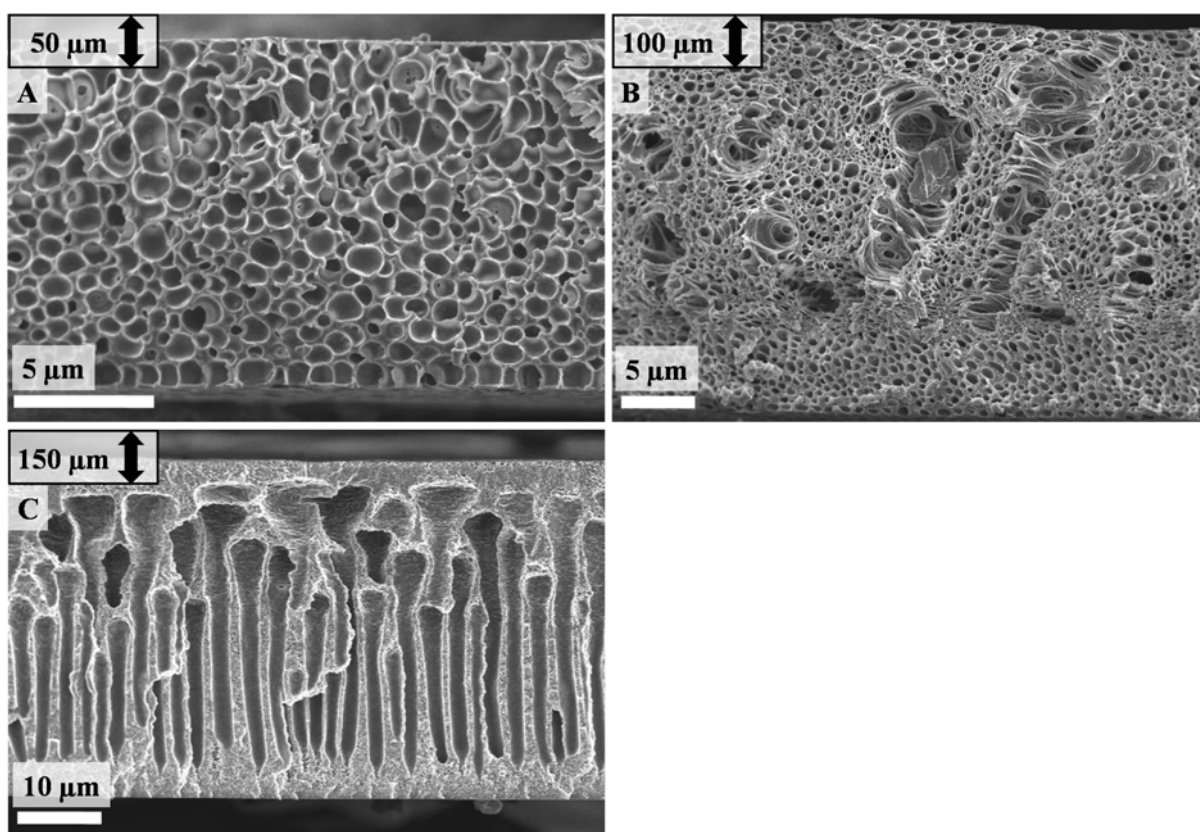


Figure 6: SEM micrographs for membranes from $S_{81}D_{19}^{75}$ cast from a mixture of THF (50%) and DMF (50%) with 60 seconds “open-time” for different film thicknesses: 50 μm (A), 100 μm (B), and 150 μm (C).

For a film thickness of 50 μm a sponge-like membrane structure was obtained (Figure 6A), very similar to the one from a 200 μm film after an “open-time” of 90 seconds (Figure 4D). Both in the volume and on the surfaces structural features in the range of 2-5 μm and with a spherical shape were visible. We suppose that this could be explained in a similar manner like for the “open-time”. For a thinner as-cast film the critical polymer concentration was reached after a shorter time period, 60 seconds in this case. This is again due to the evaporation of the THF, the better solvent for the majority block, PS. For 100 μm step height, a comparable membrane structure could be observed (Figure 6B). However, throughout the cross section also some locations were found where the cell-structure seems to be disturbed. This could already be an indication for the beginning of the macrovoid formation. Apart from that, shape and size of the obtained structures matched. The transition towards an asymmetric membrane morphology was reached if films with an initial thickness of 150 μm were cast (Figure 6C). “Finger-like” macrovoids were obtained beneath a dense skin layer with a thickness of around 5 μm . However, the structure was still not as defined as for films with 200 μm casting thickness, the macrovoids did not penetrate the whole supporting volume, and another compact layer was formed on the bottom of the membrane.

Overall, the results of variation of casted film thickness and varied “open time” could consistently be discussed based on evaporation of THF from the solvent mixture, controlled by the mass transfer to the film surface, with the same influences on the transition from anisotropic to isotropic porous cross-section morphologies. And it should also be possible to favor the formation of controlled microphase separated morphologies via casted film thickness (or its combination with “open time”) if the respective copolymer / solvent system will allow this (cf. above).

Tunable water flux

After varying the preparation parameters, the water flux through the obtained membranes was determined. First, the influence of the casting solvent mixture composition and “open-time” will be discussed. Afterwards, the double stimuli-responsive character of those structures will be highlighted using two representative examples: membranes from both $S_{81}D_{19}^{75}$ and $S_{68}D_{32}^{100}$ cast from a

mixture of 60% THF and 40% DMF with 200 μm film thickness and 60 seconds “open-time”. Water flux values obtained with de-ionized water (pH 6) at 25 °C for both polymers and different preparation conditions are summarized in Table 1.

Table 1A: water flux for different solvent compositions

Solvent composition [% THF / % DMF]	25 / 75	40 / 60	50 / 50	60 / 40	75 / 25
Water flux for $S_{81}D_{19}^{75}$ [L/m ² ·h·bar]	200	4400	2500	4100	1400
Water flux for $S_{68}D_{32}^{100}$ [L/m ² ·h·bar]	100	70	100	2100	150

Table 1B: water flux for different “open-times”

“Open-time”	0	30 sec	60 sec	90 sec	2 min	10 min
Water flux for $S_{81}D_{19}^{75}$ [L/m ² ·h·bar]	0	4800	4100	0	_ ^a	_ ^a
Water flux for $S_{68}D_{32}^{100}$ [L/m ² ·h·bar]	0	_ ^b	2100	_ ^b	100	100

a: not determined, no structural change observed for “open-times” exceeding 90 seconds

b: not determined, membrane was not prepared under these conditions

Table 1A shows the water flux values for different compositions of the solvent mixture for film casting. In the case of $S_{81}D_{19}^{75}$, high flux values were obtained except for the lowest THF content, 25%. Although this was not visible in the SEM micrographs, the skin layer for this membrane seemed to be less porous. For higher THF contents larger flux values were measured. As observed in Figure 3 concerning the morphological features, also the water flux showed no distinct tendency for THF contents ranging from 40% to 75%. The membranes cast from solutions containing 40% and 60% THF exhibited the highest flux values with around 4000. For 50% and 75% THF, permeabilities of 2500 and 1400, respectively, were determined.

For the diblock copolymer with the longer PDMAEMA block, $S_{68}D_{32}^{100}$, low flux values were measured for THF contents in the solvent mixture of 25%, 40%, and 50%. This could be explained by the compact, isotropic cross section of these membranes (cf. Figure 3B, D, and F). The membrane cast from 60% THF and 40% DMF, exhibiting

the desired asymmetric structure, showed a drastically increased flux with a value of 2100. If the THF content was increased further to 75%, the flux decreased again although the membrane cross section still was anisotropic in nature. A possible explanation is the earlier discussed transition from “finger-like” towards “pear-shaped” macrovoids. Furthermore, these structural features did not penetrate the whole membrane any more, resulting in a reduced permeability.

Table 1B summarizes the results for different “open-times”. For $S_{81}D_{19}^{75}$, no flux could be measured if this period is either too short or too long. For 0 seconds the skin layer did not exhibit any porosity (Figure 4A), for 90 seconds phase separation already started before the immersion into the water bath, leading to a sponge-like cross section. As mentioned earlier, longer “open-times” than 90 seconds did not lead to any significant change in the membrane morphology. Surprisingly, for 30 seconds “open-time” the highest water flux was measured.

Also for $S_{68}D_{32}^{100}$ no water flux was observed for 0 seconds “open-time”. Obviously, also here a certain evaporation of THF was necessary for the formation of pores in the top skin layer. For times exceeding 60 seconds, spongelike isotropic membrane cross sections were obtained again, like discussed in Figure 5. Comparable to the structures obtained for solvent mixtures with 50% THF or less, these exhibited a rather low water flux around 100, attributed to the densely packed membrane structure. This has been verified for “open-times” up to even 10 minutes.

Next, the surrounding conditions were varied to trigger both stimuli of the “smart” PDMAEMA, pH and temperature. To reach a new equilibrium state under flow-through conditions, each change in pH was performed over a time span of 2 hours. The waiting time in between two temperatures was 1 hour. Measurements were performed for two representative membranes, prepared from solutions of 60% THF and 40% DMF for both polymers. The results are shown in Figure 7.

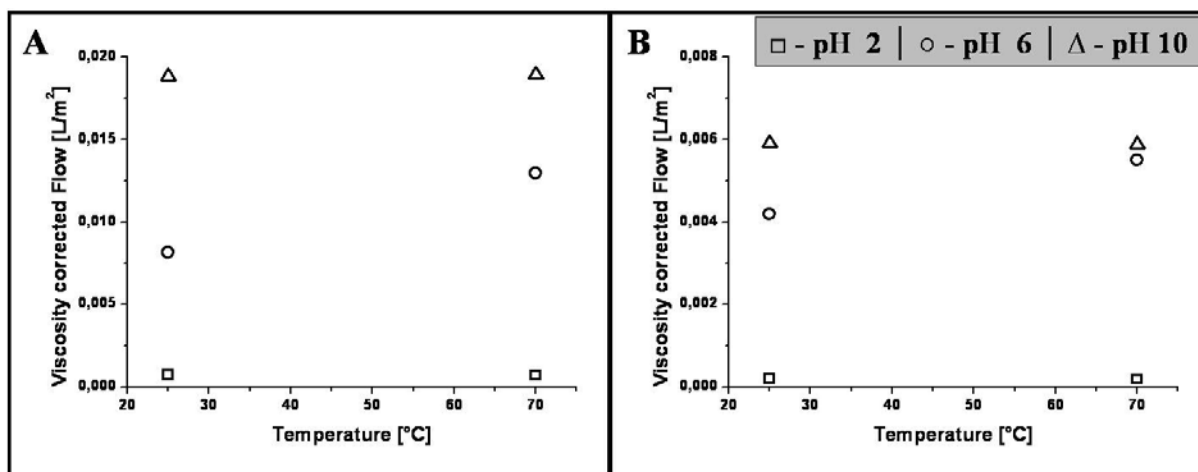


Figure 7: pH- and temperature dependent water flux (multiplied with viscosity for the respective temperatures) for $S_{81}D_{19}^{75}$ (A) and $S_{68}D_{32}^{100}$ (B), prepared from solutions of 60% THF and 40% DMF; open squares indicate measurements performed at pH 2 (\square), open spheres pH 6 (\circ), and open triangles pH 10 (Δ).

Figure 7A displays the water flux values obtained for $S_{81}D_{19}^{75}$ at different pH- and temperature conditions. At pH 2, almost no flux was measured due to the full protonation and, hence, swollen state of the PDMAEMA chains. Upon heating above the previously determined cloud point of around 65 °C for membranes prepared from this polymer,²⁴ no increase in flux could be seen. At pH 6, the PDMAEMA chains were less protonated ($pK_a \approx 7.78$ ¹⁵) and less extended, a considerably higher water flux was obtained. Raising the temperature to 70 °C further increased the water flow. Here, the LCST is applicable and at the cloud point the polymer chains collapse. Through a change to pH 10 yet another gain in flux could be achieved. Under these conditions, the PDMAEMA chains were completely uncharged. Surprisingly, upon heating no flux increase could be seen, indicating a complete collapse of the polymer chains even at room temperature.

Figure 7B summarizes the results obtained for a membrane of $S_{68}D_{32}^{100}$, prepared using the same conditions. Here, the overall flux values were lower, confirming the results presented in Table 1A. This was attributed to a more densely packed skin layer obtained for membranes of this polymer, as already discussed according to Figure 3. At pH 2, again, the hydrophilic membrane material was completely swollen, almost no flux was measured and also no gain in flux could be seen upon heating. An immense increase in terms of water flux was obtained at pH 6, almost by a factor of 20. Subsequent heating to 70 °C, like for $S_{81}D_{19}^{75}$, caused a collapse

of the temperature-sensitive PDMAEMA chains, which were less protonated under these conditions. At pH 10 the largest values could be measured, again, heating to 70 °C resulted in no further increase.

If both polymers were compared, the content of “smart” material indeed seemed to have an influence. In the case of $S_{81}D_{19}^{75}$, a change in pH from 2 to 6 induced a 10fold water flux increase whereas for $S_{68}D_{32}^{100}$ a factor of 20 could be seen. Further pH increase to a value of 10 resulted in a comparable change, a factor of 2 for $S_{81}D_{19}^{75}$ and a factor of 1.5 for $S_{68}D_{32}^{100}$. Same accounted for the situation upon triggering the LCST at pH 6. Here, the flux rises by a factor of 1.5 ($S_{81}D_{19}^{75}$) and 1.3 ($S_{68}D_{32}^{100}$). Obviously, the higher content of PDMAEMA lead to a higher degree of swelling of the whole membrane at low pH or, more precise, it facilitated a more pronounced de-swelling upon a change to pH 6. It remains a rather puzzling question why no flux increase could be detected for both membranes upon heating at pH 10. Membranes with comparable structure, casting conditions, and flux values were shown earlier to exhibit a certain LCST behavior even under these conditions.²⁴

Conclusions

We successfully prepared asymmetric membranes via the NIPS process from solutions of two amphiphilic block copolymers, $S_{81}D_{19}^{75}$ and $S_{68}D_{32}^{100}$ in mixtures of DMF and THF. Through a systematic variation of the casting conditions for both polymers, e.g. the used solvent mixture, the “open-time”, or the casted film thickness we were able to point out crucial parameters which determine the obtained membrane morphologies. These results have to be interpreted with a certain caution, as the investigated systems are rather complex and combine the aspects of at least two different ternary phase diagrams, one for each block copolymer compartment and based on the assumption that THF and DMF mix ideally. Nevertheless, this work alludes to general tendencies and principles for morphological transitions in amphiphilic membrane systems. Moreover, the effect of a higher content in hydrophilic material for $S_{68}D_{32}^{100}$ was demonstrated, leading to an improved compatibility with the non-solvent bath and, hence, slower precipitation and further developed structural features. Thus, conditions could be identified where ordered micro phase separated porous morphologies were

observed in parts of the membrane cross-section. Both polymers were shown to form self-supporting membrane systems which are able to react onto two different external stimuli in terms of water flux, pH and temperature.

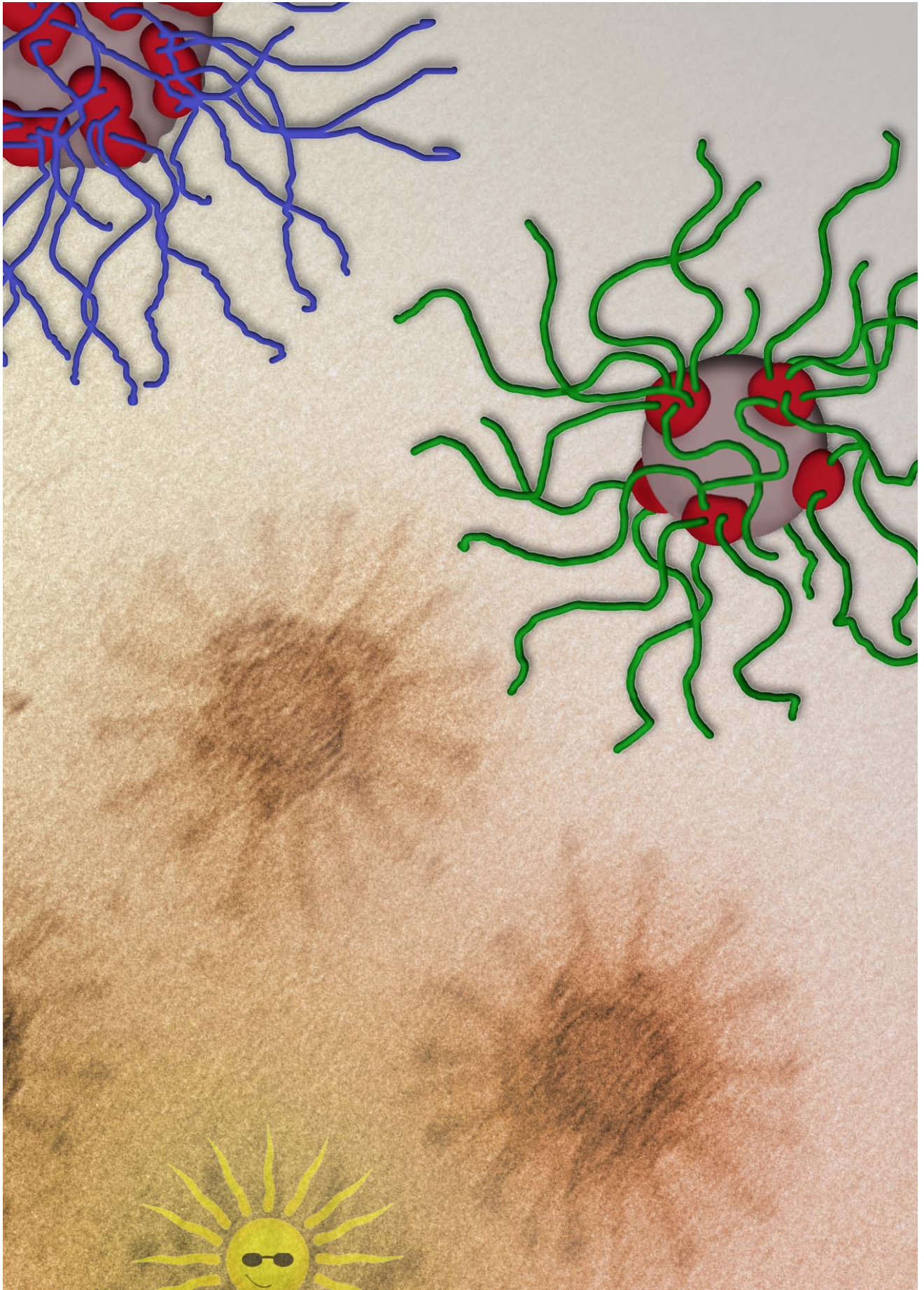
Acknowledgements:

The authors would like to thank Benjamin Gossler for the SEM measurements and Sabine Wunder, Christina Löffler and Robin Pettau for SEC measurements (all University of Bayreuth). Claudia Schenk, Marcel Gawenda and Dr. Heru Susanto are acknowledged for their help during the stay of FS at University Duisburg-Essen. Funding was received from the VolkswagenStiftung within the framework “Complex Materials”.

References:

1. Baker, R., *Membrane Technology and Applications*. Wiley: Chichester, 2004.
2. Yoo, S. H.; Kim, J. H.; Jho, J. Y.; Won, J.; Kang, Y. S. *J. Membr. Sci.* 2004, 236, 203-207.
3. Ulbricht, M. *Polymer* 2006, 47, 2217-2262.
4. Mehta, A.; Zydney, A. L. *Journal of Membrane Science* 2005, 249, 245-249.
5. Abetz, V.; Simon, P. F. W., *Phase Behavior and morphologies of block copolymers*. Springer-Verlag Berlin Heidelberg: 2005; Vol. 189, p 125-212.
6. Klok, H.-A.; Lecommandoux, S. *Adv.Mater.* 2001, 13, 1217-1229.
7. Schacher, F.; Müllner, M.; Schmalz, H.; Müller, A. H. E. *Macromol. Chem. Phys.* 2009, 210, 256-262.
8. Walther, A.; Millard, P.-E.; Goldmann, A. S.; Lovestead, T. M.; Schacher, F.; Barner-Kowollik, C.; Müller, A. H. E. *Macromolecules* 2008, 41, 8608-8619.
9. Breiner, U.; Krappe, U.; Abetz, V.; Stadler, R. *Macromol. Chem. Phys.* 1997, 198, 1051.
10. Hückstädt, H.; Göpfert, A.; Abetz, V. *Polymer* 2000, 41, 9089-9094.
11. Walther, A.; Andre, X.; Drechsler, M.; Abetz, V.; Müller, A. H. E. *J. Am. Chem. Soc.* 2007, 129, 6187-6198.
12. Sperschneider, A.; Schacher, F.; Gawenda, M.; Tsarkova, L.; Müller, A. H. E.; Ulbricht, M.; Krausch, G.; Köhler, J. *Small* 2007, 3, 1056-1063.
13. Erhardt, R.; Boker, A.; Zettl, H.; Kaya, H.; Pyckhout-Hintzen, W.; Krausch, G.; Abetz, V.; Müller, A. H. E. *Macromolecules* 2001, 34, 1069-1075.
14. Plamper, F. A.; Becker, H.; Lanzendörfer, M.; Patel, M.; Wittemann, A.; Ballauff, M.; Müller, A. H. E. *Macromol. Chem. Phys.* 2005, 206, 1813.
15. Plamper, F.; Ruppel, M.; Schmalz, A.; Borisov, O.; Ballauff, M.; Müller, A. H. E. *Macromolecules* 2007, 40, 8361-8366.
16. Plamper, F.; Walther, A.; Müller, A. H. E.; Ballauff, M. *Nano Lett.* 2007, 7, 167-171.
17. Yang, S. Y.; Ryu, I.; Kim, H. Y.; Jang, S. K.; Russell, T. P. *Advanced Materials* 2006, 18, 709-712.
18. Phillip, W. A.; Rzayev, J.; Hillmyer, M. A.; Cussler, E. L. *Journal of Membrane Science* 2006, 286, 144-152.
19. Nunes, S. P.; Peinemann, K. V., *Membrane Technology*. 2nd ed.; Wiley-VCH: Weinheim, 2006.
20. van de Witte, P.; Dijkstra, P. J.; van den Berg, J. W. A.; Feijen, J. *J. Membr. Sci.* 1996, 117, 1-31.

21. Peinemann, K. V.; Abetz, V.; Simon, P. F. W. *Nature mat.* 2007, 6, 992-996.
22. Su, Y.-L.; Li, C. *J. Membr. Sci.* 2007, 305, 271-278.
23. Ying, L.; Kang, E. T.; Neoh, K. G.; Kato, K.; Iwata, H. *J. Membr. Sci.* 2004, 243, 253-262.
24. Schacher, F.; Ulbricht, M.; Müller, A. H. E. *Adv. Funct. Mater.* 2009, 19, 1040-1045.
25. Freyss, D.; Rempp, P.; Benoît, H. *Polym. Lett.* 1964, 2, 217.
26. Quirk, R. P.; Yoo, T.; Lee, Y.; Kim, J.; Lee, B. *Adv. Polym. Sci.* 2000, 153, 67-106.
27. Brandrup, J.; Immergut, E. H.; Grulke, E. A., *Polymer Handbook*. 4th ed.; John Wiley & Sons: New York, 1999.
28. Wienk, I. M.; Boom, R. M.; Beerlage, M. A. M.; Bulte, A. M. W.; Smolders, C. A.; Strathmann, H. *J. Membr. Sci.* 1996, 113, 361-371.

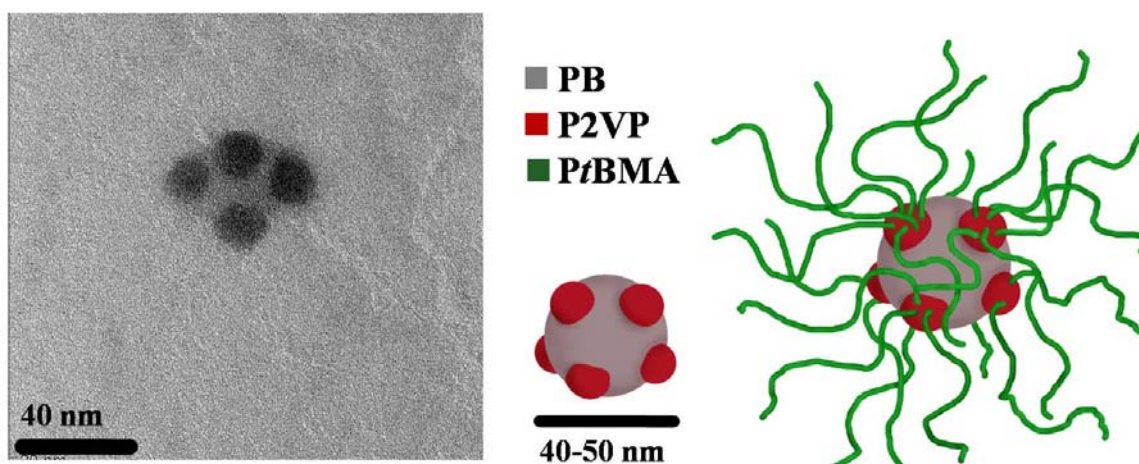


Multicompartment Core Micelles of Triblock Terpolymers in Organic Media

Felix Schacher^{1}, Andreas Walther², Markus Ruppel³, Markus Drechsler¹,
and Axel H. E. Müller^{1*}*

- [1] Makromolekulare Chemie II and Zentrum für Kolloide und Grenzflächen, Universität Bayreuth, 95440 Bayreuth, Germany,
- [2] Department of Applied Physics, Helsinki University of Technology, FIN-02015 TKK, Helsinki, Finland
- [3] Oak Ridge National Laboratory, Oak Ridge, TN 37831, USA

felix.schacher@uni-bayreuth.de; axel.mueller@uni-bayreuth.de;



ABSTRACT:

The formation of multicompartment micelles featuring a “spheres on sphere” core morphology in acetone as a selective solvent is presented. The polymers investigated are ABC triblock terpolymers polybutadiene-*b*-poly(2-vinylpyridine)-*b*-poly(*tert*-butyl methacrylate) (BVT), which were synthesized via living sequential anionic polymerization in THF. Two polymers with different block lengths of the methacrylate moiety were studied with respect to the formation of multicompartmental aggregates. The micelles were analyzed by static and dynamic light scattering as well as by transmission electron microscopy. Crosslinking of the polybutadiene compartment could be accomplished via two different methods, ‘cold vulcanization’ and with photopolymerization after the addition of a multifunctional acrylate. In both cases, the multicompartmental character of the micellar core is fully preserved and the micelles could be transformed into core-stabilized nanoparticles. The successful crosslinking of the polybutadiene core is indicated by $^1\text{H-NMR}$ and the by transfer of the aggregates into non-selective solvents like THF or dioxane.

Introduction

Multicompartment micelles can combine several properties or functionalities in close proximity and are therefore promising candidates for a new class of nanomaterials. Different research groups have worked to develop diverse strategies for the preparation of such micelles in aqueous media. The term “multicompartment micelles”, or more precisely, “multicompartment core micelles”, stands for self-assembled aggregates of block copolymers with cores that are further subdivided. The principal concept was introduced by Ringsdorf^[1] around 10 years ago and a recent review reports on the progress within this field of research.^[2] Those structures are of great interest when it comes to the simulation or understanding of biological systems, where different functionalities in close proximity are necessary to perform distinct biological functions.^[3] Multicompartment micelles are very promising candidates for drug-delivery applications, especially for entrapment and / or release of hydrophobic species in different media. Different groups investigated the selective solubilization in multicompartmental micellar cores.^[4-7] Hillmyer et. al. demonstrated the possibility of storing two different dyes in two segregated compartments of such a multicompartmental structure in various aqueous micellar solutions.^[8]

Complex structures have been prepared from ABC triblock terpolymers in solution.^[9-11] In contrast to the large number of reports on micellar aggregates from diblock copolymers or the structures of ABC triblock terpolymers in the bulk, the number of contributions on triblock terpolymer micelles in selective solvents is still limited.^[12-16] In particular, the formation and the control of the stability of such systems are yet not very well studied and understood. Most of the current approaches towards multicompartmental architectures are based on the mutual incompatibility of fluorocarbon and hydrocarbon segments of self-assembled systems in aqueous media.^[3, 8, 17, 18] One very recent example employs an ABCBA pentablock terpolymer of poly(ethylene oxide) (PEO), poly(γ -benzyl-L-glutamate) (PBLG) and poly(perfluoroether) (PFPE) in aqueous solution.^[19] Besides, complex polymer architectures may also lead to the formation of multicompartmental structures. Lodge et al. reported on ABC miktoarm star terpolymers, poly(ethylene)-*b*-poly(ethylene oxide)-*b*-poly(perfluoropropylene oxide).^[20, 21] The star architecture can suppress the formation of concentric microphase domains. This has also been

demonstrated by Hillmyer et al. for polyester-containing ABC miktoarm star polymers with arms of PEO, poly(ethylene), and poly(γ -methyl- ϵ -caprolactone).^[22] Additionally, charged polymer segments may induce a further compartmentalization of either core or corona as well, as shown by Yan et al.^[23] Theoretical aspects of the micelle formation from ABC terpolymers as model systems depending on block sequence, architecture and molecular weight have been addressed^[24-27] and broadened the scope and interest of multicompartment architectures.

In this contribution we present the formation of multicompartment core micelles in acetone solution from polybutadiene-*b*-poly(2-vinylpyridine)-*b*-poly(*tert*-butyl methacrylate) (BVT) triblock terpolymers and their stabilization by crosslinking. The polymers were synthesized via sequential anionic polymerization and exhibit a very narrow molecular weight distribution (PDI < 1.04). The formed aggregates have been investigated by transmission electron microscopy (TEM), cryogenic transmission electron microscopy (cryo-TEM) and light scattering methods. The micelles are stable with respect to the crosslinking of the double bonds of the polybutadiene compartment. Crosslinking was carried out via either “cold vulcanization” with S₂Cl₂ or through UV-photopolymerization in presence of a tetrafunctional acrylate. The effect of the amount of crosslinking agent and/or the reaction time on the size and the shape of the generated nanostructures were also studied. After performing the crosslinking reactions in solution, the micelles were again subjected to electron microscopy and light scattering analysis. The success of the crosslinking was proven by the transfer of the micellar aggregates into THF, a non-selective solvent for all the three blocks. In contrast to other works within this field, the employed building blocks here are rather simple and consist of standard, easy-to-handle monomers. It is noteworthy that in all cases only one single population of aggregates was found and the micellar solutions are stable over several months, both before and after the crosslinking steps.

Experimental part

Materials

Sec-butyllithium, S₂Cl₂ and pentaerythroltetraacrylate (Aldrich) were used without further purification. Butadiene (Messer-Griesheim) was passed through columns filled with molecular sieves (4Å) and basic aluminum oxide. Afterwards it was condensed into a glass reactor and stored over dibutylmagnesium. 2-Vinylpyridine (Fluka) was degassed and stirred with CaH₂ over night. The monomer was condensed on a high vacuum line into a round bottom flask containing 2 ml of triethylaluminum (solution in hexane, Aldrich) per 10 ml 2-vinylpyridine. The resulting yellow solution was stirred for 2 hours. Subsequently, the calculated amount of monomer was condensed into a previously weighed glass ampoule and stored in liquid nitrogen until use. *Tert*-butyl methacrylate (BASF) was first degassed by 3 freeze-thaw cycles on a high vacuum line. Then trioctylaluminum (solution in hexane, Aldrich) was added until a slight yellow color of the resulting mixture persisted. The solution was stirred for 1 hour and the calculated amount of monomer was condensed into a previously weighed glass ampoule and stored in liquid nitrogen until use. THF (Fluka) was distilled from CaH₂ and Na/K alloy. 1,1-diphenylethylene was distilled from *sec*-butyl lithium under reduced pressure. The solvents for the preparation of the micellar solutions were purchased in p.a. grade and used as delivered.

Synthesis

Sequential living anionic polymerization in THF

The linear BVT triblock terpolymers were synthesized via sequential living anionic polymerization in THF at low temperatures using *sec*-butyl lithium as initiator. Under these conditions, mainly 1,2-polybutadiene (86%, confirmed by ¹H-NMR measurements) is generated. After the polymerization of the P2VP block, 1,1-diphenylethylene was added to end-cap the living ends of the anions. In this way crossover steps and transfer reactions due to too high nucleophilicity upon addition of the third monomer could be suppressed.^[28, 29] During the polymerization of the P*t*BMA block, samples were taken from the reactor after different polymerization times and were precipitated into degassed methanol. The number-averaged molecular weight of the polybutadiene precursor and the molecular weight distributions

of the triblock terpolymers were determined by gel permeation chromatography. In the case of the polybutadiene precursor, MALDI-ToF mass spectrometry was employed to receive the absolute molecular weight. All the polymers exhibit narrow molecular weight distributions characterized by a polydispersity index between 1.02 and 1.03. Additionally, ^1H NMR spectra were recorded and the molecular weights of the P2VP and P*t*BMA blocks were calculated using the triblock terpolymer composition determined by NMR and GPC. The GPC curves for $\text{B}_{800}\text{V}_{190}\text{T}_{380}$, $\text{B}_{800}\text{V}_{190}\text{T}_{550}$ and the corresponding precursors are shown in **Figure 1** and the molecular characteristics are shown in **Table 1**. Both polymers mentioned showed a lamellar (ll) morphology in the bulk state with characteristic long periods of 78 ($\text{B}_{800}\text{V}_{190}\text{T}_{380}$) and 85 nm ($\text{B}_{800}\text{V}_{190}\text{T}_{550}$).

Table 1: Molecular characteristics of the BVT block terpolymers employed:

Composition ^a	Composition ^b	$10^{-3} M_w^c$	Polydispersity ^d
$\text{B}_{37}\text{V}_{17}\text{T}_{46}^{117}$	$\text{B}_{800}\text{V}_{190}\text{T}_{380}$	117	1.03
$\text{B}_{30}\text{V}_{14}\text{T}_{56}^{141}$	$\text{B}_{800}\text{V}_{190}\text{T}_{550}$	141	1.02

^a subscripts are weight fractions, the superscript is the overall molecular weight in kg/mol); ^b subscripts are degrees of polymerization; ^c determined by combination of MALDI-TOF MS and ^1H NMR; ^d determined via THF-SEC calibrated with 1,4-polybutadiene standards;

Crosslinking via cold vulcanization with S_2Cl_2

To a micellar solution of 1 mg/mL $\text{B}_{30}\text{V}_{14}\text{T}_{56}^{141}$ in acetone were added 1, 2 or 5 equivalents (functional groups of crosslinking agent with respect to the amount of remaining double bonds from the first block of the terpolymer) of S_2Cl_2 . Afterwards the dispersion was stirred for around two hours. The unreacted S_2Cl_2 was removed through dialysis against acetone (dialysis tube, MWCO = 10000 g/mol).

Crosslinking with pentaerythrol tetraacrylate

To a micellar solution of 1 mg/mL $\text{B}_{30}\text{V}_{14}\text{T}_{56}^{141}$ in acetone were added 0.5, 1 or 2 equivalents (functional groups of crosslinking agent with respect to the amount of remaining double bonds from the first block of the terpolymer) of multifunctional acrylate. Afterwards the dispersion was stirred for around two hours to equilibrate.

Crosslinking was performed through irradiation of the dispersion with an UV-lamp (Hoenle VG-UVAHAND 250 GS equipped with a glass filter, cut-off at 300 nm wavelength to not depolymerize the methacrylic compartment). The unreacted crosslinking agent was removed through dialysis against acetone (dialysis tube, MWCO = 10000 g/mol).

Characterization

Gel permeation chromatography measurements were performed on a set of 30 cm SDV-gel columns of 5 mm particle size having a pore size of 10^5 , 10^4 , 10^3 and 10^2 Å with refractive index and UV ($\lambda=254$ nm) detection. GPC was measured at an elution rate of 1 ml/min with THF as eluent.

$^1\text{H NMR}$ spectra were recorded on a Bruker 250 AC spectrometer using either CDCl_3 or THF as solvent and tetramethylsilane (TMS) as internal standard.

Dynamic light scattering (DLS)

DLS measurements were performed in sealed cylindrical scattering cells ($d = 10$ mm) at five scattering angles 30, 60, 90, 120 and 150° on an ALV DLS/SLS-SP 5022F equipment consisting of an ALV-SP 125 laser goniometer with an ALV 5000/E correlator and a He-Ne laser with the wavelength $\lambda = 632.8$ nm. The CONTIN algorithm was applied to analyze the obtained correlation functions. Apparent hydrodynamic radii were calculated according to the Stokes-Einstein equation. Prior to the light scattering measurements the sample dispersions were filtered using Millipore PTFE filters with a pore size of $1 \mu\text{m}$. The polydispersities were determined from unimodal peaks via the cumulant analysis.

Static light scattering

Micellar solutions of the polymers were prepared in the concentration range between 0.1 and 1 g/L. Static light scattering measurements were carried out on a Sofica goniometer with He-Ne laser ($\lambda = 632.8$ nm) at RT. Prior the measurements, sample dispersions were filtered through Millipore PTFE filters of pore size $1 \mu\text{m}$. A Zimm plot was used to evaluate the data. A diffraction refractometer DnDC2010/620 (PSS) was used to measure refractive index increment, dn/dc (0.166

L/mol for B₈₀₀V₁₉₀T₃₈₀ and 0.148 for B₈₀₀V₁₉₀T₅₅₀), of the polymer micellar solution at $\lambda = 620$ nm.

Transmission electron microscopy

TEM images were taken with a Zeiss CEM902 EFTEM electron microscope operated at 80 kV or a Zeiss EM922 OMEGA EFTEM electron microscope operated at 200 kV. Both machines are equipped with an in-column energy filter. Samples were prepared through deposition of a drop of micellar solution (concentration always 0,1 g/L) onto the TEM grid (Gold, 400 mesh). Afterwards the remaining solvent was removed with a filter paper.

Cryogenic Transmission Electron Microscopy (Cryo-TEM)

A drop of the sample solution (c ~0.5 wt-%, solvent being either THF or dioxane) was placed on a lacey carbon-coated copper TEM grid (200 mesh, Science Services, München, Germany), where most of the liquid was removed with blotting paper, leaving a thin film stretched over the grid holes. The specimens were shock vitrified by rapid immersion into liquid nitrogen in a temperature controlled freezing unit (Zeiss Cryobox, Zeiss NTS GmbH, Oberkochen, Germany) and cooled to approximately 90 K. The temperature was monitored and kept constant in the chamber during all the preparation steps. After freezing the specimens, they were inserted into a cryo-transfer holder (CT3500, Gatan, München, Germany) and transferred to a Zeiss EM922 OMEGA EFTEM instrument. Examinations were carried out at temperatures around 90 K. The transmission electron microscope was operated at an acceleration voltage of 200 kV. Zero-loss filtered images ($\Delta E = 0$ eV) were taken under reduced dose conditions (100 - 1000 e/nm²). All images were registered digitally by a bottom mounted CCD camera system (Ultrascan 1000, Gatan), combined and processed with a digital imaging processing system (Gatan Digital Micrograph 3.9 for GMS 1.4).

Matrix assisted Laser Desorption Ionization - Time of Flight Mass Spectrometry

MALDI-ToF MS analysis was performed on a Bruker Reflex III equipped with a 337 nm N₂ laser in the linear mode and 20 kV acceleration voltage. Sodium trifluoroacetate (NaTFA, Fluka, 99,5 %) was used as salt to induce ion formation. Samples were prepared from THF solution by mixing matrix (20 g/L) and the sample (1 mg) in a

ratio of 10:1. The number-average molecular weight, M_n , of the sample was determined in the linear mode.

Results and Discussion

Synthesis of BVT block terpolymers

The two polymers shown in Table 1, $B_{800}V_{190}T_{380}$ and $B_{800}V_{190}T_{550}$, were used for the investigations in this work. The indices denote the degree of polymerization of the corresponding block. These are just two out of a series of several polymers with constant length ratio of first to second block and increasing poly(*tert*-butyl methacrylate) (*Pt*BMA) content. They both display a very low polydispersity. The overall molecular weight was determined by a combination of MALDI-ToF mass spectra of the polybutadiene (PB) precursor and $^1\text{H-NMR}$ spectra of the block copolymer. First, the molecular weight of the polybutadiene precursor was determined via MALDI-ToF mass spectrometry and then the integrals of characteristic signals in NMR spectra of the two other blocks were used for the calculation of the corresponding block lengths. The mass spectrum of the polybutadiene precursor is shown in the supporting information. The SEC elution traces in THF for the PB precursor, the PB-*b*-P2VP precursor and the two BVT triblock terpolymers are shown in Figure 1.

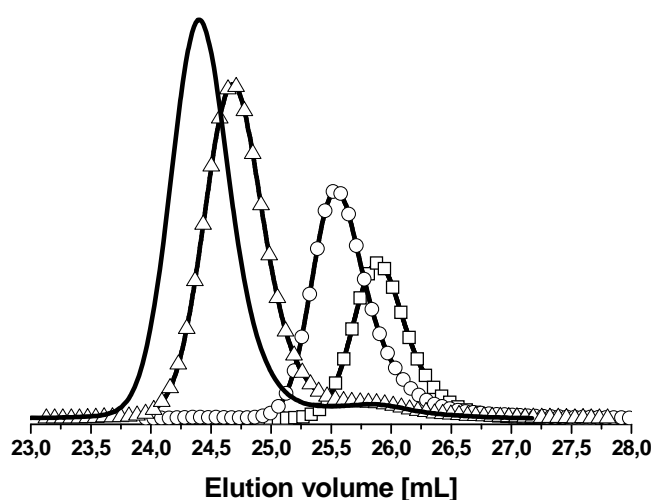


Figure 1: SEC elution traces of B_{800} ($-\square-$), $B_{800}V_{190}$ ($-o-$) and the two triblock terpolymers $B_{800}V_{190}T_{380}$ ($-\Delta-$) and $B_{800}V_{190}T_{550}$ (solid black line).

To induce micelle formation, the polymers need to be dissolved in a selective solvent. Acetone is known to be a non-solvent for polybutadiene^[30]. The micelle formation was investigated in a concentration regime from 0.1 to 3 g/L. When dispersed in acetone at room temperature, the BVT triblock terpolymers immediately form aggregates, indicated by a turbid dispersion. This process is quite fast, the polymers are completely dissolved after 5 minutes. The so-formed micelles were expected to consist of a B core and a corona consisting of V and T.

Dynamic light scattering

DLS was used to assess the average hydrodynamic sizes of the formed aggregates. The CONTIN plots for $B_{800}V_{190}T_{380}$ and $B_{800}V_{190}T_{550}$ in acetone at 1 g/L and $\Theta = 90^\circ$ are shown in Figure 2A and plots of decay rate, Γ , vs. the square of the scattering vector, q^2 , are shown in Figure 2B

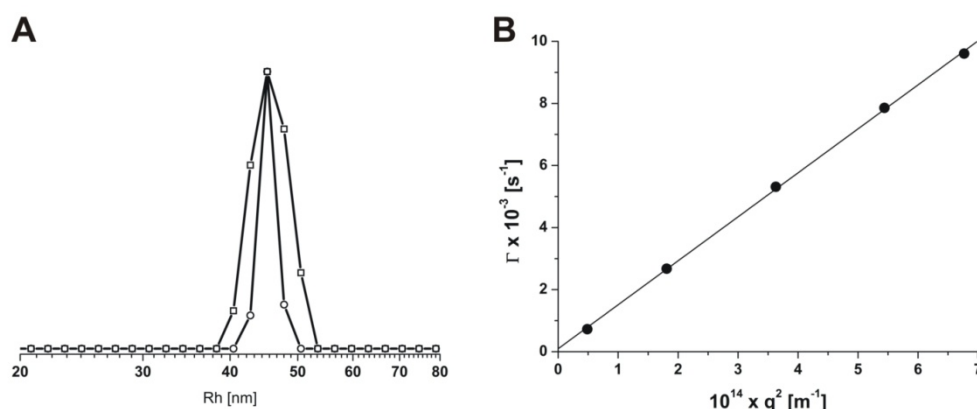


Figure 2: A: CONTIN plots (intensity weighted) for $B_{800}V_{190}T_{380}$ (grey line, $\langle R_h \rangle_z = 43$ nm) and $B_{800}V_{190}T_{550}$ (black line, $\langle R_h \rangle_z = 44$ nm) at $\Theta = 90^\circ$ in acetone ($c = 1$ g/L); B: Γ vs. q^2 for $B_{800}V_{190}T_{550}$.

The micelles are very uniform, as seen by the unimodal CONTIN plots in Figure 2A. These aggregates can be considered as almost monodisperse (PDI ~ 0.02). The hydrodynamic radii, R_h , of both polymers (from the diffusion coefficients, slope of Fig. 2B) and the corresponding polydispersities calculated via cumulant analysis at 90° measurement angle are shown in Table 2. Note that no significant change in the R_h was obtained for concentrations from 0.05 up to 5 g/L. The linearity of the decay rate plots, Γ vs. q^2 and the lack of an intercept in Figure 2B indicates pure translational diffusion, typical for spherical particles.

Static light scattering

SLS experiments were performed in acetone ($0.1 \text{ g/L} \leq c \leq 1 \text{ g/L}$) and analyzed using a Zimm plot.^[31] The results are shown in Table 2. A representative Zimm plot is shown in Figure 3 for $B_{800}V_{190}T_{380}$ at four different concentrations.

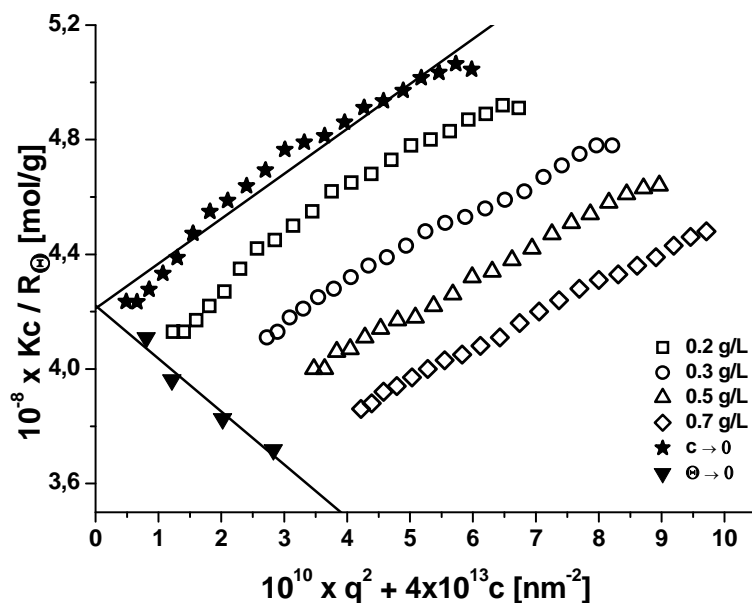


Figure 3: Zimm plot of $B_{800}V_{190}T_{380}$ in acetone.

The molecular weights of both micellar aggregates are comparable ($M_w = 2.38 \times 10^7 \text{ g/mol}$ for $B_{800}V_{190}T_{380}$ and $M_w = 1.17 \times 10^7 \text{ g/mol}$ for $B_{800}V_{190}T_{550}$), resulting in a higher aggregation number of the BVT terpolymer with lower P*t*BMA molecular weight. This corresponds to theoretical expectations and results of diblock copolymer micelles, where it was derived that $N_{agg} \sim N_A^2 N_B^{-0.8}$, where N_A and N_B correspond to the degrees of polymerization of the core- and corona-forming block of strongly segregating systems, respectively.^[32] The degrees of aggregation, N_{agg} , were calculated using the known molecular weights of the precursors and are given in Table 2. A further elucidation of the structure can be achieved by evaluating the characteristic ratio, R_g/R_h . This ratio provides an indication about the shape of the scattering particle.^[33] For hard spheres the ratio is expected to be 0.775, whereas a ratio of 1.1 is expected for polymeric stars with a high arm number. In this particular case, the value for $B_{800}V_{190}T_{380}$ fits the hard spheres model whereas the slightly

higher value for the polymer with the longer methacrylate block might indicate a tendency towards a more star-like solution structure. In both cases, low negative values for the virial coefficient A_2 are obtained, indicating that acetone is not a good solvent for the micelle. This is a known phenomenon of micellar solutions. The high aggregation numbers around 200 lead to a high segment density close to the micellar core and, hence, few solvent molecules are present in-between the single corona chains.^[34]

Recapitulating, dynamic as well as static light scattering revealed that BVT terpolymers form almost monodisperse spherical micelles in acetone as a non-solvent for polybutadiene.

Table 2: Solution characteristics of the BVT terpolymers in acetone

R_h [nm] ^a	PDI ^b	R_g [nm] ^c	R_g/R_h	N_{agg} ^c	$10^6 A_2$ ^e [mol ml/g ²] ^c
43	0.022	34	0,76	203 ± 3^d	-5.13
44	0.016	36	0.82	174 ± 3^d	-4.82

a: determined by DLS at $c = 1$ g/L; b: deviation determined by cumulant analysis at 90° ; c: determined by SLS; d: determined via a linear fit of the extrapolated values for $c \rightarrow 0$ and $\Theta \rightarrow 0$ in Figure 3; e: second virial coefficient, determined via SLS.

Transmission electron microscopy

Typically, the specimens for TEM measurements were prepared through drop-coating from micellar solutions of approximately 0.1 g/L onto carbon-coated gold grids. This concentration is above the critical aggregation concentration (c_{ac}) as indicated by DLS measurements. If not mentioned, the samples were not stained and the contrast originates only from the different polymeric microcompartments. Although TEM is an elegant way to visualize the shape and the size of particles in the nanometer range, one has to be aware that the shape of particles may be affected by the drying procedure on the TEM grids. To confirm the obtained results,

specimens were also prepared through freeze-drying and spray-coating from acetone for two examples. Unfortunately, we have been unable to perform cryo-TEM in acetone. Therefore, freeze-drying is supposed to have the smallest influence on the micellar structure obtained on the TEM specimen. The obtained micelles are very uniform in size. No larger aggregates are present, as shown in **Figure 4A** and **B** for $B_{800}V_{190}T_{550}$ employing two different preparation methods.

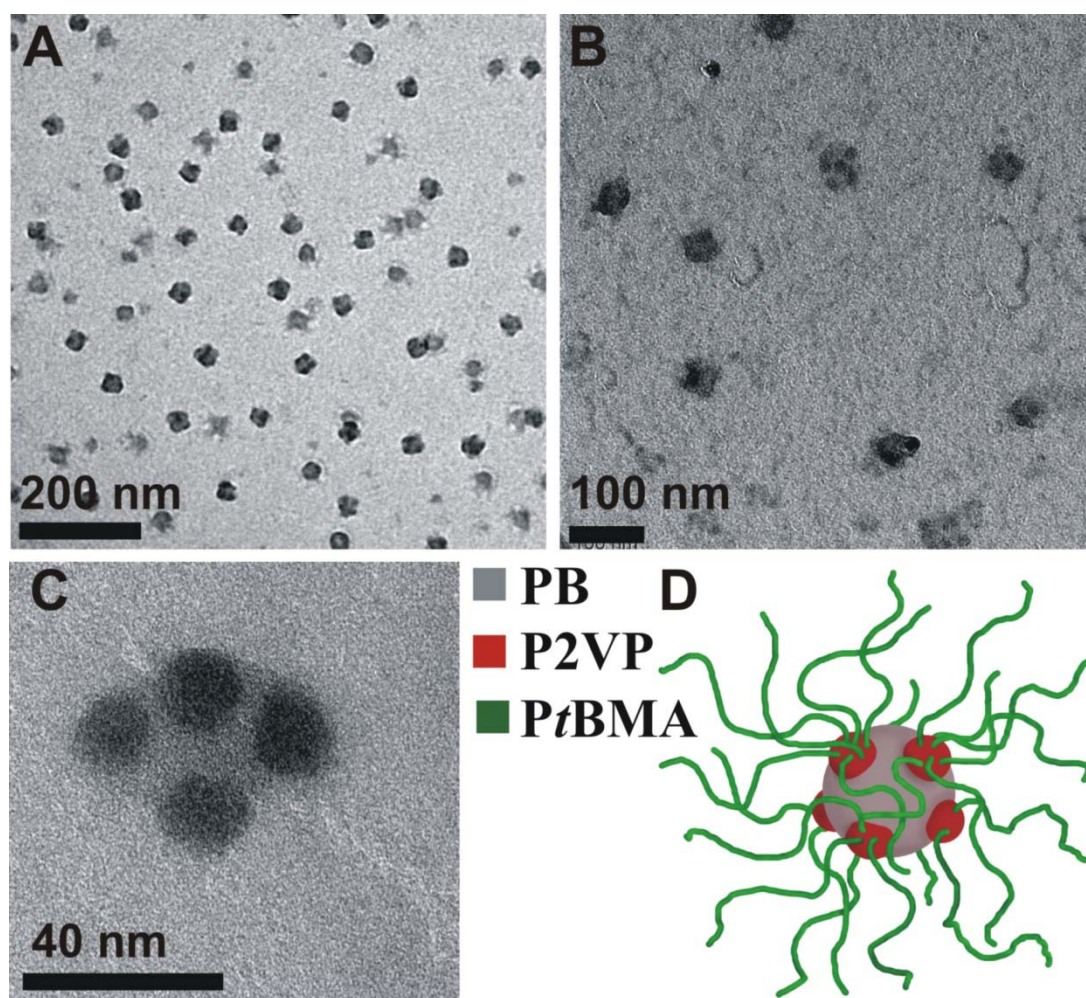


Figure 4: TEM images of multicompartment micelles from $B_{800}V_{190}T_{550}$, drop-coated (A) and freeze-dried (B) from 0.1 g/L acetone onto carbon-coated gold TEM grids. C: single micelle at high magnification; D: proposed solution structure of the micelles.

Only a single micellar population is present. The image reveals uniformly dispersed objects with an average diameter of 40-50 nm, corresponding to the micellar core, which is subdivided into segregated domains. The central element (PB, grey) bears several black objects (P2VP, black), spherical in shape with an average diameter of 10-15 nm. For the polymers investigated in this work, numbers of 3-6 PVP spheres were found. The rather strong contrast originates from the difference in electron

density between PB and P2VP. The multicompartmental character of the aggregates is unveiled in the enlargement in **Figure 4C**, whereas parts D shows the proposed solution structure of the micellar aggregates. This type of micellar core is referred to as “spheres on sphere” or “raspberry-like”.^[18] The P*t*BMA corona is not visible due to its immediate degradation upon irradiation with the electron beam.

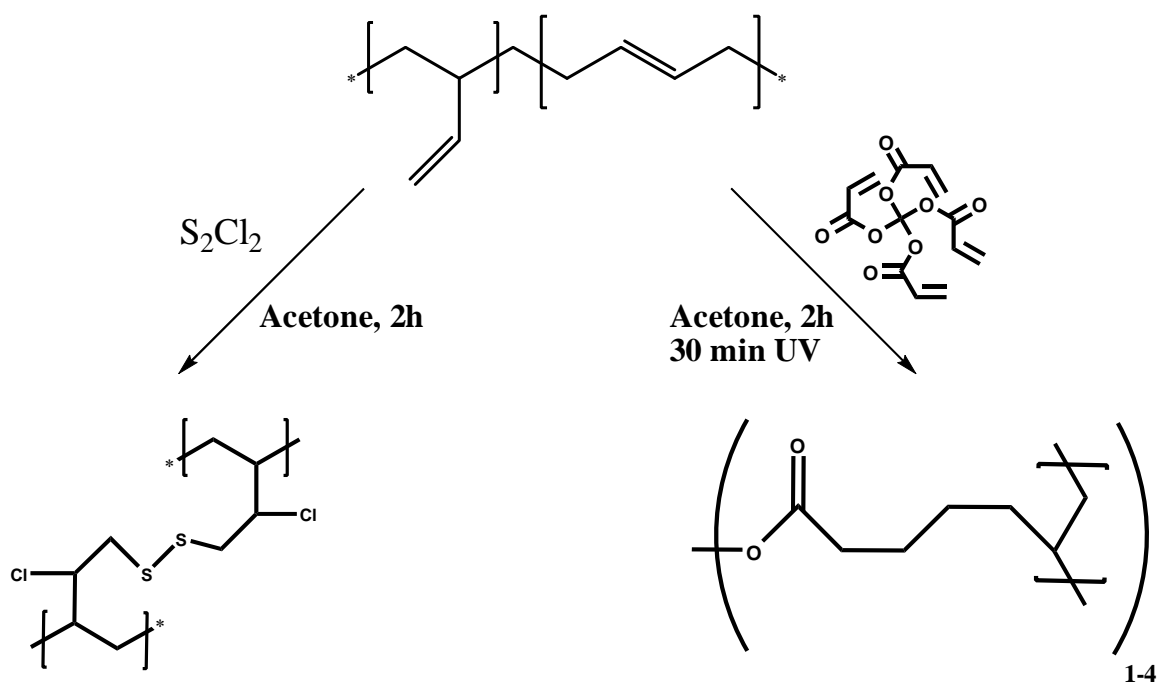
It remains puzzling that P2VP seems to be insoluble in acetone for our system. According to literature and our own experiments, P2VP homopolymer is soluble in acetone.^[35] If homopolymers of comparable molecular weight are dissolved in acetone at a comparable concentration, no aggregation is observed. For the BVT polymers, however, the formation of spherical, collapsed domains situated on the soft PB core seems to be more favorable. One tentative explanation may be the strong incompatibility between the first and the second block ($x_{BV} = 0.325$).^[36] The strong driving force for minimization of the interface between PB and P2VP could hamper the formation of a continuous shell around the micellar core and therefore result in a further compartmentalization of the P2VP phase. A similar morphology was first described by Stadler et al. for the bulk morphology of polystyrene-*b*-polybutadiene-*b*-poly(methyl methacrylate) (SBM) triblock terpolymers with a certain composition.^[37] Later, nanostructured aggregates like this one of SBM terpolymers were dispersed in a polymerizable matrix and were stabilized in that way for further examination.^[38, 39] Comparable micellar morphologies have been observed for mixtures of PS-*b*-P2VP-*b*-PEO block terpolymers with PAA in DMF.^[40] Recently, Laschewsky et al. also reported on a linear poly(4-methyl-4-(4-vinylbenzyl)morpholin-4-ium chloride)-*b*-polystyrene-*b*-poly(pentafluorophenyl 4-vinylbenzyl ether) (PVBM-*b*-PS-*b*-PVBFP) triblock terpolymer which self-assembled into micelles with a similarly compartmentalized core in aqueous solution^[18]. In their case the two hydrophobic and insoluble blocks, one of them fluorinated, built the two different core domains.

In conclusion, TEM measurements show the formation of micelles with a very low polydispersity. Furthermore, first hints towards a multicompartmental character of the micellar core are observed.

Crosslinking

There is a significant interest in the stabilization of polymer micelles. In that way, their dynamic structure can be altered to facilitate the transfer of such aggregates into non-selective solvents or to stabilize them even below the critical micellar concentration.^[41] Crosslinking of the core of the presented multicompartment micelles in acetone was performed via two different ways; “cold vulcanization” with S_2Cl_2 , generating sulphur-sulphur bonds between neighboring double bonds of the polybutadiene compartment or by applying a multifunctional acrylate (pentaerythrol tetraacrylate) (PETA) as crosslinking agent and subsequent UV irradiation. The advantage of the latter is that the so-formed junctions between different polymer chains are almost irreversible and not, as for the cold vulcanization, prone towards hydrolysis in acidic media. Both methods preferentially crosslink the 1,2-part of the polybutadiene segment. The content of 1,2-microstructure was measured via 1H -NMR to be around 86 % for the BVT terpolymers, thus facilitating the crosslinking.^[42] The pathway for the crosslinking procedure is depicted in **Scheme 1**.

Scheme 1: Crosslinking procedure for the PB core of the multicompartment micelles via two different methods; cold vulcanization with S_2Cl_2 and a pentaerythrol tetraacrylate.



Crosslinking with S_2Cl_2

In the case of $B_{800}V_{190}T_{550}$, crosslinking was carried out with one equivalent of S_2Cl_2 relative to the number of double bonds. The hydrodynamic radii of the initial micelles in acetone ($c = 1$ g/L), the crosslinked micelles in acetone and finally after exchange of the solvent to THF are shown in Figure 5A.

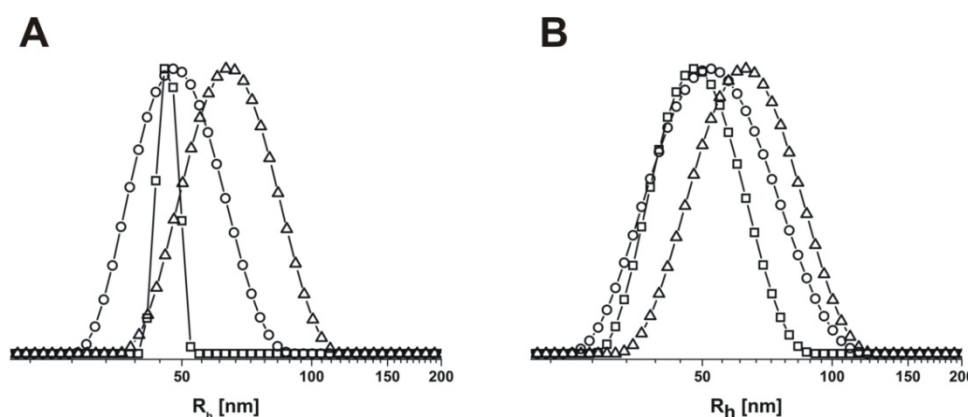


Figure 5: DLS CONTIN plots ($\Theta = 90^\circ$; $c = 1$ g/L, intensity-weighted) of micellar solutions: A: $B_{800}V_{190}T_{550}$ in acetone (\square , $\langle R_h \rangle_z = 44$ nm), after crosslinking of the polybutadiene core with 1 equivalent S_2Cl_2 (\square , $\langle R_h \rangle_z = 49$ nm) and after transfer of the crosslinked micellar aggregates into THF through dialysis (Δ , $\langle R_h \rangle_z = 64$ nm); B: $B_{800}V_{190}T_{380}$ in acetone after crosslinking with 1 eq (\square , $\langle R_h \rangle_z = 48$ nm) and 5 eq (\square , $\langle R_h \rangle_z = 53$ nm) S_2Cl_2 for 2h and 1 eq (Δ , $\langle R_h \rangle_z = 64$ nm) for 96h.

After crosslinking, the hydrodynamic radii in acetone increase from 44 nm to about 49 nm. The CONTIN analysis still reveals only one size of micellar aggregates. Furthermore, crosslinking seemed to take place only within the micelles and no intermicellar crosslinking occurs. Cumulant analysis at $\Theta = 90^\circ$ results in a PDI = 0.031. It remains unclear why a significantly higher PDI is obtained after the crosslinking procedure. The increase of the hydrodynamic radius after crosslinking in acetone is due to the incorporation of the voluminous crosslinking agent, S_2Cl_2 , into the micellar core. After transfer of the micellar solution into THF by dialysis the size of the aggregates further increases to values of about 64 nm (PDI = 0.038). This indicates that the polybutadiene part of the core is still able to swell in THF, which is a non-selective solvent for all the three blocks. However, the presence of only one popu-

lation of aggregates even in THF solution is a clear proof of the successfully performed crosslinking. The block terpolymer itself is molecularly soluble in THF.

To probe the effect of the amount of crosslinking agent and the reaction time on the size of the aggregates, $B_{800}V_{190}T_{380}$ was crosslinked with 1 and 5 equivalents of S_2Cl_2 for 2 h and with 1 equivalent for 96 h. The results are shown in Figure 5B. The hydrodynamic radius before crosslinking is around 43 nm. For 1 equivalent of crosslinking agent the size of the micellar aggregates increases slightly to about 48 nm (PDI = 0.053). For 5 equivalents of S_2Cl_2 , the value for R_h increases to 53 nm (PDI = 0.064). With increasing concentration of S_2Cl_2 , more incorporation takes place within the same reaction time. This indicates that the crosslinking is not completed after 2 h. If the reaction time is increased to 96 h, the micelles show $R_h = 64$ nm afterwards (PDI = 0.065). The crosslinking reaction proceeds very controlled as only one micellar population was obtained and no larger aggregates could be detected via the CONTIN analysis. Also here, the PDI increases after the treatment with S_2Cl_2 . To determine the actual amount of crosslinking, the solvent was removed and the residue was dissolved in deuterated THF to perform 1H -NMR measurements. The ratio of the integral of the protons of the tert-butyl group ($\delta = 1.4$ ppm) was compared to the diminished 1,2-polybutadiene signals ($\delta = 4.8$ ppm) to determine the extent of crosslinking. The obtained results were cross-checked through soxhlett-extraction with THF for 48 h and are summarized in Table 3.

Table 3: Crosslinking efficiency of S_2Cl_2 for $B_{800}V_{190}T_{380}$ in acetone

Equivalents S_2Cl_2 a	Reaction time [h]	Insoluble material [%] ^b
1	2	9
2	2	42
5	2	65
1	96	46

^a: relative to the amount of double bonds in PB; ^b: determined by 1H -NMR in THF- d_6 .

With increasing amount of crosslinking agent also the extent of crosslinking increases. For 5 equivalents of S_2Cl_2 , the crosslinked polymer could not be dissolved in THF after evaporation of the acetone. Therefore, the acetone dispersion was mixed with deuterated N-methyl pyrrolidone (NMP) and acetone was evaporated. Table 3 also demonstrates that for a lower amount of S_2Cl_2 a longer reaction time is required to reach the same crosslinking efficiency.

Crosslinking with pentaerythrol tetraacrylate (PETA)

Poly(*tert*-butyl methacrylate) can be easily transformed into poly(methacrylic acid) by acidic treatment. With regard to the micellar aggregates presented here this will generate an amphiphilic structure. In order to facilitate stable micellar solutions in aqueous media at different pH-values, another method for the crosslinking of the core had to be found to avoid the hydrolysis of the sulphur-sulphur bonds in acidic media. Contrary to the above discussed cold vulcanization technique, this multifunctional acrylate provides an efficient and convenient way of pH-robust crosslinking junctions. Acetone micellar solutions of $B_{800}V_{190}T_{550}$ ($c = 1$ g/L) were mixed with defined solutions of PETA. The actual amount of crosslinking agent is given in equivalents of functional groups crosslinking agent with respect to the amount of reactive double bonds on the polymer chains in solution. After equilibration (24 hours), the dispersions were exposed to UV light (300-400 nm) for 60 minutes. Subsequently, unreacted crosslinking agent was removed through dialysis. The hydrodynamic radii R_h of $B_{800}V_{190}T_{550}$ crosslinked with 1 eq PETA and after subsequent transfer to dioxane are shown in **Figure 6**.

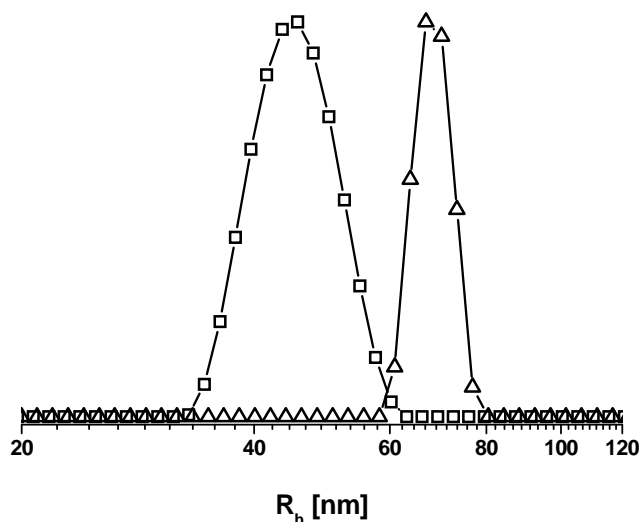


Figure 6: R_h of $B_{800}V_{190}T_{550}$ after crosslinking with 1 (-□-, $\langle R_h \rangle_z = 46$ nm) equivalent PETA in acetone and after transfer to dioxane (-△-, $\langle R_h \rangle_z = 67$ nm) ($c = 1$ g/L).

Initial R_h values for $B_{800}V_{190}T_{550}$ in acetone were 43 nm. After crosslinking with 1eq PETA basically the same values were obtained with 46 nm (PDI = 0.024). Surprisingly, in this case the micellar core does not seem to increase significantly upon crosslinking. The amount of insoluble material was determined as described for the cold vulcanization technique and was 63% for 0.5 and 67% for 1 equivalent of crosslinking agent. Transfer to dioxane resulted again in larger aggregates with $\langle R_h \rangle_z = 67$ nm (PDI = 0.025), proving the successful crosslinking. According to the literature, PETA forms an interpenetrating network upon photopolymerization.^[43, 44] We suppose that this network forms junctions with the PB core (cf. Scheme 1). Without added PETA, UV irradiation of BVT block terpolymer micelles in acetone did not lead to crosslinked aggregates.

Summarized, the presented multicompartment micelles exhibited single micellar populations in all cases demonstrated here. In order to assess structure and shape of the micelles after the various treatments the micellar solutions were drop-coated onto carbon-coated TEM grids. TEM images of different dispersions are shown in Figure 7.

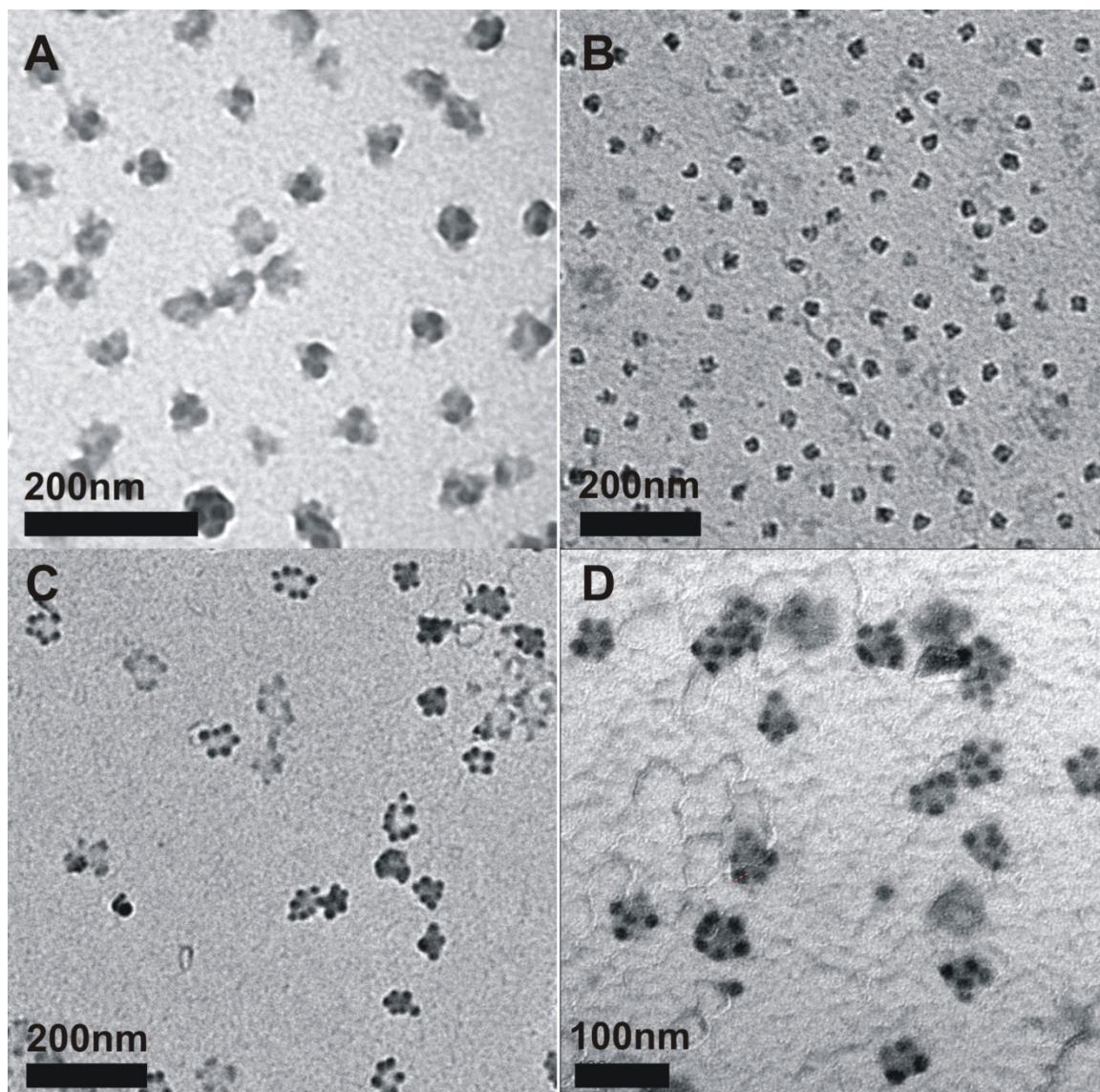


Figure 7: TEM images of micelles drop-coated from 0.1 g/L micellar solution in acetone (A, B) and THF (C, D). A: $B_{800}V_{190}T_{550}$ after crosslinking with S_2Cl_2 ; B: $B_{800}V_{190}T_{550}$ after crosslinking with PETA; C: $B_{800}V_{190}T_{550}$ dispersion of part C after dialysis to THF; D: $B_{800}V_{190}T_{550}$ dispersion of part A after staining with iodine.

Figure 7A shows $B_{800}V_{190}T_{550}$ multicompartment micelles after crosslinking with one equivalent of S_2Cl_2 from acetone. The compartmentalization of the core is still present, just the contrast decreased slightly. This could be explained by the incorporation of sulphur and chlorine into the polybutadiene compartment and therefore the convergence of the electron density for the two core-forming compartments. As already indicated by the DLS measurements in Figure 5A the size of the aggregates increases slightly. In part B of Figure 7 micelles from $B_{800}V_{190}T_{550}$ after crosslinking of the core with 1 eq PETA are presented. Again size and shape seem to be conserved. Figure 6C represents micelles from $B_{800}V_{190}T_{550}$ after crosslinking with 1 eq S_2Cl_2 and subsequent transfer of the aggregates into THF as a non-

selective solvent, which then is able to swell the partially crosslinked core, as already shown by means of DLS in Figure 5A. Part D of Figure 7 exhibits $B_{800}V_{190}T_{550}$ multicompartment micelles after crosslinking with S_2Cl_2 and subsequent staining with iodine. I_2 preferentially enhances electron density in the poly(2-vinyl pyridine) compartment. This treatment makes the two compartments of the micellar core even more distinguishable from each other. A sharp borderline can be clearly seen between the grey polybutadiene and the black poly(2 vinylpyridine). Staining with OsO_4 , which reacts with the 1,4-polybutadiene units,^[45] has also been carried out. Unfortunately, this treatment did not give any further insight.

To conclude, the multicompartmental character of the micellar aggregates is fully preserved after crosslinking with either S_2Cl_2 or PETA. The crosslinking success is proven through the successful transfer of the micelles into THF or dioxane. Iodine staining was successfully employed to enhance the phase contrast between the two core-forming departments in TEM measurements.

Cryogenic transmission electron microscopy (cryo-TEM)

Cryo-TEM can be employed to explore the micellar structure in-situ without any drying effects.^[46] Most of the work on cryo-TEM reported in the literature has been performed in water. In this work, either THF or dioxane was taken as solvent. We have recently shown that cryo-TEM in THF can successfully be used to explore complex aggregation patterns.^[47] The concentration of the samples investigated varied from 0.1 g/L to 0.7 g/L. A general effect across all the samples investigated is that instead of single micelles continuous structures could be observed. This is shown in **Figure 8** for S_2Cl_2 core-crosslinked micelles of $B_{800}V_{190}T_{550}$.

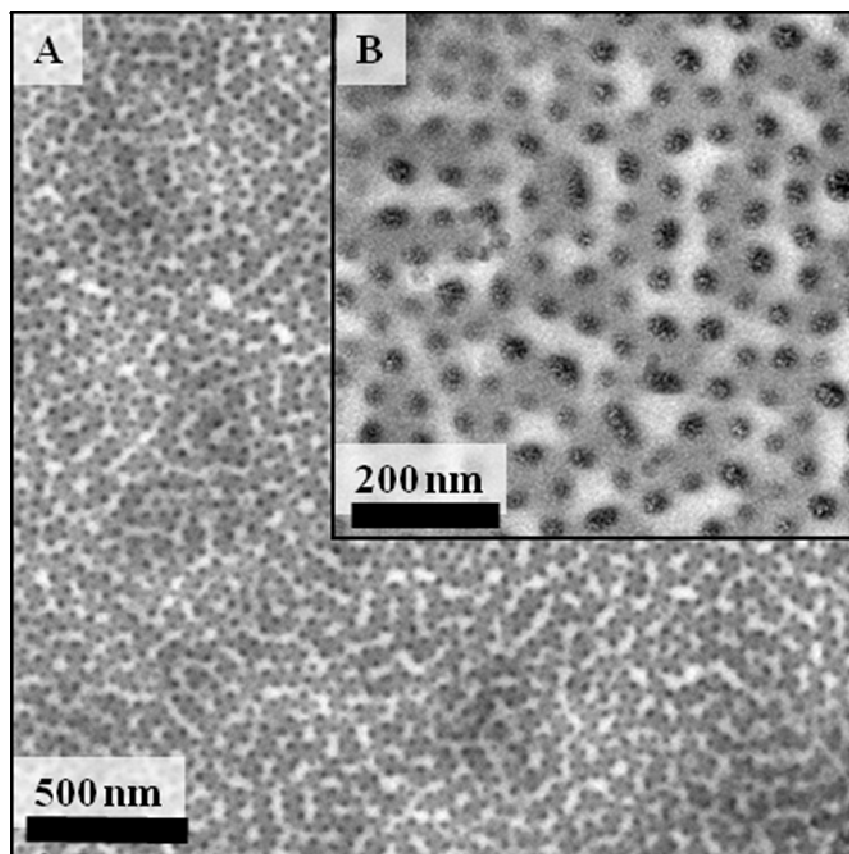


Figure 8: Cryo-TEM images of $B_{800}V_{190}T_{550}$ in THF after crosslinking of the polybutadiene core with 1 equivalent S_2Cl_2 in acetone and subsequent transfer of the aggregates into THF through dialysis; A: overview; B: enlargement; $c = 0.5$ g/L; the scale bar corresponds to 500 nm (A) and 100 nm (B).

Figure 8A shows an overview over an area with the continuous structure, part B an enlargement. Both images were taken from vitrified THF solutions at a concentration of 0.5 g/L. Similar results could be obtained in the concentration range from 0.1 g/L to 0.7 g/L. Basically the multicompartmental character can be confirmed. Grey elongated structures bearing black dots are visible. Clearly, the black parts consist of poly(2-vinylpyridine), which is the material with the highest electron density. The grayish compartments resemble the crosslinked polybutadiene and the light parts in-between are poly(*tert*-butyl methacrylate), which is well soluble and swollen with THF. In this particular case, electron density in the polybutadiene compartment is enhanced through the crosslinking step and therefore the incorporation of sulphur and chlorine atoms. The observed vermicular structures could again be formed due to the strong incompatibility between polybutadiene and poly(2-vinylpyridine).^[36] The foremost random distribution of length and orientation of the elongated structures could be the result of interface minimization. Alongside on the vermicular objects, the poly(2-vinylpyridine) compartments are

always in situated in a “zigzag” manner and never directly opposite. The formation of continuous structures could be explained through the evaporation of some solvent during the sample preparation and hence an increase in the sample concentration. It is noteworthy that the structures appear somewhat larger in cryogenic TEM measurements, again leading to the conclusion that the partially crosslinked micellar cores are still able to swell in THF to a certain extent.

Figure 9 shows an image taken from a vitrified micellar solution of $B_{800}V_{190}T_{550}$ micelles after “cold-vulcanization” and transfer into dioxane at a concentration of 0.1 g/L. For this specimen, similar aggregates were found but are not depicted here. Instead Figure 9 presents single micellar aggregates. Coexistence of both structures was found over the whole specimen. Although the contrast is worse than in Figure 8, the further compartmentalized core of the micelles can be visualized. The size shows an increase to about 60-70 nm per micellar core. That again can be explained through swelling of the partially crosslinked polybutadiene in the solvent. Some of the assemblies seem to merge, especially in the upper right corner of Figure 9. In that way this cryo-TEM image may resemble the transition from single multicompartment micelles to the previously discussed continuous structures.

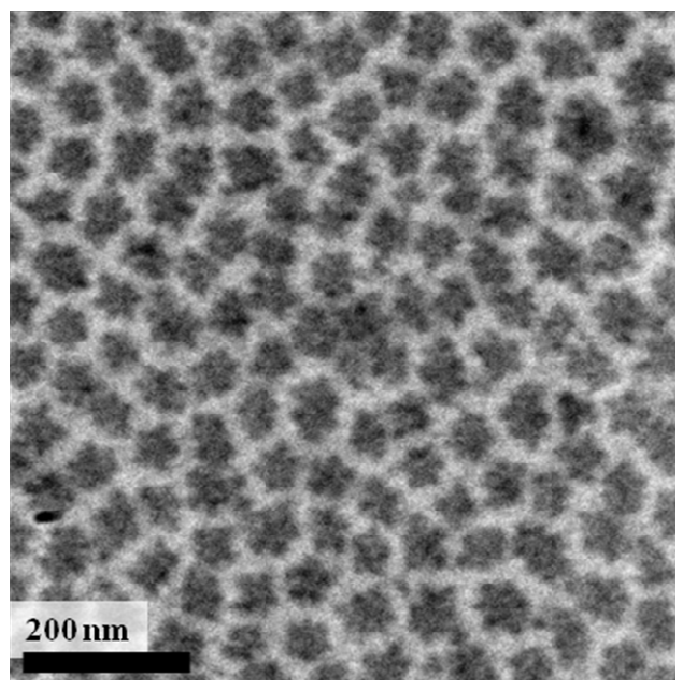


Figure 9: Cryo-TEM images of $B_{800}V_{190}T_{550}$ in dioxane after crosslinking of the polybutadiene core with 1 eq S_2Cl_2 in acetone and subsequent transfer of the aggregates into dioxane ($c = 0.2$ g/L); the scale bar corresponds to 100 nm.

In conclusion, the cryo-TEM investigations show that the multicompartment micelles exist as single aggregates in dioxane and that the solvent is able to swell the partially crosslinked core.

Conclusions

This work shows for the first time that multicompartment micelles from ABC triblock terpolymers, $B_{800}V_{190}T_{380}$ and $B_{800}V_{190}T_{550}$, can be easily prepared when dissolving them in acetone. In contrast to other works within this field, neither a complex polymer architecture nor extraordinary monomers had to be employed for the formation of a further compartmentalized micellar core, all the three monomers are common, cheap and available in large amounts. The convenient synthesis pathway allows the preparation of the triblock terpolymers on a large scale. The structure of the aggregates could be assessed via TEM and cryo-TEM measurements. The uniformity of the formed aggregates was proven with several dynamic and static light scattering experiments. The crosslinking of the polybutadiene compartment with two inherently different methods was shown not to alter the structure of the micelles. In the case of the cold vulcanization pathway, the effect of the amount of crosslinking agent and reaction time has been investigated. For the crosslinking with a multifunctional acrylates, two main differences could be observed: first the micellar core does not seem to increase through the incorporation of the pentaerythrol tetraacrylate, which definitely happened for S_2Cl_2 , and second the newly formed junctions between polymer chains are supposed to be stable with respect to the hydrolysis of the ester moiety of the poly(*tert*-butyl methacrylate) compartment and the transfer of the micelles into aqueous media at different pH values. The latter will be the subject of further research. Crosslinking was proven to be successful through the transfer of the aggregates into non-selective solvents, THF and dioxane.

Acknowledgements: The authors to thank VolkswagenStiftung for financial support. Special thanks go also to all the people who contributed to this work, in particular Dr. Markus Burkhardt for discussions, and Dr. Holger Schmalz and Denise Danz for help with the polymer synthesis.

References

1. Ringsdorf, H.; Lehman, P.; Weberskirch, R., *Book of Abstracts, 217th ACS National Meeting*. American Chemical Society, Washington, DC: Anaheim, 1999.
2. Lutz, J.-F.; Laschewsky, A. *Macromol. Chem. Phys.* **2005**, 206, 813-817.
3. Li, Z.; Hillmyer, M. A.; Lodge, T. P. *Macromolecules* **2006**, 39, 765-771.
4. Stähler, K.; Selb, J.; Barthelemy, P.; Pucci, B.; Candau, F. *Langmuir* **1998**, 14, 4765-4775.
5. Stähler, K.; Selb, J.; Candau, F. *Langmuir* **1999**, 15, 7565-7576.
6. Kotzev, A.; Laschewsky, A.; Adriaensens, P.; Gelan, J. *Macromolecules* **2002**, 35, 1091-1101.
7. Szczubialka, K.; Moczek, L.; Goliszek, A.; Nowakowska, M.; Kotzev, A.; Laschewsky, A. *J. Fluor. Chem.* **2005**, 126, 1409-1418.
8. Lodge, T.; Rasdal, A.; Li, Z.; Hillmyer, M. A. *J. Am Chem Soc.* **2005**, 127, 17608-17609.
9. Underhill, R. S.; Liu, G. *Chem. Mater.* **2000**, 12, 2082-2091.
10. Fustin, C. A.; Abetz, V.; Gohy, J. F. *Eur. Phys. J. E* **2005**.
11. Zheng, R.; Liu, G.; Yan, X. *J. Am Chem Soc.* **2005**, 127, 15358-15359.
12. Patrickios, C. S.; Forder, C.; Armes, S. P.; Billingham, N. C. *J. Polym. Sci. A: Polym. Chem.* **1997**, 35, 1181.
13. Kriz, J.; Massar, B.; Plestil, J.; Tuzar, Z.; Pospisil, H.; Duskociloca, D. *Macromolecules* **1998**, 31, 41.
14. Chen, W. Y.; Alexandridis, P.; Su, C. K.; Patrickios, C. S.; Hertler, W. R.; Hatton, T. A. *Macromolecules* **1995**, 28, 8604.
15. Yu, G. E.; Eisenberg, A. *Macromolecules* **1998**, 31, 5546-5549.
16. Stewart, S.; Liu, G. *Chem. Mater.* **1999**, 11, 1048.
17. Stähler, K.; Selb, J.; Candau, F. *Materials Science & Engineering C* **1999**, 10, 171-178.
18. Kubowicz, S.; Baussard, J.-F.; Lutz, J.-F.; Thünemann, A.; Berlepsch, H. v.; Laschewsky, A. *Angew. Chem. int. Ed.* **2005**, 44, 5262-5265.
19. Thünemann, A.; Kubowicz, S.; Berlepsch, H. v.; Möhwald, H. *Langmuir* **2006**, 22, 2506-2510.
20. Li, Z.; Hillmyer, M. A.; Lodge, T. *Langmuir* **2006**, 22, 9409-9417.

21. Li, Z.; Kesselman, E.; Talmon, Y.; Hillmyer, M. A.; Lodge, T. P. *Science* **2004**, 306, 98-101.
22. Saito, N.; Liu, C.; Lodge, T. P.; Hillmyer, M. A. *Macromolecules* **2008**, 41, (22), 8815-8822.
23. Mao, J.; Ni, P.; Mai, Y.; Yan, D. *Langmuir* **2007**, 23, 5127-5134.
24. Dormidontova, E. E.; Khokhlov, A. R. *Macromolecules* **1997**, 30, (7), 1980-1991.
25. Chou, S.-H.; Tsai, H.-K.; Sheng, Y.-J. *J. Chem. Phys.* **2006**, 125, 194903.
26. Zhong, C.; Liu, D. *Macromol. Theory & Simulations* **2007**, 16, 141-157.
27. Ma, Z.; Jiang, W. *J. Polym. Sci. B: Polym. Phys.* **2009**, 47, (5), 484-492.
28. Freyss, D.; Rempp, P.; Benoit, H. *Polym. Lett.* **1964**, 2, 217.
29. Quirk, R. P.; Yoo, T.; Lee, Y.; Kim, J.; Lee, B. *Adv. Polym. Sci.* **2000**, 153, 67-106.
30. David, R. L., *CRC Handbook of chemistry and physics*. 81st ed.; CRC Press: Boca Raton, 2000.
31. Zimm, B. H. *J. Chem. Phys.* **1948**, 16, 1099.
32. Förster, S.; Zisenis, M.; Wenz, E.; Antonietti, M. *J. Chem. Phys.* **1996**, 104, 9956-9970.
33. Burchard, W. *Adv. Polym. Sci.* **1999**, 143, (Branched Polymers II), 113-194.
34. Erhardt, R.; Boker, A.; Zettl, H.; Kaya, H.; Pyckhout-Hintzen, W.; Krausch, G.; Abetz, V.; Mueller, A. H. E. *Macromolecules* **2001**, 34, 1069-1075.
35. Brandrup, J.; Immergut, E. H.; Grulke, E. A., *Polymer Handbook*. 4th ed.; John Wiley & Sons: New York, 1999.
36. Barton, A. F., *CRC Handbook of Polymer Liquid Interaction Parameters and Solubility Parameters*. CRC Press: Boca Raton, 1990.
37. Breiner, U.; Krappe, U.; Jakob, T.; Abetz, V.; Stadler, R. *Polym. Bull.* **1998**, 40, 219.
38. Ritzenthaler, S.; Court, F.; David, L.; Girard-Reydet, E.; Leibler, L.; Pascault, J. P. *Macromolecules* **2002**, 35, 6245.
39. Ritzenthaler, S.; Court, F.; Girard-Reydet, E.; Leibler, L.; Pascault, J. P. *Macromolecules* **2003**, 36, 118.
40. Gohy, J. F.; Khouzakoun, E.; Willet, N.; Varshney, S. K.; Jérôme, R. *Macromol. Rap. Comm.* **2004**, 25, 1536-1539.
41. O'Reilly, R. K.; Hawker, C.; Wooley, K. L. *Chem. Soc. Rev.* **2006**, 35, 1068-1083.
42. Hsieh, H. L.; Quirk, R. P., *Anionic Polymerization-Principles and Practical Applications*. Marcel Dekker: New York, 1996.

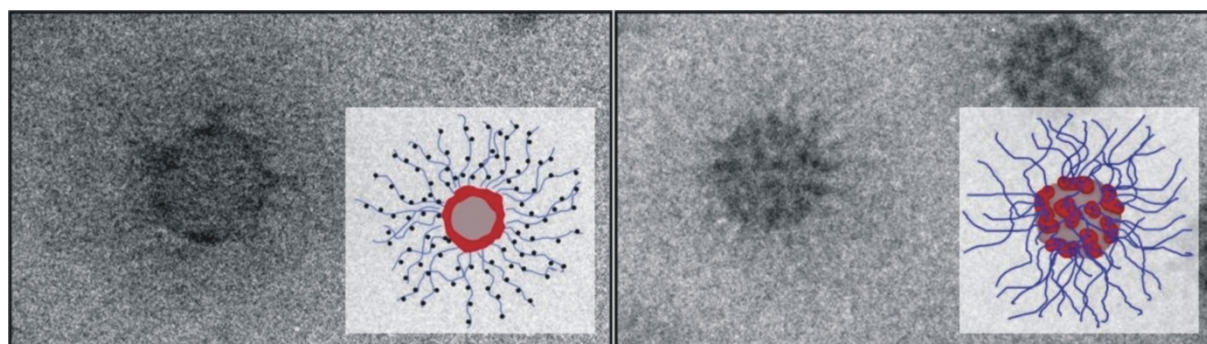
43. Petrov, P.; Bozukov, M.; Tsvetanov, C. B. *J. Mater. Chem.* **2005**, 15, (14), 1481-1486.
44. Petrov, P.; Yuan, J.; Yoncheva, K.; Müller, A. H. E.; Tsvetanov, C. B. *J. Phys. Chem. B* **2008**, 112, (30), 8879-8883.
45. Kato, K. *J. Polym. Sci. Polymer Letters* **1966**, 4, 35.
46. Adrian, M.; Dubochet, J.; Lepault, J.; McDowell, A. W. *Nature* **1984**, 32, 308.
47. Walther, A.; Andre, X.; Drechsler, M.; Abetz, V.; Muller, A. H. E. *J. Am. Chem. Soc.* **2007**, 129, (19), 6187-6198.

Dynamic Multicompartment-Core Micelles in Aqueous Media

Felix Schacher, Andreas Walther and Axel H. E. Müller**

Makromolekulare Chemie II and Zentrum für Kolloide und Grenzflächen,
Universität Bayreuth, 95440 Bayreuth, Germany.

axel.mueller@uni-bayreuth.de; felix.schacher@uni-bayreuth.de;



PB-P2VP-PMAA

PB-P2VP_q-PMAA

ABSTRACT:

We investigate micellar aggregates of amphiphilic block terpolymers, polybutadiene-*block*-poly(2-vinyl pyridine)-*block*-poly(methacrylic acid) (PB₈₀₀P2VP₁₉₀PMAA₅₅₀) and their quaternized analogues polybutadiene-*block*-poly(*N*-methyl-2-vinylpyridinium)-*block*-poly(methacrylic acid) (PB₈₀₀P2VP_{q190}PMAA₅₅₀) in aqueous solution using light scattering (DLS, SLS) and cryogenic transmission electron microscopy (cryo-TEM). At high pH, PB₈₀₀P2VP₁₉₀PMAA₅₅₀ forms core-shell-corona micelles with a hydrodynamic radius $R_h \sim 100$ nm and a continuous shell of P2VP. However, at pH 4 partial intramicellar interpolyelectrolyte complex (*im*-IPEC) formation between P2VP and PMAA results in a patchy, collapsed shell. This is far more pronounced for the quaternized analog, PB₈₀₀P2VP_{q190}PMAA₅₅₀, which forms aggregates of similar size, also exhibiting a non-continuous, patchy shell. Here, these *im*-IPECs of the positively charged poly(*N*-methyl-2-vinylpyridinium) and the partially negatively charged poly(methacrylic acid) are present over the whole investigated pH-range (4-10). We further demonstrate that size and charge of the corona can be tuned through the block terpolymer composition, in particular the ratio between P2VP_q and PMAA. These micelles are dynamic and able to react to changes in pH or salinity in terms of corona diameter and aggregation number.

Introduction

Block terpolymers form a great variety of complex and interesting nanostructures and their self-assembly has been studied intensively in solution,¹⁻⁴ thin films,⁵⁻⁷ and the bulk.⁸⁻¹⁴ However, so far bulk structures have been studied to the greatest extent. Such ternary systems, if compared to ordinary AB diblock and ABA triblock copolymers, can lead to a greatly diversified area of self-assembled morphologies, depending on the actual composition. As increasing complexity of such polymer topologies enables the preparation of highly developed functional systems, many efforts have been made in the last few years to obtain well-defined micellar aggregates and, alongside, polymeric nanoparticles from block terpolymer systems.^{15, 16}

Typical morphologies for micelles from block terpolymers in solution are cylinders,¹⁷ spheres,¹⁸ and vesicles,^{19, 20} but also more complex structures like multicompartment micelles²¹⁻²³ have been reported. Complex compartmentalized nanostructures are promising candidates for the generation of inorganic-organic hybrid structures²⁴ or controlled release applications, e.g. entrapment of hydrophobic species in different media. Lodge et al. showed recently that two different dye molecules can be stored in two variable compartments of such micelles.²⁵ In general, there are different approaches for the preparation of multicompartment micelles in solution. The most common way is to use a selective solvent, forcing a block terpolymer to self-assemble. If the polymer is not directly soluble in the specific solvent, it is first dissolved in a non-selective solvent and then afterwards this is exchanged against the desired one by dialysis.²⁶ Another facile and straightforward way to obtain compartmentalized colloids from block terpolymers in solution is based on crosslinking of well-defined bulk structures. Here, bulk films of the material are prepared. Very complex compartmentalized colloids with a precisely defined cross-section and tunable dimensions can be obtained in this way. This procedure has been successfully applied to produce spherical,²⁷ cylindrical,²⁸ and disc-shaped²⁹ Janus particles.

The complexation between two oppositely charged polyelectrolyte blocks is another method to prepare micelles. The resulting structures are often referred to as interpolyelectrolyte complexes (IPECs) or block ionomer complexes (BICs).³⁰ This method has been used to prepare micellar aggregates with complex coacervate

cores from two oppositely charged AB and CD diblock copolymers.³¹ Comparable procedures have been employed to form the shell of core-shell-corona micelles.³² Typically, first micelles with a charged shell are prepared from amphiphilic AB diblock copolymers and afterwards an oppositely charged water-soluble polyion is added. Depending on pH, temperature, charge equilibrium and concentration, this results in the formation of core-shell-corona micelles where the shell is made out of an IPEC between the two oppositely charged blocks. One interesting feature of such block ionomer complexes is their ability to participate in cooperative polyion exchange reactions with other polyelectrolytes present in solution.^{33, 34}

Here we present an approach to direct the self-assembly of amphiphilic block terpolymers in aqueous solution. Polybutadiene-*block*-poly(2-vinyl pyridine)-*block*-poly(*tert*-butyl methacrylate) PB-P2VP-P*t*BMA block terpolymers are modified in order to render them amphiphilic and to generate micelles in aqueous systems. This is performed by hydrolysis of the ester moiety of P*t*BMA in dioxane to PMAA, a weak polyelectrolyte.³⁵ In that way, PB-P2VP-PMAA core-shell-corona micelles with a polybutadiene core, a poly(2-vinyl pyridine) shell and a poly(methacrylic acid) corona are formed. Different micellar aggregates are obtained if the middle block, P2VP, is previously quaternized and turned into the strong polyelectrolyte poly(*N*-methyl-2-vinyl pyridinium) P2VPq, providing an ampholytic ABC system. Here, micelles exhibiting a non-continuous shell are found, due to *im*-IPEC formation between negatively charged PMAA and positively charged P2VPq. To the best of our knowledge, this is the first example where interpolyelectrolyte formation can be shown to take place in such a manner. Moreover, the multicompartmental PB-P2VPq-PMAA micelles are able to react in a dynamic fashion to changes in salinity. Both PB-P2VP-PMAA and PB-P2VPq-PMAA block terpolymers also exhibit pH-responsive properties due to the pH-dependent solubility of PMAA and the non-quaternized P2VP. We further investigated the effect of the block length ratio between both blocks participating in the formation of these *im*-IPECS, P2VPq and PMAA. The micelles were characterized by means of dynamic and static light scattering and cryogenic transmission electron microscopy.

Experimental part

Synthesis

Materials

The solvents for the preparation of the micellar solutions were purchased in p.a. grade and used as delivered. Methyl iodide (MeI) and hydrochloric acid (32%) were used as delivered. Buffer solutions with pH 10 ($\text{H}_3\text{BO}_3/\text{KCl}/\text{NaOH}$) were purchased from Fluka. All other buffer solutions mentioned were prepared from citric acid (0.15 mol/L) and K_2HPO_4 (0.15 mol/L) in different ratios.

Synthesis of the PB-P2VP-PtBMA triblock terpolymers

The linear block terpolymers were synthesized via sequential living anionic polymerization in THF at low temperatures using sec-butyl lithium as initiator. A more detailed description of the synthetic procedure has been reported elsewhere.³⁶ Exemplarily THF-SEC traces for PB_{800} , $\text{PB}_{800}\text{P2VP}_{190}$, and $\text{PB}_{800}\text{P2VP}_{190}\text{PtBMA}_{550}$ are provided in the supporting information (Figure S1, Supporting information).

Quaternization of the poly(2-vinyl pyridine) block

PB-P2VP-PtBMA block terpolymers were dissolved in dioxane at a concentration of 1 g/L. Afterwards, MeI (10 eq corresponding to the 2-vinyl pyridine groups) was added and the solution was stirred for at least 72 hours at room temperature. During the reaction, the solution became slightly yellowish. The excess of quaternization agent was removed by dialysis against dioxane. The resulting solution of polybutadiene-*block*-poly(*N*-methyl-2-vinyl pyridinium)-*block*-poly(*tert*-butyl methacrylate) PB-P2VPq-PtBMA was directly used for the subsequent hydrolysis of the ester moiety of the methacrylate block. DLS CONTIN plots for $\text{PB}_{800}\text{-P2VPq}_{190}\text{-PtBMA}_{550}$ and $\text{PB}_{800}\text{-P2VPq}_{190}\text{-PMAA}_{550}$ (Figure S2, Supporting information) and IR spectra of $\text{PB}_{800}\text{-P2VP}_{190}\text{-PtBMA}_{550}$ and $\text{PB}_{800}\text{-P2VPq}_{190}\text{-PMAA}_{550}$ (Figure S3, Supporting information) are included in the supporting information. From the IR measurements and iodometric titrations with diluted AgNO_3 solutions we determined a degree of quaternization of 70-90 %.

Dialysis

Dialysis membrane tubes (MWCO 3.500 g/mol, Regenerated Cellulose ester) were purchased from Spectra/Por. Prior to use, the tubes were immersed into de-ionized water for 1h to open the pores.

Hydrolysis of the poly(*tert*-butyl methacrylate) block

Depending on the situation, either a solution of PB-P2VP-P*t*BMA or PB-P2VP_q-P*t*BMA in dioxane ($c = 1$ g/L) was treated with a 5-fold excess of hydrochloric acid relative to the ester moieties. Afterwards, the reaction mixture was refluxed at 120 °C for 24 hours.

Preparation of the micellar solutions

Directly after hydrolysis of the P*t*BMA block, micellar stock solutions ($c = 1$ g/L) were prepared via dialysis against pH 10 buffer solution. From these stock solutions, changes in pH or salinity were performed by dialysis against the corresponding solutions. “Staining” of the PMAA corona with CsCl (0.05 M) was performed in an analogous way.

Characterization

Dynamic light scattering

All experiments were performed using the same concentrations ($c = 1$ g/L). DLS measurements were performed in sealed cylindrical scattering cells ($d = 10$ mm) at an angle of 90° on an ALV DLS/SLS-SP 5022F equipment consisting of an ALV-SP 125 laser goniometer with an ALV 5000/E correlator and a He-Ne laser with the wavelength $\lambda = 632.8$ nm. The CONTIN algorithm was applied to analyze the obtained correlation functions. Apparent hydrodynamic radii were calculated according to the Stokes-Einstein equation. Prior to the light scattering measurements the sample solutions were filtered using Millipore PTFE filters with a pore size of 1 μ m for organic solvents like dioxane or Millipore nylon filters with a pore size of 1.2 or 5 μ m in the case of aqueous solutions. The polydispersities were determined from unimodal peaks via the cumulant analysis.

Static light scattering

For SLS, solutions of the polymers were prepared in the concentration range between 0.1 and 1 g/L. Measurements were carried out on a Sofica goniometer with a He-Ne laser ($\lambda = 632.8$ nm) at 25 °C. Prior to the measurements, sample solutions were filtered through Millipore nylon filters with the pore size 1.2 or 5 μm . A Zimm plot was used to evaluate the data. A differential refractometer DnDC2010/620 (PSS) was used to measure the refractive index increment, dn/dc (PB₈₀₀P2VPq₁₉₀PMAA₅₅₀; 0.278 ± 0.007 at pH 10 and 0.103 ± 0.007 at pH 10 and 1.0 M added NaCl), of the polymer solutions at $\lambda = 620$ nm. Note that the dn/dc decreases drastically with the addition of 1.0 M NaCl. This can be explained through the deregulation of the Manning condensation occurring. Counterions are now everywhere in the solution and, hence, the counterion contribution to the measured dn/dc is significantly smaller.

Cryogenic Transmission Electron Microscopy (cryo-TEM)

For cryo-TEM studies, a drop of the sample solution ($c \approx 0.1$ wt-%) was placed on a lacey carbon-coated copper TEM grid (200 mesh, Science Services, München, Germany), where most of the liquid was removed with blotting paper, leaving a thin film stretched over the grid holes. The specimens were shock vitrified by rapid immersion into ethane in a temperature-controlled freezing unit (Zeiss Cryobox, Zeiss NTS GmbH, Oberkochen, Germany) and cooled to approximately 90 K. The temperature was monitored and kept constant in the chamber during all the preparation steps. After freezing the specimens, they were inserted into a cryo-transfer holder (CT3500, Gatan, München, Germany) and transferred to a Zeiss EM922 Omega EFTEM instrument. Examinations were carried out at temperatures around 90 K. The microscope was operated at an acceleration voltage of 200 kV. Zero-loss filtered images ($\Delta E = 0$ eV) were taken under reduced dose conditions. All images were registered digitally by a bottom mounted CCD camera system (Ultrascan 1000, Gatan), combined and processed with a digital imaging processing system (Gatan Digital Micrograph 3.9 for GMS 1.4).

Zeta-potential

The zeta-potential was determined on a Malvern Zetasizer Nano ZS in conjunction with an MPT2 autotitrator (Malvern). The electrophoretic mobilities (u) were con-

verted into ζ potentials via the Smoluchowski equation $\zeta = u\eta/\epsilon_0\epsilon$, where η denotes the viscosity and $\epsilon_0\epsilon$ the permittivity of the solution.

Results and Discussion

Synthesis of block terpolymers

The synthesis and the characterization of the polymeric precursors, (e.g. PB₈₀₀P2VP₁₉₀PtBMA₅₅₀, $M_n = 141 \cdot 10^3$ g/mol, PDI = 1.02; subscripts denoting the degree of polymerization of the corresponding block) as well as their micellization in acetone has been published earlier.²³ The two different pathways for the preparation of micellar aggregates in aqueous systems are shown in **Figure 1**. In the one-step procedure (left part), only the PtBMA block is modified. The middle block, P2VP, remains unaltered and therefore only hydrophilic at acidic conditions ($pK_a \sim 4$).³⁷ The two-step procedure, however, first leads to a quaternized and permanently hydrophilic middle block, P2VPq. Afterwards, the PtBMA is hydrolyzed, rendering ampholytic PB-P2VPq-PMAA block terpolymers.

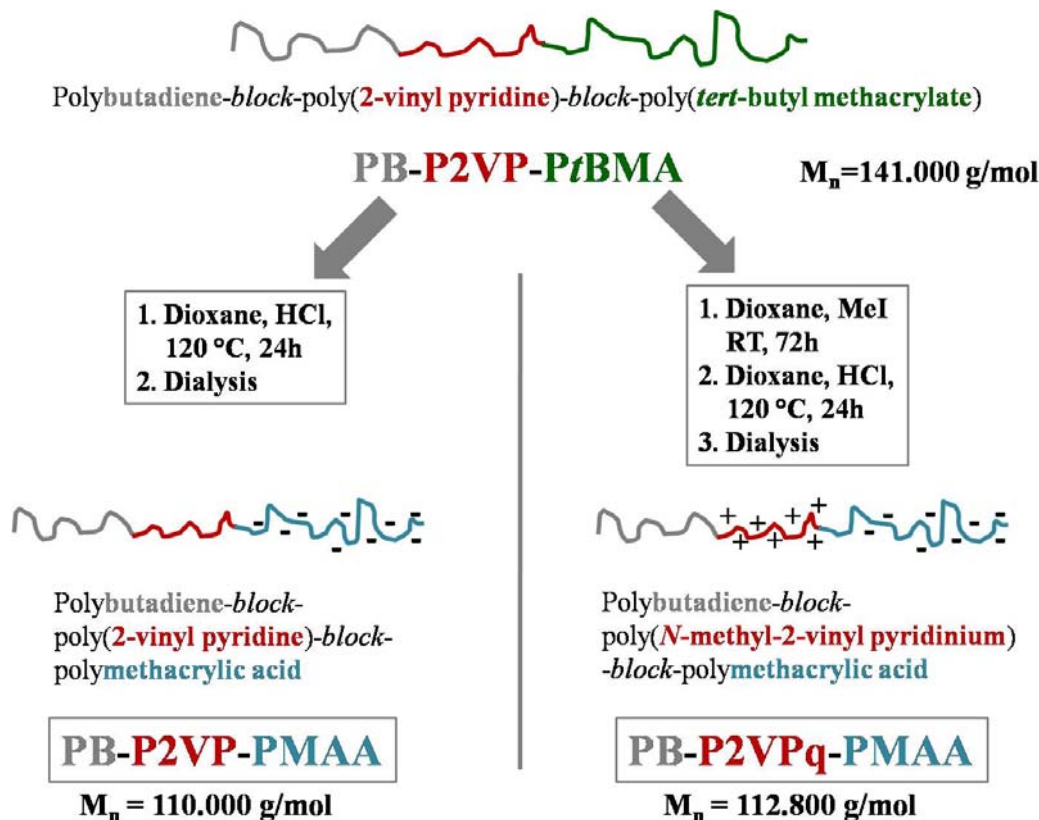


Figure 1: Schematic depiction of the two different pathways for the preparation of micelles from PB-P2VP-PMAA or PB-P2VPq-PMAA in water.

After quaternization, the PB-P2VPq-P*t*BMA terpolymers already start to aggregate in dioxane. The DLS CONTIN plot exhibits a maximum at a hydrodynamic radius of 27 nm (Figure S2, Supporting information). This is far above the observed size of a single polymer chain in a non-selective solvent. Also, FTIR spectroscopy clearly indicates a successful quaternization (Figure S3, Supporting information). In the following, first the micellization of PB₈₀₀P2VP₁₉₀PMAA₅₅₀ and PB₈₀₀P2VPq₁₉₀PMAA₅₅₀, depending on the preparation conditions, are shown and discussed in detail. Afterwards, the effects of the block length ratio between P2VPq and PMAA on the micellar corona formed are discussed for three different PB-P2VPq-PMAA block terpolymer systems.

Core-shell-corona micelles of PB₈₀₀P2VP₁₉₀PMAA₅₅₀

After hydrolysis of the poly(*tert*-butyl methacrylate) block, amphiphilic block terpolymers with two pH-responsive hydrophilic compartments, poly(2-vinylpyridine) as middle (DP = 190) and poly(methacrylic acid) as end block (DP = 550) are obtained. Starting from the stock solution at pH 10, these can be transferred into aqueous solutions at different pH-values, rendering micelles with a soft polybutadiene core, a glassy poly(2-vinyl pyridine) shell with a certain degree of swelling depending on the pH and a poly(methacrylic acid) corona.

Poly(methacrylic acid) is a weak polyelectrolyte and its solubility in aqueous systems is strongly depending on the pH and the polymer topology.³⁸ At pH > 5.5, part of the PMAA units are deprotonated and negatively charged, whereas below this value the solubility in water decreases. For the middle block, P2VP, the situation is entirely different.^{39, 40} Only under acidic conditions (pH ≤ 4), the nitrogen moiety of the 2-vinyl pyridine is protonated and it becomes water-soluble.³⁹ Solutions of pH 4, 6 and 10 were chosen to demonstrate the pH-responsive behavior of this system. The corresponding hydrodynamic radius distributions are shown in **Figure 2**.

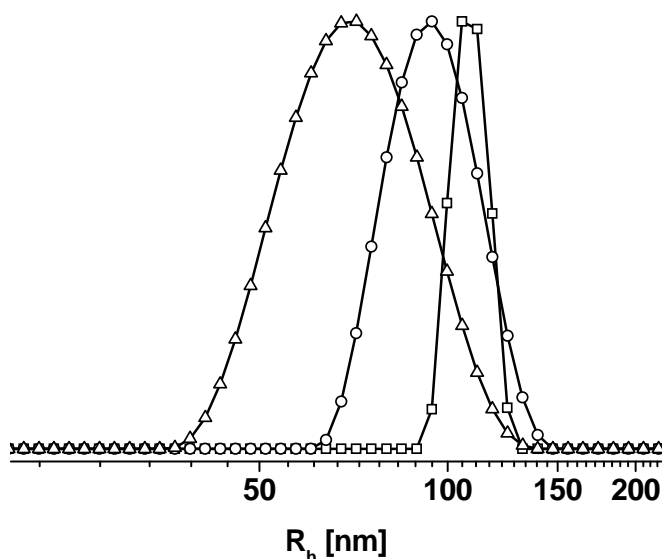


Figure 2: DLS CONTIN plots for $\text{PB}_{800}\text{P2VP}_{190}\text{PMAA}_{550}$ in aqueous buffers at different pH-values; pH 10 ($\langle R_h \rangle_z = 105$ nm, $-\square-$, PDI = 0.06), pH 6 ($\langle R_h \rangle_z = 94$ nm, $-\square-$, PDI = 0.12) and pH 4 ($\langle R_h \rangle_z = 71$ nm, $-\Delta-$, PDI = 0.16).

At pH 10 the micellar aggregates are distinctly larger than at lower pH values ($\langle R_h \rangle_z = 105$ nm). This is explained by the well-known pH-responsive behavior of the poly(methacrylic acid). At high pH the complete ionization of the polyelectrolyte chains leads to a more stretched conformation in solution. With decreasing pH, the number of negative charges per polymer chain decreases and therewith the corona of the micellar aggregates shrinks. The hydrodynamic radius obtained at pH 6 is significantly smaller ($\langle R_h \rangle_z = 94$ nm). Upon further acidification, the aggregates continue diminishing in size ($\langle R_h \rangle_z = 71$ nm at pH 4). For all samples, a spherical shape is indicated by DLS measurements through an extrapolation of the decay rate, $\Gamma_{(q=0)} = 0$. Alongside with the contraction of the PMAA, the polydispersity of the micelles observed via DLS increases (PDI = 0.06 (pH 10), 0.12 (pH 6), 0.16 (pH 4)). A rather broad distribution function was obtained at pH 4. Furthermore, in contrast to other pH-values, the micelles were not stable at pH 4 for a long time. After several days precipitation could be observed, indicating that the increasing hydrophilicity of the poly(2-vinyl pyridine) block is not able to compensate the increasing hydrophobicity of the corona, PMAA.

To obtain further insight into the micellar structure, we performed cryogenic transmission electron microscopy (cryo-TEM) in water. Cryo-TEM is an outstand-

ing method for in-situ imaging of complex structures in solution without having to consider drying artifacts or interactions with the substrate.⁴¹ To increase contrast for the micellar corona, the micellar solution was dialyzed against a buffer containing 0.05M CsCl to exchange the counter ions for the carboxylate group of the poly(methacrylic acid). Without Cs⁺ counter ions, the corona could not be visualized in cryo-TEM. However, this is the only example where we added CsCl to the micellar solutions. The result can be seen in **Figure 3A and B**.

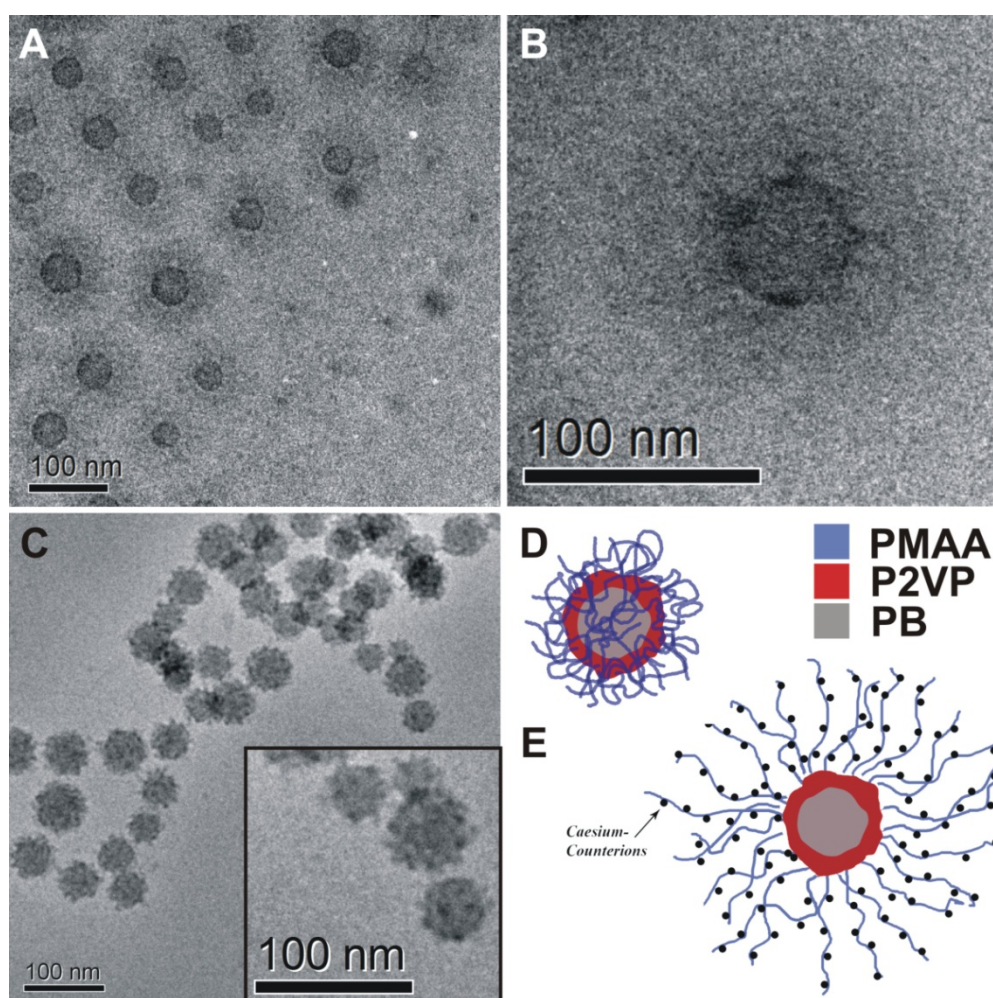


Figure 3: Cryo-TEM micrographs of PB₈₀₀P2VP₁₉₀PMAA₅₅₀ in aqueous solution at pH 10 (0.05M CsCl, c = 1 g/L), Overview (A) and single core-shell-corona micelle (B); at pH 4 (c = 1 g/L) (C), the inset shows an enlargement; schematic depiction of the proposed solution structure of PB₈₀₀P2VP₁₉₀PMAA₅₅₀ depending on the pH; core-shell-corona structure with an expanded PMAA corona at pH 10 (E) and micelles with a collapsed PMAA corona at pH 4 (D).

Micrograph A provides an overview over a larger section of the vitrified micellar solution while B depicts a single core-shell-corona micelle. The latter clearly shows the predicted structure of the triblock terpolymer micelles in solution. They exhibit a grey core with an approximate radius of 20-25 nm in this case. A thin dark shell of P2VP is observed surrounding the PB core. The P2VP is hydrophobic at high pH but still immiscible with polybutadiene, providing a rather hard shell around the soft PB core. Emerging from the P2VP shell, the ionized PMAA arms can be seen, stained by the addition of heavy Cs^+ counter ions. Note that the micelles are always separated from each other by the efficient repulsion of the corona chains and that no clustering could be found. The good contrast between the PB core and P2VP shell without additional staining can be explained by the relatively high difference in mass density between the two blocks. The overall number-average radius of the core-shell-corona micelle in Figure 3B is around 75 nm. Considering that with increasing distance from the micellar core the PMAA arms spread more and more and therefore may not be distinguishable in the cryo-TEM micrograph any more, the average core to core distance in Figure 3A was measured and found to be 150 nm ($= 2 \cdot 75$ nm) as well. This is somewhat smaller than the expected radius from DLS measurements, which was found to be $\langle R_h \rangle_z = 105$ nm. However, this behavior can be understood in terms of that a number-average (TEM) is compared to a z-average (DLS) for a moderately polydisperse sample. The number-average hydrodynamic radius, as calculated from a number-weighted CONTIN plot is $\langle R_h \rangle_n = 63$ nm.

To compare the micelles at lower pH, we also conducted cryo-TEM in water at pH 4 and a representative micrograph is shown in Figure 3C. The appearance of the micellar aggregates has changed. Instead of the very well-defined core-shell-corona structure present at higher pH, now rough, slightly ill-defined yet round-shaped objects are observed. The size of the polybutadiene core is comparable to that at high pH values. Additionally, clustering of the micelles is taking place, originating from the lower charge density in the corona and therefore less electrostatic repulsion between them. The PMAA corona is not visible anymore because the PMAA chains start to collapse upon acidification. This can also explain the uneven appearance of the aggregates. The inset in Figure 3C shows an enlargement. Here, dark spots are observed on the PB core. This could be due to proton transfer from

the carboxylic groups of the PMAA chains onto the nitrogen atoms of the P2VP at this pH, resulting in partial *im*-IPEC formation. Figure 3D shows the micelles with a collapsed PMAA corona at pH 4 while Figure 3E depicts the charged and, thus, expanded core-shell-corona micelle at pH 10 with Cs⁺ as coronal counterions.

Multicompartment-Core Micelles of PB₈₀₀P2VP_{q190}PMAA₅₅₀

After quaternization of the nitrogen moiety of the poly(2-vinyl pyridine) with methyl iodide followed by hydrolysis of the poly(*tert*-butyl methacrylate) block, amphoteric block terpolymers with one permanently hydrophilic block are obtained. The middle block, after modification now poly(*N*-methyl-2-vinylpyridinium iodide) behaves as a strong polyelectrolyte. The corresponding micelles should again exhibit a polybutadiene core, but the situation in the micellar shell or corona has changed as compared to the previous section. Depending on the pH, *im*-IPECs may be formed between the positively charged poly(*N*-methyl-2-vinylpyridinium) and the (at high pH) negatively charged PMAA chains. However, since the positively charged block is much shorter than the negatively charged one, the aggregates in solution will still exhibit an excess negative charge at high pH. In case of *im*-IPEC formation occurring, a salt-responsive behavior can be expected as high concentrations of salt can suppress the formation of IPECs. DLS CONTIN plots are shown for pH 4, pH 10 in the absence of added salt, and pH 10 in the presence of 1.0 M NaCl in Figure 4.

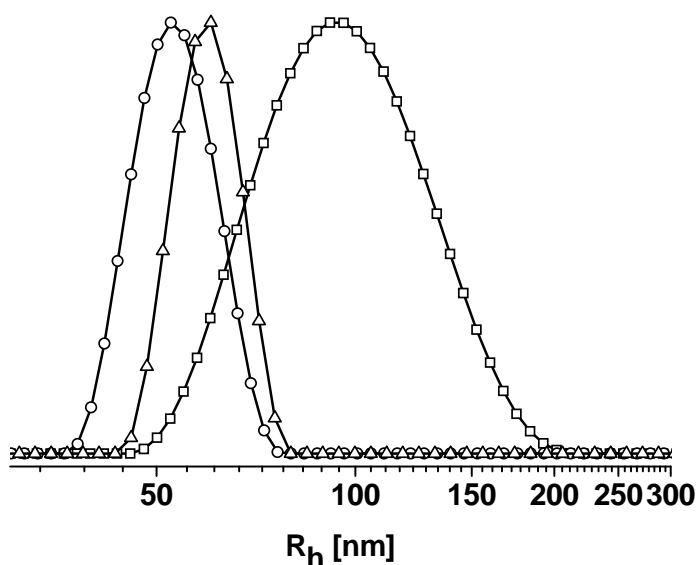


Figure 4: DLS CONTIN plots for PB₈₀₀P2VPq₁₉₀PMAA₅₅₀ in aqueous buffers at different pH-values; pH 10 ($\langle R_h \rangle_z = 102$ nm, \square , PDI = 0.15), pH 4 ($\langle R_h \rangle_z = 52$ nm, \circ , PDI = 0.08) and pH 10 with 1.0 M NaCl ($\langle R_h \rangle_z = 60$ nm, Δ , PDI = 0.09).

At pH 10, a rather broad micellar distribution can be seen (\square). The size ($\langle R_h \rangle_z = 102$ nm, PDI = 0.15) is also in the same range like for the micelles with a non-quaternized middle block ($\langle R_h \rangle_z = 105$ nm). Upon decreasing the pH to 4, the aggregates again contract (\circ), the resulting size ($\langle R_h \rangle_z = 52$ nm, PDI = 0.08) being almost half, and the distribution of the micelles becomes narrower. Again, a spherical shape is indicated by the DLS measurements for all samples through the extrapolation of the decay rate, $\Gamma_{(q=0)} = 0$. Contrary to the PB₈₀₀P2VP₁₉₀PMAA₅₅₀ core-shell-corona micelles discussed in the previous section, the apparent polydispersity of the aggregates in the CONTIN plot does not increase upon acidification, indicating a sufficient stability of the polymeric particles even at low pH. This suggests the formation of an inherently different micellar system due to the change in solubility from P2VP to P2VPq. The corresponding cryo-TEM micrographs are shown in Figure 5A, B, and E.

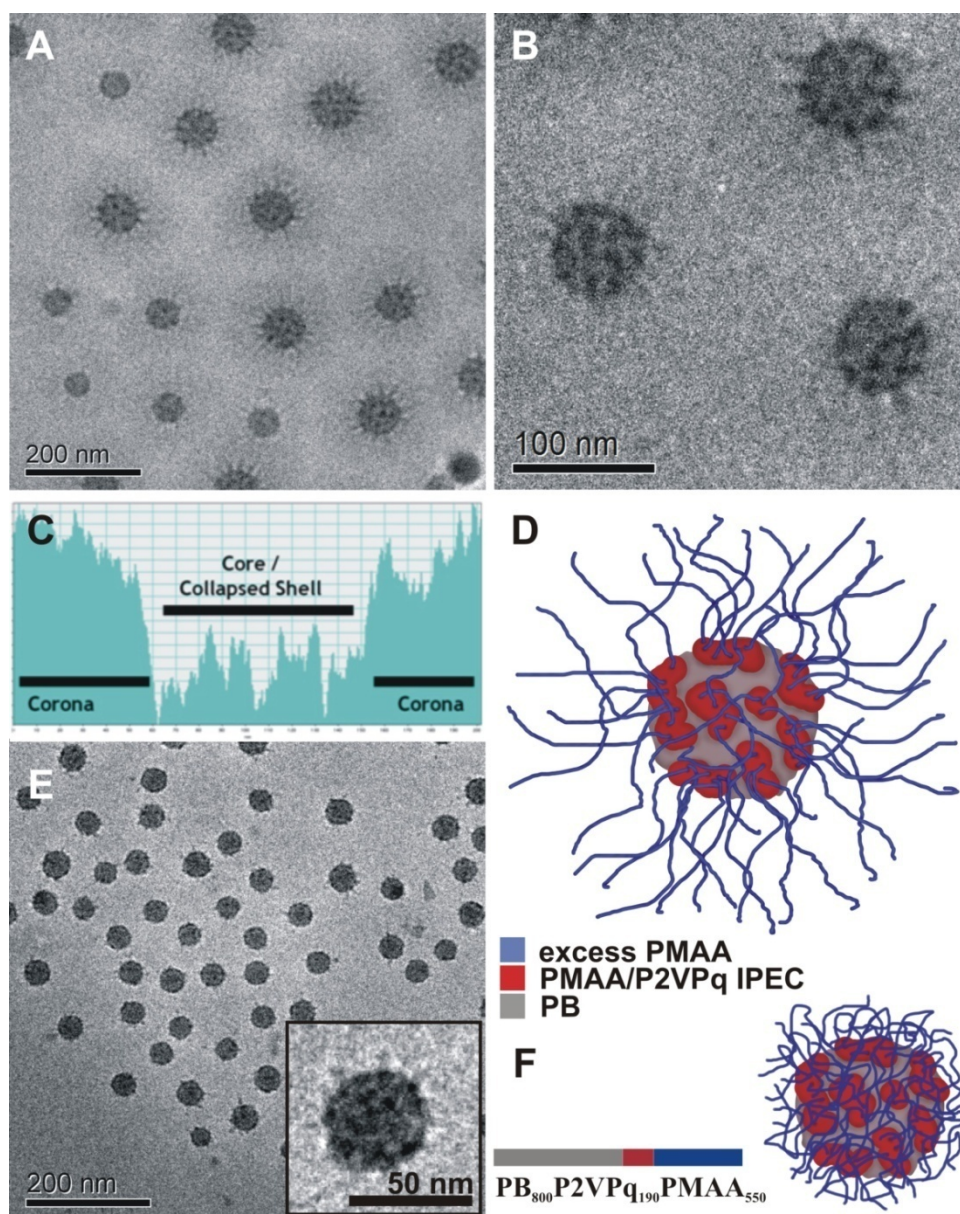


Figure 5: Cryo-TEM micrographs of $PB_{800}P2VPq_{190}PMAA_{550}$ in aqueous solution; (A+B) pH 10, ($c = 1$ g/L); (C) grey-scale analysis of a micellar cross-section; (D) proposed solution structure at pH 10, expanded PMAA corona; (E) cryo-TEM micrograph at pH 4, ($c = 1$ g/L), the inset shows an enlargement of a single micelle; (F) schematic depiction of the block terpolymer composition and proposed solution structure at low pH, collapsed PMAA corona.

Figure 5A presents several micelles, again featuring a constant core to core distance, due to the charged corona of the system. This distance here has an average of around 200 nm, fitting with the values obtained for the hydrodynamic radius of the micelles from dynamic light scattering experiments. The micelles presented are spherical in shape and exhibit a multicompartmental core, observable through several dark spots on the grey polybutadiene part. This is even more pronounced in

Figure 5B, displaying an enlargement of 5A. The micellar cores exhibit a pattern of black, round-shaped objects with the size of around 10 nm and a constant distance of around 15 nm. These patches on the polybutadiene core are the result of *im*-IPEC formation between poly(*N*-methyl-2-vinylpyridinium) polycations and polymethacrylate anions. This also explains the rather high contrast in cryo-TEM, compared to the micellar core. Considering the degrees of polymerization of PMAA and P2VP, the degree of quaternization and the IPEC formation, ~400 units of PMAA per polymer chain form the corona of the micelles. Strikingly, the *im*-IPEC formation, triggered by the quaternization of the P2VP, induces significant changes to the multicompartmental character. Further insight is provided through the grey-scale analysis of one micellar aggregate in Figure 5C. Here, the corona and the core are nicely visible. Within the cross-section of the core, several discontinuities are present, referring again to the patchy *im*-IPECs present on the soft polybutadiene core. Figure 5D shows a schematic depiction of the multicompartment micelle at pH 10. To the best of our knowledge, this is the first example of such complex micellar aggregates with a non-continuous shell formed by *im*-IPECs.

A change to pH 4 results in the collapse of the PMAA corona and a considerable contraction of the aggregates. Figure 5E shows a cryo-TEM micrograph of this sample. The distinct change in micellar size can again be explained by two reasons: the collapse of the corona and / or a certain dynamic character of the aggregates. While DLS gave just an apparent hydrodynamic size, cryo-TEM clearly shows that indeed not only the corona, but also the micellar core shrinks, indicating a change in the aggregation number, N_{agg} . While at pH = 10 the core has a radius of about 30-35 nm (Figure 5A and B), at pH 4 the radius is around 20-25 nm (Figure 5E). Nevertheless, the dark spots representing the IPECs are still present, although somewhat hidden among the collapsed corona chains. This is shown in the inset in Figure 5E, depicting a single micelle. Figure 5F displays a drawing of the proposed micellar structure at low pH values. To further elucidate the ability of these multicompartment micelles to react in a dynamic manner towards environmental stimuli, the micellar solution was dialyzed against 1.0 M NaCl at pH 10. High salinity should lead to a screening of charges,⁴² causing both a breakup of the IPECs and, alongside, a change in the hydrophilic-to-hydrophobic balance of the whole system. Indeed, the DLS CONTIN plot in Figure 4 ($\langle R_h \rangle_z = 60$ nm, $-\Delta-$, PDI = 1.09) shows that the micelles

shrink considerably upon salt addition. Nevertheless, both middle and end block should stay water-soluble. Cryo-TEM of the $\text{PB}_{800}\text{P2VP}_{190}\text{PMAA}_{550}$ micelles at pH 10 with 1.0 M NaCl was performed and is shown in **Figure 6**.

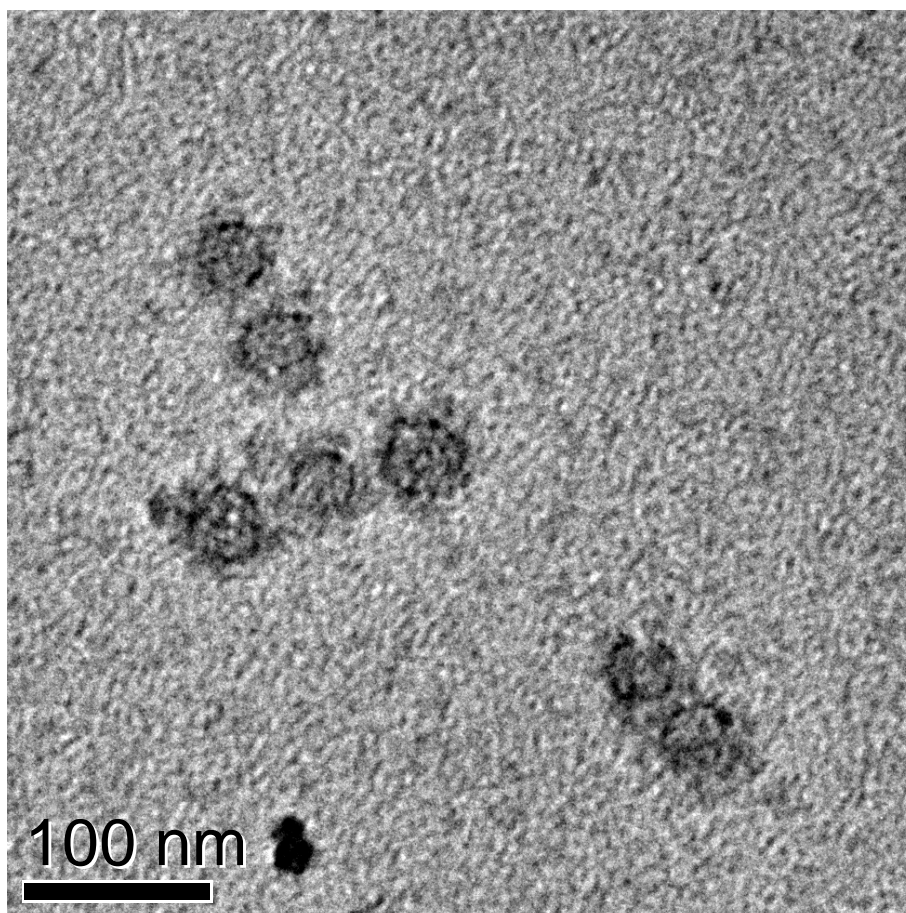


Figure 6: Cryo-TEM micrograph of $\text{PB}_{800}\text{P2VP}_{190}\text{PMAA}_{550}$ micelles at pH 10 and 1.0 M NaCl.

The appearance of the aggregates distinctly changed: instead of dark spots on the grey polybutadiene core a thin dark shell around it can be observed. This is an indication for the breakup of the *im*-IPECs, rendering a poly(*N*-methyl-2-vinylpyridinium) shell comparable to the one observed for the core-shell-corona particles described earlier in this article. Moreover, the screening of the charges leads to a certain clustering of the micelles, shown in Figure 6. The PMAA corona is not visible in Figure 6 but the polybutadiene core is with $R_{\text{core}} = 20$ nm significantly smaller, if compared to the micelles in absence of salt ($R_{\text{core}} = 30\text{-}35$ nm). Again, two factors can explain the contraction of the aggregates. First, the screening of the charges leads to a lowered repulsion of the corona chains and thus to a lowered extension of them. Secondly, the soft polybutadiene core is far above its glass tran-

sition temperature ($T_g = -15^\circ\text{C}$ for ~85% 1,2-polybutadiene), rendering a dynamic micellar system, capable of undergoing changes in its aggregation number and core size. This is even more pronounced as the quaternized P2VPq is completely water-soluble and, therefore, also able to participate in unimer or polyion exchange reactions. To investigate a possible dynamic behavior reflected in a change in the aggregation number, static light scattering experiments for both systems at $\text{pH} = 10$ have been performed. The molar mass for $\text{PB}_{800}\text{P2VPq}_{190}\text{PMAA}_{550}$ was calculated according to the DP of the corresponding blocks and was 112.800 g/mol . The results are shown in **Table 1**. As an alternative to the ZIMM method, N_{agg} was also determined from the micellar core size of the cryo-TEM experiments according to **Equation 1**.

$$N_{\text{agg}} = m_{\text{core}} / m_{\text{PB}} = \frac{4\pi}{3} R^3 \rho_{\text{PB}} / (M_{\text{PB}} / N_A) \quad (1)$$

Table 1: Solution characteristics of the double-hydrophilic $\text{PB}_{800}\text{P2VPq}_{190}\text{PMAA}_{550}$ block terpolymers;

Sample	$R_h[\text{nm}]^a$	$R_g[\text{nm}]^b$	R_g/R_h	$10^{-6} \cdot M_w$ [g/mol] ^b	N_{agg}^b	N_{agg}^c	$10^6 \cdot A_2$ [mol·mL/g ²] ^b
pH 10	102	86	0.84	26.7 ± 0.8	237 ± 7	194 ± 15	-3.43
pH 10, 1.0M NaCl	60	50	0.83	13.6 ± 0.7	121 ± 6	92 ± 11	-4.14

a: determined by dynamic light scattering at 90° angle; b: determined by static light scattering; c: determined by equation (1).

Indeed, upon addition of 1.0 M NaCl the molecular weight and the corresponding aggregation number of the micelles significantly decrease to half of their original values. There are two effects associated with a change in the aggregation number for such systems: the screening of the charges by the addition of high amounts of salt should lead to a less stretched conformation of the corona chains, PMAA, and a decrease in R_h , accompanied by an increase in N_{agg} . On the other hand, the addition of salt disintegrates the IPECs. The quaternized and, hence, wa-

ter-soluble P2VPq chains now are swollen and occupy more space. This in combination with the uncomplexed PMAA chains renders the whole system more hydrophilic and results in a decreased aggregation number N_{agg} . Based on the experimental results presented here, the latter effect seems to be dominating.

The ratio R_g/R_h , which is indicative for the micellar shape, is 0.84 in the absence of added salt and 0.83 for 1.0 M NaCl. Hard spheres are supposed to give a value of 0.775,⁴³ the micelles investigated here exhibit a tendency towards a more star-like structure. This fits with the theory of stretched polyelectrolyte chains as a micellar corona. The theoretical value obtained from R_g/R_h for star-like micelles is 1.1.

Effect of the polymer composition

The ratio of the two *im*-IPEC forming blocks, P2VPq and PMAA, should directly affect the size of the micellar corona. If the PMAA block exhibits a higher degree of polymerization than the P2VPq block, uncomplexed, negatively charged PMAA remains after IPEC formation, serves as the corona, and further stabilizes the block terpolymer micelles. Here, we compare three different systems at pH 10: $PB_{800}P2VPq_{190}PMAA_{550}$, $PB_{800}P2VPq_{190}PMAA_{345}$, and $PB_{800}P2VPq_{190}PMAA_{140}$. We assume that the degree of quaternization of the P2VP block is the same for all the polymers. For $PB_{800}P2VPq_{190}PMAA_{550}$, the PMAA block has a threefold DP if compared to P2VPq. Thus, micelles with a rather thick corona are expected and were shown in Figure 5A and B. For $PB_{800}P2VPq_{190}PMAA_{345}$, the DP of PMAA is approximately twice the DP of P2VPq and the resulting corona should be considerably smaller. Finally, for $PB_{800}P2VPq_{190}PMAA_{140}$, the DP of P2VPq is higher than that for PMAA. Here, complete complexation of PMAA is expected, leading to block terpolymer micelles with very short corona chains made out of P2VPq. However, the remaining positive charge of P2VPq is supposed to render these aggregates still water-soluble. **Figure 7** shows cryo-TEM micrographs, DLS CONTIN plots, and the proposed micellar structure for $PB_{800}P2VPq_{190}PMAA_{345}$ and $PB_{800}P2VPq_{190}PMAA_{140}$.

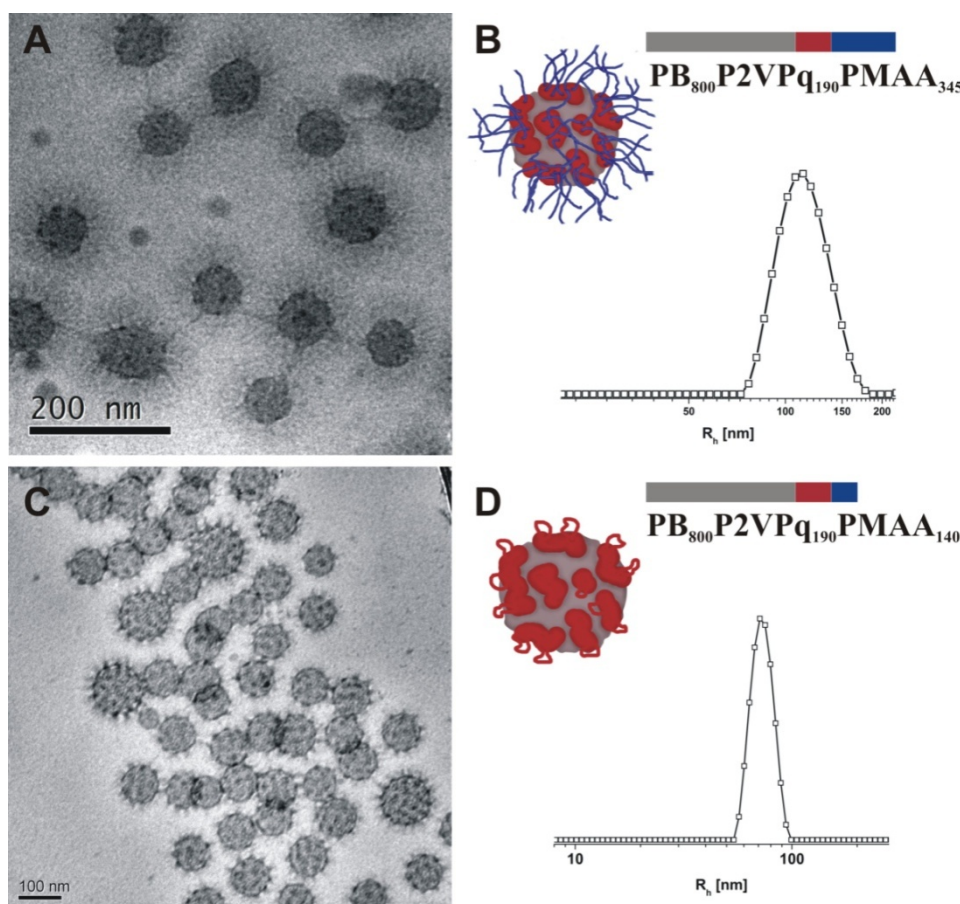


Figure 7: Cryo-TEM micrographs of $\text{PB}_{800}\text{P2VPq}_{190}\text{PMAA}_{345}$ (A) and $\text{PB}_{800}\text{P2VPq}_{190}\text{PMAA}_{140}$ (C); schematic block length depiction, proposed solution structure, and DLS CONTIN plot at pH 10 for $\text{PB}_{800}\text{P2VPq}_{190}\text{PMAA}_{345}$ (B, $\langle R_h \rangle_z = 118$ nm, PDI = 1.18) and $\text{PB}_{800}\text{P2VPq}_{190}\text{PMAA}_{140}$ (D, $\langle R_h \rangle_z = 72$ nm, PDI = 1.08).

The colored bars in Figure 7B and D represent the corresponding block lengths for the PB-P2VPq-PMAA block terpolymers. The cryo-TEM micrograph for $\text{PB}_{800}\text{P2VPq}_{190}\text{PMAA}_{550}$ has already been shown in Figure 5A. Here, the micellar corona exhibited a thickness of approx. 50-60 nm. The micelles formed from $\text{PB}_{800}\text{P2VPq}_{190}\text{PMAA}_{345}$, displayed in Figure 7A, feature a significantly thinner corona of about 30 nm whereas for $\text{PB}_{800}\text{P2VP}_{190}\text{PMAA}_{140}$ very short and straightened corona chains are observed. This could be parts uncomplexed P2VPq chains. Moreover, here the *im*-IPECs present on the core surface are most pronounced. To further elucidate these findings, the zeta-potential of all three micellar solutions at pH 10 and a comparable concentration was measured. For $\text{PB}_{800}\text{P2VPq}_{190}\text{PMAA}_{550}$, a value of -35.8 mV was determined; $\text{PB}_{800}\text{P2VPq}_{190}\text{PMAA}_{345}$ gave -20.5 mV and for $\text{PB}_{800}\text{P2VPq}_{190}\text{PMAA}_{140}$ +1.5 mV were obtained. This in combination with the presented cryo-TEM micrographs confirms that indeed size and charge of the micellar corona can be controlled via the block lengths of both blocks participating in *im*-

IPEC formation, P2VPq and PMAA. The results of this part are summarized in Table 2.

Table 2: Solution characteristics of the different block terpolymer systems.

Block Terpolymer	Ratio P2VPq/PMAA ^a	$\langle R_h \rangle_z$ [nm] ^b	PDI ^c	Zeta-potential ^d [mV]
PB ₈₀₀ P2VPq ₁₉₀ PMAA ₅₅₀	0.35	102	1.15	-35.8
PB ₈₀₀ P2VPq ₁₉₀ PMAA ₃₄₅	0.55	118	1.18	-20.5
PB ₈₀₀ P2VPq ₁₉₀ PMAA ₁₄₀	1.35	72	1.08	+1.5

a: determined according to the block lengths of P2VPq and PMAA; b: determined via the CONTIN algorithm from DLS measurements; c: determined via cumulant analysis of DLS measurements; d: converted from electrophoretic mobilities via the Smoluchowski equation.

Conclusions

Different block terpolymer micelles starting from PB-P2VP-P*t*BMA precursors were prepared: Hydrolysis of the P*t*BMA block leads to PB-P2VP-PMAA, which in aqueous solution forms core-shell-corona micelles with a PB core surrounded by a glassy P2VP shell and a (depending on the pH) negatively charged PMAA corona. The micelles react to changes in pH, due to the pH-responsive nature of PMAA. At pH 4, partial *im*-IPEC formation was observed as a result of proton-transfer from PMAA to P2VP. Quaternization of the P2VP middle block followed by hydrolysis of the ester moiety leads to PB-P2VPq-PMAA, forming multicompartment micelles. The combination of a weak and a strong polyelectrolyte within the same polymer chain resulted in *im*-IPEC formation over the whole addressed pH-range. These IPECs form a patchy, non-continuous shell around the soft PB core. We demonstrate that the block ionomer complexes respond in an elegant way to the addition of salt, rendering smart, dynamic colloids whose shape and / or dimension can be triggered by pH and salinity. We further show that the size and charge of the corona of these micelles can be controlled through the composition of the block terpolymers, in particular the block length ratio in between P2VP and PMAA. Such aggregates with *im*-IPECs could serve as model systems for the control of charge and shape in polymer-

ic micelles. The further complexation of the charged micellar aggregates with, for example, functional particles and block copolymers will be the subject of further studies.

Acknowledgements: The authors acknowledge the VolkswagenStiftung for financial support within the framework “Complex Materials”. Special thanks go to Prof. Adi Eisenberg, Dr. Dmitry Pergushov, and Dr. Markus Burkhardt for fruitful discussions, and Dr. Holger Schmalz and Denise Danz for help with the polymer synthesis. Christopher Synatschke is gratefully acknowledged for the preparation of micellar solutions from PB₈₀₀P2VP_{q190}PMAA₃₄₅ during his labcourse. We also thank Dr. Markus Drechsler for the cryo-TEM measurements of PB₈₀₀P2VP_{q190}PMAA₃₄₅.

Supporting Information Available: THF-SEC traces for the PB₈₀₀P2VP₁₉₀P*t*BMA₅₅₀ terpolymer precursor, DLS CONTIN plots in dioxane after the modification steps, and FTIR spectra of PB₈₀₀P2VP₁₉₀P*t*BMA₅₅₀ and PB₈₀₀P2VP_{q190}PMAA₅₅₀ (Figures S1-S3). This material is available free of charge via the internet at <http://pubs.acs.org>.

References

1. Riess, G. *Prog. Polym. Sci.* **2003**, *28*, 1107-1170.
2. Fustin, C. A.; Abetz, V.; Gohy, J. F. *Eur. Phys. J. E* **2005**.
3. Chen, W.-Y.; Alexandridis, P.; Su, C.-K.; Patrickios, C. S.; Hertler, W. R.; Hatton, T. A. *Macromolecules* **1995**, *28*, 8604-8611.
4. Stewart, S.; Liu, G. *Angew. Chemie Int. Ed.* **2000**, *39*, 340-344.
5. Elbs, H.; Stadler, R.; Magerle, R.; Krausch, G. *Macromolecules* **1999**, *1999*, 1204-1211.
6. Fukunaga, K.; Hashimoto, T.; Elbs, H.; Krausch, G. *Macromolecules* **2003**, *36*, 2852-2861.
7. Böker, A.; Müller, A. H. E.; Krausch, G. *Macromolecules* **2001**, *34*, 7477-7488.
8. Stadler, R.; Giebeler, E. *Macromol. Chem. Phys.* **1997**, *198*, 3815-3825.
9. Auschra, C.; Stadler, R. *Macromolecules* **1993**, *26*, 2171.
10. Abetz, V.; Stadler, R.; Leibler, L. *Polym. Bull.* **1996**, *37*, 135-142.
11. Breiner, U.; Krappe, U.; Abetz, V.; Stadler, R. *Macromol. Chem. Phys.* **1997**, *198*, 1051-1083.
12. Goldacker, T.; Abetz, V.; Stadler, R.; Erukhimovich, I.; Leibler, L. *Nature* **1999**, *398*, 137-139.
13. Bates, F. S.; Fredrickson, G. H. *Phys Today* **1999**, *52*, 32-38.
14. Goldacker, T.; Abetz, V. *Macromol. Rapid Comm.* **2000**, *21*, 16-34.
15. Cui, H.; Chen, Z.; Zhong, S.; Wooley, K. L.; Pochan, D. J. *Science* **2007**, *317*, 647-650.
16. Yu, G. E.; Eisenberg, A. *Macromolecules* **1998**, *31*, 5546-5549.
17. Schmalz, H.; Schmelz, J.; Drechsler, M.; Yuan, J.; Walther, A.; Schweimer, K.; Mihut, A. M. *Macromolecules* **2008**, *41*, 3235-3242.
18. Tsitsilianis, C.; Roiter, Y.; Katsampas, I.; Minko, S. *Macromolecules* **2008**, *41*, 925-934.
19. Zheng, R.; Liu, G. *Macromolecules* **2007**, *40*, 5116-5121.
20. Bieringer, R.; Abetz, V.; Müller, A. H. E. *Eur. Phys. J. E* **2001**, *5*, 5.
21. Lutz, J.-F.; Laschewsky, A. *Macromol. Chem. Phys.* **2005**, *206*, 813-817.
22. Li, Z.; Hillmyer, M. A.; Lodge, T. *Langmuir* **2006**, *22*, 9409-9417.
23. Schacher, F.; Walther, A.; Ruppel, M.; Drechsler, M.; Müller, A. H. E. *Macromolecules* **2009**, *42*, 3540-3548
24. Yelamanchili, R. S.; Walther, A.; Müller, A. H. E.; Breu, J. *Chem. Commun.* **2008**, 489-491.
25. Lodge, T.; Rasdal, A.; Li, Z.; Hillmyer, M. A. *J. Am Chem Soc.* **2005**, *127*, 17608-17609.

26. Gao, Z.; Varshney, S. K.; Wong, S.; Eisenberg, A. *Macromolecules* **1994**, *27*, 7923-7927.
27. Erhardt, R.; Boker, A.; Zettl, H.; Kaya, H.; Pyckhout-Hintzen, W.; Krausch, G.; Abetz, V.; Müller, A. H. E. *Macromolecules* **2001**, *34*, 1069-1075.
28. Liu, Y.; Abetz, V.; Müller, A. H. E. *Macromolecules* **2003**, *36*, 7894-7898.
29. Walther, A.; Andre, X.; Drechsler, M.; Abetz, V.; Müller, A. H. E. *J. Am. Chem. Soc.* **2007**, *129*, 6187-6198.
30. Kabanov, V. A. *Russ. Chem. Rev.* **2005**, *74*, 3-20.
31. Voets, I.; de Keizer, A.; de Waard, P.; Frederik, P. M.; Bomans, P.; Schmalz, H.; Walther, A.; King, S. M.; Leermakers, F. A. M.; Cohen Stuart, M. A. *Angew. Chemie Int. Ed.* **2006**, *45*, 6673-6676.
32. Pergushov, D. V.; Remizova, E. V.; Feldthusen, J.; Zezin, A. B.; Müller, A. H. E.; Kabanov, V. A. *J. Phys. Chem.* **2003**, *107*, 8093-8096.
33. Chelushkin, P. S.; Lysenko, E. A.; Bronich, T. K.; Eisenberg, A.; Kabanov, V. A.; Kabanov, A. V. *J. Phys. Chem. B* **2007**, *111*, 8419-8425.
34. Chelushkin, P. S.; Lysenko, E. A.; Bronich, T. K.; Eisenberg, A.; Kabanov, V. A.; Kabanov, A. V. *J. Phys. Chem. B* **2008**, *112*, 7732-7738.
35. Burkhardt, M.; Martinez-Castro, N.; Tea, S.; Drechsler, M.; Babin, I.; Grishagin, I.; Schweins, R.; Pergushov, D. V.; Gradzielski, M.; Zezin, A. B.; Müller, A. H. E. *Langmuir* **2007**, *23*, 12864-12874.
36. Sperschneider, A.; Schacher, F.; Gawenda, M.; Tsarkova, L.; Müller, A. H. E.; Ulbricht, M.; Krausch, G.; Köhler, J. *Small* **2007**, *3*, 1056-1063.
37. Ripoll, C.; Muller, G.; Selegny, E. *Europ. Polym. J.* **1971**, *7*, 1393-1409.
38. Leyte, J.; Mandel, M. *J. Polym. Sci. Part A* **1964**, *2*, 1879-1891.
39. Gohy, J. F.; Varshney, S. K.; Antoun, S.; Jerome, R. *Macromolecules* **2000**, *33*, 9298-9305.
40. Gohy, J.-F.; Varshney, S. K.; Jerome, R. *Macromolecules* **2001**, *34*, 3361-3366.
41. Cui, H.; Hodgdon, T. K.; Kaler, E. W.; Abezgauz, L.; Danino, D.; Lubovsky, M.; Talmon, Y.; Pochan, D. J. *Soft Matter* **2007**, *3*, 945-955.
42. Burkhardt, M.; Ruppel, M.; Tea, S.; Drechsler, M.; Schweins, R.; Pergushov, D. V.; Gradzielski, M.; Zezin, A. B.; Müller, A. H. E. *Langmuir* **2008**, *24*, 1769-1777.
43. Burchard, W.; Richtering, W. *Progr. Colloid & Polymer Sci.* **1989**, *80*, 151.

Supporting information to the paper:

Dynamic Multicompartment-Core Micelles in Aqueous Media

by Felix Schacher, Andreas Walther and Axel H. E. Müller

Experimental

Gel permeation chromatography. GPC measurements were performed on a set of 30 cm SDV-gel columns of 5 mm particle size having a pore size of 10^5 , 10^4 , 10^3 and 10^2 Å with refractive index and UV ($\lambda=254$ nm) detection. GPC was measured at an elution rate of 1 ml/min with THF as solvent.

Fourier-transform infrared spectroscopy. FTIR measurements were performed using a Perkin Elmer Spectrum One FTIR spectrometer. The samples were introduced as freeze-dried powders.

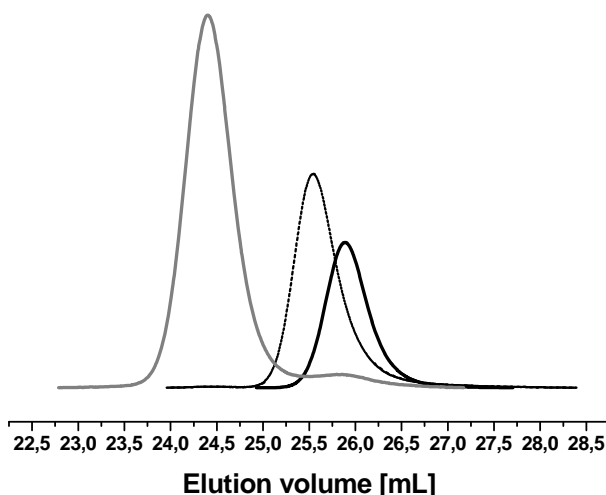


Figure S1: THF-SEC elution traces of the B_{800} precursor (solid black line, PDI = 1.04), the $B_{800}V_{190}$ diblock copolymer (dashed black line, PDI = 1.04), and the $B_{800}V_{190}T_{550}$ block terpolymer (solid grey line, PDI = 1.02).

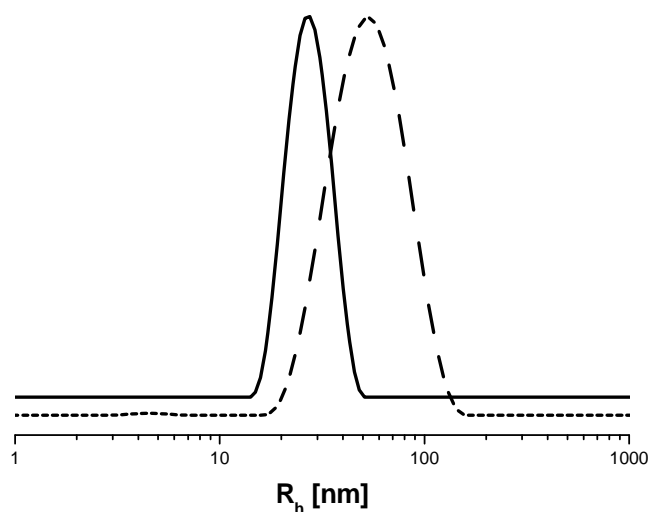


Figure S2: DLS CONTIN plots for $B_{800}Vq_{190}T_{550}$ in dioxane after quaternization ($\langle R_h \rangle_z = 27$ nm, solid black line, PDI = 0.06) and $B_{800}Vq_{190}MAA_{550}$ in dioxane after quaternization and subsequent hydrolysis ($\langle R_h \rangle_z = 53$ nm, dashed black line, PDI = 0.11).

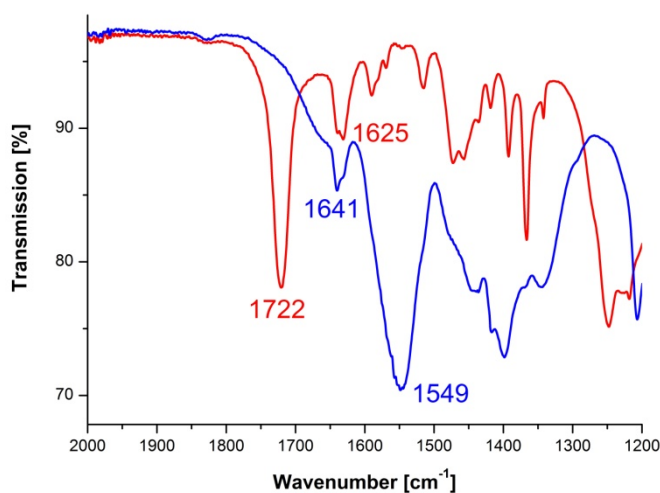


Figure S3: FTIR spectra for $B_{800}V_{190}T_{550}$ (red line) and $B_{800}Vq_{190}MAA_{550}$ (blue line).

For the $B_{800}V_{190}T_{550}$ block terpolymer, an IR band at 1625 cm^{-1} is observed. After quaternization, this band shifted to 1641 cm^{-1} , indicating a successful modification

of the P2VP block. This is in rather good agreement with the results of Biesalski et al., who reported on the quaternization of P4VP.¹ The hydrolysis of the ester moiety can nicely be seen as the IR band for the carboxylic group, 1722 cm^{-1} , vanishes and a broad band for the carboxylate is obtained at 1549 cm^{-1} . Unfortunately, the baseline of the IR measurements was not completely flat, preventing a quantitative evaluation of the data.

1. Biesalski, M.; R uhe, J. *Langmuir* **2000**, *16*. 1943-1950

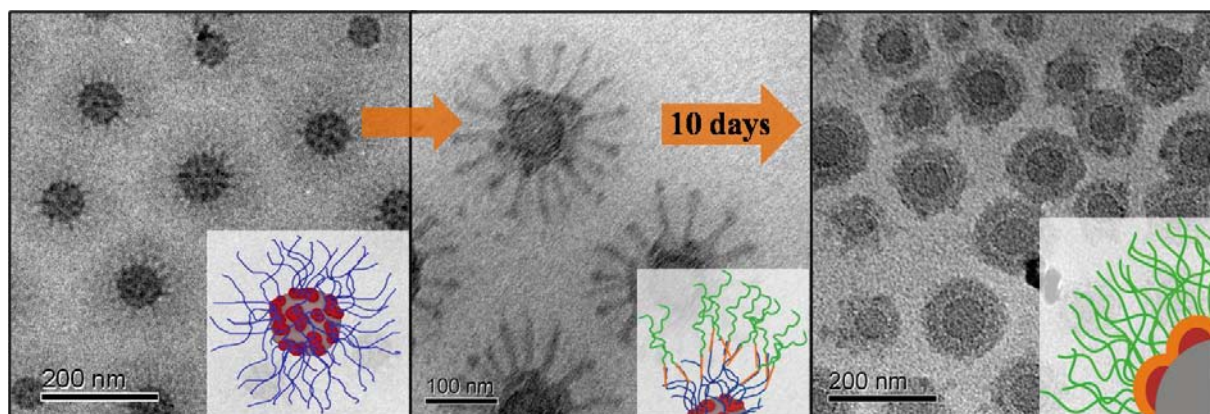
Interpolyelectrolyte Complexes of Dynamic Multicompart- ment Micelles

Felix Schacher,^{1} Eva Betthausen,¹ Andreas Walther^{1,2} Holger Schmalz,¹ Dmitry V. Pergushov,³ and Axel H. E. Müller^{1*}*

[1] Makromolekulare Chemie II and Bayreuther Zentrum für Kolloide und Grenzflächen, Universität Bayreuth, Universitätsstraße 30, D-95440 Bayreuth, Germany

[2] Department of Applied Physics, Helsinki University of Technology, FIN-02015 TKK, Helsinki, Finland

[3] Department of Polymer Science, School of Chemistry, Moscow State University, Vorob'evy Gory, 119991 Moscow, Russia



Abstract

Dynamic core-shell-shell-corona micelles are formed between two oppositely charged block copolymer systems. Preformed polybutadiene-*block*-poly(*N*-methyl-2-vinylpyridinium)-*block*-poly(methacrylic acid) (PB-P2VPq-PMAA) block terpolymer micelles with a soft polybutadiene core, an interpolyelectrolyte complex (IPEC) shell made out of poly(*N*-methyl-2-vinylpyridinium) and poly(methacrylic acid), and a negatively charged PMAA corona were mixed in different ratios at high pH with positively charged poly(*N*-methyl-2-vinylpyridinium)-*block*-poly(ethylene oxide) (P2VPq-PEO) diblock copolymers. Under these conditions, mixing results in the formation of a second IPEC shell onto the PB-P2VPq-PMAA precursor micelles, surrounded by a PEO corona. The resulting multicompartmented IPECs exhibit dynamic behavior, highlighted by a structural relaxation within a period of 10 days, investigated by dynamic light scattering (DLS), cryogenic transmission electron microscopy (cryo-TEM), and scanning force microscopy (SFM). After a short mixing time of 1h, the IPECs exhibit a star-shaped structure whereas after 10 days spherical core-shell-shell-corona objects could be observed. To further increase complexity and versatility of the presented systems, the in-situ formation of gold nanoparticles (Au-NPs) in both the precursor micelles and the equilibrated IPEC was tested. For the PB-P2VPq-PMAA micelles, NP formation resulted in narrowly distributed Au-NP located within the PMAA shell whereas for the core-shell-shell-corona IPEC the Au-NPs were confined within the IPEC shell and shielded from the outside through the PEO corona.

Introduction

Bottom-up processes are one of the key strategies for the preparation of materials matching the demands of today's and future nanotechnology.^[1, 2] Such requirements are, for example, defect-free spatial ordering over several microns, control over interfacial energies, or the positioning of different functional groups within close proximity. During the last decades, co- or self-assembly processes have proven to be the method of choice, providing tailored materials through the careful adjustment of supramolecular and interfacial forces and interactions. Often, block copolymers with suitable functional moieties in different compartments are taken as unimolecular building blocks for the formation of compartmentalized structures in the bulk,^[3-5] in thin-films,^[6, 7] or in solution.^[8-10] In all these cases, the driving force for structural evolution originates from the mutual incompatibility of the unlike segments. Another facile and straightforward method to induce co-assembly of block copolymers is the formation of interpolyelectrolyte complexes (IPECs) through electrostatic interactions between two oppositely charged segments,^[11] either inter-^[12] or intramolecular.^[13] Furthermore, these interpolyelectrolyte complexes are capable of undergoing dynamic polyion exchange reactions, rendering smart colloidal objects responsive to changes in pH or salinity.^[14-18]

The formation of so-called hybrid or composite materials is another way to generate structures with manifold functionalities. The most common examples are organic-inorganic hybrid materials where metal or semiconductor nanoparticles are incorporated into a polymeric matrix material.^[19-22] The idea behind is the combination of both the unique properties of metal nanoparticles regarding catalysis,^[23] chemical sensing,^[24] or data storage together with the cohesion, the processability, and the flexibility of polymer chains. Moreover, if carried out in solution, nanoparticles generated in this way are significantly stabilized through the coordination to the polymer chains, preventing further aggregation taking place and facilitating a narrow particle size distribution,^[25] which is directly related to the materials properties.^[26, 27] A prominent example are hybrid materials of block copolymers and gold nanoparticles, both in the bulk^[28] and in solution.^[29] Gold nanoparticles are of particular interest due to their electronic and optic properties but also due to their biocompatibility.^[25]

Within this work we present a combination of all three previously mentioned approaches for the generation of novel complex materials: first, the self-assembly

of an amphiphilic ABC block terpolymer in a selective solvent and the generation of dynamic complex multicompartiment micelles. Second, the electrostatically driven co-assembly at pH 10 between negatively charged polybutadiene-*block*-poly(*N*-methyl-2-vinylpyridinium)-*block*-poly(methacrylic acid) (PB-P2VPq-PMAA, the degree of polymerization for PMAA has to be significantly higher than that for P2VPq) block terpolymer micelles and positively charged poly(*N*-methyl-2-vinylpyridinium)-*block*-poly(ethylene oxide) (P2VPq-PEO) diblock copolymers is investigated. Finally, the synthesis and encapsulation of narrowly dispersed gold nanoparticles within the intermediate shell of these IPECs is presented.

Both polymers were synthesized via living sequential anionic polymerization. Upon mixing at certain Z-ratios ($Z (+/-)$ being the overall ratio of positive to negative charges) core-shell-shell-corona IPECs are formed with a soft PB core, 2 adjacent IPEC shells consisting of PMAA and P2VPq, and a PEO corona. We show that these complexes first exhibit a star-like appearance which changes to a spherical shape during 10 days due to the dynamic nature of such IPECs. For $Z(+/-) < 1$ uncomplexed PMAA is still present in the intermediate shell formed by both PMAA and P2VPq, providing a suitable environment for the in-situ formation of gold nanoparticles. After preparation, these nanoparticles are protected by the outer PEO shell. The aggregates were analyzed with light scattering, scanning force (SFM), and transmission electron microscopy (TEM, cryo-TEM).

Experimental Part

Synthesis

The synthesis and characterization of poly(2-vinyl pyridine)-*block*-poly(ethylene oxide)^[18] and polybutadiene-*block*-poly(2-vinyl pyridine)-*block*-poly(*tert*-butylmethacrylate)^[30] as well as its modification into polybutadiene-*block*-poly(1-methyl-2-vinylpyridinium)-*b*-poly(methacrylic acid)^[13] have been described elsewhere.

Quaternization

Poly(2-vinyl pyridine)-*b*-poly(ethylene oxide) V₉₄EO₁₂₄₅ (1g, 0.015 mmol) was dissolved in dioxane (50 ml). A 20-fold excess of dimethyl sulfate (3.56 g, 28 mmol, calculated with a degree of polymerization of 94 for the P2VP) was added via syringe. After stirring at 40 °C for 5 days, the excess of dimethyl sulfate was removed by dialysis (regenerated cellulose membranes, MWCO 3.500 g/mol, spectra/por)

against deionized water. Poly(*N*-methyl-2-vinylpyridinium)-*b*-poly(ethylene oxide) was obtained via freeze drying. The degree of quaternization was estimated via FTIR measurements and iodometric titrations and was around 80%.^[13]

Preparation of the interpolyelectrolyte complexes

Both Vq₉₄EO₁₂₄₅ (5 g/L) and B₈₀₀Vq₁₉₀MAA₅₅₀ (1 g/L) were dissolved in a pH 10 buffer solution (VWR®, AVS Titrinorm). Afterwards, the corresponding volumes to reach a certain Z-value (overall-ratio of positive to negative charges) were mixed in small glass vials and stirred at RT.

Preparation of the Au-nanoparticles

HAuCl₄ was dissolved in deionized water (1 g/L) and kept in the dark. The Au load was calculated according to the number of uncomplexed PMAA units present in solution (depending on the Z-value in case of the IPECs). Typically, the Au load was 10% or, 0.1 equivalent compared to the number of PMAA units. The necessary amount of HAuCl₄ in solution was added to the micellar solution at pH 10, stirred for 24 h at RT and kept dark. Excess of HAuCl₄ was removed afterwards via dialysis against pH 10 buffer solution (RC membranes, MWCO 3.500 g/mol, spectra/por). Already after this step, the solutions appeared slightly purple, indicating the formation of Au nanoparticles. For the final nanoparticle formation the solution was exposed to UV-irradiation (Hoenle VG UVAHAND 250 GS) for 30 minutes.

Dynamic light scattering

DLS measurements were performed in sealed cylindrical scattering cells (d = 10 mm) at an angle of 90° on an ALV DLS/SLS-SP 5022F equipment consisting of an ALV-SP 125 laser goniometer with an ALV 5000/E correlator and a He-Ne laser with the wavelength $\lambda = 632.8$ nm. The CONTIN algorithm was applied to analyze the obtained correlation functions. Apparent hydrodynamic radii were calculated according to the Stokes-Einstein equation. Prior to the light scattering measurements the sample solutions were filtered using Millipore Nylon filters with a pore size of 1.2 or 5 μm . Apparent polydispersities for the aggregates in solutions were calculated using the cumulant analysis.

Transmission electron microscopy

TEM images were taken with a Zeiss CEM902 EFTEM electron microscope operated at 80 kV or a Zeiss EM922 OMEGA EFTEM electron microscope operated at 200 kV. Both machines are equipped with an in-column energy filter. Samples were pre-

pared through deposition of a drop of micellar solution (concentration always 0.1 g/L) onto the TEM grid (Gold, 400 mesh). Afterwards the remaining solvent was removed with a blotting paper.

Cryogenic transmission electron microscopy

For Cryo-TEM studies, a drop ($\approx 2 \mu\text{L}$) of the sample solution ($c \approx 0.1 \text{ wt-\%}$) was placed on a lacey carbon-coated copper TEM grid (200 mesh, Science Services, München, Germany), where most of the liquid was removed with blotting paper, leaving a thin film stretched over the grid holes. The specimens were shock vitrified by rapid immersion into liquid ethane in a temperature controlled freezing unit (Zeiss Cryobox, Zeiss NTS GmbH, Oberkochen, Germany) and cooled to approximately 90 K. The temperature was monitored and kept constant in the chamber during all the preparation steps. After freezing the specimens, they were inserted into a cryo-transfer holder (CT3500, Gatan, München, Germany) and transferred to a Zeiss EM922 OMEGA EFTEM instrument. Examinations were carried out at temperatures around 90 K. The transmission electron microscope was operated at an acceleration voltage of 200 kV. Zero-loss filtered images ($\Delta E = 0 \text{ eV}$) were taken under reduced dose conditions. All images were registered digitally by a bottom mounted CCD camera system (Ultrascan 1000, Gatan), combined and processed with a digital imaging processing system (Gatan Digital Micrograph 3.9 for GMS 1.4).

Scanning force microscopy

SFM images were recorded on a Digital Instruments Dimension 3100 microscope operating in Tapping ModeTM. Samples were prepared on polished silicon wafers through dip-coating. The wafer were previously cleaned in toluene, dried on a heating plate and finally treated with a snow jetTM. Afterwards, the pre-cleaned silicon wafers were dipped into the sample solution for 20 seconds and the excess of solution was afterwards removed with a dust-free blotting paper. All images were treated with the Nanoscope 7.20 software.

Zeta-potential

The zeta-potential was determined on a Malvern Zetasizer Nano ZS in conjunction with an MPT2 autotitrator (Malvern). The electrophoretic mobilities (u) were converted into ζ potentials via the Smoluchowski equation $\zeta = u\eta/\epsilon_0\epsilon$, where η denotes the viscosity and $\epsilon_0\epsilon$ the permittivity of the solution.

UV-VIS spectroscopy. The UV spectra of the gold nanoparticle solution were recorded on a Hitachi U-3000 spectrophotometer with a scanning speed of 300 nm / min and a sampling interval of 0.50 nm.

Results and Discussion

Dynamic Multicompartment Micelles from B₈₀₀Vq₁₉₀MAA₅₅₀

Recently we reported on the unique micellization behavior of polybutadiene-*block*-poly(*N*-methyl-2-vinylpyridinium)-*block*-poly(methacrylic acid) B₈₀₀Vq₁₉₀MAA₅₅₀ ($M_n = 110$ kg/mol, PDI = 1.02) block terpolymers in aqueous systems. The subscripts denote the number-average degrees of polymerization of the corresponding block. Dynamic multicompartment micelles which showed response to changes in salinity or pH were formed and exhaustively characterized.^[13] A cryo-TEM micrograph of such micelles at pH 10 and the proposed solution structure are shown in **Figure 1**. The micelles consist of a soft polybutadiene core, a patchy intra-micellar interpolyelectrolyte complex shell formed by P2VPq and parts of the PMAA, and a negatively charged and, thus, stretched corona of excess PMAA (DP (PMAA) > DP (P2VPq)).

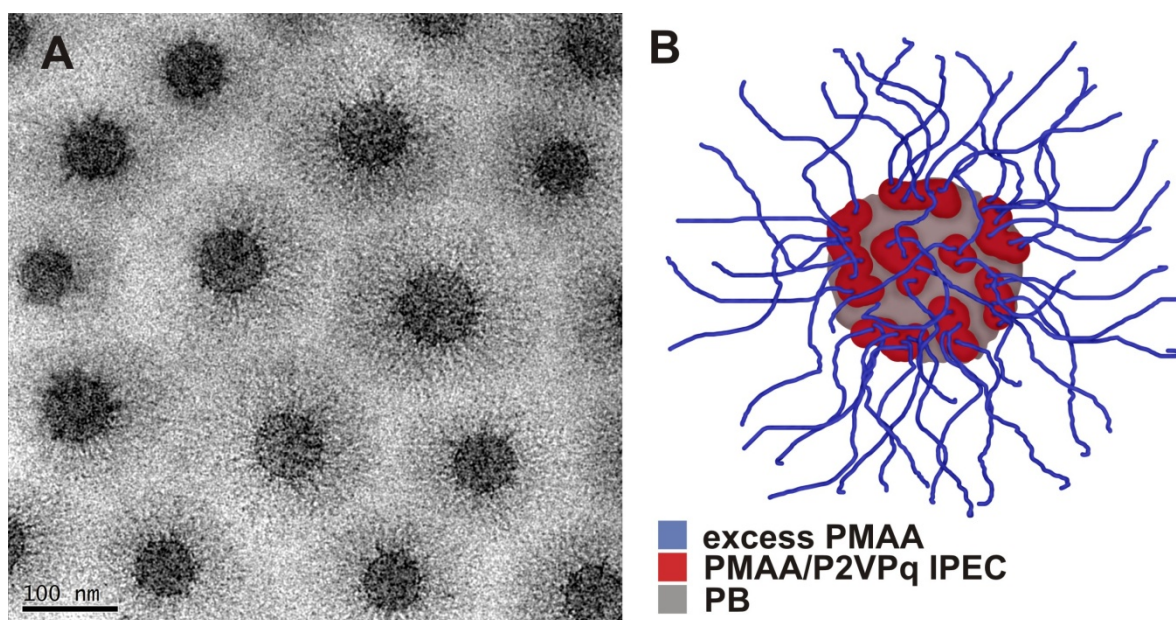


Figure 1: Cryo-TEM of B₈₀₀Vq₁₉₀MAA₅₅₀ micelles at pH 10 (A); proposed multicompartment architecture of the micelles (B).

Interpolyelectrolyte Complex Formation between $B_{800}Vq_{190}MAA_{550}$ and $Vq_{94}EO_{1245}$

For the IPEC formation these aggregates were mixed with quaternized poly(1-methyl-2-vinylpyridinium)-*block*-poly(ethylene oxide) $Vq_{94}EO_{1245}$ diblock copolymers in a ratio so that the overall ratio of positive to negative charges $Z = 1$ (taking into account the estimated quaternization efficiency of 80% for the P2VPq block). The degrees of polymerization are 94 (Vq) and 1250 (EO). Note that the Z-ratio is the overall ratio of positive to negative charges. The mixing process as well as the proposed structure of the resulting IPECs is shown in **Figure 2**. As described earlier,^[13] we assume a remaining DP of 360 of the negatively charged PMAA for the multi-compartment micellar precursor after the intra-micellar IPEC formation. More precisely, for one molecule $B_{800}Vq_{190}MAA_{550}$ approximately 3.8 molecules $Vq_{94}EO_{1245}$ are added.

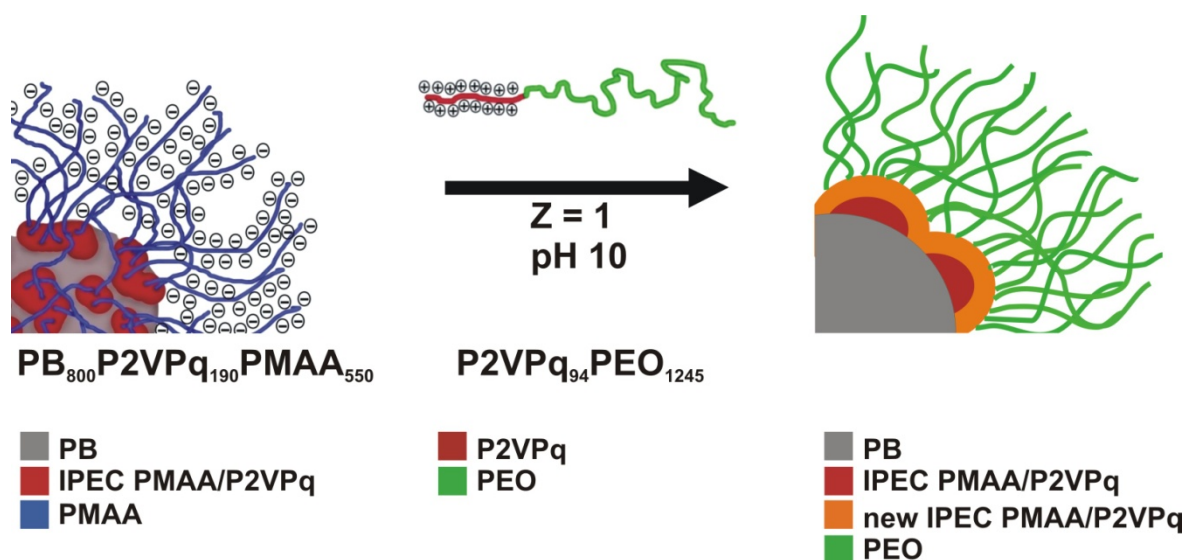


Figure 2: scheme for the formation of IPECs between negatively charged $B_{800}/V_{190}MAA_{550}$ block terpolymer micelles and positively charged $Vq_{94}EO_{1250}$ diblock copolymers at $Z (+/-) = 1$; please note that the precursor micelles on the left are shown according to an “on-top” view whereas the IPEC on the right is shown as a cross section.

By mixing with positively charged $Vq_{94}EO_{1245}$ diblock copolymers in solution at pH 10 further IPEC formation takes place, providing a new shell around the PB core as depicted in the right part of Figure 2. Although, for clarity reasons, the right part in Figure 2 displays two different IPEC shells (the red one being the former patchy shell of the precursor particles and the orange shell the newly formed IPEC) surrounding the PB core it is rather unlikely that both can be distinguished, as

they consist of the same two charged polymer segments. After IPEC formation, the whole core-shell-shell micelle is further surrounded by a PEO corona, depicted in green in Figure 2. Dynamic light scattering (DLS) was performed to compare both solutions (Figure 3). The “precursor” micelles have a hydrodynamic radius $\langle R_h \rangle_z = 99$ nm (PDI = 1.18). After 1h of mixing at $Z = 1$, the size of the aggregates increased significantly, resulting in $\langle R_h \rangle_z = 155$ nm (PDI = 1.19). Moreover, if the same experiment is performed again after 10 days, the radius decreased to 133 nm (PDI = 1.08). No significant decrease in size was observed after these 10 days. Furthermore, the distribution of the hydrodynamic radii significantly narrows after 10 days, indicating a certain equilibration of the system.

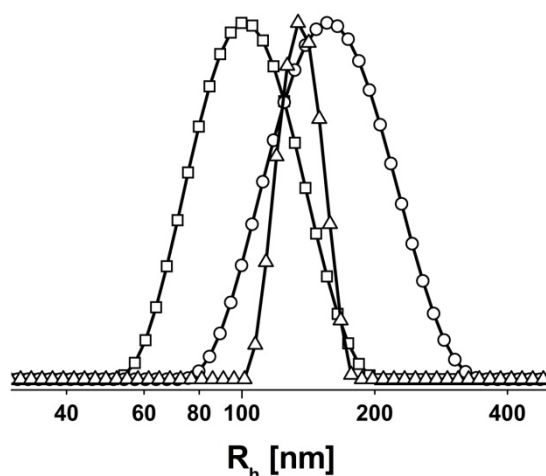


Figure 3: DLS CONTIN plots for the $B_{800}Vq_{190}MAA_{550}$ block terpolymer precursor micelles ($\langle R_h \rangle_z = 99$ nm, PDI = 1.18, \square), the IPECs at $Z (\pm) = 1$ after 1h ($\langle R_h \rangle_z = 155$ nm, PDI = 1.19, \circ) and 10 days mixing time ($\langle R_h \rangle_z = 133$ nm, PDI = 1.08, Δ).

One possible explanation is that the formed IPECs are capable of undergoing polyion exchange reactions in aqueous solution and that this is the effect of some structural rearrangement of the formed polymeric micelles.^[11, 17] To evaluate this, cryo-TEM of a sample was performed 1h after mixing (Figure 4A and 4B).

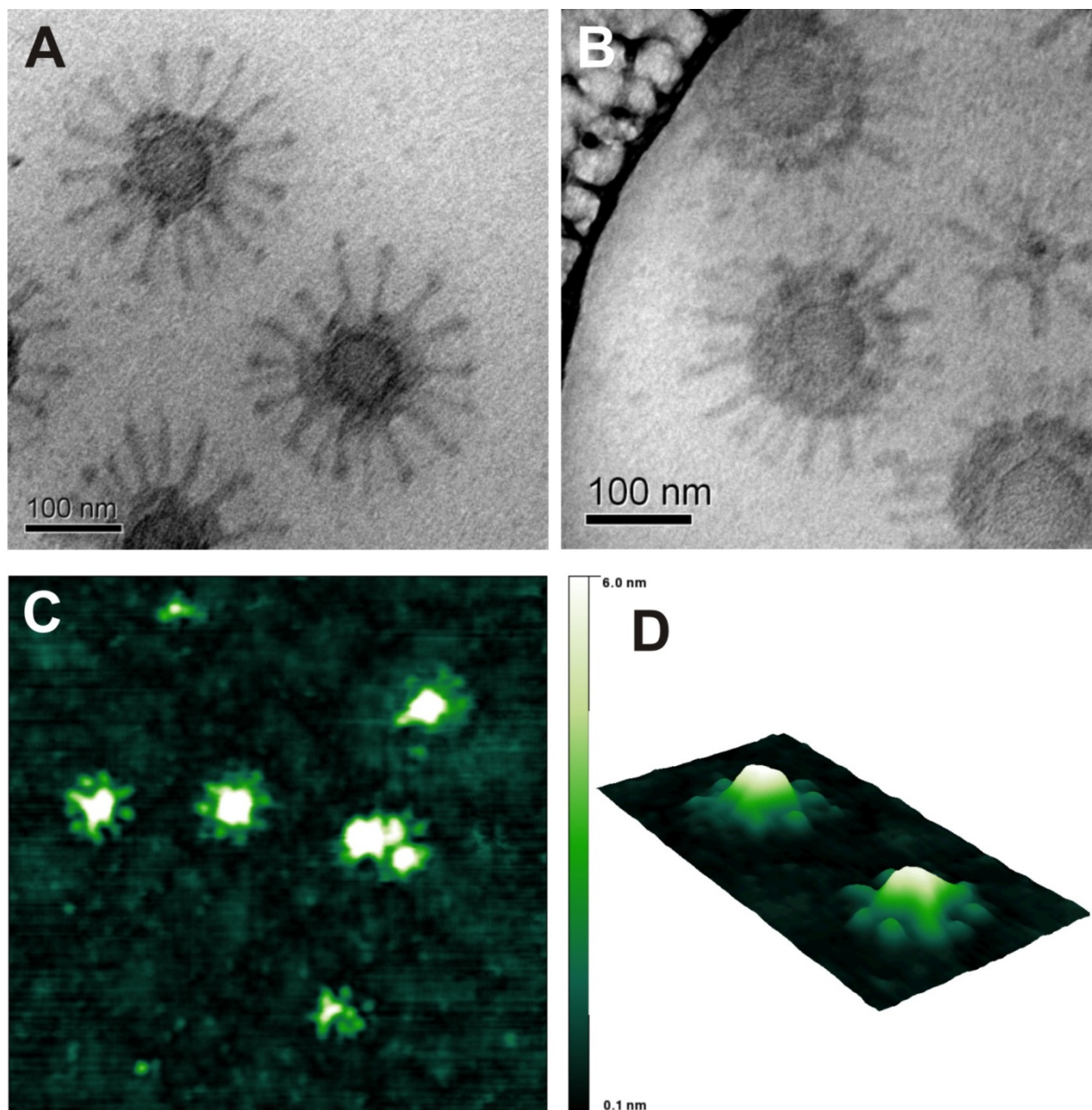


Figure 4: A, B: cryo-TEM micrograph of IPECs at $Z (+/-) = 1$ and pH 10 after 1h mixing time at different locations of the same sample; C, D: SFM height images of an IPEC solution at $Z (+/-) = 1$ and pH 10 after deposition on a carbon coated TEM grid (image size is $2 \times 2 \mu\text{m}$ (C) and $1 \times 0.5 \mu\text{m}$ (D), z-scale in both cases is 6 nm), D displaying an enlargement of C.

Figure 4A displays star-like micellar aggregates with a radius of around 125 nm. The PB core has a radius of 30-35 nm and is surrounded first by a very thin dark ring ($d \sim 10$ nm), and then by a 10-20 nm thick lighter grey shell ending up in several (typically 12-16) stretched arms. In Figure 4B, at a first glance the structure appears similar, but the thin dark ring around the PB core has almost vanished and the surrounding grey shell is thicker and more continuous. Also the arms appear shorter, if compared to Figure 4A. In our opinion, Figures 4A and 4B represent

different states of a dynamic system on its way to equilibrium. A possible illustration for the formation of this intermediate structure is shown in **Figure 5**. Such structural rearrangements after the initial formation of an IPEC have been reported for the IPEC formation between polyisobutylene-*block*-poly(methacrylic acid) micelles with positively charged poly(*N*-ethyl-4-vinylpyridinium).^[15]

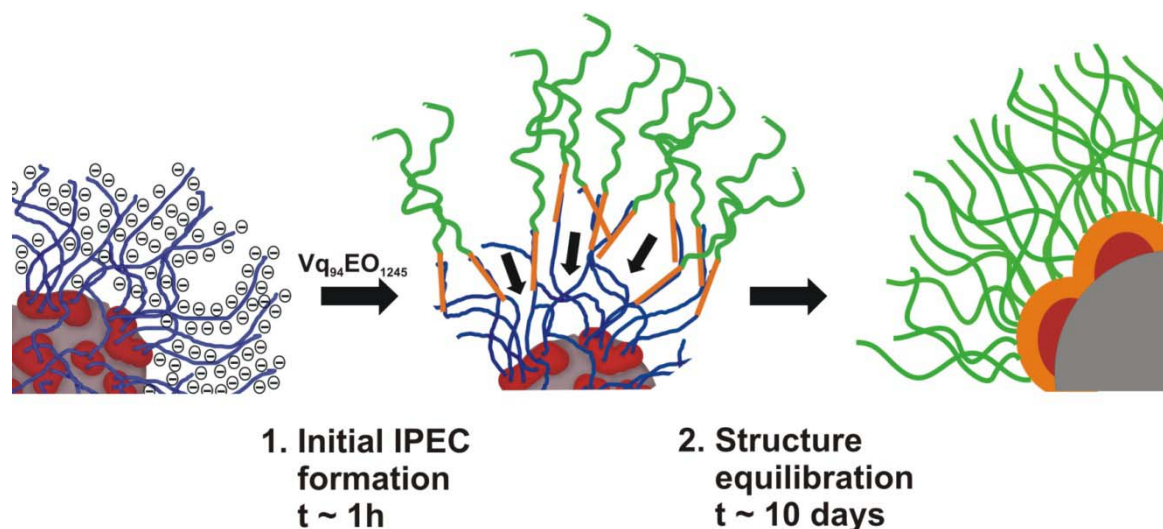


Figure 5: Schematic depiction of the formation of the star-like intermediate structures of the IPECs between $B_{800}Vq_{190}MAA_{550}$ and $Vq_{94}EO_{1245}$; please note that the precursor micelles on the left are shown according to an “on-top” view whereas the IPEC on the right is shown as a cross section.

In the beginning, the corona chains of $B_{800}Vq_{190}MAA_{550}$ micelles at pH 10 are charged and, hence, stretched. The same accounts for the positively charged part of $Vq_{94}EO_{1245}$. Upon mixing, first IPEC formation takes place between two stretched, oppositely charged polymer chains. Afterwards, upon charge neutralization and, thus, less repulsion in-between the chain segments, the formed IPECs start to fuse, form a continuous shell around the PB core and overlap with the already existing “patchy” shell of the precursor micelles. The star-like appearance of the aggregates in Figure 4A and 4B could be explained in this way. If the aggregation number determined for the precursor micelles $(243)^{13}$ is taken into account, each of these “ray-like” protrusions should consist of 15-20 PMAA chains and the respective 3.8-fold number of oppositely charged P2VPq chains. Furthermore, the thin dark ring around the PB core in Figure 4A seems to represent the former, non-continuous shell of the $B_{800}Vq_{190}MAA_{550}$ multicompartiment micelles. Figure 4B depicts a system already somewhat closer to equilibrium, visible by the thicker and more developed IPEC shell around the PB core and the shorter arms. In addition, the dark ring has almost vanished, indicating the formation of a continuous inter-

face between the “old” and the newly formed IPECs. The presence of aggregates at different stages of the equilibration process after a short mixing time could also explain the decreasing polydispersity of the IPECs during the 10 days of mixing.

The same aggregates at $Z = 1$ after 1h mixing time were also analyzed by scanning force microscopy (SFM) on polished silicon wafers. Figure 4C provides an overview ($2.0 \times 2.0 \mu\text{m}$, height image, z-scale = 7 nm) with several IPECs of similar size and shape and Figure 3D shows the height image of two single IPECs. The single IPECs in Figure 4D have an overall radius of around 150 nm with a core of 75 nm and 9 bumps of 10-15 nm surrounding both. The increase in size is caused by the flattening of the aggregates on the silicon substrate. Also the arms seem to be less stretched than in the corresponding cryo-TEM micrographs (Figure 4A and 4B). The (according to DLS) equilibrated IPECs at $Z (+/-) = 1$ after 10 days mixing were also analyzed by cryo-TEM. The resulting cryo-TEM micrographs are shown in **Figure 6**.

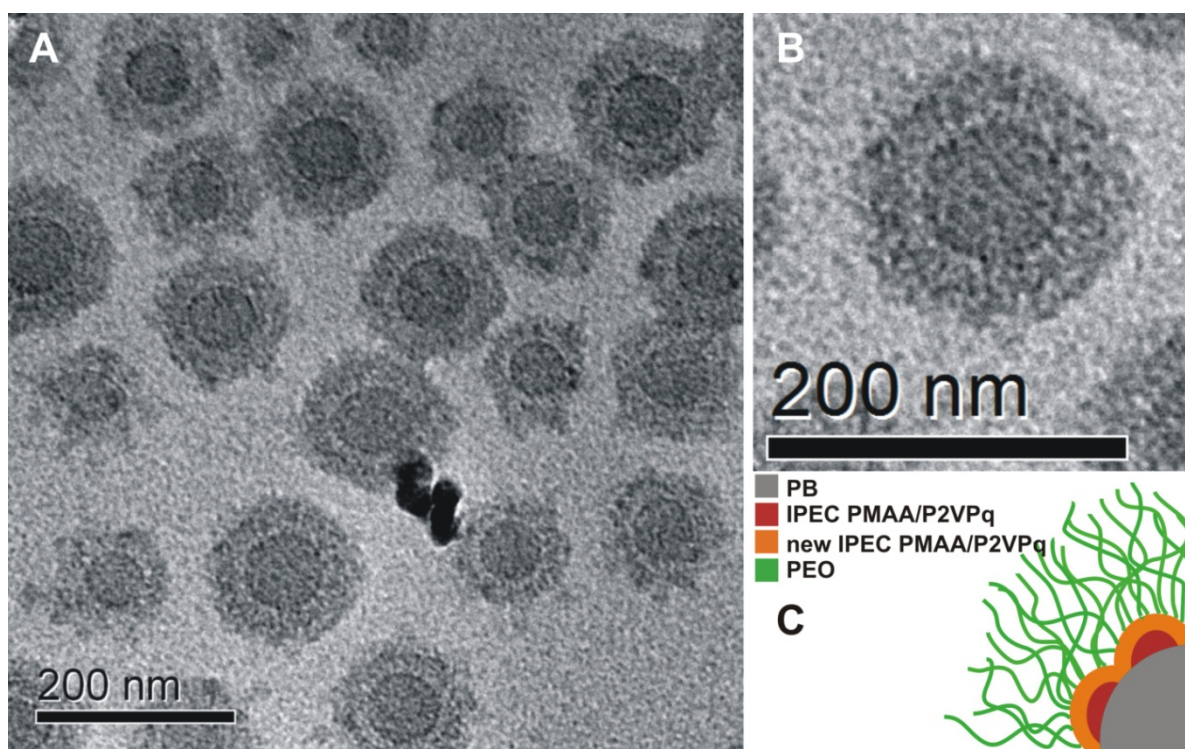


Figure 6: Cryo-TEM micrograph of the IPEC formed between $B_{800}Vq_{190}MAA_{550}$ and $Vq_{94}EO_{1245}$ at $Z (+/-) = 1$ after 10 days mixing time (A); enlargement of a single IPEC (B); proposed structure of the assembly (C).

Indeed, the appearance of the structures has significantly changed. Instead of the former core-patchy shell-corona micelles, now a thick, fuzzy, continuous shell can be observed. The core size has remained constant; in both cases a radius of 30-35 nm was measured. The shell thickness is around 20-30 nm. We propose that this continuous shell is made of both the former, intra-micellar IPEC and the newly formed one between excess PMAA and Vq₉₄EO₁₂₄₅. As expected, the two different parts of the IPEC shell are not distinguishable. The rather fuzzy appearance of the micellar shell could be due to an incomplete mixing of the two IPEC shells. According to the volume of the newly formed IPEC shell compared to the volume of the two polyelectrolyte chains participating (243 PMAA chains¹³ with a DP of 360 and ~900 P2VPq chains with a DP of 94), it is quite likely that also PEO chains are incorporated or buried into this shell. This would also lead to a certain swelling of this shell through the solvent, water. A PEO corona, surrounding the shell, is expected, though not visible in cryo-TEM. However, charge neutrality of the outmost part of the micellar aggregates can be assumed as the micelles do not show repulsion apparent through a strongly deviating core-to-core distance. To confirm this, the zeta-potential of these solutions was determined, revealing -35.8 mV (B₈₀₀Vq₁₉₀MAA₅₅₀ precursor micelles), + 14.7 mV (Vq₉₄EO₁₂₅₀ diblock copolymer in aqueous solution) and + 0.2 mV (resulting IPEC at Z = 1) at comparable concentrations (c ≈ 1 g/L). Although one has to be careful about a quantitative evaluation of these measurements, the general message is quite clear. At Z = 1 almost uncharged particles are obtained.

Effect of the overall Z (+/-) ratio

All data presented so far has been obtained for Z (+/-) = 1. To elucidate the effect of this ratio on particle size, micelle polydispersity, or the remaining particle charge we prepared IPECs at different Z-values 0.1, 0.2, 0.5, and 0.75. DLS CONTIN plots and zeta-potential measurements for these solutions after 10 days mixing are shown in **Figure 7**.

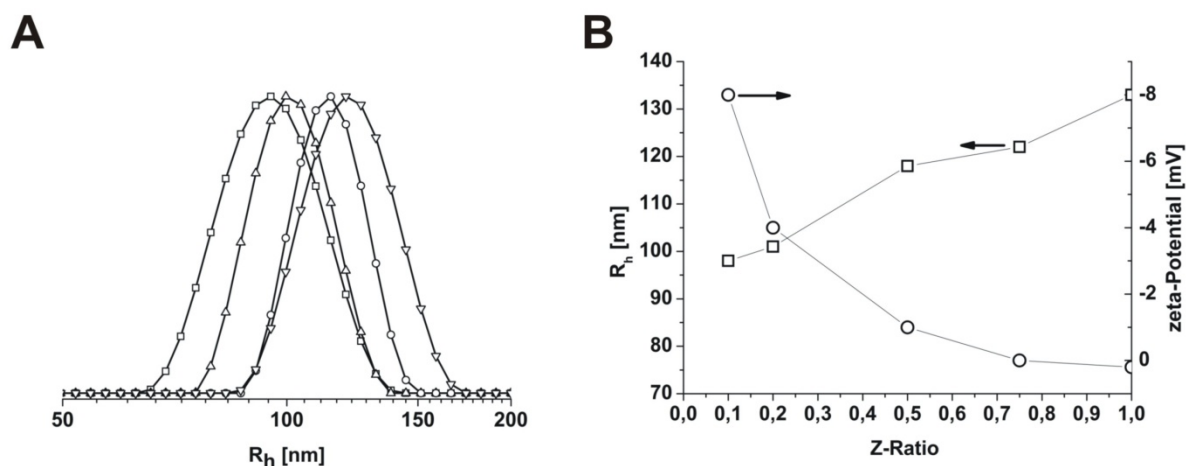


Figure 7: DLS CONTIN plots for IPECs of $B_{800}Vq_{190}MAA_{550}$ and $Vq_{94}EO_{1245}$ after 10 days mixing at different Z (+/-) = 0.1 ($\langle R_h \rangle_z = 98$ nm, PDI = 1.17, -□-), 0.2 ($\langle R_h \rangle_z = 102$ nm, PDI = 1.16, -Δ-), 0.5 ($\langle R_h \rangle_z = 117$ nm, PDI = 1.11, -○-), and 0.75 ($\langle R_h \rangle_z = 123$ nm, PDI = 1.12, -▼-) (A); hydrodynamic radii (-□-) and zeta-potential (-○-) depending on the prepared Z (+/-) - ratio (B).

With increasing Z, the radius of the IPECs measured by DLS increases steadily. In the beginning, for Z = 0.1 and $\langle R_h \rangle_z = 98$ nm (PDI = 1.17), almost no change can be seen as compared to the block terpolymer precursor micelles ($\langle R_h \rangle_z = 99$ nm, PDI = 1.18). At Z = 0.2, the radius increases slightly to 102 and the distribution narrows (PDI = 1.16). This effect becomes more pronounced at higher Z-values (Z = 0.5: $\langle R_h \rangle_z = 117$ nm, PDI = 1.11; Z = 0.75: $\langle R_h \rangle_z = 123$ nm, PDI = 1.12; Z = 1.0: $\langle R_h \rangle_z = 133$ nm, PDI = 1.08). The measured zeta-potential for these solutions follows the same trend: -8 mV (Z = 0.1), -6 mV (Z = 0.2), -2.5 mV (Z = 0.5), -0.2 mV (Z = 0.75), and +0.2 mV (Z = 1.0) were obtained. The zeta-potential at Z = 0.75 does not seem to be different from that for Z = 1. We assume that in this case the shell of the $B_{800}Vq_{190}MAA_{550}$ precursor micelles is already completely covered with $Vq_{94}EO_{1245}$ molecules, burying any remaining uncomplexed PMAA within the IPEC shell.

To further increase the complexity of these dynamic multicompartamental systems, the preparation of gold nanoparticles inside the IPECs was tested. We therefore prepared IPEC solutions at Z(+/-) = 0.2.

Nanoparticle Generation inside the IPECs:

There is a general and growing interest in the generation of gold nanoparticles within or on polymeric scaffolds^[20, 31], either for applications in electronic or catalytic devices. There are several examples about the ability of PAA, PMAA, or comparable weak polyelectrolytes as carriers for noble metal nanoparticles in the literature. For example, Bi et al. generated Ag nanoparticles inside the PAA core of PS-

b-PAA diblock copolymer micelles in toluene.^[32] Caruso et al. reported the loading of PbS and Au nanoparticles on polymer spheres coated with PAA / poly(allylamine hydrochloride) (PAH) multilayers.^[33] To elucidate the use of the presented IPECs as carriers for gold nanoparticles, they were mixed with HAuCl₄ in solution. The precursor micelles with a PMAA corona serve as a reference system. For the system presented here, both PMAA and P2VPq could serve as stabilizers for Au NPs. However, we assume that the P2VPq compartments are almost completely located within the collapsed IPEC domains and, hence, by far less accessible for the AuCl₄⁻ ions. Even so, it cannot be completely neglected that some metal particles are located at either the P2VPq or the IPEC. Typically, the PMAA chains of both the reference system and the IPEC at $Z = 0.2$ were loaded with 10% HAuCl₄, calculated on the proposed remaining DP for PMAA of 360^[13] in combination with the charge ratio. After 24 h in the dark and subsequent dialysis for another 24 h to remove non-coordinated HAuCl₄, the solutions were exposed to UV-irradiation for 30 minutes. Afterwards, pink solutions were obtained. The reaction scheme is shown in **Figure 8**.

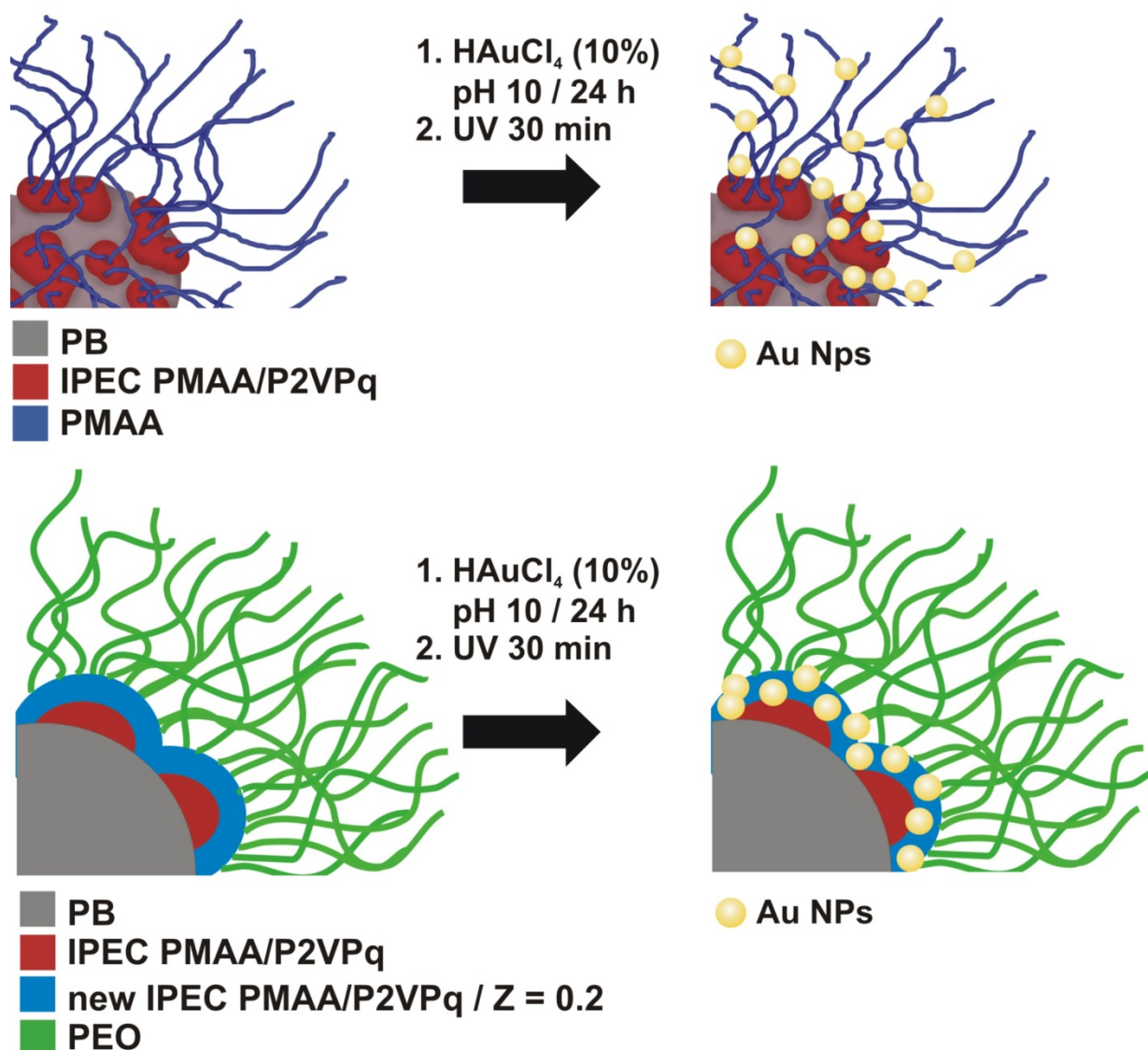


Figure 8: Schematic depiction of the formation of Au nanoparticles on negatively charged B₈₀₀V_{q190}MAA₅₅₀ terpolymer micelles (upper scheme) and IPECs from B₈₀₀V_{q190}MAA₅₅₀ and V_{q94}EO₁₂₄₅ at Z (+/-) = 0.2 after mixing for 10 days (lower row);

For the IPECs prepared at Z = 0.2, the newly formed shell still exhibits a negative charge and, hence, uncomplexed PMAA units; thus enabling the formation of gold nanoparticles within the IPEC. This is confirmed by zeta-potential measurements (cf. Figure 7B). According to the proposed solution structure of the IPECs the Au NPs should be formed within the shell shielded from the outside by the PEO corona. Here we assume that for this charge ratio the equilibrium structure is comparable but with uncomplexed PMAA present. After loading with the Au NPs, the B₈₀₀V₁₉₀MAA₅₅₀ terpolymer micelles were analyzed by TEM. The nanoparticle loading of the IPECs was investigated by cryo-TEM. The results are shown in Figure 9.

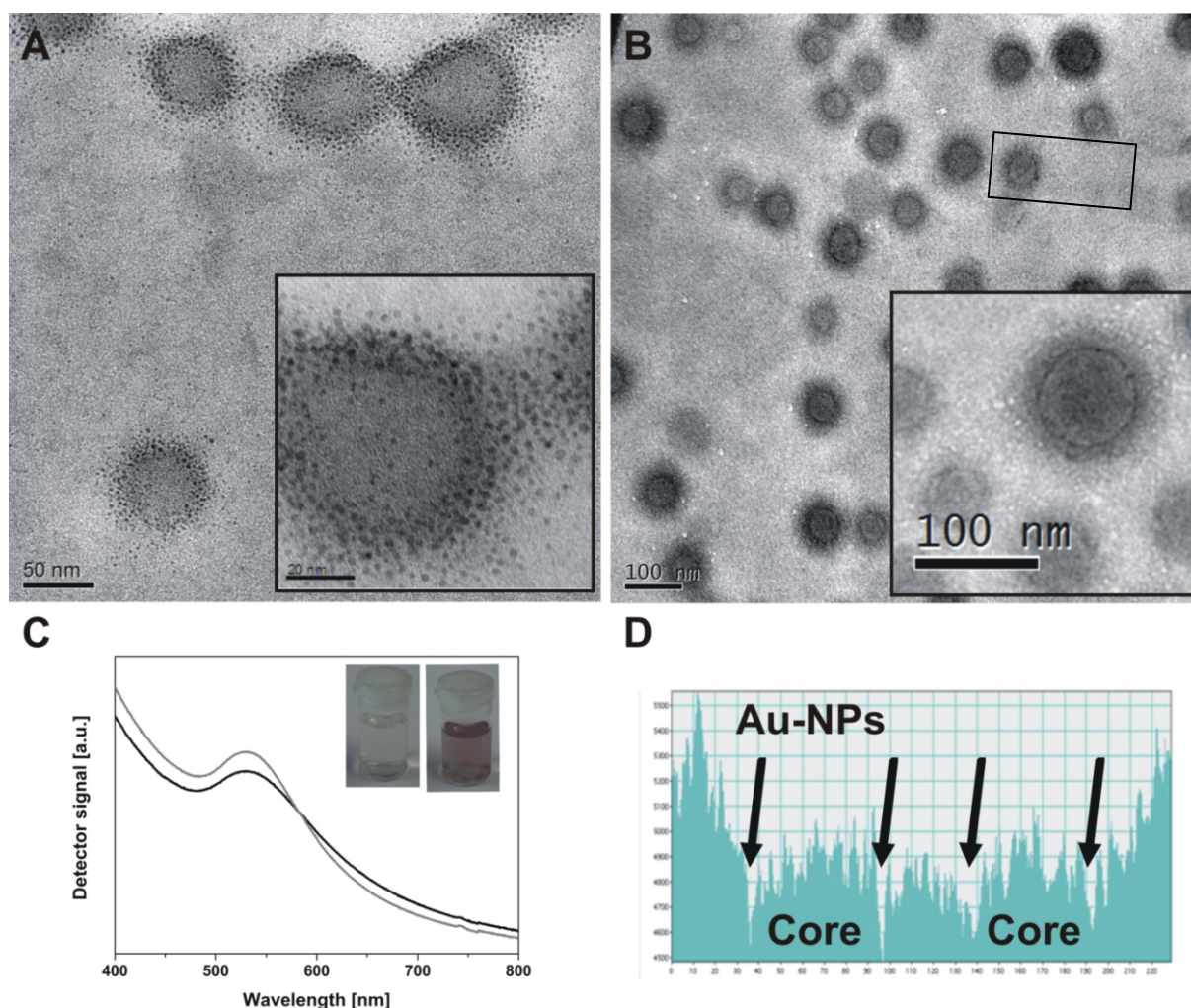


Figure 9: TEM micrograph of $B_{800}Vq_{190}MAA_{550}$ terpolymer micelles loaded with Au-NPs on a carbon-coated copper grid (A), the inset displays an enlargement; cryo-TEM micrograph of the IPEC at $Z = 0.2$ loaded with Au-NPs (B), the inset shows an enlargement; UV-VIS spectra of both the $B_{800}Vq_{190}MAA_{550}$ micelles (solid black line) and the IPEC (solid grey line) loaded with Au-NPs (C), the insets are photographs taken of the IPEC solutions before (left) and after (right) nanoparticle formation; grey-scale analysis of two adjacent IPECs in (B, marked via the black rectangle), highlighting the location of the nanoparticles inside the structure (D).

As depicted in Figure 9A, the Au nanoparticles formed within the PMAA shell of the $B_{800}Vq_{190}MAA_{550}$ micelles are narrowly distributed and around 3-4 nm in diameter as shown in the enlargement in Figure 9A. They are densely located directly within the IPEC shell around the soft PB core and less packed with growing distance. The patchy shell of these micelles is not visible here as the contrast of the metal particles simply is too high compared to the different block polymer compartments. Strikingly, only very few free Au-NP can be seen, indicating a strong tendency of the $HAuCl_4$ -precursor to coordinate within the IPEC shell or the PMAA corona. Figure 5B shows a cryo-TEM of the IPEC solution at $Z = 0.2$ after being loaded with Au NPs in a similar manner. Round-shaped objects with a radius of 60-

75 nm can be seen, each exhibiting a thin dark ring inside the grey shell. These must be the Au NPs, located within the IPEC shell and still surrounded by the PEO corona. This is highlighted more clearly in the inset in Figure 8B showing an enlargement of one single IPEC. A thin, continuous dark ring with a thickness of around 5 nm is embedded within the grey IPEC micelle. Furthermore, almost no free nanoparticles can be observed in the cryo-TEM in Figure 9B.

Besides electron microscopy, UV-VIS spectroscopy is one of the standard methods to determine the aggregation state of noble metal colloids in solution.^[34] UV-VIS spectra of the B₈₀₀Vq₁₉₀MAA₅₅₀ micelles (solid black line) and the IPECs loaded with Au-NPs (solid grey line) are shown in Figure 9C. In both cases, an absorption maximum at around 520 nm was obtained, also indicating the formation of rather small gold particles without further aggregation occurring. The inset are two photographs taken from the IPEC solution before (left) and after (right) Au NP formation. The pink color in the right image supports the drawn conclusions. In addition, grey-scale analysis on two adjacent IPECs was performed and is depicted in Figure 9D. The sharp inclusions (arrows) on both sides of the cores present the thin dark ring and thus, the nanoparticles. Both electron microscopic and spectroscopic techniques convincingly show that the formation of Au-NP selectively within the IPEC shell of complex particles in solution was successfully performed.

Conclusion

We have successfully prepared dynamic and multicompartmental colloidal objects with a radius of around 100-150 nm through the combination of 3 inherently different approaches: non-solvent induced self-assembly, ionic complexation, and coordination chemistry. IPEC formation between negatively charged core-patchy shell-corona micelles from B₈₀₀Vq₁₉₀MAA₅₅₀ terpolymers and positively charged Vq₉₄EO₁₂₅₀ diblock copolymers rendered core-shell-shell-corona objects, which showed a dynamic relaxation behavior within 10 days, changing from a star-like to a spherical shape. The remaining charge of these colloids could be adjusted via the mixing ratio of both polymers. The IPECs could be even further modified through the in-situ reduction of HAuCl₄ through UV-irradiation within the IPEC shell, resulting in narrowly distributed Au-NPs with a diameter of 3-4 nm. These systems could be interesting candidates for catalytic application or act as carriers for sensitive substances through the protective PEO corona.

ACKNOWLEDGMENT: We thank Jiayin Yuan for performing the UV-VIS measurements, Markus Hund for help during the SFM measurements and Katharina Schatz for help with the illustrations. The Volkswagenstiftung is gratefully acknowledged for financial support within the framework “Complex Materials”.

References

- [1] M. Lazzari, M. A. Lopez-Quintela, *Adv. Mater.* **2003**, *15*, 1583.
- [2] A. Ruzette, L. Leibler, *Nature Mater.* **2005**, *4*, 19.
- [3] A. Walther, X. Andre, M. Drechsler, V. Abetz, A. H. E. Muller, *J. Am. Chem. Soc.* **2007**, *129*, 6187.
- [4] F. S. Bates, G. H. Fredrickson, *Phys Today* **1999**, *52*, 32.
- [5] T. Goldacker, V. Abetz, R. Stadler, I. Erukhimovich, L. Leibler, *Nature* **1999**, *398*, 137.
- [6] S. B. A. Ludwigs, A. Voronov, N. Rehse, R. Magerle, G. Krausch, *Nature Mater.* **2003**, *2*, 744.
- [7] S. Guo, J. Rzaev, T. S. Bailey, A. S. Zalusky, R. Olayo-Valles, M. A. Hillmyer, *Chem. Mat.* **2006**, *18*, 1719.
- [8] R. Erhardt, M. Zhang, A. Böker, H. Zettl, C. Abetz, P. Frederik, G. Krausch, V. Abetz, A. H. E. Müller, *J. Am. Chem. Soc.* **2003**, *125*, 3260.
- [9] Z. Li, M. A. Hillmyer, T. P. Lodge, *Langmuir* **2006**, *22*, 9409.
- [10] H. Cui, T. K. Hodgdon, E. W. Kaler, L. Abezgauz, D. Danino, M. Lubovsky, Y. Talmon, D. J. Pochan, *Soft Matter* **2007**, *3*, 945.
- [11] V. A. Kabanov, *Russ. Chem. Rev.* **2005**, *74*, 3.
- [12] D. V. Pergushov, E. V. Remizova, J. Feldthusen, A. B. Zezin, A. H. E. Mueller, V. A. Kabanov, *J. Phys. Chem.* **2003**, *107*, 8093.
- [13] F. Schacher, A. Walther, A. H. E. Müller, **2009**, submitted.
- [14] M. Burkhardt, N. Martinez-Castro, S. Tea, M. Drechsler, I. Babin, I. Grishagin, R. Schweins, D. V. Pergushov, M. Gradzielski, A. B. Zezin, A. H. E. Muller, *Langmuir* **2007**, *23*, 12864.
- [15] M. Burkhardt, M. Ruppel, S. Tea, M. Drechsler, R. Schweins, D. V. Pergushov, M. Gradzielski, A. B. Zezin, A. H. E. Muller, *Langmuir* **2008**, *24*, 1769.
- [16] P. S. Chelushkin, E. A. Lysenko, T. K. Bronich, A. Eisenberg, V. A. Kabanov, A. V. Kabanov, *J. Phys. Chem. B* **2007**, *111*, 8419.
- [17] P. S. Chelushkin, E. A. Lysenko, T. K. Bronich, A. Eisenberg, V. A. Kabanov, A. V. Kabanov, *J. Phys. Chem. B* **2008**, *112*, 7732.
- [18] I. K. Voets, A. de Keizer, P. de Waard, P. M. Frederik, P. H. H. Bomans, H. Schmalz, A. Walther, S. King, F. A. M. Leermakers, M. A. Cohen Stuart, *Angew. Chem. Int. Ed.* **2006**, *118*, 6825.
- [19] S. Förster, M. Antonietti, *Adv. Mater.* **1998**, *10*, 195.
- [20] A. Haryono, W. H. Binder, *Small* **2006**, *2*, 600.
- [21] J. He, R. Tangirala, T. Emrick, T. P. Russell, A. Böker, X. Li, J. Wang, *Adv. Mater.* **2007**, *19*, 381.

- [22] Y. Lin, A. Boker, J. He, K. Sill, H. Xiang, C. Abetz, X. Li, J. Wang, T. Emrick, S. Long, Q. Wang, A. Balazs, T. P. Russell, *Nature* **2005**, *434*, 55.
- [23] M. V. Seregina, L. M. Bronstein, O. A. Platonova, D. M. Chernyshov, P. M. Valetsky, J. Hartmann, E. Wenz, M. Antonietti, *Chem. Mat.* **1997**, *9*, 923.
- [24] G. Schmid, *Chem. Rev.* **1992**, *92*, 1709.
- [25] P. Zheng, X. Jiang, X. Zhang, W. Zhang, L. Shi, *Langmuir* **2006**, *22*, 9393.
- [26] C. Carrot, J. C. Valmalette, C. J. G. Plummer, S. M. Scholz, J. Dutta, H. Hofmann, J. G. Hilborn, *Colloid Polym. Sci.* **1998**, *276*, 853.
- [27] M. Valden, X. Lai, D. W. Goodman, *Science* **1998**, *281*, 1647.
- [28] J. J. Chiu, B. J. Kim, E. J. Kramer, D. J. Pine, *J. Am. Chem. Soc.* **2005**, *127*, 5036.
- [29] J. Q. Lu, S. S. Yi, *Langmuir* **2006**, *22*, 3951.
- [30] F. Schacher, A. Walther, M. Ruppel, M. Drechsler, A. H. E. Müller, *Macromolecules* **2009**, *42*, 3540.
- [31] R. Djalali, S. Y. Li, M. Schmidt, *Macromolecules* **2002**, *35*, 4282.
- [32] Z. Lei, X. Wei, L. Zhang, S. Bi, *Colloids and Surfaces A: Physicochem. Eng. Aspects* **2008**, *317*, 705.
- [33] P. Schuetz, F. Caruso, *Chem. Mat.* **2004**, *16*, 3066.
- [34] P. B. Johnson, R. W. Christy, *Physical Review B* **1972**, *6*, 4370.

Publications:

1. E. Tullberg, F. Schacher, D. Peters, and T Frejd, "*Solvent-free Heck-Jeffery reactions under ball-milling conditions applied to the synthesis of unnatural amino acids precursors and Indoles*", *Synthesis* 7, 2006, 1183-1189
2. M. Gawenda, A. Sperschneider, F. Schacher, G. Krausch, A.H.E. Müller, and M. Ulbricht, "*Toward Nanoporous Composite Membranes with Tailored Block Copolymers as Selective Layers*", *Desalination* 200, 2006, 29-31
3. F. Schacher, A. Walther, M. Ruppel, and A.H.E. Müller, "*Multicompartment Micelles from ABC Triblock Terpolymer*", *Polym. Mater. Sci. Eng.* 94, 2007, 96-97
4. A. Sperschneider, F. Schacher, M. Gawenda, L. Tsarkova, A.H.E. Müller, M. Ulbricht, and G. Krausch, "*Towards Nanoporous Membranes based on ABC Triblock Terpolymers*", *Small* 3(6), 2007, 1056-1063
5. J. Yuan H. Schmalz, Y. Xu, N. Miyajima, M. Drechsler, M.W. Möller, F. Schacher, and A.H.E. Müller, "*Room-Temperature Growth of Uniform Tellurium Nanorods and the Assembly of Tellurium or Fe₃O₄ Nanoparticles on the Nanorods*", *Adv. Mater.* 20, 2008, 947
6. S. Tea, F. Schacher, and A.H.E. Müller, "*Methacrylate Nanoparticles by Crosslinking of Block Copolymer Micelles in Organic Solvents*", *Polym. Prepr. (Am. Chem. Soc., Div. Polym. Chem.)* 49(2), 2008, 745
7. A. Walther, P. Millard, A. Goldmann, T. Lovestead, F. Schacher, C. Barner-Kowollik, and A.H.E. Müller, "*Bis-Hydrophilic Block Terpolymers via RAFT Polymerization: Toward Dynamic Micelles with Tunable Corona Properties*", *Macromolecules* 41(22), 2008, 8608
8. F. Schacher, M. Ulbricht, and A.H.E. Müller, "*Self-Supporting, Double Stimuli-responsive Porous Membranes from Polystyrene-block-poly(N,N-*

- dimethylaminoethyl methacrylate) Diblock Copolymers*", Adv. Funct. Mater. 19, 2009, 1040-1045
9. F. Schacher, M. Müllner, H. Schmalz, and A.H.E. Müller, "New Block Copolymers with Poly(N,N-dimethylaminoethyl methacrylate) as Double Stimuli-responsive Block", Macromol. Chem. Phys. 210, 2009, 256-263
 10. F. Schacher, T. Rudolph, M. Ulbricht, and A.H.E. Müller, "Double Stimuli-Responsive Porous Membranes from Polystyrene-block-poly(N,N-dimethylaminoethyl methacrylate) Diblock Copolymers", Polym. Mater. Sci. Eng. 100 2009
 11. J. Yuan, Y. Lu, F. Schacher, T. Lunkenbein, S. Weiss, H. Schmalz, and A.H.E. Müller, "Template-directed Synthesis of Titania Hybrid Nanowires within Core-Shell Cylindrical Polymer Brushes", Chem. Mat., 2009, submitted
 12. F. Schacher, A. Walther, M. Ruppel, M. Drechsler, and A.H.E. Müller, "Multicompartment Core Micelles of ABC Block Terpolymers in Organic Media", Macromolecules 42, 2009, 3540-3548 (Cover Article)
 13. J. Yuan, H. Gao, F. Schacher Y. Xu, R. Richter, W. Tremel, and A.H.E. Müller, "Alignment of Tellurium Nanorods via a Magnetization-Alignment-Demagnetization ("MAD") Process Assisted by an External Magnetic Field", ACS Nano, 2009, accepted (DOI: 10.1021/nn9002715)
 14. F. Schacher, A. Walther, and A.H.E. Müller, "Dynamic Multicompartment Core Micelles in Aqueous Media", Langmuir, 2009, accepted (DOI: 10.1021/la901182c)
 15. F. Schacher, E. Betthausen, A. Walther, H. Schmalz, D. Pergushov, and A.H.E. Müller, "Interpolyelectrolyte Complexes of Dynamic Multicompartment Micelles", ACS Nano, 2009, submitted

16. F. Schacher, S. Reinicke, A. Walther, H. Schmalz, and A.H.E. Müller, *New amphiphilic nanostructures based on block terpolymers made by anionic polymerization* in: *"New smart materials via metal mediated macromolecular engineering: from complex to nano structures"*, E. Khosravi, Y. Yagci, Eds., NATO ASI Series, 2009, in press

17. F. Schacher, T. Rudolph, F. Wieberger, M. Ulbricht, and A.H.E. Müller, *"Double Stimuli-Responsive Ultrafiltration Membranes from Polystyrene-block-poly(N,N-dimethylaminoethyl methacrylate) Diblock Copolymers"*, ACS Applied Materials & Interfaces, 2009, *accepted* (DOI: 10.1021/am900175u)

Conference presentations:

1. F. Schacher, A. Walther, M. Ruppel, A.H.E. Müller. "*Multicompartment Micelles from triblock terpolymers*", Poster presentation at workshop "Structure and properties of self-organized amphiphilic systems", October 3-6, 2006, Prague (CZE)
2. F. Schacher, A. Sperschneider, M. Gawenda, J. Köhler, G. Krausch, M. Ulbricht, A.H.E. Müller. "*Towards nanoporous membranes from linear ABC triblock terpolymers*", Oral presentation at symposium "Complex materials", March 18-21, 2007, Rolduc abbey, Kerkrade (NL)
3. F. Schacher, A. Walther, A.H.E. Müller. "*Multicompartment micelles from linear ABC triblock terpolymers*", Oral presentation at 233rd ACS national meeting, March 25-29, 2007, Chicago (US)
4. F. Schacher, A. Walther, A.H.E. Müller. "*Multicompartment micelles from linear ABC triblock terpolymers*", Oral presentation at symposium "Modern problems in polymer science", April 17-21, 2007, St. Petersburg (RUS)
5. F. Schacher, M. Müllner, H. Schmalz, A.H.E. Müller. "*New block copolymers with DMAEMA prepared via anionic polymerization*", Poster presentation at "IUPAC international symposium on ionic polymerization", September 2-7, 2007, Banz Abbey, Banz (GER)
6. F. Schacher, A. Walther, A.H.E. Müller. "*Core cross-linked multicompartment micelles*", Poster presentation at conference "STIPOMAT, Stimuli-responsive polymeric materials", October 14-17, 2007, Les Diablerets (CH)

7. F. Schacher, A. Walther, A.H.E. Müller. "*Directing the self-assembly of ABC triblock terpolymers in aqueous solution through selective quaternization of the middle block*", Poster presentation at symposium "Self-assembled structures of amphiphilic copolymers and biopolymers", February 10-14, 2008, Biarritz (FR)
8. F. Schacher, A. Sperschneider, A.H.E. Müller. "*Well-defined block copolymers as membrane precursors*", Poster presentation at the E-MRS spring meeting, May 26-30, 2008, Strasbourg (FR)
9. F. Schacher, A. Walther, A.H.E. Müller. "*Dynamic multicompartment interpolyelectrolyte complexes*", Poster presentation at ECIS conference, August 31 - September 5, 2008, Krakow (POL)
10. F. Schacher, M. Ulbricht, A.H.E. Müller. "*Asymmetric membranes from double stimuli-responsive amphiphilic diblock copolymers*", Poster presentation at conference "Bio & Polymers", September 28-30, 2008, Aachen (GER)
11. F. Schacher, M. Ulbricht, A.H.E. Müller. "*Double stimuli-responsive porous membranes from polystyrene-block-poly(N,N-dimethylaminoethyl methacrylate) diblock copolymers*", Poster presentation at Makromolekulares Kolloquium 2009, February 25-28, 2009, Freiburg (GER)
12. F. Schacher, T. Rudolph, M. Ulbricht, A.H.E. Müller. "*Double stimuli-responsive porous membranes from polystyrene-block-poly(N,N-dimethylaminoethyl methacrylate) diblock copolymers*", Oral presentation at 237th ACS national meeting, March 22-26, 2009, Salt Lake City (US)

Abbreviations:

ALD	Atomic layer deposition
ATRP	Atom transfer radical polymerization
BIC	Block ionomer complex
BVT	Polybutadiene- <i>block</i> -poly(2-vinylpyridine)- <i>block</i> -poly(<i>tert</i> -butyl methacrylate)
CPB	Cylindrical polyelectrolyte brush
DEAEMA	N,N-diethylaminoethyl methacrylate
DLS	Dynamic light scattering
DMAEMA	N,N-dimethylaminoethyl methacrylate
DMSB	Dimethylsilacyclobutane
DMF	Dimethylformamide
DPE	1,1-diphenylethylene
DPLi	1,1-diphenylhexyllithium
GTP	Group transfer polymerization
IPEC	Interpolyelectrolyte complex
LB	Langmuir-Blodgett
LCST	Lower critical solution temperature
MALDI-ToF	Matrix assisted laser desorption ionization - time of flight mass spectrometry
NIPS	Non-solvent induced phase separation
NIR	Near infrared
NMR	Nuclear magnetic resonance
NPs	Nanoparticles
ODT	Order-disorder transition
P2VP	Poly(2-vinylpyridine)
P4VP	Poly(4-vinylpyridine)
PAA	Polyacrylic acid
PB	Polybutadiene
PCEMA	Poly(cinnamoyl ethyl methacrylate)

PDMAEMA	Poly(N,N-dimethylaminoethyl methacrylate)
PDMS	Poly(dimethylsilane)
PE	Polyethylene
PEE	Poly(ethyl ethylene)
PEO	Poly(ethylene oxide)
PFEMS	Poly(ferrocenylethylmethylsilane)
PFPO	Poly(perfluoropropylene oxide)
PFS	Poly(ferrocenyl silane)
PI	Polyisoprene
PIB	Polyisobutylene
PL	Perforated lamella
PLA	Poly(D,L-lactide)
PMAA	Poly(methacrylic acid)
PMMA	Poly(methyl methacrylate)
PMVP	Poly(1-methyl-2-vinylpyridine)
PS	Polystyrene
P <i>t</i> BMA	Poly(<i>tert</i> -butyl methacrylate)
P <i>t</i> BS	Poly(<i>tert</i> -butoxystyrene)
PVDF	Poly(vinylidene fluoride)
RAFT	Reversible addition fragmentation transfer
SAXS	Small angle X-ray scattering
SBM	Polystyrene- <i>block</i> -polybutadiene- <i>block</i> -poly(methyl methacrylate)
SBT	Polystyrene- <i>block</i> -polybutadiene- <i>block</i> -poly(<i>tert</i> -butyl methacrylate)
SBV	Polystyrene- <i>block</i> -polybutadiene- <i>block</i> -poly(2-vinylpyridine)
SEC	Size exclusion chromatography
SEM	Scanning electron microscopy
SFM	Scanning force microscopy
SLS	Static light scattering
SPB	Spherical polyelectrolyte brush

SVT	Polystyrene- <i>block</i> -poly(2-vinylpyridine)- <i>block</i> -poly(<i>tert</i> -butyl methacrylate)
TBAB	Tetrabutylammonium bromide
TEM	Transmission electron microscopy
TFC	Thin-film composite
THF	Tetrahydrofuran
TMS	Tetramethylsilane
UCST	Upper critical solution temperature

Danksagung

Das Merkwürdigste an der Zukunft ist wohl die Vorstellung, daß man unsere Zeit später die gute alte Zeit nennen wird.

(John Steinbeck)

Zuallererst möchte ich mich bei Herrn Prof. Müller bedanken. Die mittlerweile 3,5 Jahre in seiner Gruppe waren sehr unterhaltsam, lehrreich, und vor allem eines: produktiv. Am meisten beeindruckt hat mich eigentlich das entgegengebrachte Vertrauen, mich meine Doktorarbeit zu großen Teilen selbst gestalten zu lassen. Weiterhin durfte und konnte ich vielen nationalen und internationalen Tagungen beiwohnen, Erfahrungen sammeln, andere Forschungsgruppen kennenlernen und Wissen austauschen. Auch daß ist keineswegs selbstverständlich.

Des weiteren möchte ich mich auch bei Herrn Prof. Ulbricht ganz herzlich für Gespräche, Anregungen, Korrekturen und ganz einfach eine angenehme Zusammenarbeit bedanken.

Wie an den zahlreichen Co-Autoren unschwer zu erkennen ist, ist diese Arbeit nicht nur das Resultat meiner, sondern auch der Bemühungen und Hilfe vieler anderer Kollegen und Freunde.

Ganz besonders möchte ich mich bei Andreas bedanken. Du hast mir anfangs und auch später viele Ideen gegeben, mir gezeigt wie ich Resultate sinnvoll und wirksam zusammenstelle und warst immer ein guter Ansprechpartner und Freund.

Dima, Dir danke ich für viele nette Diskussionen und für einen wunderschönen Abend in Moskau.

Sascha, auch hier noch einmal ein herzliches Dankeschön für eine unvergessliche Woche in St. Petersburg.

Die Liste aller Lehrstuhlmitarbeiter, die zum Gelingen dieser Arbeit beigetragen haben, ist lang, darum hier an dieser Stelle nur ein kleiner Auszug:

Markus, der beste schnarchende Zimmergenosse aller Zeiten // Felix, mein Seelenverwandter in Sachen Reise- und Sprachangelegenheiten // Alexandra, erprobte Reisegefährtin, Lactose-Beraterin und Projekt-(Leidens)-Genossin // Manuela, versierte Konferenz-Touristin und Kummerkasten // Jiayin und Youyong, die ersten offiziellen Grill-Botschafter der Volksrepublik China // Sandrine, einfach zu viele F´s // Harald, unser Mann am Aluminium-Band // Holger, das wandelnde Anionik-Lexikon // Stefan, wer braucht schon Zahnbürsten wenn man sich dieselbe Ampulle teilt... // Benni, eine Bank am REM

...und viele mehr...

Vieles liegt aber auch einfach an der Atmosphäre und dem Umfeld eines Lehrstuhls. Es war immer wieder ein Vergnügen mit euch allen zusammen zu arbeiten: Anja, Susanne, Annika, Karina, Jeannine, Daniela, Denise, Cornelia, Anette, Kerstin, Andre, Alexander, Markus, Stephan, Sergey, Pierre, Andrea, Joe, Thomas, Melanie, Hansi, Evis, Xavier, Alexandre, Markus, Markus...

Gabi, nochmals danke für Deine stete Hilfe bei allem bürokratischen Firlefanz, dafür, daß Du immer ein offenes Ohr hattest, und für stilsichere Hochzeitsberatung.

Während der Zeit hier durfte ich mehrere Vertiefungspraktikanten und HiWis betreuen: ihr habt mir viel geholfen, und ein bisschen Spaß war ja schließlich auch dabei. Danke an André, Markus, Simone, Eva, Christian, Alexander, Tobias, Christopher.

Auch die Zusammenarbeit mit anderen Lehrstühlen hat wunderbar funktioniert und viele Sachen erleichtert oder die Wege verkürzt. Ein herzliches Dankeschön an dieser Stelle an alle Kollegen an den Lehrstühlen für Organische, Anorganische, Physikalische oder Makromolekulare Chemie.

Mehr als 7 Jahre an der Uni Bayreuth hinterlassen aber auch andere Spuren. Ich freue mich, daß mir, gerade aus meinem Semester, ein großer Freundeskreis vergönnt war. Nicht zuletzt deshalb haben wir es geschafft, den ersten Alumniverein der Chemie, die CSG e.V., aus dem Boden zu stampfen.

Mike, Markus, Eva, Bertram, Roland, Dominik, André, Sandra, Florian, Daniel, Dunja... - Wir haben uns doch das eine oder andere Mal gegenseitig davor bewahrt, verrückt zu werden.

Benjamin, vielen Dank für die Hilfe mit den Illustrationen der einzelnen Kapitel.

Meiner Familie danke ich für die fortwährende Unterstützung auf sämtlichen verfügbaren Wellenlängen. Moralisch, finanziell, dafür, daß ich immer selbst entscheiden konnte, für den Rückhalt, und für das Vertrauen.

Katharina, Du hast es in allen nur erdenklichen Situationen geschafft mir die Stütze zu sein die ich brauche. Ich weiß nicht wie, aber es gibt Sachen die muss man nicht verstehen. Ohne Dich wäre ich nur ein Schatten meiner selbst.

Erklärung

Die vorliegende Arbeit wurde von mir selbstständig verfasst und ich habe keine anderen als die angegebenen Hilfsmittel verwendet.

Ferner habe ich nicht anderweitig versucht, mit oder ohne Erfolg eine Dissertation einzureichen oder mich der Doktorprüfung zu unterziehen.

Bayreuth, den 04.02.2009

(Felix Schacher)